nature

THE INTERNATIONAL WEEKLY JOURNAL OF SCIENCE

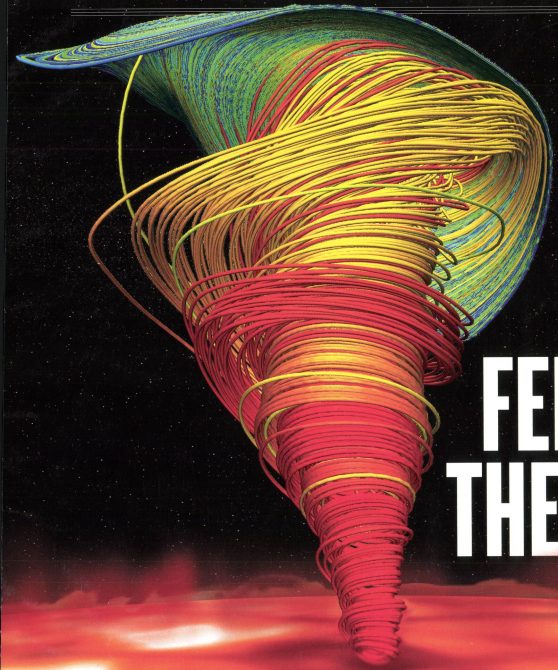

How super-tornadoes up the temperature in the Sun's outer atmosphere

PAGES 476 & 505

FEELING THE HEAT

AVIAN FLU

H5N1 — FIVE BIG QUESTIONS

What it will take to size up the threat

PAGE 456

AGRICULTURE

PIGS WEANED OFF DRUGS

Danish farmers cut dependence on antibiotics

PAGE 465

SCIENCE FICTION

ARCHITECT OF THE FUTURE

David Brin celebrates Ray Bradbury's vision

PAGE 471

NATURE.COM/NATURE

28 June 2012 £10

Vol. 486, No. 7404

9 770028 083095 26

nature podcast

science... wherever you are.

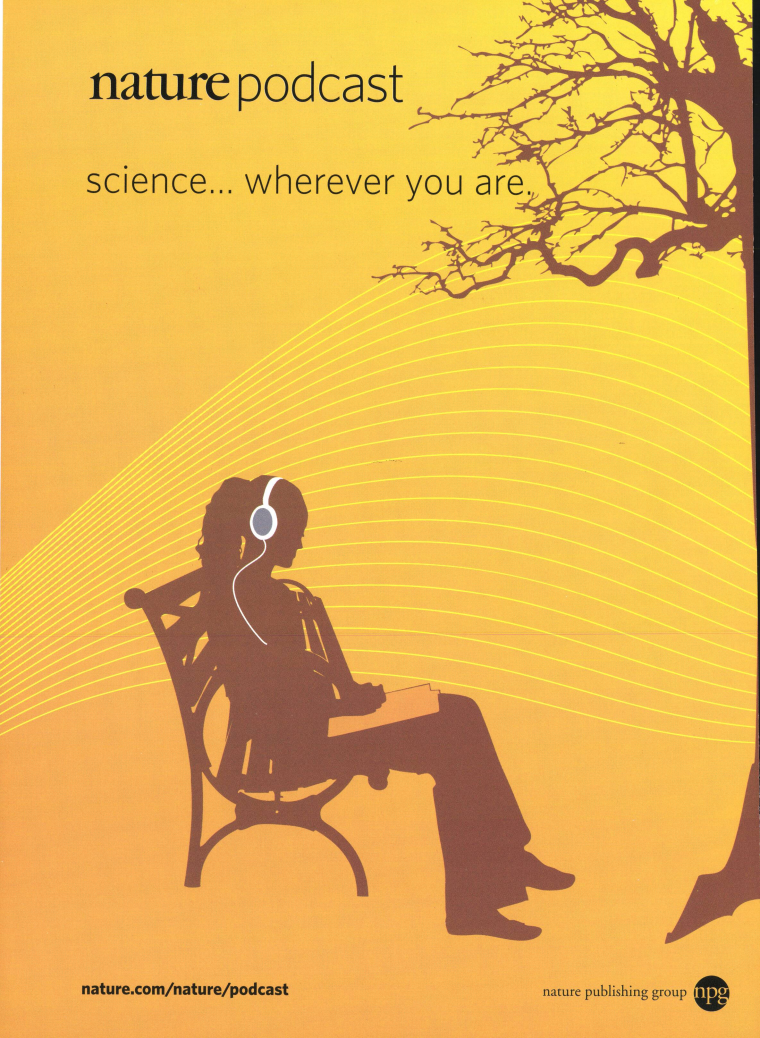

nature.com/nature/podcast

nature publishing group npg

BioResearch

Lonza

A Clear Pathway to Results

For Biologically Relevant Gene Expression Analysis

Help free your gene expression experiments from biases and interference with targeted research tools for every step of your workflow.

Our flexible, integrated solutions bring you biological relevance from sample preparation, to qPCR, all the way through protein confirmation.

- FlashGel® System for rapid, simple assurance of quality RNA
- StellARray™ qPCR Arrays for accurate, unbiased, disease- and pathway-specific qPCR reactions
- PAGEr® Precast Gels and reagents for consistent, reliable protein validation by Western blot

The direct route to results starts with Lonza.

Lonza Research Solutions
© 2011 Lonza Walkersville, Inc. www.lonza.com/research

www.lonza.com/gex

Hypertension Research

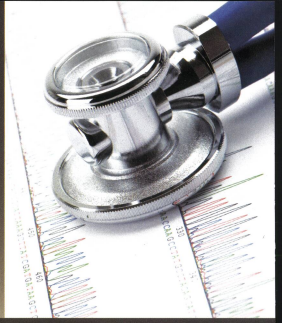

Recent Progress and Future Prospects in Genetics of Hypertension

Review Series and Web Focus

Hypertension Research features a special **Review Series and Web Focus** on the **Recent Progress and Future Prospects in Genetics of Hypertension**, which provides a series of review articles and carefully selected papers dealing with the study of genetic factors influencing blood pressure.

Featured articles include:

The stroke-prone spontaneously hypertensive rat: still a useful model for post-GWAS genetic studies?
Toru Nabika, Hiroki Ohara, Norihiro Kato and Minoru Isomura

Ethnic differences in genetic predisposition to hypertension
Norihiro Kato

Hunting for genes for hypertension: the Millennium Genome Project for Hypertension
Yasuharu Tabara, Katsuhiko Kohara and Tetsuro Miki
and behalf of the study group of the Millennium Genome Project for Hypertension

To access the Web Focus on Recent Progress and Future Prospects in Genetics of Hypertension visit:
www.nature.com/hr/focus/genetics_hypertension

nature publishing group npg

Instruments that are music to your hands.

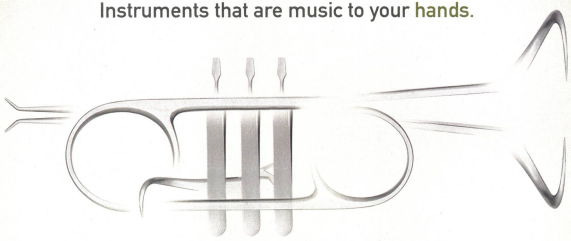

FINE SURGICAL INSTRUMENTS FOR RESEARCH™

SHIPPING GLOBALLY SINCE 1974

Request a catalog at finescience.com or call 1-800-521-2109.

F · S · T®

FINE SCIENCE TOOLS

The Norwegian Academy of Science and Letters
announces the

2012 WINNERS OF

THE KAVLI PRIZE℠

Seven scientists whose discoveries have dramatically expanded human understanding in the fields of astrophysics, nanoscience and neuroscience have been recognized with the award of the million-dollar Kavli Prizes.

The laureates were chosen for work that has led to a major revision of knowledge about our planetary system, pioneering contributions to the field of nanotechnology, and new discoveries of how the brain receives and responds to sensations such as sight, sound and touch

The Kavli Prize is a partnership between The Norwegian Academy of Science and Letters, The Kavli Foundation (US) and The Norwegian Ministry of Education and Research.

HM King Harald presents the Kavli Prize to the 2012 Laureates on September 4, 2012 at a ceremony in Oslo, Norway.

THE KAVLI PRIZE IN ASTROPHYSICS

MICHAEL E. BROWN
California Institute of Technology,
Pasadena, CA USA

DAVID C. JEWITT
University of California
Los Angeles, CA USA

JANE X. LUU
MIT Lincoln Laboratory,
Lexington, MA USA

"for discovering and characterizing the Kuiper Belt and its largest members, work that led to a major advance in the understanding of the history of our planetary system."

THE KAVLI PRIZE IN NANOSCIENCE

MILDRED S. DRESSELHAUS
Massachusetts Institute of Technology,
Cambridge, MA, USA

"for her pioneering contributions to the study of phonons electron-phonon interactions, and thermal transport in nanostructures."

THE KAVLI PRIZE IN NEUROSCIENCE

CORNELIA I. BARGMANN
The Rockefeller University
New York, NY, USA

WINFRIED DENK
Max Planck Institute for
Medical Research
Heidelberg, Germany

ANN M. GRAYBIEL
Massachusetts Institute of Technology,
Cambridge, MA, USA

"for elucidating basic neuronal mechanisms underlying perception and decision"

To learn more about The Kavli Prize please visit

www.kavliprize.no
www.kavlifoundation.org

CONTENTS

28 June 2012 / Vol 486 / Issue No 7404

THIS WEEK

EDITORIALS

439 OPEN ACCESS
Openness costs
Making data freely available will require a shift in business models

439 EARTH SUMMIT
A first step
Could the latest Earth conference be the start of a new journey?

440 ANTIBIOTICS
Pig out
Countries should follow Denmark and slash antibiotic use in farming

WORLD VIEW

441 **Open your minds and share your results**
Geoffrey Boulton
Publicly funded research should be treated as a public resource

RESEARCH HIGHLIGHTS

442 SELECTIONS FROM THE SCIENTIFIC LITERATURE
Turtles fossilized in flagrante / 'Ring' species found in plants / Diversity link to languages / A puzzling exoplanet pair / Martian snow / Information rays

SEVEN DAYS

444 **The news in brief**
United Nations to set up international science board / Lonesome George dies / Royal Society condemns data hoarding / Japanese people protest against restart of nuclear reactors

CAREERS

559 GRANT APPLICATIONS
Find me the money
Are funding consultants the answer for the cash-strapped researcher?

561 CAREERS NEWS

NEWS IN FOCUS

447 ENVIRONMENT
Rio+20's ambitions collide with global wealth gap

449 BIOSECURITY
Work on H5N1 avian flu virus to restart — along with controversy

450 CLIMATE
In North Carolina, even measuring sea-level rise is the stuff of politics

451 SPECIES RECOVERY
Why threatened California condor still eats lead

452 POLITICS
Presidential candidates promise to boost spending on Mexican science

453 GENETIC ENGINEERING
Transgenic-pig disease models pose a tricky problem for regulators

454 GENETICS
Lawsuits complicate debut of non-invasive fetal tests

FEATURES

456 INFLUENZA
Five questions on H5N1
What do we still need to know about the pandemic potential of avian flu?

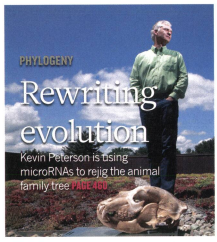

COMMENT

463 ENVIRONMENT
Save the Baltic Sea
Daniel J Conley
Forget geoengineering, removing nutrients at source will save the Baltic

465 AGRICULTURE
Get pigs off antibiotics
Frank Aarestrup
Danish farmers have given up using antibiotics as growth promoters

BOOKS & ARTS

468 PHYSICS
A shining life
Frank Close

469 BOOKS IN BRIEF

470 CITIES
Metropolitan mash-up
Anthony King

471 FICTION
Ray Bradbury, an appreciation
David Brin

472 Q&A
The sound catcher
Imogen Heap uses Tom Mitchell's high-tech gloves to both write and play new music

CORRESPONDENCE

473 Bring back DDT / Breast best for cancer prevention /Smart drugs survey/ Supernova over Otford

OBITUARY

474 **Andrew Fielding Huxley (1917–2012)**
Yale E Goldman, Clara Franzini-Armstrong & Clay M Armstrong

FUTURES

564 **Celestial bodies**
Ken Liu

Any sample, any application — no limits

Maximize success with QIAGEN sample technologies

- Innovative, room-temperature sample collection and stabilization
- DNA, RNA, and protein purification from any sample
- Hands-free automated sample preparation
- Reliable genetic, epigenetic, and gene expression analysis from FFPE samples
- Whole genome and transcriptome amplification to overcome sample limitations

Contact QIAGEN today or visit www.qiagen.com/sample-technologies

QIAGEN®

Sample & Assay Technologies

CONTENTS

28 June 2012 / Vol 486 / Issue No 7404

RESEARCH

NEW ONLINE

475 Papers published this week at nature.com

NEWS & VIEWS

476 SOLAR PHYSICS
Swirls in the corona
Energy conduits in the Sun's outer atmosphere
Stephen J Bradshaw SEE LETTER P.505

477 AGEING
A healthy diet for stem cells
Calorie restriction preserves the functions of stem cells
Fresnida J Ramos & Matt Kaeberlein
SEE ARTICLE P.490

478 ORGANIC CHEMISTRY
Directors extend their reach
Functionalization at the *meta*-position of benzene rings
Matthew O Kitching & Victor Snieckus
SEE LETTER P.518

479 PHARMACOLOGY
A false sense of non-self
Drug-induced hypersensitivity can result from altered antigen display
Ellis L Reinherz SEE LETTER P.554

481 NEUROSCIENCE
Genes and human brain evolution
A gene duplication may have helped to make our brains big and adaptable
Daniel H Geschwind & Genevieve Konopka

482 CANCER
Pinprick diagnostics
Rare drug-resistant clones detected in circulating tumour DNA
Eduardo Vilar & Josep Tabernero
SEE LETTERS P.532 & P.537

ARTICLES

485 ECOLOGY **Dimensionality of consumer search space drives trophic interaction strengths**
S Pawar, A I Dell & V M Savage

490 STEM CELLS **mTORC1 in the Paneth cell niche couples intestinal stem-cell function to calorie intake**
Ö H Yilmaz et al. SEE N&V P.477

496 GENOMICS **A map of nucleosome positions in yeast at base-pair resolution**
K Brogaard, L Xi, J-P Wang & J Widom

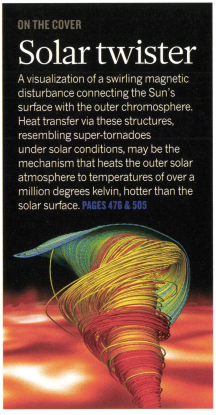

ON THE COVER

Solar twister

A visualization of a swirling magnetic disturbance connecting the Sun's surface with the outer chromosphere. Heat transfer via these structures, resembling super-tornadoes under solar conditions, may be the mechanism that heats the outer solar atmosphere to temperatures of over a million degrees kelvin, hotter than the solar surface. PAGES 476 & 505

LETTERS

502 ASTRONOMY **The signature of orbital motion from the dayside of the planet τ Boötis b**
M Brogi et al.

505 ASTRONOMY **Magnetic tornadoes as energy channels into the solar corona**
S Wedemeyer-Böhm et al. SEE N&V P.476

509 NUCLEAR PHYSICS **The limits of the nuclear landscape**
J Erler et al.

513 PHYSICS **Fractal morphology, imaging and mass spectrometry of single aerosol particles in flight**
N D Loh et al.

518 ORGANIC CHEMISTRY **Activation of remote *meta*-C–H bonds assisted by an end-on template**
D Leow, G Li, T-S Mei & J-Q Yu
SEE N&V P.478

523 PALAEONTOLOGY **Three-dimensional limb joint mobility in the early tetrapod *Ichthyostega***
S E Pierce, J A Clack & J R Hutchinson

527 GENOMICS **The bonobo genome compared with the chimpanzee and human genomes**
K Prüfer et al.

532 CANCER **Emergence of *KRAS* mutations and acquired resistance to anti-EGFR therapy in colorectal cancer**
S Misale et al. SEE N&V P.482

537 CANCER **The molecular evolution of acquired resistance to targeted EGFR blockade in colorectal cancers**
L A Diaz Jr et al. SEE N&V P.482

541 MOLECULAR BIOLOGY **Autoregulation of microRNA biogenesis by *let-7* and Argonaute**
D G Zisoulis, Z S Kai, R K Chang & A E Pasquinelli

545 IMMUNOLOGY **Generalized Lévy walks and the role of chemokines in migration of effector CD8⁺ T cells**
T H Harris et al.

549 IMMUNOLOGY **PPAR-γ is a major driver of the accumulation and phenotype of adipose tissue T_{reg} cells**
D Cipolletta et al.

554 IMMUNOLOGY **Immune self-reactivity triggered by drug-modified HLA-peptide repertoire**
P T Illing et al. SEE N&V P.479

PALAEONTOLOGY

Shore thing

Ichthyostega was an inelegant mover when out of the water.
PAGE 523

COVER IMAGE USES VAPOR AND COSBOLD SOFTWARE

nature

28 June 2012 / Vol 486 / Issue No. 7404

EDITORIAL

LONDON, MUNICH, WASHINGTON DC, NEW YORK, BOSTON, PARIS, SAN FRANCISCO, TOKYO nature@nature.com

EDITOR-IN-CHIEF: Philip Campbell
EXECUTIVE EDITOR: Nick Campbell
PUBLISHING EXECUTIVE EDITOR: Maxine Clarke **EXECUTIVE EDITOR:** Véronique Kiermer
CHIEF MAGAZINE EDITOR: Tim Appenzeller
THIS WEEK/NEWS/FEATURES: Alison Abbott, David Adam, Ananyo Bhattacharya, Geoff Brumfiel, Declan Butler, Ewen Callaway, Erika Check Hayden, Daniel Cressey, David Cyranoski, Natasha Gilbert, Eric Hand, Heidi Ledford, Corrie Lok, Brendan Maher, Emma Marris, Richard Monastersky, Brian Owens, Helen Pearson, Mark Peplow, Eugenie Samuel Reich, Ivan Semeniuk, Quirin Schiermeier, Jeff Tollefson, Richard Van Noorden, Meredith Wadman, M Mitchell Waldrop **COMMENT:** Sara Abdulla, Joanne Baker, Rosalind Cotter, Barbara Kiser, Alison McCook, Lucy Odling-Smee, Sarah Tomlin **NATURE PODCAST/VIDEO:** Adam Rutherford, Thea Cunningham, Geoff Marsh, Kerri Smith, Charlotte Stoddart **NEWS AND VIEWS:** Sadaf Shadan, Ana Lopes, Andrew Mitchinson, Cesar Sanchez, Marian Turner **RESEARCH:** Ritu Dhand, Karl Ziemelis, Francesca Cesari, I-han Chou, Tanguy Chouard, Rosamund Daw, Alex Eccleston, Angela Eggleston, Joshua Finkelstein, Henry Gee, Patrick Goymer, Noah Gray, Marie-Thérèse Heemels, Magdalena Helmer, Karen Howell, Claudia Lupp, Barbara Marte, Andrew Mitchinson, Juliane Mössinger, Deepa Nath, Wayne Peng, Leslie Sage, Magdalena Skipper, Clare Thomas, Maria Trajkovska, John VanDecar, Liesbeth Venema, Ursula Weiss, Michael White **INSIGHTS/REVIEWS/PERSPECTIVES:** Ursula Weiss **CAREERS:** Gene Russo, Karen Kaplan **TECHNOLOGY FEATURES:** Monya Baker **WOOD FEATURES:** Henry Gee **SUPPLEMENTS:** Herb Brody, Michelle Grayson, Tony Scully **SUBEDITORS:** Colin Sullivan, Sarah Archibald, Nicola Bailey, Anne Blewett, Nicolas Fanget, Isobel Flanagan, Paul Fletcher, Afsaneh Gray, Sasha Lewis, Dinah Loon, Louisa Lyon, Anna Novitzky, Yukie Ozawa, Katherine Perry, David Price, Jenny Rooke, David Winters, Anna York **PRODUCTION:** Jenny Henderson, Leonora Dawson-Bowling, Dan Foley, Stewart Fraser, Susan Gray, Simon Gribbin, Hazel Mayhew, James McQuat, Emilia Orviss, Yvonne Strong, Robert Sullivan, Roberta Tarran, Charles Wenz **ART AND DESIGN:** Kelly Buckheit Krause, Wesley Fernandes, Madeline Hutchinson, Barbara Izdebska, Paul Jackman, Jasiek Krzyszteluk, Annthea Lewis, Chris Ryan, Nik Spencer, Claire Welsh, Mark Wood **JAPAN EDITION:** Eiji Matsuda, Mika Ishida, Mitsuyo Utsugi, Sayaka Ayame **PRESS OFFICE:** Ruth Francis, Neda Afsarmanesh, Lisa Boucher, Rachel Twinn, Rebecca Walton **ADMINISTRATION:** Paul Sng, Liz Bankes, Roseann Campbell, Peter Cary, Ffion Cleverley, Dana Coles, Faye Forrassier, Ashlee Gagui, Amy Invernizzi, Diane Kempinski, Caroline McLean, Rina Nozawa, Anastasia Panoutsou, Kenneth Simpson

PUBLISHING

LONDON feedback@nature.com
MANAGING DIRECTOR & PUBLISHER: Steven Inchcoombe
ASSOCIATE PUBLISHER: Arash Hejazi
PUBLISHING PROJECT MANAGER: Christian Manco
TOKYO feedback@naturasia.com
REGIONAL MANAGING DIRECTOR — ASIA-PACIFIC: David Swinbanks
DIRECTOR — ASIA-PACIFIC: Antoine E Bocquet
OPERATIONS DIRECTOR — ASIA-PACIFIC: Hiroshi Minemura

DISPLAY ADVERTISING, SPONSORSHIP & NATUREJOBS

GLOBAL HEAD: Andrew Douglas a.douglas@nature.com
DISPLAY ADVERTISING AND SPONSORSHIP
GLOBAL HEAD: Gerard Preston g.preston@nature.com
ASSISTANT SPONSORSHIP MANAGER: Reya Silao Tel: +44 (0)20 7843 4977 (rsilao@nature.com)

EUROPE/REST OF WORLD display@nature.com Tel: +44 (0)20 7843 4960
GERMANY/SWITZERLAND/AUSTRIA: Sabine Hugi-Fürst Tel: +41 52761 3386
UK/IRELAND/SCANDINAVIA/SPAIN/PORTUGAL: Evelina Rubio Hakansson Tel: +44 (0)20 7843 4079
FRANCE/BELGIUM/THE NETHERLANDS/LUXEMBOURG/ITALY/OTHER EUROPE: Nicola Wright Tel: +44 (0)20 7843 4959

NORTH AMERICA display@natureny.com
NEW ENGLAND/ EASTERN CANADA: Sheila Reardon Tel: +1 617 494 4900
NEW YORK/ MID-ATLANTIC/ SOUTHEAST: Jim Breault Tel: +1 212 726 9334
MIDWEST: Mike Rossi Tel: +1 212 726 9255
WEST COAST/ WESTERN CANADA: George Lui Tel: +1 415 781 3804
WEST COAST NORTH: Kayla McCutchan Tel: +1 415 403 9038

ASIA-PACIFIC display@natureasia.com
ASIA-PACIFIC HEAD: Kate Yoneyama
JAPAN: Keri Mikami Tel: +81 3 3267 8765
GREATER CHINA/SINGAPORE: Gloria To Tel: +852 2811 7191
INDIA: Vikas Chawla Tel: +91 124 288 1057

SPONSORSHIP
BUSINESS DEVELOPMENT MANAGER: David Bagshaw Tel: +1 212 726 9215
BUSINESS DEVELOPMENT MANAGER: Patrick Murphy Tel: +1 617 475 9216

NATUREJOBS naturejobs@nature.com
EUROPEAN HEAD OFFICE, LONDON: Tel: +44 (0)20 7843 4961
EUROPEAN SALES MANAGER: Nils Moeller (n.moeller@nature.com) **BUSINESS DEVELOPMENT MANAGER, MIDDLE EAST:** Jon Giuliani (j.giuliani@nature.com) **ADVERTISING PRODUCTION MANAGER:** Stephen Russell **NATUREJOBS ONLINE PRODUCTION:** Dennis Chu
US HEAD OFFICE, NEW YORK: naturejobs@natureny.com **US SALES MANAGER:** Ken Finnegan
JAPAN HEAD OFFICE, TOKYO: Tel: +81 3 3267 8765 **ASIA-PACIFIC HEAD:** Kate Yoneyama
ASIA-PACIFIC SALES & BUSINESS DEVELOPMENT MANAGER: Yuki Fujiwara **BUSINESS DEVELOPMENT MANAGER, GREATER CHINA, SINGAPORE:** Gloria To Tel: +852 2811 7191
INDIA: Vikas Chawla Tel: +91 1242881057 (vchawla@nature.com)

MARKETING & SUBSCRIPTIONS

USA/CANADA/LATIN AMERICA subscriptions@us.nature.com
Tel: (USA/Canada)+1 866 363 7860; (outside USA/Canada) +1 212 726 9223
MARKETING: Sara Girard **FULFILMENT:** Karen Dawson

JAPAN/CHINA/KOREA subscriptions@natureasia.com
Tel: +81 3 3267 8751 **MARKETING:** Sachiyo Ikeda **FULFILMENT:** Masayo Tanaka

EUROPE/REST OF WORLD subscriptions@nature.com
Tel: +44 (0)1256 329242
MARKETING: Elena Woodstock, Marcus Parker, Hannah Phipps **FULFILMENT:** Jean Burrows

INDIA npgindia@nature.com
Tel: +91 124 2881053/54
HEAD OF BUSINESS DEVELOPMENT, INDIA: Debashish Brahmachari **MARKETING:** Hargat Singh Gill

ANNUAL SUBSCRIPTIONS (UK/Europe, including post and packing)
FULL RATE: £1,400
PERSONAL RATES: UK £135; Europe €209; Rest of World £210
STUDENT RATES: UK £79; Europe €122; Rest of World £125
Individual rates apply to payments by personal cheque or credit card. Back issues: £20.00.

ANNUAL SUBSCRIPTIONS (USA, including post and packing)
INSTITUTIONAL/CORPORATE RATE: $2,730 ; **PERSONAL RATE:** $199; **STUDENT RATE:** $99;
POSTDOC RATE: $119
Printed in USA. Individual rates available only to subscribers paying by personal check or credit card. Orders for student/postdoc subscriptions must be accompanied by a copy of student ID. Rates apply to USA, Canada, Mexico/Central & South America. Add 7% GST tax in Canada (Canadian GST number 140911595). **BACK ISSUES:** US$20.00.

ANNUAL SUBSCRIPTIONS (Asia, including post and packing)
JAPAN: 年間購読料金： *Nature* のみ 437,800 円 +21,890 円 (消費税) =459,690 円 (合計)
Nature + *Nature Digest* 466,550 円 +23,328 円 (消費税) =489,878 (合計)
お問い合わせ 日本出版貿易株式会社 国内営業 1 部
〒101-0064 東京都千代田区猿楽町1-2-1 Tel: 03-3292-3767 Fax: 03-3292-8766
個人/学生購読について
NPG ネイチャー アジア・パシフィック フルフィルメント & カスタマーサービス
〒162-0843 東京都新宿区市谷田町2-37 千代田ビル Tel: 03-3267-8759 Fax: 03-3267-8752
CHINA: www.natureasia.com/cn/subscribe; **KOREA:** www.natureasia.com/korea/subscribe

NATURE ONLINE WWW.NATURE.COM/NATURE

CHIEF TECHNOLOGY OFFICER: Howard Ratner **ASSOCIATE DIRECTOR, NATURE.COM:** Daniel Pollock
PLATFORM DEVELOPMENT: Jeremy Macdonald **WEB PRODUCTION:** Alexander Thurrell, Deborah Anthony **WEB DESIGN:** Juan-Carlos Sobrino, Luke Stavenhagen **PLATFORM INTERFACES:** Amanda Ward

SITE LICENCES, FULFILMENT & CUSTOMER SERVICES

SITE LICENCES: npg.nature.com/libraries feedback@nature.com
CHIEF OPERATIONS OFFICER: John Carroll **ASSOCIATE DIRECTOR OF OPERATIONS:** Dominic Pettit
CUSTOMER SERVICE: Liz Davidson **ORDER PROCESSING OPERATIONS:** Steve Poulter

NATURE PUBLISHING GROUP OFFICES

LONDON: The Macmillan Building, 4 Crinan Street, London N1 9XW Tel: +44 (0)20 7833 4000 Fax: +44 (0)20 7843 4596/7

BASINGSTOKE: Nature Publishing Group, Subscriptions, Brunel Road, Basingstoke, Hants RG21 6XS, UK Tel: +44 (0)1256 329242

WASHINGTON DC: 968 National Press Building, 529 14th St NW, Washington DC 20045-1938 Tel: +1 202 737 2355

NEW YORK: 75 Varick St, 9th Floor, New York, NY 10013-1917 Tel: +1 212 726 9200

BOSTON: 25 First Street, Suite 104, Cambridge, MA 02141 Tel: +1 617 475 9275

SAN FRANCISCO: 225 Bush Street, Suite 1453, San Francisco, CA 94104 Tel: +1 415 403 9027

MUNICH: Nymphenburger Strasse 14, D-80335 München Tel: +49 89 549057-13

PARIS: Moulin de Malicorne, Sainte Maure de Touraine, Paris 37800 Tel: +33 2 47 35 72 15

TOKYO: Chiyoda Building, 2-37 Ichigayatamachi, Shinjuku-ku, Tokyo 162-0843 Tel: +81 3 3267 8751

INDIA: Nature Publishing Group, 3A, 4th Floor, DLF Corporate Park, Gurgaon 122002 Tel: +91 124 2881053/54

Nature® (ISSN 0028-0836) is published by Nature Publishing Group, a division of Macmillan Publishers Ltd (The Macmillan Building, 4 Crinan Street, London N1 9XW). Registered as a newspaper at the British Post Office. North and South American orders to subscriptions@natureny.com (Tel: +1 866 363 7860). Other orders to subscriptions@nature.com (Tel. +44 (0)1256 329242. Fax +44 (0)1256 812358). Authorization to photocopy material for internal or personal use, or internal or personal use of specific clients, is granted by *Nature* to libraries and others registered with the Copyright Clearance Center (CCC) Transactional Reporting Service, provided the relevant copyright fee is paid direct to CCC, 222 Rosewood Drive, Danvers MA 01923, USA. Identification code for *Nature*: 0028-0836/03. CPC PUB AGREEMENT #40032744. In the US, *Nature* (ISSN 0028-0836) is published weekly on Thursday, except the last week in December by Nature Publishing Group, 75 Varick St, 9th Fl, New York NY 10013-1917, USA. US Periodicals postage paid at New York NY, and additional mailing post offices. US POSTMASTER: send address changes to *Nature*, Subscription Dept, 75 Varick St, 9th Fl, New York NY 10013-1917, USA. Published in Japan by NPG Nature Asia-Pacific, Chiyoda Building, 2-37 Ichigayatamachi, Shinjuku-ku, Tokyo 162-0843, Japan. ® 2012 Macmillan Publishers Limited. All rights reserved.

THIS WEEK

EDITORIALS

PIGS Antibiotic use now less rotten in the state of Denmark **p.440**

WORLD VIEW Open data is the future for you and me **p.441**

RING CYCLE Mexican plants open second front on evolution **p.442**

Openness costs

Two reports highlight key aspects of the global trend towards open access to research results: who will pay, and how much, to supply what to whom?

Britain has become involved in something of a national debate recently over access to the research literature. And within the past week, two reports have appeared that will be relevant to researchers everywhere. The Royal Society published an analysis of openness in scientific data (see go.nature.com/of89t1 and page 441). And a committee set up by the UK government reported on how access could be enhanced, and how policy-makers could promote a gradual shift towards publishing research papers in journals that allow or require authors to pay article publishing charges (APCs) up front. The published paper would then be freely available to all from the moment of publication. That is a shift that *Nature* in principle supports (see *Nature* **481,** 409; 2012).

The UK government's report, widely referred to as the Finch report after Janet Finch, who chaired the committee that delivered it, examines in depth the issues facing the United Kingdom (see go.nature.com/solui2). The country's funding structure in principle enables it more readily than many to shift some of the funds currently spent on university library subscriptions to a stream for APCs partly funded by research funding councils.

The report is also timely in an international context, because funders elsewhere are thinking about this transition. All are aware of the complexities that Finch highlights, and in practice it may take several years for progress to be made towards mandated open access. But the mood to make the shift is strong.

A key issue is the cost of publishing, and here the parallels between the Finch report and the Royal Society report (whose authors include *Nature*'s editor-in-chief) are striking. Both make the point that scientific output, whether research papers or research data, needs to be rendered usable, and that the costs of curation, hosting, editing and enrichment with metadata, and the continual renewal of such activities, must all be met.

In its advocacy of open data, the Royal Society report does not estimate potential costs but provides examples of their likely scale. The preprint server arXiv, which does little more than host papers sent to it in raw form, requires six full-time staff. The Worldwide Protein Databank and the UK Data Archive each require a multi-million-dollar budget and around 65 full-time staff. (By acute contrast, a survey of UK universities revealed that they deploy on average 1.4 full-time staff to run their institutional repositories, and that only 40% of such repositories receive research data.)

The Finch report's attention to national financial models provides an important component for debate. The report models (albeit with highly uncertain assumptions) scenarios in a transition that includes both subscriptions and author-paid open access, also taking into account assumed international shifts in policy. UK researchers publish well over 100,000 articles a year. In one example, assuming that 50% of these are published fully open access at an average APC of £1,450 (US$2,260), the transition would be cost-neutral to the United Kingdom. Under more pessimistic assumptions about international uptake, and if the average APC were £2,200, the additional cost to the UK higher-education sector is estimated at £70 million, in a current annual expenditure on journals of £175 million in a research budget of more than £5 billion. (Papers published in highly selective journals such as *Nature*, whose costs would point towards much higher APCs, would represent a small proportion of the national output.)

Publishers in such an environment will need all the more to demonstrate that they add value to the research process. This sits alongside their need to deliver a reasonable profit — whether to fund learned-society activities or to reduce their publishing charges (the aim of the Public Library of Science) or, like many suppliers of services and equipment to researchers, to deliver a return to their investors. The perception of publishers as profiteers is strong, and understanding of the value they add is weak. Not noted for their transparency, publishers will have to work hard to develop trust amid a fundamental shift in their customer base.

"The mood to make the shift towards mandated open access is strong."

The transition poses a particular challenge to universities. The Finch report rightly concludes that universities will need to set up dedicated funds for APCs. Issues of principle and practice in the deployment of such funds will take time to become established, especially in highly decentralized universities. As the number of papers published by their researchers has increased over the past few years, so the proportion of university funds devoted to libraries has declined. And yet, as the Royal Society report clearly demonstrates, the information obligations of these institutions, both internal and external, can only grow. ■

A first step

Perhaps the Earth conference was not a wasted opportunity but the start of a new journey.

The agreement for modest commitments to sustainable development after 2015, reached at last week's Earth conference in Rio de Janeiro, has been roundly condemned as inadequate, or even an outright failure. The document is full of legalese and vague assertions, and it postpones the making of potentially significant decisions and assigning accountability to an uncertain future. When it comes to sustainable development, the agreement neither secures new resources nor defines the parameters for success. But did anybody, really, expect more?

Rio was never intended as a venue for the signing of major new environmental treaties, so it should come as no surprise that governments did not do so. But the actual purpose of the conference was never made

clear. In the run-up to the meeting, *Nature* said that the event presented an opportunity to take stock, acknowledge past failures and identify opportunities to break political deadlock. It may have succeeded with the first two, but has certainly fallen flat with the all-important third.

The world needs hope, a sustainable goal and a clear path to reach it. It needs a strong message to invigorate the global conversation and to motivate current and future generations of scientists, thinkers and leaders. Right now, politicians need to lay the groundwork and implement productive policies on the ground. They also need to find practical and politically viable ways to scale things up. With a clear aim in view and a workable means to achieve it, political leaders would find it much harder to turn their backs on the problems the world faces.

Perhaps Rio really was a failure, but not for the reasons levelled at the conference over the past week. Put simply, the agreement failed to capture the imagination. The wording does not lay out a clear and compelling vision — a brave new message that will spark debate among friends, family and colleagues. Sadly, it doesn't even capture the spirit and energy that enlivened the conference itself over the past two weeks.

For the more than 45,000 people who attended the conference, the picture was very different. Countless individuals, businesses and non-profit organizations unveiled their latest ideas to eager audiences. Governments announced initiatives to reduce emissions, protect forests, expand access to energy and generally make the world a cleaner and greener place for all. Visitors from around the world were introduced to global problems — and, in the case of Rio's favelas, smart solutions — clarifying the connection between poverty and the need for sustainable development. Millions of Brazilians, at least, were bombarded with news coverage detailing the full suite of issues under discussion. This is not enough, but it is not nothing either. By focusing too much on the final text and what it contains, critics are ignoring what was there.

Although the agreement that came out of Rio last week did not define sustainable-development goals, it did create a process to do so. These goals will need to be informed by science if they are to be meaningful. And policy-makers will need to find a way to assess whether they are making progress on the social, economic and environmental issues they face. Governments must cope with a dizzying array of interrelated challenges, from freshwater shortages and carbon emissions to issues of food, poverty, biodiversity and demographics. They have limited resources with which to tackle a bewildering portfolio of complex problems, and they need to understand where the environmental boundaries lie when they try to solve them.

> ***"The world needs hope, a sustainable goal, and a clear path to reach it."***

At its heart, this is a scientific challenge, and one that scientists and funding agencies have already set out to tackle through the Future Earth initiative, a framework of research into sustainable development paid for by the National Science Foundation. It represents an opportunity to analyse and assess competing uses for various resources across the global landscape. To help translate this useful work into relevant information, scientists must find a way to integrate their knowledge of natural systems with economics and other social sciences, to better assess the solutions that people will be willing to accept and to encourage new technologies and ideas to ripple through society. Speaking in Rio, Hans Joachim Schellnhuber, a physicist by training and director of the Potsdam Institute for Climate Impact Research in Germany, said that the next decade could be "the decade of the social sciences". He may well be right. Just as fear does not sell, it should also be clear by now that simply presenting the bare facts on their own, no matter how starkly, will not be enough. ■

Pig out

If farmers do not rein in the use of antibiotics for livestock, people will be severely affected.

The spread of dangerous bacteria that are resistant to antibiotics is fuelled by overuse of the drugs — and not just in people. Farmers around the world routinely feed antibiotics to their animals, not only to prevent and treat infections, but also to make their animals grow faster. This leads to drug-resistant bacteria in the animals, and this resistance can spread to the bacteria that infect us.

The overuse of antibiotics in farm animals is a global issue. Human propensity for trade and travel ensures that resistant bacteria spread easily around the world, so as long as any one country pumps its pigs and poultry full of the drugs, everyone is at risk.

In 1998, the Danish poultry industry took the unusual step of volunteering to stop using antibiotics for the promotion of animal growth. Two years later, the country's pork farmers did the same. Denmark might be a small country, but it is the world's largest exporter of pork. And it didn't stop there, writes Frank Aarestrup in a Comment piece on page 465. Denmark went on to reduce its overall use of antibiotics in livestock by 60%. It achieved this by creating a comprehensive surveillance system to monitor overuse, and limiting the amount of money that vets could make from selling the drugs to farmers.

Many feared that the changes would cripple Denmark's pork production. Instead, production rose by 50%. "Any country trying to limit the use of antibiotics in livestock can learn from what my colleagues and I did in Denmark, adjusting what worked to local needs," Aarestrup writes. These are encouraging words, but it is unlikely to be that simple.

The biggest obstacle is likely to be generating the political resolve and public support needed to crack down on the lucrative trade in antibiotics. This was possible in Denmark because there, perhaps uniquely, warnings from the medical community were picked up by the media, creating widespread public awareness of the problems caused by the overuse of antibiotics. People in other countries may not be so engaged, particularly when faced with the inevitable lobbying of the agricultural and veterinary sectors, which make big profits from selling antibiotics.

Also a problem is the fact that in many countries, farmers tend to work independently of each other. Almost all Danish farmers, by contrast, are members of the Danish Agriculture and Food Council, through which they frequently communicate and interact. This meant that they had a convenient forum in which to debate the issue and come to the decision to stop using antibiotics for growth. Denmark also has a detailed system in place to keep track of the effects of antibiotic use by farmers, which helps to enforce the regulations. In the United States, drug companies provide the Food and Drug Administration with data on the quantity of antibiotics sold to farmers, although they do not routinely say what types of animal the drugs are given to, or what the drugs are used for. The nation therefore has the necessary infrastructure and reporting system to monitor and regulate the use of antibiotics for animal growth, should it wish to do so, as do other countries. And the European Union has already banned such drug use.

The first step to building the case for tighter control is to obtain more specific data. Researchers should be able to survey ten farms in ten US states, for example, and extrapolate those data nationally to build up an accurate picture of antibiotic use. The drugs are almost certainly overused, and are almost certainly having a damaging impact on public health, so publishing the results would help in raising awareness of the problem and generating the necessary support. The people of Denmark deserve praise for their efforts, and other countries, and their people, should look more carefully at what their animals are being fed. ■

NATURE.COM
To comment online, click on Editorials at:
go.nature.com/xhunqv

MERCK MILLIPORE

Break free from routine sample prep. Go from boring to bold.

The Samplicity™ Filtration System takes sample prep in a flexible, new direction. This vacuum-powered system filters one sample or eight, of virtually any viscosity or composition, into HPLC vials in seconds—with minimal manual effort.

With the Samplicity filtration system and Millex Samplicity™ filters, Merck Millipore has transformed multi-sample filtration forever.

Samplicity makes it simple.

Discover how at www.millipore.com/GoBold

Merck Millipore is a division of MERCK

Merck Millipore, the M mark, Samplicity and Millex Samplicity are trademarks of Merck KGaA, Darmstadt, Germany.
© 2012 EMD Millipore Corporation, Billerica MA USA. All rights reserved.

King Abdullah International Medical Research Center

Got Ethics?

We do. Ethics is doing the right thing, even if nobody is watching.

KAIMRC aims to disseminate biomedical ethic concepts into the health care system and community through education and public awareness. In an Islamic matrix of ethics and morality, we strive to set our own trends to formulate policies and guidelines, carry out and coordinate teaching and research, stimulate informed public debate, and provide a resource service for health professionals in our community and beyond. Ethical work behavior is a crucial part of success; all our employees possess a high degree of integrity and an outstanding level of professionalism.

At KAIMRC, a segment in the enormous healthcare system of King Abdulaziz Medical City, we felt the overwhelming sense of obligation towards both the healthcare profession and our institution to launch a Masters Degree program in Biomedical Ethics with the incorporation of Islamic Law. Healthcare professionals who show genuine interest in applying their knowledge and expertise to the ethical aspects of healthcare would be considered for program.

KAIMRC takes pride in its Bioethics Section, as it is home for the UNESCO chair of Saudi Arabia, held by its head Dr. Amin Kashmeery.

"*Whoever works righteousness, man or woman, and has faith, verily, to them will We give a new Life, a life that is good and pure, and We will bestow on such their reward according to the best of their actions.*" - Holy Qur'an, Chapter 16, Verse 97

"*It is better for a leader to make a mistake in forgiving than to make a mistake in punishing.*"- Prophet Mohammed (PBUH)

"*In law a man is guilty when he violates the rights of others. In ethics he is guilty if he only thinks of doing so.*" – Immanuel Kant

"*Ethics is knowing the difference between what you have a right to do and what is right to do.*" – Potter Stewart

cientists Vacancies at King Abdullah ternational Medical Research Center

Today's Question, Tomorrow's Answer

AIMRC provides an opportunity to serve in a dynamic, ulticultural environment with state-of-the-art facilities for mpetent and motivated persons who are willing to dedicate emselves and make a difference in the world of scientific medical search. If you are interested in being involved in demanding and novative projects within one of the leading medical research centers orldwide, then search KAIMRC on Naturejobs.com to find our latest cancies or apply with us by sending your resume to recruitment@kaimrc.ed.sa. Please identify the position that you are applying to in the subject ading of your e mail.

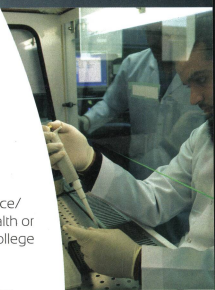

AIMRC Is Looking To Hire The Following:

1. Senior Research Scientist:

Education & Qualifications:

Doctorate Degree (PhD) in Health Science or in a related discipline from an accredited university(Essential).

Experience:

Minimum of twelve (12) years of experience in a well recognized research institution, coupled with two (2) years supervisory experience in a senior management position(Essential).

2. Research Scientist:

Education & Qualifications:

- PhD IN Science/Pathology or in a related discipline from an accredited University (Essential).

Preferably post-doctoral research experience

Experience:

- Eight (8) years working experience in clinical /research institution or Five (5) years experience with one or more publication as Principal Investigator in journal with 12 or more impact factor(Essential).

3. Associate research scientist:

Education & Qualifications:

- Doctorate Degree (PhD) in Health Science or equivalent from an accredited university (Essential).

Experience:

- Completion of Post Doctoral Fellowship (Essential).
- Minimum of three (3) years of experience in a clinical/research institution(Essential).

4. Research Assistant:

Education & Qualifications:

- Master's Degree in Health Science/ Health Management/Public Health or equivalent from an accredited college or university(Essential).

Experience:

- Minimum of four (4) years working experience in clinical research or scientific field(Essential).

5. Research Associate:

Education & Qualifications:

- Master's Degree in Health Science/ Health Management/Public Health or equivalent from an accredited college or university (Essential).

Experience:

- Minimum of seven (7) years of experience in a clinical/research institution(Essential).

For further information
Please visit our website: www.kaimrc.med.sa
To know more about our activities, the available positions or our collaboration policies,
Email: researchl@ngha.med.sa

CPT: Pharmacometrics & Systems Pharmacology

An Official Journal of ASCPT and ASoP

Summer 2012

A new online open access journal in quantitative methods from *Clinical Pharmacology & Therapeutics*

CPT: PSP is a cross-disciplinary journal that provides a unique international forum for scientists in the pharmacometrics and systems pharmacology space.

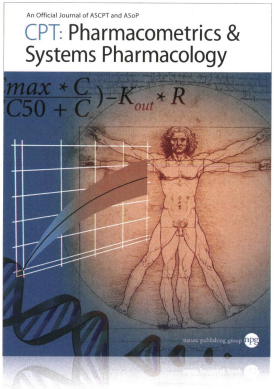

Editor-in-Chief:
Piet van der Graaf, PharmD, PhD

Publishing original research in:

- Modeling and simulation as applied to the design and evaluation of clinical trials
- Quantitative methods that improve our understanding of pharmacology and therapeutics in humans

Accepting submissions May 2012

www.nature.com/psp

nature publishing group npg

© JOAN R. BOZ, EDINBURGH

Open your minds and share your results

An open approach is the best way to maximize the benefits of research for both scientists and the public, says **Geoffrey Boulton**.

There is a compelling case for having open access to scientific papers, to enhance the efficacy and reach of scientific communication. But important though this is, the open-access debate has drawn attention away from a deeper issue that is at the heart of the scientific process: that of 'open data'. In an attempt to focus much-needed attention on this subject, I chaired a group that produced *Science as an Open Enterprise*, a policy report from the Royal Society in London, published last week.

Open enquiry has been at the heart of science since the first scientific journals were printed in the seventeenth century. Publication of scientific theories — and the supporting experimental and observational data — permits others to identify errors, to reject or refine theories and to reuse data. Science's capacity for self-correction comes from this openness to scrutiny and challenge.

Modern techniques to gather, store and manipulate data make this more difficult. In the 1980s, I published a paper that presented seven hard-won data points showing the relationship between stress and velocity beneath a glacier. Two years ago, I was involved in an analogous experiment on the Antarctic ice sheet that created more than a billion times more data points. No journal could publish these data, so for them to be accessible, the only option was to deposit the information in a recognized repository, complete with metadata (data about data), and to signpost it in published papers, preferably through live links in the papers' electronic versions.

In the Royal Society report, we argue that this procedure must become the norm, required by journals and accepted by the scientific community as mandatory. As scientists, we have some way to go to achieve this. A recent study of the 50 highest-impact journals in biomedicine showed that only 22 required specific raw data to be made available as a condition of publication. Only 40% of papers fully adhered to the policy and only 9% had deposited the full raw data online (A. A. Alsheikh-Ali *et al. PLoS ONE* **6**, e24357; 2011).

We also need to be open towards fellow citizens. The massive impact of science on our collective and individual lives has decreased the willingness of many to accept the pronouncements of scientists unless they can verify the strength of the underlying evidence for themselves. The furore surrounding 'Climategate' — rooted in the resistance of climate scientists to accede to requests from members of the public for data underlying some of the claims of climate science — was in part a motivation for the Royal Society's current report. It is vital that science is not seen to hide behind closed laboratory doors, but engages seriously with the public.

There is, of course, a problem in making data sets open to non-specialists. They are rarely in the form of an Excel spreadsheet, an illusion under which many politicians labour in their laudable but problematic calls for open data. True openness requires data to be not only accessible, but also intelligible, assessable (who produced the data, what are their qualifications, do they have conflicts of interest?) and reusable.

Everyone will benefit from a more open approach. The digital and communications revolutions bring opportunities for research that demand openness and a willingness to share data. These include the assembly of massive data sets from diverse sources, and linking them to allow data integration, dynamic updating and the manipulation of data within electronic publications. Such data-led science offers ways to explore massive data sets for patterns and relationships.

Yet this, too, presents a problem. Too often, we scientists seek patterns in data that reflect our preconceived ideas. And when we do publish the data, we too frequently publish only those that support these ideas. This cherry-picking is bad practice and should stop.

For example, there is strong evidence that the partial reporting of the results of clinical trials, skewed towards those with positive outcomes, obscures relationships between cause and effect. We should publish all the data, and we should explore them not just for preconceived relationships, but also for unexpected ones. Without rigorous use and manipulation of data, science merely creates myths. At the same time, communications technologies are displacing the printed page from its dominant role as the medium of scientific communication. This is already exploiting the collective intelligence of the scientific community and shifting the social dynamic of research towards collaboration.

SCIENCE'S CAPACITY FOR SELF-CORRECTION COMES FROM ITS OPENNESS TO SCRUTINY AND CHALLENGE.

This shift has not been mandated by research councils, governments or national academies, but is the consequence of scientists finding more productive and creative ways to do science. Pathfinder disciplines include bioinformatics, astronomy, mathematics, nanotechnology and social and health statistics. Likewise, to extend the reach and depth of these approaches does not need top-down orchestration. It merely requires some constraints to be removed and some enabling changes to be made.

What about costs? Data curation should be viewed as a necessary cost of research. Creative data generation should be a source of scholarly esteem and a criterion for promotion. We need a revolution in the role of the science library, with data scientists supporting the management of data strategies for both institutions and researchers. We need strategic funding to develop software tools to automate and simplify the creation and exploitation of data sets. And above all, we need scientists to accept that publicly funded research is a public resource. ■

➲ **NATURE.COM**
Discuss this article online at:
go.nature.com/u5lazh

Geoffrey Boulton *is regius professor of geology emeritus at the University of Edinburgh, UK.*
e-mail: g.boulton@ed.ac.uk

RESEARCH HIGHLIGHTS

Selections from the scientific literature

DEVELOPMENTAL BIOLOGY

Blood vessel directs cells

The first blood vessel formed in the embryo — the dorsal aorta — coordinates the formation of the sympathetic nervous system and the medulla of the adrenal gland, both of which marshal the body's fight-or-flight response.

The nervous system and the adrenal medulla are derived from progenitor neural-crest cells — some of which migrate towards the dorsal aorta during early development. Yoshiko Takahashi of Kyoto University in Japan and her colleagues studied developing chick and mouse embryos and found that the dorsal aorta secretes bone morphogenetic proteins. These stimulate the production of signalling molecules that, in turn, attract some of the neural-crest cells. Bone morphogenetic proteins are then involved in the formation of the separate lineages that give rise to the adrenal gland and the sympathetic nervous system.

Science 336, **1578–1581 (2012)**

SENCKENBERG NATURALMUSEUM FRANKFURT

PALAEONTOLOGY

Turtle sex recorded in rock

A pit in Germany has yielded the first fossilized evidence of mating behaviour: copulating turtles preserved about 47 million years ago.

Walter Joyce of the University of Tübingen in Germany and his colleagues analysed the remains of nine pairs of *Allaeochelys crassesculpta* turtles (pictured). On the basis of anatomical differences, the researchers discerned that each pair comprised one male and one female. In two of the pairs, the partners' tails were aligned, consistent with turtle mating positions.

The researchers propose that the couples began mating in the habitable surface waters of a volcanic lake and met their untimely end as they sank into deeper, toxic waters.

Biol. Lett. **http://dx.doi.org/10.1098/rsbl.2012.0361 (2012)**

For a longer story on this research, see go.nature.com/ld1rbi

ECOLOGY

One ring species to rule them all

Researchers have found the first evidence in plants of a 'ring' species — one that arises when a population expands its range along two fronts in a ring around unsuitable habitat. When organisms from the two groups meet, they behave as separate species.

Ivalú Cacho and David Baum at the University of Wisconsin-Madison sequenced two genes from 40 populations of Caribbean slipper spurge (*Euphorbia tithymaloides*). The sequences revealed that the plant spread from Mexico along two trajectories: one population (**pictured right**) headed through South America and then north to the Lesser Antilles, and the other (**left**) spread by hopping east across islands such as Jamaica and Puerto Rico.

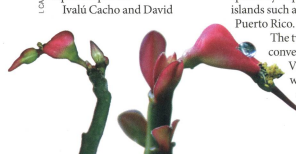

I. CACHO

The two populations converged on the Virgin Islands, where they coexist as distinct subspecies on the island of St Croix. Despite being in close proximity to one another, there has not been significant gene flow between the subspecies.

Proc. R. Soc. B **http://dx.doi.org/10.1098/rspb.2012.0498 (2012)**

CELL BIOLOGY

p53 triggers cell death in stroke

The protein p53 is known to suppress tumour growth, which it does in part by initiating apoptosis, or programmed cell death. However, p53 also triggers another form of cell death — necrosis — that occurs in conditions such as stroke.

Ute Moll at Stony Brook University in New York and her team studied the effects of adding purified p53 to mitochondria — the cell's power-generating organelles — isolated from mouse cells. The authors found that p53 causes certain pores in the mitochondrial membrane to open up by interacting with a protein, cyclophilin D, that regulates the pore. Treating cells with an oxidizing chemical kicks off this process, which ultimately leads to necrosis.

The researchers detected the two-protein complex in injured brain tissue from mice in which a cerebral artery had been temporarily blocked as

a model of stroke. Preventing complex formation protected against stroke-induced injury. ***Cell*** 149, **1536–1548 (2012)**

ASTRONOMY

Similar orbits but not densities

Data from NASA's Kepler spacecraft have revealed two extrasolar planets with similar orbits around the same star but radically different densities — challenging planetary formation theories.

Joshua Carter at the Harvard-Smithsonian Center for Astrophysics in Cambridge, Massachusetts, Eric Agol at the University of Washington in Seattle and their team found the two planets, which have orbital periods of 14 and 16 days. The inner planet has a density consistent with a rocky planet like Earth, whereas the outer one has the density of a gaseous planet, such as Neptune. This is puzzling to theorists who had expected gaseous planets to form much further out, as in the Solar System. When viewed from the Earth-like planet, the Neptune-like planet would be 2.5 times the size of the Moon. ***Science*** **http://dx.doi.org/10.1126/science.1223269 (2012)**

PHOTONICS

Data travel on spiralled light

The amount of information that can be crammed into a beam of light can be increased by splitting the photon stream into different shaped spirals that act as independent channels.

Jian Wang at the Wuhan National Laboratory for Optoelectronics in China, Alan Willner at the University of Southern California, Los Angeles, and their team used the technique to send terabits of information per second through free space. The technique could be combined with more conventional methods of high-density data transfer — such as splitting a beam into two different polarizations or multiple wavelengths — to achieve massive data-flow.

The method could prove particularly well-suited to cable-free information transfer over short distances, or to communication in space. ***Nature Photon.*** **http://dx.doi.org/10.1038/nphoton.2012.138 (2012)**

MOLECULAR BIOLOGY

Protein crawls on chromosome

Proteins that control gene expression by attaching to specific DNA sequences amble along chromosomes until they hit their targets, according to a single-molecule imaging study.

In the 1970s, researchers theorized that one such protein, or transcription factor, called the *lac* repressor (LacI) would act in this way. Johan Elf and his team at Uppsala University in Sweden provide the first evidence of this behaviour *in vivo*. In *Escherichia coli* cells, the team found that LacI took 3–5 minutes to bind to the correct DNA site — the speed predicted by theoretical models of 'chromosome crawling'. When other proteins are bound to the chromosome, they act like roadblocks and slow the search. Moreover, the transcription factor typically slides over its target several times before binding to it. ***Science*** 336, **1595–1598 (2012)**

PLANETARY SCIENCE

Carbon dioxide snow on Mars

Clouds of snow — frozen carbon dioxide crystals — at the Martian poles are made up of particles just 8–44 micrometres in diameter.

The Martian atmosphere consists mainly of carbon dioxide, which condenses at the poles during the winter. Renyu Hu and his colleagues at the Massachusetts Institute of Technology in Cambridge analysed temperature, pressure and topography data gathered over more than 9 years by the Mars Global Surveyor and Mars Reconnaissance Orbiter. The researchers found that snow accumulation is greater at the south pole than at the north and that the clouds spread halfway towards the equator before retreating in the spring. ***J. Geophys. Res.*** **http://dx.doi.org/10.1029/2012JE004087 (2012)**

COMMUNITY CHOICE

The most viewed papers in science

ENVIRONMENTAL SCIENCE

Biodiverse and language-diverse

HIGHLY READ on www.pnas.org in May

An analysis of a global data set tracking the geographical extent of some 6,900 languages has revealed that highly biodiverse areas accounting for 24% of Earth's land surface contain about 70% of the world's languages.

Biologists and linguists have previously noted that areas with high species diversity also tend to show high language diversity. The data set, published in 2010, has enabled Larry Gorenflo at Pennsylvania State University in University Park and his colleagues to perform a more detailed analysis. Regions that are particularly rich linguistically include parts of west Africa and southeast Asia and some of the Indonesian islands, which have more than 250 native languages each. These languages are often unique to their regions and many are at risk of extinction.

The authors suggest a range of possible reasons for this link. For one, the spread of a few dominant European languages tended to occur in more temperate areas, and not in the biodiverse tropics. ***Proc. Natl Acad. Sci. USA*** 109, **8032–8037 (2012)**

STROBEL/AFP/GETTY

CLIMATE CHANGE

Cyclones on the move

Tropical cyclones in the North Indian Ocean will tend to occur later in the year, during the peak monsoon season, as the climate warms.

Hiroyuki Murakami, now at the University of Hawaii at Manoa in Honolulu, and his colleagues used several versions of an atmospheric circulation model to project changes in cyclone activity in the North Indian Ocean in 2075–99 relative to 1979–2003. The researchers found that, in a simulated warmer future, fewer cyclones formed in the pre-monsoon season in spring, whereas a greater number of storms occurred in the peak-monsoon season in summer. Overall cyclone frequency in the region did not change significantly, however.

Increased sea surface temperature and a reduction in vertical wind shear — which pulls cyclones apart — could explain the projected increase in storm frequency during the summer monsoon season. ***Clim. Dyn.*** **http://dx.doi.org/10.1007/s00382-012-1407-z (2012)**

NATURE.COM

For the latest research published by *Nature* visit:
www.nature.com/latestresearch

SEVEN DAYS *The news in brief*

POLICY

UN science advice

The United Nations is to set up an international board of science advisers, to be selected by its Environmental, Scientific and Cultural Organization (UNESCO). The board's remit is to promote cooperation on science-related issues between UN agencies, and with the international scientific community. UNESCO's director-general, Irina Bokova, announced the decision on 22 June at the Rio+20 conference on sustainable development. See go.nature.com/2zxlep for more. The conference itself concluded with modest and mostly voluntary commitments to sustainable-development goals after 2015. See page 447 for more.

Romania plagiarism

More than 6,000 scientists and academics have signed an online petition calling on Romanian Prime Minister Victor Ponta to resign, after *Nature* revealed allegations of extensive plagiarism in Ponta's doctoral thesis (see *Nature* **486**, 305; 2012).

Primate transport

Israeli airline El Al has added itself to the list of air carriers refusing to transport monkeys for medical research. Its decision follows an Israeli supreme-court ruling this month that banned a breeding facility near Tel Aviv from exporting wild-caught monkeys to the United States. Activists worldwide mounted a campaign to pressure El Al not to fly even captive-born monkeys (which the court ruling had permitted). The airline's decision was announced on 18 June in a terse letter to the Israeli animal-advocacy group Let the Animals Live. See go.nature.com/3sqalw for more.

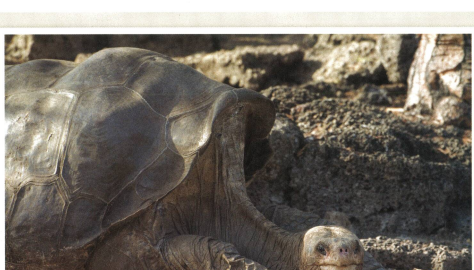

K. SZULDKAR/PA

Farewell, Lonesome George

Lonesome George, the Galapagos giant tortoise widely known as the rarest in the world, died unexpectedly on 24 June, at the age of around 100. George was discovered in 1971, and conservationists had hoped to coax his subspecies (*Chelonoidis nigra abingdoni*) back from the brink of extinction. But no others of his kind were ever found, and George stayed mainly indifferent to female tortoises of different subspecies that were introduced to him. He became a conservation icon: a quiet but powerful ambassador for the Galapagos Islands and for endangered species everywhere. See go.nature.com/hamvew for more.

Korean creationism

In response to a public outcry over the removal of examples of evolution from school biology textbooks (see *Nature* **486**, 14; 2012), South Korea's Ministry of Education, Science and Technology is to set up a panel to oversee future revisions of science textbooks. See go.nature.com/fcivld for more.

Drug approvals

US legislation that allows drug-makers to pay a fee in return for a speedier approval process looks likely to be renewed for the next five years. The bill, called the Prescription Drug User Fee Act (PDUFA), was first enacted in 1992; its fifth version reached a near-final step on 20 June, when the House of Representatives voted to re-authorize it. Up to 2017, PDUFA V is expected to generate billions of dollars for the US Food and Drug Administration in new fees from generic and biosimilar drug-makers. See go.nature.com/kp5ixp for more.

RESEARCH

Open data

Hoarding research data is a "serious impediment" to the scientific process, the UK Royal Society notes in a 21 June report, *Science as an Open Enterprise*. It urges funders, institutions and scientists to "shift away from a research culture where data is viewed as a private preserve" and to give greater recognition to the importance of generating and curating data. See page 441 and go.nature.com/nkt9ls for more.

Agriculture reform

A major global agricultural network — the CGIAR Consortium — launched its reshaped science programme at the Rio+20 conference in Brazil last week. The consortium, which supports some 8,000 scientists and staff in 15 centres around the world, has restructured its work into 15 research programmes, ranging from improving the yields of crops to studies on agricultural

policies and markets. Its budget will be around US$1 billion a year from 2013. See go.nature.com/bogcnz for more.

EVENTS

China dock and dive

China is celebrating feats of technological prowess in space and under the sea. On 24 June, three astronauts on the country's *Shenzhou 9* spacecraft achieved a first-ever manual docking with its orbiting space module, Tiangong 1. On the same day, the country's manned research submersible *Jiaolong* successfully completed its deepest test dive, to 7,020 metres in the Mariana Trench in the western Pacific Ocean. See go.nature.com/bocfdj for more.

Nuclear protests

In the largest of many demonstrations against the imminent restart of nuclear reactors in Japan (**pictured**), around 40,000 protesters rallied in front of the prime minister's residence in Tokyo on 22 June. The protests, unusual in a country not known for political activism, followed approvals earlier this month by local and central government to restart two reactors at the Ohi power station in Fukui prefecture. They would be the first shuttered plants to reopen since the Fukushima nuclear disaster

R. REYES MARIN/AFLO/NIPPON NEWS/CORBIS

in March 2011, and would start generating power in July.

PEOPLE

Psychology fraud

Erasmus University Rotterdam in the Netherlands announced on 25 June that after an internal investigation it would retract two papers from social psychologist Dirk Smeesters, and had accepted his resignation. Smeesters is a professor specializing in consumer behaviour at the university's Rotterdam School of Management. His misconduct comes in the wake of findings of fraud by another social psychologist, Diederik Stapel, at Tilburg University in the Netherlands (see *Nature*, **479**, 15; 2011).

Turkish arrest

Kemal Gürüz, a prominent academic reformer in Turkey, was arrested and jailed in Ankara on 25 June. Charges have not yet been formally published, but reportedly concern the allegation that Gürüz informed the military about the political orientation of Turkish university rectors when he was president of the Turkish Council of Higher Education between 1995 and 2003. Many academics and human-rights workers say the charges are trumped up. Gürüz, a defender of secularism in universities, was also arrested in 2009 with other academics and charged with membership of an antigovernment organization (see *Nature* **470**, 436; 2011); that case is ongoing. See go.nature.com/14nawu for more.

Kyoto prizewinners

This year's ¥50-million (US$626,000) Kyoto prizes in science have been won by Yoshinori Ohsumi and Ivan Sutherland. Ohsumi, a molecular biologist at the Tokyo Institute of Technology, won the basic-sciences prize for his work in the field of autophagy. Computer scientist Sutherland at Portland State University in Oregon was awarded the advanced-technology prize for his work on graphics and user interfaces.

Egypt's elections

Scientists in Egypt are hoping for a renaissance after a politician with a background in materials science and engineering won the country's presidential elections. Mohammed Morsi, the candidate for the Muslim Brotherhood, gained a PhD at the University of Southern California in Los Angeles, and from 1985 to 2010 headed the materials-science department at Zagazig University in Egypt. He has promised to increase research spending. See go.nature.com/dxnur4 for more.

COMING UP

1–6 JULY
More than 25 Nobel prizewinners meet with hundreds of young researchers at the Lindau Nobel Laureate Meeting in Germany, which this year is dedicated to physics.
www.lindau-nobel.org

4–11 JULY
Expect more results in the hunt for the Higgs boson, as the latest data from CERN, Europe's particle-physics laboratory, are discussed at a conference on high-energy physics in Melbourne, Australia.
ichep2012.com.au

STANDING UP FOR SCIENCE
Nominations are invited for the John Maddox Prize, which will reward an individual in any country who has promoted sound science and evidence on a matter of public interest. The £2,000 (US$3,000) prize puts emphasis on those who have faced difficulty or hostility for their efforts. The prize is awarded by *Nature* and Sense About Science, and is supported by the Kohn Foundation. The deadline for nominations is 20 August 2012. See go.nature.com/9rvd1t.

TREND WATCH

The fishing power of fleets in the world's oceans (measured by factors including ship engine power and vessel size) has increased 10-fold since the 1950s — and 25-fold in Asia. Yet the amount of fish caught for each standardized unit of fishing effort has halved (see chart), illustrating the decline in fish resources, according to an analysis led by an international team of fisheries scientists, published on 19 June (R. A. Watson *et al. Fish Fish.* http://doi.org/hz2; 2012).

DIMINISHING RETURNS ON FISHING
For each unit of fishing power expended by fleets, fish catches are now half what they were in 1950.

SOURCE: R. A. WATSON *ET AL. FISH FISH.* HTTP://DOI.ORG/HZ2 (2012)

NATURE.COM
For daily news updates see:
www.nature.com/news

nature MIDDLE EAST

Emerging science in the Arab world

twitter facebook google+

The Arab world has a rich history of scientific breakthroughs. Ensure you're part of the scientific and medical community gaining access to **breaking news in the region**.

From the latest news, in-depth features, expert commentaries and research highlights to regional jobs, event listings and alerts direct to your inbox – ***Nature Middle East*** is your free comprehensive portal keeping you at the centre of science in the Arabic speaking Middle East.

nature.com/nmiddleeast

Download the free app for your phone at **http://gettag.mobi**

Sponsored by

nature publishing group npg

NEWS IN FOCUS

MEXICO Presidential candidates promise a boost for science **p.452**

BIOMEDICINE Little GM piggies stay at home, waiting for approval **p.453**

GENOMICS Patent tussle mars debut of fetal DNA tests **p.454**

BIRD FLU What we still need to know about H5N1 **p.456**

F. DANA/AFP/GETTY

Environmental activists push an inflatable globe through the streets of Rio de Janeiro, Brazil, during multilateral talks on sustainable development.

ENVIRONMENT

Wealth gap curbs Rio goals

Outcome of last week's Earth Summit reflects the divided priorities of rich and poor nations.

BY JEFF TOLLEFSON IN RIO DE JANEIRO

Brazil's celebrated coastal metropolis is defined by stark contrasts, both geographic and economic. Extravagant wealth rings the city's luxurious beaches, while poverty looks on from the haphazard developments called favelas that sprawl across the surrounding hills. Such conspicuous inequality is symbolic of the challenge humanity faces on a global scale — a problem that restricted progress at the Rio+20 meeting last week to a modest and mostly voluntary set of commitments.

"What has been agreed to is entirely insufficient to tackle the problems that are before us on environment and development," says Manish Bapna, acting president of the World Resources Institute, a global environment think tank in Washington DC.

The 49-page document adopted on 22 June at the close of Rio+20 — the United Nations Conference on Sustainable Development — does many small things. Called *The Future We Want*, it establishes a process for crafting a set of sustainable-development goals that would come into effect just as the UN Millennium Development Goals expire in 2015. It endorses efforts to reduce consumption, improve energy systems and encourage a greener world economy, and calls for an international governance system for conserving biodiversity in the high seas.

But the agreement offers little in the way of relief for an increasingly pressured biosphere. Whereas the first Earth Summit in Rio de Janeiro in 1992 served as a launch pad for landmark agreements such as the Convention on Biological Diversity and the UN Framework Convention on Climate Change, the 2012 ▶

➲ NATURE.COM
For *Nature*'s special on the Rio meeting, see:
go.nature.com/d69weu

meeting instead revolved around the thorny question of global inequality.

Poverty, not global warming or the environment, is "the greatest challenge that we face in the world today", said Luiz Alberto Figueiredo Machado, Brazil's chief negotiator, when a draft that ultimately became the final agreement was announced on 19 June. One of Brazil's slogans for the conference was "To grow, to include, to protect", and as talks commenced, developing countries aligned their priorities in that order.

Throughout the meeting, the developing countries that make up the Group of 77 negotiating bloc (G77) objected to language that they felt might constrain their ability to grow and lift citizens out of poverty. In one case, the G77, along with the United States, blocked a European proposal to acknowledge the existence of global environmental thresholds that should not be surpassed. Such 'planetary boundaries' could include levels of carbon dioxide in the atmosphere and acidification of the oceans. Developing countries also fought against commitments to pursue a green economy unless they were phrased in the context of economic and social development. For such nations, "inclusive growth and a rapid increase in per capita income levels are development imperatives", declared Indian Prime Minister Manmohan Singh in his conference address.

Yet industrialized countries, including the United States and those in the European Union, seemed to be too preoccupied with their own economic woes to step forward with major new financial commitments for poor countries. The final text of the agreement provided no concrete answers to long-standing questions about development aid.

Although talks among high-level officials made little headway, there was a flurry of activity at hundreds of side meetings. The UN counted more than 100 individual initiatives on renewable energy by governments, businesses and multilateral financial institutions such as the World Bank, and monetary commitments of more than US$513 billion for a range of public and private initiatives on sustainable development. Many observers took such announcements as a sign that action is happening from the bottom up, even as international negotiations stall at the top. But others regarded the initiatives as too little, too late.

"There is compelling scientific evidence that we will lose invaluable species, ecosystems and their services under global warming as generated by business as usual with a few green speckles," says Hans Joachim Schellnhuber, director of the Potsdam Institute for Climate Impact Research in Germany. Schellnhuber says that governments are ignoring planetary boundaries at their own peril. "In this respect, the second Rio summit has utterly failed."

HUMAN INVESTMENT

Brazil as a country is emblematic of the economic imbalance that hung over the meeting and that threatens to hamper progress at future global environment talks. With the sixth largest economy in the world, Brazil is regarded abroad as an emerging power, but the country sinks to 101st in a ranking of gross domestic product per capita.

Rio de Janeiro's poorest districts, such as Cachoeirinha in the west, also offer a glimpse of the future for much of the planet. UN projections suggest that by 2025, the world's cities could contain one billion new residents, most of whom will begin their lives in slums and poor communities throughout the developing world.

Jilson Roberto is head of the Cachoeirinha community association, and attended the 1992 Earth Summit to advocate for a green-development plan on behalf of favelas. Roberto says that his community has little to show for the effort 20 years later. Cachoeirinha still lacks basic rubbish collection and floods regularly when it rains. The area also remains in the hands of drug traffickers, their territory marked by a pair of sofas blocking the road outside the community centre. Governments shouldn't forget about the current generation as they plan for the future, Roberto says. "We need to invest in human beings today."

To that end, the summit agreement calls for a high-level political forum to promote work on sustainable development. Its role and function remain to be worked out, but the Rio agreement suggests that the forum would conduct a regular scientific assessment of progress towards sustainable-development initiatives, says Gisbert Glaser, senior adviser at the International Council for Science in Paris, which represented scientists' interests in the Rio+20 negotiations.

More than ever, Glaser says, scientists need to work across disciplines to advise policymakers on a host of interrelated issues, from climate, energy and water to food, poverty and development. He adds that researchers need to develop metrics to help define sustainable development, similar to the carbon dioxide levels and temperature thresholds used to assess global warming, and then work with social scientists and economists to look for politically viable solutions. "This is a difficult thing to do," he says, "but we have to do it."

Examples of such complexity abound. When it comes to biofuels, for instance, governments must learn how to account for water use and international trade to understand the broader impacts of biofuel production on land use, biodiversity and food prices.

Biologist John Sulston of the University of Manchester, UK, who chaired a UK Royal Society working group that investigated links between global population and consumption, laments that the final agreement fails to link population to sustainable development. To Sulston, this is like planning a party without a guest list, "but on a unimaginably vast scale". In another example of the competing agendas at work behind such issues, the Vatican led a small group of countries in removing the term 'reproductive rights' from the text, despite pressure from family-planning groups.

Rather than complaining that global leaders have failed in the negotiations, Sulston says, scientists can and should work to help countries to develop new sustainable-development goals in the coming years. "Delving into the [agreement] text, we can see the skeleton of what we need to ensure our planet's future," he says. "From these bare bones we can raise an army." ■

V. R. CAVANO/AP/PA

In the Manguinhos neighbourhood of Rio de Janeiro, talk of reducing consumption seems a world away.

BIOSAFETY

Freeze on mutant-flu research set to thaw

But some fear that if more labs work on the viruses, the risk of accidental release will multiply.

BY DECLAN BUTLER

If you thought that the controversy was over, think again. Last week's publication of the second of two papers describing how to make mammalian-transmissible forms of the H5N1 avian influenza virus merely closes one chapter of a smouldering debate about the risks of the research. That debate seems certain to reignite in the coming months once researchers lift a voluntary moratorium on the work.

The research published last week, led by Ron Fouchier at the Erasmus Medical Centre in Rotterdam, the Netherlands, showed that introducing as few as five genetic mutations made the H5N1 virus capable of airborne spread between ferrets[1,2]. It followed similar work published in May[3] by Yoshihiro Kawaoka's groups at the University of Wisconsin–Madison and the University of Tokyo.

In December 2011, the US National Science Advisory Board for Biosecurity (NSABB) had recommended that only redacted portions of the papers should be published, mainly on the grounds that divulging the detailed methods could increase the risk of bioterrorism. But, after much wrangling, the NSABB in March finally agreed to the publication of updated versions of the full papers[4].

Supporters of the research say that it could help public-health experts to detect ominous genetic changes in nature, providing an early warning of an emerging flu pandemic. Others are sceptical, and point out that an expansion of research to pursue this goal would probably see similar mutant viruses being created in dozens more labs worldwide — some of which may lack adequate biosafety standards. That would multiply the risk of an accidental release of a pathogen capable of sparking a pandemic.

For now, the research moratorium agreed by 39 leading flu scientists in January and extended at a meeting convened by the World Health Organization (WHO) in Geneva in February[5] is allowing the field to discuss how to proceed safely. The moratorium would only be lifted, experts at the meeting agreed, once funders and regulators had worked out the biosafety and biosecurity conditions that would allow such research to be conducted with reasonable guarantees of safety. The meeting also resulted in a public-relations campaign to influence public opinion about the research and its potential benefits.

Flu researchers will soon be able to argue that those conditions have been met. "We have heard from several researchers that they would like to lift the moratorium sooner rather than later," says Fouchier, one of its signatories.

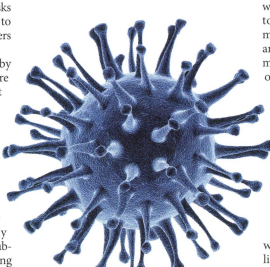

Just a few genetic tweaks can enable the H5N1 avian flu virus to transmit between mammals.

In a few weeks, the WHO will unveil non-binding biosafety and biosecurity guidelines for mutant-flu research. Over the following months, national regulatory authorities are expected to produce their own biosafety rules. In the United States, which is the main funder of this type of flu research, a joint committee of federal agencies — the Intragovernmental Select Agents and Toxins Technical Advisory Committee — is expected to issue its own biosafety rules soon. A more detailed plan — the United States Government Policy for Local Institutional Oversight of Dual Use Research of Concern — is also likely to be released for public comment soon, possibly within weeks, says Anthony Fauci, director of the US National Institute of Allergy and Infectious Diseases (NIAID) in Bethesda, Maryland.

➲ NATURE.COM
For more, see *Nature*'s mutant-flu special:
go.nature.com/mhmibi

But Fauci says that he is keen to restart the research before the final policy is published months from now. He intends to hold a discussion on future plans for this work at the annual meeting of the NIAID Centers of Excellence for Influenza Research and Surveillance in New York at the end of July, which will be attended by many of the moratorium's signatories. "I can't say that the moratorium will officially end then, but we are certainly going to address the topic at that meeting," he says, "to get some research going on an interim basis."

The moratorium only involves the handful of groups, mostly funded by the US National Institutes of Health, that currently work on 'gain-of-function' experiments that increase the transmissibility or pathogenicity of flu viruses, emphasizes Fauci. "Many people think that the entire field of influenza research is on hold because of this moratorium, and that's not the case."

Some scientists, however, question whether funders should be driving the proliferation of this research. Ilaria Capua, a flu researcher at the Veterinary Public Health Institute in Legnaro, Italy, and a signatory to the moratorium, says that there remains a "central strategic question of whether these experiments should continue at all".

PROLIFERATION CONCERNS

Advocates of expanding the research say that finding genetic mutations that might make viruses more likely to trigger a pandemic could improve surveillance efforts. But this would require extensive experiments in ferrets and other animals, because the work would involve testing multiple mutations of the many types of wild H5N1 virus and the diverse range of other flu viruses with pandemic potential, such as H9 and H7 viruses.

"What is going to happen if we decide to continue funding research on this topic, and in 20 years' time we have 200 labs which have such viruses?" asks Capua. With advances in technology bringing mutant-flu research within the reach of many modest labs, even in the world's poorest countries, she worries about its unchecked proliferation in politically volatile regions. "Do we need to continue working on making these viruses

PASIEKA/SPL

more and more dangerous, and more and more transmissible? Do the research benefits outweigh the risks?"

The WHO's imminent biosafety guidelines will try to address such proliferation concerns, says one WHO official. Beyond making recommendations about biological containment levels and other physical precautions, the WHO will also suggest that labs should meet the highest standards of safety, attaining international standards for staff training and managing biological risks. The idea, says the WHO official, is to set a high bar for entry into this type of work.

Four leading public-health scientists also called for caution in an article[6] published in the same issue of *Science* as Fouchier's paper. Any predictions of flu's behaviour based on its complex genetics and host interactions are "highly speculative", they write, which raises questions about the potential benefit of mutant-virus work to flu surveillance. Moreover, current systems of genetic surveillance of flu viruses are too patchy, and years can pass before samples are sequenced[7]. Contrasting the uncertain benefits with an "exceptional level of risk should motivate exceptional caution by scientists, funders, and regulators worldwide", the authors write[6].

But Fouchier says that the mutant flu viruses that he and Kawaoka have worked on raise few new biosafety issues. "For over a century, the infectious-disease community has published work on dangerous pathogens while relying on national governments, institutional biosafety offices and the responsibility of scientists to ensure that the work is done under appropriate conditions," Fouchier adds. "Very little has gone wrong so far, so why would that be different now?"

The debate over risks and benefits is likely to come to a head at a meeting that the WHO will convene early next year to discuss the wider implications of high-risk biological research and how researchers, institutions and governments might best assess and manage risk. "The meeting will not be restricted to flu researchers, or virologists or researchers of any sort," says the WHO official. "They will certainly be represented, but so too will other groups which have very legitimate interests and perspectives on this whole question." ■

1. Herfst, S. *et al. Science* **336,** 1534–1541 (2012).
2. Yong, E. *Nature* http://dx.doi.org/10.1038/nature.2012.10875 (2012).
3. Imai, M. *et al. Nature* http://dx.doi.org/10.1038/nature10831 (2012).
4. Butler, D. & Ledford, H. *Nature* http://dx.doi.org/10.1038/nature.2012.10369 (2012).
5. Butler, D. *Nature* **482,** 447–448 (2012).
6. Lipsitch, M., Plotkin, J. B., Simonsen, L. & Bloom, B. *Science* **336,** 1529–1531 (2012).
7. Butler, D. *Nature* **483,** 520–522 (2012).

CLIMATE

Sea versus senators

North Carolina sea-level rise accelerates while state legislators put the brakes on research.

BY LEIGH PHILLIPS

Could nature be mocking North Carolina's law-makers? Less than two weeks after the state's senate passed a bill banning state agencies from reporting that sea-level rise is accelerating, research has shown that the coast between North Carolina and Massachusetts is experiencing the fastest sea-level rise in the world.

Asbury Sallenger, an oceanographer at the US Geological Survey in St Petersburg, Florida, and his colleagues analysed tide-gauge records from around North America. On 24 June, they reported in *Nature Climate Change* that since 1980, sea-level rise between Cape Hatteras, North Carolina, and Boston, Massachusetts, has accelerated to between 2 and 3.7 millimetres per year. That is three to four times the global average, and it means the coast could see 20–29 centimetres of sea-level rise on top of the metre predicted for the world as a whole by 2100 (A. H. Sallenger Jr *et al. Nature Clim. Change* http://doi.org/hz4; 2012).

"Many people mistakenly think that the rate of sea-level rise is the same everywhere as glaciers and ice caps melt," says Marcia McNutt, director of the US Geological Survey. But variations in currents and land movements can cause large regional differences. The hotspot is consistent with the slowing measured in Atlantic Ocean circulation, which may be tied to changes in water temperature, salinity and density.

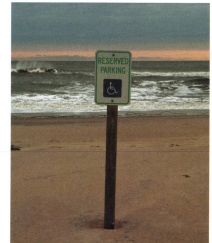

The tide will not be held back by law-makers.

K. KASMAUSKI/NAT. GEOGRAPHIC SOC./CORBIS

North Carolina's senators, however, have tried to stop state-funded researchers from releasing similar reports. The law approved by the senate on 12 June banned scientists in state agencies from using exponential extrapolation to predict sea-level rise, requiring instead that they stick to linear projections based on historical data.

Following international opprobrium, the state's House of Representatives rejected the bill on 19 June. However, a compromise between the house and the senate forbids state agencies from basing any laws or plans on exponential extrapolations for the next three to four years, while the state conducts a new sea-level study.

According to local media, the bill was the handiwork of industry lobbyists and coastal municipalities who feared that investors and property developers would be scared off by predictions of high sea-level rises. The lobbyists invoked a paper published in the *Journal of Coastal Research* last year by James Houston, retired director of the US Army Corps of Engineers' research centre in Vicksburg, Mississippi, and Robert Dean, emeritus professor of coastal engineering at the University of Florida in Gainesville. They reported that global sea-level rise has slowed since 1930 (J. R. Houston and R. G. Dean *J. Coastal Res.* **27,** 409–417; 2011) — a contention that climate sceptics around the world have seized on.

Speaking to *Nature*, Dean accused the oceanographic community of ideological bias. "In the United States, there is an overemphasis on unrealistically high sea-level rise," he says. "The reason is budgets. I am retired, so I have the freedom to report what I find without any bias or need to chase funding." But Sallenger says that Houston and Dean's choice of data sets masks acceleration in the sea-level-rise hotspot.

North Carolina is not the only hotspot for efforts to legislate away the reality of sea-level rise. In 2011, the Texas Commission on Environmental Quality removed all references to rising sea levels from a scientific study of Galveston Bay on the Gulf of Mexico. And this month, the Virginia General Assembly passed a bill commissioning a study on rising sea levels — but only after references to sea-level rise and climate change had been removed. ■

K. KOMATICK & J. EASTCOTT/MINDEN PICTURES/FLPA

Despite a ban on toxic bullets, the carcasses left by US hunters are poisoning this majestic carrion feeder.

SPECIES RECOVERY

California condors face lead menace

Signature species may need perpetual conservation.

BY MEERA SUBRAMANIAN

After more than three decades on the brink of extinction, the California condor (*Gymnogyps californianus*) — the largest and most threatened wild bird species in the United States — is making a modest recovery, thanks to intensive captive breeding and medical intervention. But troubling data reported this week suggest that unless hunters change their practices, the condor will require extensive support in perpetuity if it is to survive in the wild.

The cause of the problem is that the condors ingest lead when they feed on the carcasses of animals that hunters have shot. A multidisciplinary study published on 26 June (M. Finkelstein *et al. Proc. Natl Acad. Sci. USA* http://dx.doi.org/10.1073/pnas.1203141109; 2012) shows that chronic lead poisoning persists among condors, despite a 2008 California ban on the use of lead shot in regions where the birds are being reintroduced.

Building on earlier studies, the researchers collected feathers and blood samples from trapped birds and found no discernible difference in lead levels before and after the ban. Condors feed by scavenging; the results show that many of those sampled have dangerous levels of lead in their bodies. Lead poisoning can severely damage the birds' nervous systems and impair liver and kidney function, among other problems, and it can be fatal. The study also found that approximately 20% of condors in the wild have lead levels that are high enough to require costly treatment with chemical agents to remove the toxic metal from their bodies.

"By any measure, the lead poisoning rates in condors are of epidemic proportions," says Myra Finkelstein, a toxicologist at the University of California at Santa Cruz, who led the research.

The California condor population fell to an all-time low of 22 individuals in 1982, but captive-breeding and monitoring programmes have brought it back up to nearly 400 birds. Of those, half reside in captive-breeding centres, which provide a steady supply of new releases. In California, only 24 chicks have fledged in the wild. At that rate, the study shows, it would take 1,800 years for the population in California to reach 150 — the number called for in the recovery plan — without the ongoing release of birds bred in captivity.

Finkelstein's team did an isotopic analysis of the lead in the birds and identified lead shot or bullets as the main source of contamination. Even though hunters must use copper bullets or other alternatives in condor habitat, some are apparently ignoring the ban. Condors must consume 75–150 carcasses every year to maintain a healthy weight. The study found that even if fewer than 2% of the carcasses contain lead, there is a 50% chance that a condor will eat contaminated meat (see 'Loaded odds').

"Kudos to the hunters who are using copper [bullets], but it isn't going to be effective until you get all the lead out," says Jeff Miller, conservation advocate for the Center for Biological Diversity (CBD), based in Tucson, Arizona. Lead ammunition is cheaper and popular with hunters. The American Bird Conservancy in The Plains, Virginia, which advocates for lead-free hunting, argues that publicizing the risk of lead shot to human health might persuade hunters to use alternatives.

Pedro Nava, a former member of the California State Assembly who spearheaded the lead ban, says that a lack of resources for enforcing the ban means that the condor's future depends on the good will of hunters. He says that the California Department of Fish and Game needs more enforcement personnel. "They have 300 game wardens in the state. If they were to be consistent with other states in terms of population, they should have a thousand," he says.

Nava says that he would like to see the ban expand beyond condor habitat, starting with state-owned uplands favoured by hunters. On 7 June, the CBD filed a lawsuit to require the US Environmental Protection Agency (EPA) to ban lead ammunition, but the agency maintains that it lacks the legal authority to do so.

Despite general acceptance in the United States for the need to restrict lead in nearly all commercial products, the National Rifle Association (NRA), based in Washington DC, says that applying such rules to ammunition would infringe US gunowners' rights. "We'd look at it as an anti-gun move," said Susan Recce, the NRA's director of conservation, wildlife and natural resources. The NRA is lobbying for legislation that would prevent any EPA intervention.

Finkelstein says that the problem has to be addressed somehow, or the California condors will never recover. "We're spending an exorbitant amount of time tracking, trapping and hospitalizing these condors to manage their lead poisoning episodes," she says. "It's just not an effective way to go about this problem." ■

LOADED ODDS

A condor is likely to be poisoned even if just a small proportion of the carcasses it consumes contain lead.

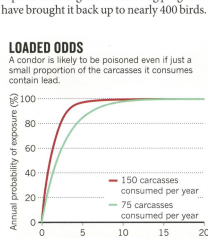

SOURCE: PROC. NATL ACAD. SCI. USA

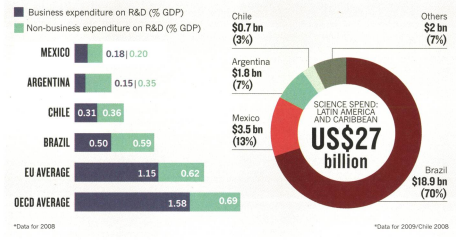
PALTRY PESOS
Mexico's gross expenditure on research and development (R&D) relative to its gross domestic product (GDP) lags behind that of rivals in Latin America, the European Union (EU) and the Organisation for Economic Co-operation and Development (OECD).
Business expenditure on R&D (% GDP)
Non-business expenditure on R&D (% GDP)
MEXICO 0.18 | 0.20
ARGENTINA 0.15 | 0.35
CHILE 0.31 0.36
BRAZIL 0.50 0.59
EU AVERAGE 1.15 0.62
OECD AVERAGE 1.58 0.69
*Data for 2008
Chile $0.7 bn (3%)
Others $2 bn (7%)
Argentina $1.8 bn (7%)
Mexico $3.5 bn (13%)
SCIENCE SPEND: LATIN AMERICA AND CARIBBEAN
US$27 billion
Brazil $18.9 bn (70%)
*Data for 2009/Chile 2008
SOURCE: RICYT/UNESCO/BRAZILIAN MINISTRY OF SCIENCE AND TECHNOLOGY

POLITICS

Science at stake in Mexican election

Presidential candidates vow to restore research reputation.

BY ERIK VANCE IN MEXICO CITY

Mexican scientists have watched with dismay as their country, Latin America's second-largest economy, has slipped down the research-spending ranks in recent years. Candidates in this week's presidential election have pledged to change that.

Back in 2000, presidential candidate Vicente Fox promised to raise Mexico's gross expenditure on research and development from about 0.4% to 1% of gross domestic product (GERD per GDP, often known as research intensity). Fox won, but despite legislation meant to guarantee the increase, Mexico's GERD per GDP has remained below 0.5%. Science has barely featured in campaigns for subsequent elections, presidential or otherwise.

Now it is back with a vengeance. In presidential debates, all three leading candidates have sworn to make good on Fox's promise. "This is the very first time that I have heard the candidates make positive pronouncements about science," says José Franco López, president of the Mexican Academy of Sciences in Mexico City. "Before, science was nowhere in their speeches. This time they are acknowledging that science and technology and innovation are engines for economic development."

The attention to research investment comes as Mexico faces competition from other emerging economies. "Brazil has almost caught up with Mexico in GDP per capita, in less than a generation," says Andrew Selee, director of the Mexico Institute at the Woodrow Wilson Center in Washington, DC. "Mexicans are starting to ask why."

For much of the twentieth century, Mexico was considered to be the leader in Latin American science. Yet although the country still has pockets of research excellence, Mexico's GERD per GDP now ranks among the very lowest in the world's top 40 economies (see 'Paltry pesos').

"This is the very first time that I have heard the candidates make positive pronouncements about science."

Brazil, by contrast, has consistently spent more than 1% of its GDP on research since 2006. Its gross expenditure on science, including industrial research, totals almost US$20 billion per year — roughly five times Mexico's tally — despite cuts this year of almost 20% to the US$3.8-billion budget of the Brazilian Ministry of Science, Technology and Innovation (L. Amorim *Science and Development Network* 6 March 2012).

"Knowledge, research, development and innovation have not been a priority for Mexican decision-makers," says Juan Pedro Laclette, head of the Scientific and Technological Consultative Forum, a leading think-tank for science based in Mexico City. "If you plant peanuts, you are going to harvest peanuts. What Mexican politicians have planted — have invested — is peanuts."

The presidential candidate who talks the most about reviving research is Andrés Manuel López Obrador, who leads the left-wing Party of the Democratic Revolution. Polls put him just ahead of Josefina Vázquez Mota of the right-leaning National Action Party, which has held the presidency since 2000, but behind Enrique Peña Nieto of the left-wing Institutional Revolutionary Party, which controlled the Mexican government for more than seven decades until 2000, and became a symbol of corruption and voter fraud.

In the most recent presidential election, in 2006, Obrador came second by such a narrow margin that he held regular protests for five months, during which time he named himself president and even set up an alternative government — machinations that have damaged his credibility this time around. His party, however, has deep roots in academia and enjoys wide support from scientists. René Drucker Colín, a neuropathologist and former coordinator of basic science at the National Autonomous University of Mexico in Mexico City, one of Latin America's biggest universities, is among the researchers who have taken to the campaign trail on Obrador's behalf.

Obrador plans to remedy what many researchers complain is a major handicap for Mexican science: the lack of a clear national research strategy with long-term commitments to nurturing particular fields. He has pledged to boost spending and promote the country's biggest science funder, the National Council on Science and Technology, to a fully fledged ministry — with Drucker Colín at its head — that would control the nation's entire science budget.

Peña Nieto, the current presidential front runner, has said less publicly about science. But in an e-mail to *Nature*, he wrote: "We need to create a National System for Innovation that promotes it through effective stimuli, intellectual property rights protection, better access to credit and coordination between the public and private sectors."

Industry contributes less than half of Mexico's GERD per GDP, and the country's scientists, including Pedro Laclette, have long bemoaned the schism between industry and academic research. In the future, wrote Peña Nieto, "private funding will be instrumental to the success of the system".

Whoever wins the election, researchers are adamant that the time for broken promises is past. "If you take the difference between what they give and what they were supposed to be giving, they owe science a huge amount of money," says Franco López. ■

GENETIC ENGINEERING

Model pigs face messy path

As approvals for engineered food animals stall, pigs may be US regulators' next challenge.

BY AMY MAXMEN

The three litters of Yucatan miniature piglets, born in late May, dwell in a space more like a neonatal care unit than a barn. They require hand-feeding and frequent veterinary attention from the staff at Exemplar Genetics in Sioux Center, Iowa. Their muscles already show the signs of deterioration that they were bred for.

As the United States' first genetically engineered (GE) pigs with muscular dystrophy, the creatures could be used to test treatments for the disease. But their utility will remain limited for the time being, while the US Food and Drug Administration (FDA) works out how to regulate them.

Exemplar Genetics, which aims to sell GE pig models for use in academic and pharmaceutical laboratories, has so far bred about 275 pigs — some with cystic fibrosis, others with heart disease, arrhythmia or cancer, and now muscular dystrophy. Because pigs mimic these human diseases more closely than mice, they are desirable models for drug testing and for studying the disease process.

However, as the first company to seek approval for a disease model in a GE animal that could, in theory, also be eaten, Exemplar is navigating a dimly lit regulatory path. In 2009, the company submitted its first application to the FDA for approval of its cystic fibrosis pig model. "We don't really know what additional steps we need to do in order to get FDA approval for full commercialization," says John Swart, president of Exemplar. Nevertheless, the company remains hopeful that its pigs will skirt the hardships that have befallen other GE animals in the pipeline.

As early as 1999, the FDA spoke about the promise of GE animals for both food and pharmaceutical purposes. Ten years later, the agency created a framework to judge their safety. In 2009, it applied the guidelines in approving a GE goat that produces a blood-clotting drug in its milk.

Since then, however, FDA approvals for two GE food animals have stalled: a salmon with a gene prompting faster growth, and a hog engineered to excrete less-toxic manure. Members of Congress have voiced their fears about such 'frankenfish,' and environmental groups are concerned that transgenic animals might escape and interbreed with wild populations.

In April, amid the delays, the University of Guelph in Ontario, Canada, which was sponsoring the environmentally friendly hog, backed out of the approval process. Last month, the experimental hogs were put down. AquaBounty, the GE salmon company, based in Maynard, Massachusetts, fears that it, too, may have to pull its product if delays persist. "We've done everything we've been asked to do, and nothing has happened for so long that it's threatening the existence of our company," says Ronald Stotish, AquaBounty's president. The FDA declined to comment on any pending GE animal applications.

With salmon frozen in the pipeline, Exemplar's piglets might skip to the front of the queue. "GE pigs for medical models could move more quickly because there's a strong need for them in the medical community," suggests David Edwards, director of animal biotechnology at the Biotechnology Industry Organization based in Washington DC. Although animal-rights advocates may object to disease-model pigs, Swart predicts that they will avoid intense public scrutiny because they aren't meant to be eaten.

Nonetheless, Swart is worried about the regulatory process for 'new animal drugs' (NAD), which applies to all GE animals, whether they're bred to produce food, drugs or, in Swart's case, disease. "The NAD process doesn't fit us real well," he says. When Swart asked the FDA how to demonstrate the requirement that his products are safe for human consumption, he says the FDA revised the rule: Exemplar must ensure that no unintended consequences befall the animals themselves. But Swart points out that diseases have variable symptoms. "We don't know much about these diseases, which is why we need a model."

While the pigs plod through the process one step at a time, a handful of investigators at US universities have already begun to study how diseases develop in the transgenic animals. Because the pigs aren't federally approved, Exemplar must track each pig from birth to beyond the grave. If a scientist in Iowa sends tissue from one of the animals to a colleague in California, Exemplar knows. Moreover, without approval, Exemplar cannot promote the pig models for drug testing based on what the researchers find.

Exemplar has repeatedly asked for an exemption from the NAD category, such as that granted to transgenic mice, but so far the FDA has not provided one. Although delays have nearly driven other GE animal companies under, Swart calls the wait worthwhile if Exemplar's pigs can help pharmaceutical companies to predict whether a drug will work. "It's critical to figure out how to do this right with the FDA," he says. ■

EXEMPLAR GENETICS

Drug companies want to test therapies on Yucatan piglets engineered to develop diseases.

MORE ONLINE

TOP STORY

There may be many more species of shark than we thought
go.nature.com/xyaz0y

JOIN THE CONVERSATION

- Injected proteins protect mice from radiation poisoning go.nature.com/aajrqe
- Future of the sagebrush lizard hinges on voluntary measures go.nature.com/ouybug
- Shell gears up for Arctic oil rush go.nature.com/7fu5oa

WATCH THE MOVIE

Astronomers manage to capture film of near-miss asteroid
go.nature.com/qqiwzu

N. PROBST/IMAGEBROKER/PLUS

R. P. BINZEL, M. LOCKHART (MIT); B. GOLISCH, S. J. BUS, T. DENAULT, J. RAYNER, A. TOKUNAGA (IVAA-IAU) [+ KOLLAR/CAVIT]

GENETICS

Fetal tests spur legal battle

A newborn industry based on non-invasive genetic testing turns combative.

BY ERIKA CHECK HAYDEN

Genetic tests that analyse fetal DNA from a pregnant woman's blood are arriving in a rush, giving parents powerful tools for gleaning information about their unborn offspring. Three companies have launched versions of such tests in the past 12 months, and a fourth plans to do so later this year.

But the commercialization of these tests has brought a legal battle that could not only affect corporate profits, but also limit which patients will be able to access the tests and under what terms. The tangle of lawsuits may also offer a taste of future conflicts in the rapidly growing medical-genomics industry.

"If a single company has a monopoly on the market, it will essentially be able to dictate the standard of care and the quality of care," says Mildred Cho, a bioethicist at the Stanford University School of Medicine in California.

The four firms are all based in California — Sequenom in San Diego, Ariosa Diagnostics in San Jose, and Verinata Health and Natera, both in Redwood City — and use similar techniques to identify fetal DNA in maternal blood samples. The tests can spot genetic abnormalities, such as those that cause Down's syndrome, as early as ten weeks after conception — several weeks sooner than tests already in use. In studies of women at high risk of carrying offspring with Down's syndrome, the tests also produced fewer false positives.

Patents are at the core of the conflict (see 'Blood feuds'). Sequenom licensed the method for detection of cell-free fetal DNA in a mother's bloodstream in 2005, and it now says that other companies are infringing this patent.

In January this year, Sequenom filed a lawsuit against Ariosa (formerly Aria Diagnostics) for patent infringement, then requested a preliminary injunction to stop the company from using its test. As a result, Ariosa, Natera and Verinata (together with Stanford University, which was involved in Verinata's patent) have all sued Sequenom, arguing that the slight differences in their testing methods mean that they are not infringing on the patent.

This week, Judge Susan Illston of the US District Court of Northern California will hear arguments in Sequenom's lawsuit against Ariosa. On 29 June, she will conduct pre-trial meetings with lawyers for Natera, Verinata and Sequenom. Decisions in the cases are not expected for many months.

NATURE.COM
To read a Comment on fetal gene screening, see: go.nature.com/vnjsms

The lawsuits are driven by the promise of a lucrative market that is poised to become a routine part of prenatal care. Observers expect the advantages of the non-invasive tests to expand the pool of women who opt for prenatal genetic screening in the United States each year from fewer than 100,000 to as many as 3 million.

LUCRATIVE MARKET

David Ferreiro, an investment banker at Oppenheimer based in New York, has estimated that the non-invasive prenatal-testing market could exceed US$1 billion a year. So far, sales volumes reported by Sequenom — the only publicly traded company of the four — have "substantially exceeded expectations", says Ferreiro.

And the technology will probably become more powerful. Earlier this month, for example, a team of researchers at the University of Washington in Seattle announced that they had used non-invasive sequencing to read a whole fetal genome (J. O. Kitzman *et al. Sci. Transl. Med.* **4**, 137ra76; 2012). The reading of whole genomes could tell potential parents about a much wider range of genetic variations. Because it covers non-medical traits and genetic variants not certain to cause disease, prenatal sequencing will also raise thorny ethical issues.

Although demand for prenatal testing is likely to increase, cost disparities have already made some of the tests unaffordable for low-income or uninsured women. At present, costs range from $795 (for Ariosa's test) to $2,762 (for Sequenom's, although out-of-pocket costs are capped at $235 for women who have health insurance). In California, Ariosa's test is covered by Medi-Cal — a state programme that pays for prenatal health care for low-income women — but Sequenom's and Verinata's tests are not.

If one company were to have a monopoly on prenatal testing, it could dictate the price of the test, potentially pushing costs out of reach for government programmes such as Medi-Cal, which pays for 40% of the births in California each year, or Medicaid, which covers as many as 60% of the births in some states. Many potential parents would be affected.

"The bigger policy issue is whether society should allow monopolies on medical practice, especially for medical technologies that benefited from public funding," Cho says. ■

BLOOD FEUDS

A spate of prenatal DNA tests has brought with it a host of legal disputes.

BSIP/PHOTOTAKE

14 OCTOBER 2005 Sequenom licenses a patent for non-invasive prenatal diagnosis.

10 AUGUST 2010 Sequenom's lawyers send Verinata Health a letter warning that Verinata is developing tests that will infringe on Sequenom's patent and patent application.

30 AUGUST 2011 Stephen Quake — founder of Verinata — and Hei-Mun Fan, both at Stanford University in California, are issued a patent for 'Determination of fetal aneuploidies by massively parallel DNA sequencing'.

17 OCTOBER 2011 Sequenom launches the MaterniT21 test.

6 DECEMBER 2011 Sequenom sends Aria Diagnostics a letter warning about patent infringement.

19 DECEMBER 2011 Aria files a complaint against Sequenom.

6 JANUARY 2012 Natera files a complaint against Sequenom.

24 JANUARY 2012 Sequenom sues Aria.

22 FEBRUARY 2012 Verinata and Stanford University sue Sequenom.

1 MARCH 2012 Verinata launches the Verifi prenatal test.

7 MAY 2012 Ariosa (formerly Aria) launches the Harmony prenatal test.

naturejobs CAREER EXPO LONDON 2012

20 SEPTEMBER 2012

BUSINESS DESIGN CENTRE, LONDON

The *Naturejobs* Career Expo in London is the UK's largest career fair and conference focused exclusively on the scientific world.

- **FREE** exhibition
- Expected **50+ employers**
- **Networking** opportunities
- Insightful **conference sessions**
- In-depth **company workshops**

For more information and to register visit:
www.naturejobs.com/careerexpo

naturejobs

nature publishing group npg

IN222277E

5 QUESTIONS ON H5N1

BY ED YONG

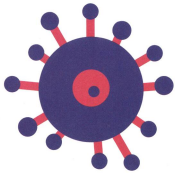

Scientists now know that the deadly bird flu virus is capable of causing a human pandemic. That makes tackling the remaining unknowns all the more urgent.

The biology of the H5N1 avian influenza virus is rife with paradoxes. The virus is widespread, but hard to detect. It kills more than half of the people known to be infected, but thousands of those exposed have no apparent problems. It seems to be just a few mutations away from gaining the ability to spread from person to person, but despite more than 16 years of fast-paced evolution, it has failed to do so.

This week saw the publication of the second of two papers identifying mutations that give H5N1 the ability to spread through the air between ferrets. The papers, the latest[1] from a group led by Ron Fouchier at the Erasmus Medical Center in Rotterdam, the Netherlands, and the earlier one[2] by Yoshihiro Kawaoka at the University of Wisconsin-Madison and his colleagues, have been controversial because they offer what some see as a recipe for disaster — that they increase the risk of accidental or intentional release of a deadly human pathogen. But what is most unsettling about them, say many in the flu community, is the evidence they provide that the wild virus could spark a pandemic on its own. That threat makes the outstanding scientific mysteries about this tiny RNA virus — its genome just 14,000 letters long — even more pressing. Here are five of the biggest puzzles, and what researchers are doing to solve them.

1 WHY IS IT SO SUCCESSFUL?

H5N1 influenza gets its name from the combination of two proteins on its surface: haemagglutinin (HA) and neuraminidase. But there are many different strains of H5N1. The highly pathogenic strain that has grabbed headlines for more than a decade was first identified in 1996. Called Gs/Gd because it was found in domestic geese in China's Guangdong province, it is "totally different to any avian influenza virus in the past", says Robert Webster, a virologist at St Jude Children's Research Hospital in Memphis, Tennessee. Most avian influenza viruses ride harmlessly aboard wild fowl, occasionally flaring into lethal but short-lived outbreaks in domestic birds. The Gs/Gd lineage, however, has jumped back from poultry into wild fowl. It also infects mammals, including humans, tigers, pikas, civets and more. It has spread to 63 countries, and is endemic in bird populations in six of them.

"What is so special about this virus that allows it to spread through the animal world so effectively?" asks Jeremy Farrar, a tropical-medicine specialist at the University of Oxford, UK. There are no firm answers.

China's crowded farms and markets, which offer a smorgasbord of potential hosts, might have selected for viruses that are adept at crossing the species barrier. The virus evolved quickly in 1999 and 2000, its family tree sprouting many new branches after efforts to stamp it out among domestic birds failed. During this time, one clade of the Gs/Gd lineage, known as 2.2, picked up a mutation in *PB2*, one of three polymerase genes that allow the virus to copy its genome. The mutation is widely considered to be an adaptation to mammalian hosts.

In 2002, for reasons that are still unclear, the viruses started hopping back into wild birds and killing them. At first, there were just a few isolated deaths, but in May 2005, clade 2.2 viruses killed more than 6,000 geese, gulls and ducks at Qinghai Lake — China's largest lake, and a major breeding spot for migratory birds. This outbreak heralded the start of a global tour in which the virus spread through bird trade and wild migrations to the rest of Asia, Europe and Africa. Vaccination controlled the virus in Hong Kong and Vietnam, but where applied haphazardly, it has helped to speed up the virus's evolution. In Egypt, it led to the birth of several new sub-clades[3], and the country has had more new human cases than any other nation every year since 2009.

There is some good news: infections in wild birds have fallen sharply since 2006. But even as old lineages wane, new ones arise, such as clade 2.3.2.1, which has swept through poultry in Asia since early 2011. "That's the one that is of great concern to me," says Webster. "It seems to be becoming dominant and it goes into wild birds readily." H5N1 may be evolving faster than our ability to understand it.

2 WHERE IS IT NOW?

H5N1 seems to be both everywhere and nowhere at the same time, making it hard to predict when, where and whether it will bloom into a human pandemic.

Wild birds carry H5N1, but the virus can be hard to detect because very few become ill. No one knows how widespread it is in humans, either. As of 7 June, the World Health Organization had counted 606 H5N1 infections in humans, 357 of them fatal. Many think that the real number is much larger, which would mean that the death rate would be much lower than 60%. Peter Palese, a virologist at Mount Sinai School of Medicine in New York, looked at a number of studies that had found evidence of H5N1 infection in the blood of healthy people. He estimates that 1–2% of people in populations exposed to the virus become infected, but most have only mild or no symptoms[4].

Palese's arguments are controversial. Farrar, who has treated patients in Asia, says that most of the cases he has seen have been severe. "If many mild infections were occurring, we'd expect to see some less severe patients in hospital, given the heightened awareness in the public and the medical profession," he says.

Underlying the debate about the infection rate is a poor understanding of how the immune system responds to the virus. People who become infected produce antibodies and T cells that recognize the virus, but no one knows how these responses rise and fall over time, or how they manifest in people who show no symptoms. The signals could also be false alarms. "If you go into henhouses every day to clean up bird droppings that are loaded with virus antigen, you may get an antibody response without being infected," says Fouchier. More thorough surveillance of suspected cases will be needed to resolve the debate about how often people are infected, says Fouchier. Farrar adds that to understand how immune responses change over time, such studies will have to be done over several years. Many researchers have called for better surveillance of domesticated and wild animals, too.

To Ilaria Capua, a veterinary virologist at the Experimental Animal Health Care Institute of Venice in Legnaro, Italy, the distribution of H5N1 is the most important issue, and the hardest to work out. "Any prediction about whether this virus will go pandemic is a function of where it is, how much of it there is and how possible the human–animal contacts are. But there are big black holes of information."

3 HOW DOES IT KILL?

Bit by bit, scientists are teasing out the genetic factors that make H5N1 so deadly. The virus has several mutations in its three polymerase genes that allow it to replicate aggressively, and patients who die carry the highest levels of viral RNA. Certain changes to *HA*, which codes for a protein that latches onto host cells, also allow the virus to infect tissues beyond the lungs and gut, including the brain. This all-access pass helps the virus to kill ferrets, mice and birds, but it is apparently less important in primates. "In humans, it still looks predominantly like a respiratory disease kills the patients," says Malik Peiris, a clinical virologist from the University of Hong Kong. Autopsies might paint a clearer picture, but Peiris says that these are rarely allowed in Asia because of cultural demands for whole-body burials.

H5N1 also drives the immune system berserk. Immune cells flock to sites of infection and produce inflammatory chemicals called cytokines, which attract more immune cells. The result, a cytokine 'storm' that floods the lungs with fluid and fatally damages surrounding tissues, is often what kills people. H5N1 triggers a more extensive storm than the human flu viruses H1N1 or H3N2 (ref. 5).

These factors may explain the severity of recorded cases, but not why infections are so rare. "Why is it that there are tens of thousands of kids running around playing with sick chickens, but we've only had 600 infections over nine years?" asks immunologist Anthony Fauci, who heads the National Institute of Allergy and Infectious Diseases in Bethesda, Maryland.

"IN PRINCIPLE, H5N1 CAN BECOME AIRBORNE. THE CRITICAL QUESTION IS WHETHER IT WILL."

Palese suspects that the severe cases have simply inhaled high doses of the virus. But Peiris says that this cannot be the sole explanation. "Infection and disease are not directly proportional to exposure. Ninety-nine point nine per cent of the people who are massively exposed don't have disease, and don't have antibodies in their blood. But in people who get sick, the virus replicates like crazy."

Notably, cases are often clustered within families, specifically blood relatives. These people might be genetically susceptible to H5N1 infection, or others may have genetic variants that protect them. Identifying such variants will be hard because fewer than 300 people around the world have survived the infection, but studies are starting to reveal clues.

A few months ago, a group from the Wellcome Trust Sanger Institute in Hinxton, UK, found that the gene *IFITM3* plays a pivotal part in responses to some flu infections[6]. One variant of the gene, which encodes a stunted protein, was overrepresented in people who had been hospitalized with pandemic and seasonal flu strains, and even a mild H3N2 virus ran amok in the lungs of mice that lacked the gene[6]. Farrar has just completed a similar study, of 67 Asian patients who had been hospitalized with H5N1. The results, which have been submitted for publication, identify variants in two other genes that seem to confer susceptibility to the virus.

"IN PEOPLE WHO GET SICK, THE VIRUS REPLICATES LIKE CRAZY."

4 WILL IT BECOME TRANSMISSIBLE IN HUMANS?

So far, people seem to catch H5N1 only through close contact with infected birds. To spread from person to person, the virus would have to become transmissible through airborne droplets. The two papers just published[1,2] have shown that that is possible.

Fouchier's strategy was to tweak *HA* so that its protein recognized receptors in the upper airways of mammals rather than those on the surface of bird cells[1]. He then allowed the virus to pass between ferrets until it evolved such that it started spreading through coughs and sneezes. Kawaoka took a similar approach[2], but he fused a mutated *HA* from H5N1 with other genes from a 2009 pandemic H1N1 strain. "In principle, H5N1 can become airborne," says Fouchier. "The critical question is whether it will."

One of the biggest questions about H5N1 is why it hasn't become transmissible after circulating for so many years — but no-one has a good answer. Many of the mutations that Fouchier and Kawaoka identified are already found in the wild. By searching surveillance databases, Derek Smith, a bioinformatician from the University of Cambridge, UK, found that many wild clades are already two to four mutations away from the sets that Fouchier and Kawaoka identified[7].

Smith was unable to determine the actual risk because surveillance data masks the genetic diversity of the virus. H5N1 reproduces with errors, so any one patient carries a swarm of viruses with subtle genetic differences. The databases contain just the 'consensus' sequence, essentially a mash-up of the most common variant at every position in the genome. Only deeper sequencing, in which each position is read many times over, will reveal all the variants.

Even if the same combination of *HA* mutations that Fouchier and Kawaoka identified arises naturally, no one knows whether the resultant viruses would spread between humans as easily as they do between ferrets in the lab. It is also not clear how H5N1's other genes contribute to transmissibility, or whether different combinations of mutations would achieve the same effect. "These guys have only scratched the surface," says Webster.

Fouchier and Kawaoka say that the value of their work lies in identifying the physical traits that make H5N1 transmissible. Some mutations allowed HA to recognize mammalian receptors, whereas others stabilized the protein. "If you take those traits, can you then make any flu virus go airborne?" asks Fouchier. The virulence of a transmissible strain is another unknown. One hypothesis suggests that as transmissibility goes up, virulence will become muted. An airborne H5N1 might recognize receptors in the upper airways, for example, but be less likely to descend into the lungs to cause the extensive damage inflicted by wild strains. "Theoretically, one could imagine such a scenario," says Pereis. "But I wouldn't want to stake my life on it."

Fouchier and Kawaoka's mutant viruses caused milder disease in ferrets than their wild counterparts do, but both men note that such comparisons are misleading because wild H5N1 has to be administered to the animals directly, which can introduce high doses deep within the lungs. And, Kawaoka notes, transmissible strains do not have to have a fatality rate of 60% to kill millions of people: the H1N1 pandemic of 1918 had a mortality rate of 2.5%, yet claimed around 50 million lives.

5 WHAT ELSE COULD CAUSE A PANDEMIC?

The Gs/Gd strain is what is known as a reassortant. It was born from a flu version of sex, in which different viruses infecting the same cell swap genes, and it probably includes genes from the H6N1 and H9N2 viruses[8]. Since then, H5N1's descendants have swapped genes mostly with each other. "H5N1 is not very sexually promiscuous," says Capua. "It likes to reassort within its own lineage." But the H1N1 strain responsible for the 2009 pandemic could shake H5N1 from its insularity. That strain is itself a cocktail of genes from swine H1N1, avian H1N1 and human H3N2 and includes a set of genes called the triple-reassortant internal gene (TRIG) cassette, which seems to make flu viruses more prone to reassortment. "That virus loves to mate," says Webster.

Kawaoka's team has shown that the two viruses are compatible, and will reassort spontaneously when they infect the same cells[9]. This is made more likely by their shared ability to infect pigs. Furthermore, Stacey Schultz-Cherry, a virologist at St Jude Children's Research Hospital, has found that reassortant viruses containing *HA* from H5N1 and other genes from pandemic H1N1 are better at replicating in human lung cells than either parent is, and that they become more virulent after a few rounds of replication[10].

Wendy Barclay, a virologist at Imperial College London, cautions that although these experiments reveal that reassortment is possible, they do not quantify the odds that it will happen. "If you force the event, it'll happen, but I haven't seen anyone do the experiment in a more natural way," she says. That would involve housing uninfected pigs with ones carrying pandemic H1N1, and poultry carrying H5N1. "Do they catch both viruses and do the viruses mix up?" asks Barclay. "It's an unknown and a pretty important one."

The upside of an H5N1–H1N1 reassortant is that many people have already been infected with H1N1 and so might have some immunity. But few people have encountered any of the flu viruses that circulate in birds. "I think the great worry is that a purely avian virus somehow crosses over to us," says Farrar. H5N1 tops the list of concerns because of the severe nature of the known infections, but other subtypes could escalate into pandemics first.

"H9N2 may be an equally plausible pandemic candidate," says Peiris. It generally goes unnoticed, but has hunkered down among Asia's poultry, caused occasional outbreaks in humans and can reassort with seasonal flu. Some strains already have mutations that are associated with greater transmissibility in mammals. H7N7 is similarly widespread and under-reported. In 2003, it flared up in the Netherlands, infecting 89 people and killing a veterinarian. Virologists hope that by understanding the secrets that allow H5N1 to spread and kill, they are in a better position to assess the risk posed by other subtypes. "With flu, nothing is predictable," says Capua. ■

Ed Yong *is a freelance writer based in London and author of the blog 'Not Exactly Rocket Science'.*

1. Herfst, S. *et al. Science* **336,** 1534–1541 (2012).
2. Imai, M. *et al. Nature* http://dx.doi.org/10.1038/nature10831 (2012).
3. Cattoli, G. *et al. Vaccine* **29,** 9368–9375 (2011).
4. Wang, T. T., Parides, M. K. & Palese, P. *Science* **335,** 1463 (2012).
5. de Jong, M. D. *et al. Nature Med.* **12,** 1203–1207 (2006).
6. Everitt, A. R. *et al. Nature* **484,** 519–523 (2012).
7. Russell, C. A. *et al. Science* **336,** 1541–1547 (2012).
8. Hoffman, E. *et al. J. Virol.* **74,** 6309–6315 (2000).
9. Octaviani, C. P., Ozawa, M., Yamada, S., Goto, H. & Kawaoka, Y. *J. Virol.* **84,** 10918–10922 (2010).
10. Cline, T. D. *et al. J. Virol.* **85,** 12262–12270 (2011).

nature REVIEWS CANCER

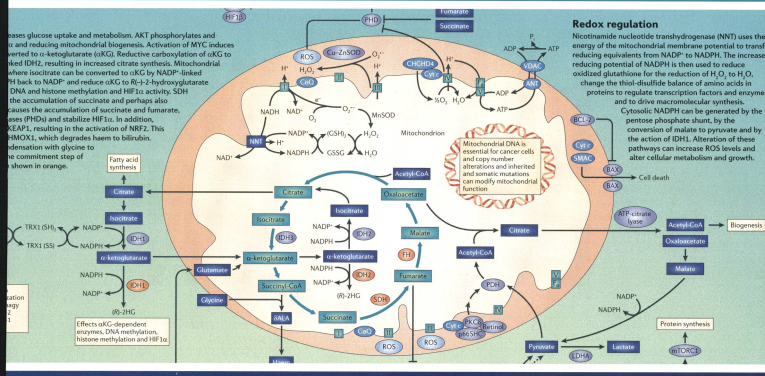
HIF1β
PHD
Fumarate
Succinate
Redox regulation
Nicotinamide nucleotide transhydrogenase (NNT) uses the energy of the mitochondrial membrane potential to transf reducing equivalents from NADP+ to NADPH. The increase reducing potential of NADPH is then used to reduce oxidized glutathione for the reduction of H2O2 to H2O. change the thiol-disulfide balance of amino acids in proteins to regulate transcription factors and enzyme and to drive macromolecular synthesis.
Cytosolic NADPH can be generated by the pentose phosphate shunt, by the conversion of malate to pyruvate and by the action of IDH1. Alteration of these pathways can increase ROS levels and alter cellular metabolism and growth.
ases glucose uptake and metabolism. AKT phosphorylates and
ix and reducing mitochondrial biogenesis. Activation of MYC induces
verted to α-ketoglutarate (αKG). Reductive carboxylation of αKG to
ked IDH2, resulting in increased citrate synthesis. Mitochondrial
where isocitrate can be converted to αKG by NADP+-linked
PH back to NADP+ and reduce αKG to R-(-)-2-hydroxyglutarate
DNA and histone methylation and HIF1α activity. SDH
the accumulation of succinate and perhaps also
causes the accumulation of succinate and fumarate,
ases (PHDs) and stabilize HIF1α. In addition,
KEAP1, resulting in the activation of NRF2. This
HMOX1, which degrades haem to bilirubin.
idemation with glycine to
he commitment step of
shown in orange.
Fatty acid synthesis
Citrate
Isocitrate
IDH3
α-ketoglutarate
IDH1
(R)-2HG
Effects αKG-dependent enzymes, DNA methylation, histone methylation and HIF1α
Glutamate
Glycine
Succinyl-CoA
SDH
Succinate
GAT
GABA
Pyruvate
ROS
Glu-Zn-SOD
CHCHD4
Cyt c
Apaf-1
MnSOD
NNT
Mitochondrion
Mitochondrial DNA is essential for cancer cells and copy number alterations and inherited and somatic mutations can modify mitochondrial function
Acetyl-CoA
Oxaloacetate
Malate
FH
Fumarate
PDH
PC
Cyt c
PKCδ
Retinoic acid
HB6 SHC
BCL-2
Cyt c
SMAC
BAX
BAX
Cell death
ATP citrate lyase
Acetyl-CoA
Oxaloacetate
Malate
Biogenesis
Protein synthesis
Lactate
LDHA
mTORC1
TRX1 (SH)2
TRX1 (SS)

FREE POSTER

Mitochondrial function and cancer

Author: Douglas C. Wallace

This Poster highlights some recent discoveries that have led to a renewed interest in the function of mitochondria in cancer cells. Mitochondria carry out a number of crucial functions in cells and these can be altered through mutations in either the nuclear DNA or the mitochondrial DNA.

Access the Poster FREE online!
www.nature.com/nrc/posters/mitochondria

This Poster is freely available thanks to sponsorship from

abcam® discover more

nature publishing group npg

REWRITING EVOLUTION

Tiny molecules called microRNAs are tearing apart traditional ideas about the animal family tree.

BY ELIE DOLGIN

Kevin Peterson grabs a pen and starts to scribble an evolutionary tree on the paper tablecloth of a bar in Hanover, New Hampshire. Drawing upside down to make it easier for me to see, he maps out the standard phylogenetic tale for placental mammals. First, Peterson scratches a line leading to elephants, which branched away from the rest of the placentals around 90 million years ago. Then came dogs, followed by primates (including humans) and finally rodents — all within a frenetic 20 million years. This family tree is backed up by reams of genomic and morphological data, and is well accepted by the palaeontological community. Yet, says Peterson, the tree is all wrong.

A molecular palaeobiologist at nearby Dartmouth College, Peterson has been reshaping phylogenetic trees for the past few years, ever since he pioneered a technique that uses short molecules called microRNAs to work out evolutionary branchings. He has now sketched out a radically different diagram for mammals: one that aligns humans more closely with elephants than with rodents.

"I've looked at thousands of microRNA genes, and I can't find a single example that would support the traditional tree," he says. The technique "just changes everything about our understanding of mammal evolution".

Peterson didn't set out to rewrite textbooks. A mild-mannered but straight-talking Montanan, Peterson had made a quiet career studying how bilateral body plans originated more than 500 million years ago. He has a particular interest in marine invertebrates and had intended to stick with that relatively obscure branch of the animal tree. But a chance investigation of microRNAs in microscopic creatures called rotifers led him to examine these regulatory molecules in everything from insects to sea urchins. And as he continues to look, he keeps uncovering problems, from the base of the animal tree all the way up to its crown.

That has won him many critics, but also some strong supporters. "Peterson and his colleagues have demonstrated that microRNAs are a powerful tool in determining the relationships of major animal groups," says Derek Briggs, director of the Yale Peabody Museum of Natural History in New Haven, Connecticut.

Now, together with his colleagues around the world, Peterson is putting it all on the line with mammals. "If we get this wrong, all faith that anyone has in microRNAs [for phylogenetics] will be lost," says Philip Donoghue, a palaeobiologist at the University of Bristol, UK, who has teamed up with Peterson. And there is more at stake than just the technique. "It could well be the end of all our careers," he says.

➲ NATURE.COM
For more on microRNAs and evolution, see:
go.nature.com/lcvohc

FOSSIL FIND

If Peterson does end up switching careers, it won't be the first time. In the early 1990s, he was working the night shift unloading trucks at a freight company in his hometown of Helena, Montana, trying to figure out what to do with his life. He had recently graduated with a pre-medical degree from a local liberal arts college, but he knew he didn't want to become a doctor. Then, rummaging in his parents' barn, he happened on the first fossil he had ever collected, as a four-year-old: a crinoid, or sea lily, about the size of a button. "After I found it, I knew right away that this was what I wanted to do," he says. "I applied to graduate school the next week."

He soon enrolled in a PhD programme in the Department of Earth and Space Sciences at the University of California, Los Angeles. There, he teamed up with developmental geneticists Eric Davidson and Andrew Cameron at the California Institute of Technology in Pasadena, and over the course of his

Kevin Peterson has kicked many mammals, including the Alaskan Brown Bear, off their traditional perch on the evolutionary tree.

DANA SMITH

graduate and postdoctoral work the three men developed a provocative idea, dubbed the set-aside cell hypothesis[1]. They posited that the ancestor of modern-day animals was a larva-like creature containing a group of undifferentiated cells that retained the capacity to give rise to the spectrum of adult body types seen during the Cambrian explosion. The idea subsequently came under fire from the evolutionary and developmental-biology communities.

A few years after moving to Dartmouth in 2000 to start his own lab, Peterson was looking for a way to test the hypothesis when he became intrigued with microRNAs. First discovered in 1993 by Victor Ambros, now at the University of Massachusetts Medical School in Worcester, these short, hairpin-shaped molecules bind to messenger RNAs and stop them from making proteins. A team that included Davidson had shown that a microRNA called let-7 was present in animal lineages that had bilateral body plans but not in simpler organisms such as jellyfish and sponges[2], hinting that microRNAs could hold the secret to morphological complexity.

Peterson teamed up with Lorenzo Sempere, then a graduate student working with Ambros at Dartmouth, and the pair began to search for let-7 and a handful of other microRNAs in relatively simple invertebrates, including rotifers, and in more complex creatures. As they added more microRNAs, they found a clear pattern: the farther away from the trunk of the evolutionary tree the animals were, the more microRNAs they had accumulated[3]. The pair started to realize that the molecules provided "a brand new way to do phylogeny, using a set of rare genomic characters that no one had ever considered before", Peterson says.

"IT COULD WELL BE THE END OF ALL OUR CAREERS."

MicroRNAs, Peterson and Sempere discovered, are unlike any of the other molecular metrics that biologists typically use to tease apart evolutionary relationships. DNA binding sites, for example, continuously mutate; microRNAs, by contrast, are either there or they aren't, so their interpretation doesn't require such complex sequence and alignment analyses. And once gained, microRNAs usually remain functional, which means that their signal stays intact for hundreds of millions of years. "No gene family was known to evolve in this way," Peterson says. In addition, these small molecules are often expressed in specific tissues and help to regulate the development of certain organs, so they could explain the origin of morphological innovations over geological time[3].

According to Peterson's latest tally, 778 microRNA families have arisen during the 600 million or so years of animal evolution, and only 48 have been lost. This pattern of inheritance leaves an easy-to-follow evolutionary trail for phylogenetic sleuths. Eugene Berezikov, a geneticist who studies microRNAs at the Hubrecht Institute in Utrecht, the Netherlands, says that microRNAs give a clearer answer than other molecular markers of evolution "because the analysis is much simpler".

OUT OF OBSCURITY

At first, Peterson and Sempere had a tough time publishing their results suggesting that animals had accumulated regulatory microRNAs. "One of the reviewers said it was impossible, what we were describing," says Peterson. In the end, the work was published in a specialized zoology journal[3]. Subsequent papers, however, won over some sceptics and Peterson was soon publishing in *Nature* and *Science*, and using his growing microRNA

library to resolve relationships within and between an assortment of evolutionary lineages, from jawless fishes[5] and reptiles[6] to fruit-flies[7] and acoelomorph worms[8].

"It is a really clever and fresh approach to phylogeny," says Peter Stadler, an evolutionary bioinformatician at the University of Leipzig in Germany. "I don't quite know why presence/absence of microRNAs is not used more frequently in deep phylogeny approaches."

Still, not everyone is convinced that microRNA genes trump other types of phylogenetic data. A key point of contention is whether microRNAs only rarely drop out of the genome, as Peterson contends. Andreas Hejnol, who studies invertebrate evolution at the Sars International Centre for Marine Molecular Biology in Bergen, Norway, is sceptical. "MicroRNAs behave like other genes — namely, they can be lost," he says. "There's no special mystery about them." Travis Glenn, an evolutionary biologist at the University of Georgia in Athens, agrees, saying that microRNA losses are probably underestimated. In May, he and his colleagues published a retort[9] to a paper[6] in which Peterson had argued that turtles are more closely related to lizards than to birds and crocodiles — the opposite of what most genomic data sets had indicated. Glenn argued that ultraconserved DNA elements — ones that evolution has kept intact over a long time — show that the conventional view is correct.

The critics have mostly been a vocal minority, but as Peterson climbs up the evolutionary ladder with his microRNA analyses, he will be reaching a much bigger audience — and the detractors are likely to become a lot louder. "We're mammals, so this matters," he says.

UP A TREE

When Peterson started his work on the placental phylogeny, he had originally intended to validate the traditional mammal tree, not chop it down. As he was experimenting with his growing microRNA library, he applied it to mammals because their tree was so well established that they seemed an ideal test. Alas, the data didn't cooperate. If the traditional tree was correct, then an unprecedented number of microRNA genes would have to have been lost, and Peterson considers that highly unlikely. "The microRNAs are totally unambiguous," he says, "but they give a totally different tree from what everyone else wants."

The results change the image of the proto-placental mammal. Because microRNAs place mice and rats at the base of the placental tree, they suggest that rodent-like traits, such as continuously growing incisor teeth, were common in the first placentals, then lost in the lineage that leads to primates, elephants, dogs and cows (see 'Duelling trees'). The findings also shift the geographical origin of placental mammals, suggesting that they started in the Northern Hemisphere, where the first rodent fossils are found, not in the Southern Hemisphere, as many researchers have assumed on the basis of fossil and DNA data.

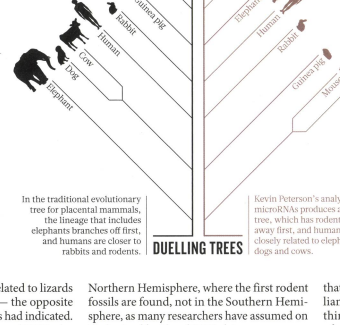

In the traditional evolutionary tree for placental mammals, the lineage that includes elephants branches off first, and humans are closer to rabbits and rodents.

Kevin Peterson's analysis of microRNAs produces a different tree, which has rodents splitting away first, and humans more closely related to elephants, dogs and cows.

At first, Peterson was shocked by his results, which still haven't been published. But he has spent the past year validating his tree with gene-expression libraries and genomic sequences, all of which he says support his findings.

Many supporters of the traditional tree suspect that something peculiar is happening with the microRNAs — probably large losses in the mammalian lineage. "He's talking about the entire genome that has to be wrong," says Robert Asher, a mammalian palaeontologist at the University of Cambridge, UK. "I don't give it any serious consideration," says Mark Springer, a molecular phylogeneticist at the University of California, Riverside, who last year published the most comprehensive genomic data set so far in support of the traditional mammalian tree[10]. "There have to be other explanations," he says.

Peterson and his team are now going back to mammalian genomes to investigate why DNA and microRNAs give such different evolutionary trajectories. "What we know at this stage is that we do have a very serious incongruence," says Davide Pisani, a phylogeneticist at the National University of Ireland in Maynooth, who is collaborating on the project. "It looks like either the mammal microRNAs evolved in a totally different way or the traditional topology is wrong. We don't know yet."

Hoping to resolve the issue, Donoghue and phylogeneticist Ziheng Yang at University College London have spent the past year amassing DNA sequences that span more than 14,600 genes from 36 mammalian species — a data set that dwarfs the one used by Springer. They are trying to determine whether the larger crop of DNA data produces the same tree as microRNAs yield. They have been able to date the origin and diversification of placental mammals[11], but they are still working to resolve which lineages branched off first — a key test for the phylogenies.

Peterson would like to put it all behind him. "What sucks about this mammal project is that it's all-consuming," he says. "Ultimately, I don't really care how mammals are related to one another — it doesn't matter to me. But what does matter is the validity of the data set."

If it turns out that the traditional mammal tree is right, Peterson won't see that result as a defeat for microRNAs. It would just mean that something odd happened with mammalian microRNAs, he says. "That says something really interesting about the evolution of microRNAs and the construction of gene regulatory networks in mammalian evolution."

For now, he's trying to amass the best evidence he can before publishing the mammal study. Then he wants to return to the quiet life of an ancient-invertebrate biologist. But if Peterson's voyage upends the mammalian phylogeny, he'll have left a furry mess in his wake. ■

Elie Dolgin *is a news editor with* Nature Medicine *in Cambridge, Massachusetts.*

1. Davidson, E. H., Peterson, K. J. & Cameron, R. A. *Science* **270,** 1319–1325 (1995).
2. Pasquinelli, A. E. *et al. Nature* **408,** 86–89 (2000).
3. Sempere, L. F., Cole, C. N., McPeek, M. A. & Peterson, K. J. *J. Exp. Zool. B Mol. Dev. Evol.* **306,** 575–588 (2006).
4. Peterson, K. J., Dietrich, M. R. & McPeek, M. A. *Bioessays* **31,** 736–747 (2009).
5. Heimberg, A. M., Cowper-Sal-lari, R., Sémon, M., Donoghue, P. C. J. & Peterson K. J. *Proc. Natl Acad. Sci. USA* **107,** 19379–19383 (2010).
6. Lyson, T. R. *et al. Biol. Lett.* **8,** 104–107 (2012).
7. Wiegmann B. M. *et al. Proc. Natl Acad. Sci. USA* **108,** 5690–5695 (2011).
8. Philippe, H. *et al. Nature* **470,** 255–258 (2011).
9. Crawford, N. G. *et al. Biol. Lett.* http://dx.doi.org/10.1098/rsbl.2012.0331 (2012).
10. Meredith, R. W. *et al. Science* **334,** 521–524 (2011).
11. dos Reis, M. *et al. Proc. Biol. Sci.* http://dx.doi.org/10.1098/rspb.2012.0683 (2012).

COMMENT

HEALTH How to cut antibiotic use in livestock to help stop resistance in humans **p.465**

BIOGRAPHY A life of Hans Bethe, Nobelist and veteran of the Manhattan project **p.468**

FICTION Author David Brin on sci-fi giant Ray Bradbury **p.471**

OBITUARY Nobel biophysicist Andrew Fielding Huxley, remembered **p.474**

ENVISAT/ESA

Cyanobacteria cover the Baltic Sea in green slime, spurred by flows of nitrogen and phosphorous.

Save the Baltic Sea

Geoengineering efforts to bring oxygen into the deep Baltic should be abandoned, says **Daniel J. Conley**.

The Baltic Sea holds the world's largest human-induced dead zone: a body of water that has all the symptoms of nutrient overload and oxygen deprivation. Dumping from sewage-treatment plants, farming and industry has poured about 20 million tonnes of nitrogen and 2 million tonnes of phosphorus into the Baltic over the past 50 years[1], spurring algal blooms.

In summer, cyanobacteria cover the beaches in green slime. As these blooms die, they fall to the sea floor and decay, using up available oxygen in the process. The oxygen-deprived bottom waters can no longer support higher forms of life, and the viable habitat for fish such as cod is greatly reduced. Over the past decade, an average of 60,000 square kilometres of the Baltic Sea has been 'hypoxic' each year: lacking enough oxygen to support its normal ecosystem.

Several large-scale geoengineering interventions have been proposed as solutions to this problem. Such radical remediation measures promise impressive improvements in water quality on short timescales. They are popular in the media and politically attractive. But they could also be dangerous. We should not let such schemes detract from the action plan that is already in place to reduce nutrient flows into the Baltic. Models predict that this plan will greatly reduce hypoxia (see 'Breathing life into the Baltic').

STIFLED SEAS

The problem of hypoxic waters is on the rise around the globe. Climate warming is likely to exacerbate matters — warmer temperatures speed up algal decomposition and reduce the rate at which oxygen from the air seeps into ocean surface waters[2]. Low oxygen levels kill sea-floor organisms and change how elements cycle through the system. In hypoxic conditions, the phosphorus-bearing iron oxyhydroxides in sediments dissolve, increasing the release of phosphate into the water. At the same time, low oxygen inhibits denitrifying bacteria in the sediments, boosting nitrogen levels. The net effect is an excess of phosphorous, which fuels nitrogen-fixing cyanobacteria and algal blooms. These decay and lead to ever more hypoxia — a vicious circle.

One potential countermeasure entails using pumps to mix the water[3]. This comes with significant challenges. About ▶

▶ 100 pumping stations would be needed throughout the Baltic to transport oxygen-rich water from a depth of about 50 metres to a depth of 125 m, and the pumps must remain operational for several decades. This is projected to cost at least €200 million (US$254 million).

The problem lies in the volumes involved. It has been estimated[4] that between 2 million and 6 million tonnes of oxygen would be required to keep the bottom waters of the Baltic Sea at a level above 2 milligrams of oxygen per litre — the limit for hypoxia. Theoretically, renewable energy sources such as wind power could be used to drive the required pumps at sea[5]. But pumping would also move less-salty water from the surface to deeper regions, potentially interfering with natural patterns of water circulation and the reproductive success of some fish species.

WARMED WATERS

In 2009, the Swedish government spent 30 million Swedish kronor (US$3.8 million) investigating this pumping option. Recent reports from those pilot studies show that the experiments were able to add oxygen (see go.nature.com/gqx2kq). However, some of the effect was counterbalanced by increases in water temperature, which can lower oxygen levels by spurring the metabolism of microbes in sediment. Bottom waters warmed as much as 8 °C at a test site in the coastal waters of Finland, for example. The raised temperatures also increased levels of ammonium, which can stimulate the growth of harmful algae.

In western Sweden, the pumping disturbed the layers of varying salinity in a deep fjord, altering water turnover and circulation patterns (see go.nature.com/gqx2kq). So far, these projects have been evaluated mostly by proponents of geoengineering. They must be subjected to unbiased, thorough scrutiny.

A second geoengineering approach, currently being trialled on a local scale in Swedish coastal waters, is the addition of chemicals to bind phosphorus in sediments. Tests are being carried out in the Stockholm archipelago using polyaluminium chloride[5], which is used in the treatment of waste water and drinking water. A small-scale field test was successfully conducted in 2011 for a few months, and the research group has received a permit from the regional government for a larger experiment.

Most tests of this technique have been confined to small lakes because of the cost of the chemicals. It is hard to know whether it will work in salty environments, how long the aluminium-bound phosphorus will stay buried in sediments, or what the effects might be on water acidity. Large-scale implementation in the Baltic Sea would have to abide by the 1972 Convention on the Prevention of Marine Pollution by Dumping of Wastes and Other Matter (the London Convention). This legal framework prevents the use of iron to sequester carbon dioxide in the oceans.

Rapid oxygenation of deep waters by any mechanism carries the risk of releasing a different toxic problem on the Baltic. Waters that are rich in oxygen can attract and support some species, such as deep-digging worms, that physically mix the sediment. This, in turn, can release old contaminants, such as polychlorinated biphenyl and DDT (dichlorodiphenyltrichloroethane), that are currently locked away under the Baltic. Thorough risk analyses of these issues have not been completed.

Yet geoengineering schemes are moving forwards. For example, the Oslo-based company Inocean announced plans to build a demonstration wind-driven pump in the southern Baltic Sea. This project, led by oceanographer Anders Stigebrandt of the University of Gothenburg in Sweden, received 2 million Swedish kronor ($288,000) in funding from the Swedish Agency for Marine and Water Management in Gothenburg this May, with co-funding from the Nordic Investment Bank and the Nordic Environment Finance Corporation, both headquartered in Helsinki. Stigebrandt stresses that full environmental impact studies will be carried out before the project begins.

A better, more cost-effective solution is to attack the root of the problem: excess nutrients. The nine countries that border the Baltic Sea have worked hard to reduce nutrient flows through the Baltic Marine Environmental Protection Commission in Helsinki — also known as the Helsinki Commission — and, since 2008, through the European Union's Marine Strategy Framework Directive. Flows of both nitrogen and phosphorus into the Baltic have fallen since their peaks in the 1980s, mostly because of improved treatment of municipal waste water and reduced discharges from industry.

Phosphorus inputs have dropped by about 30,000 tonnes per year (a 40% reduction from peak loads), and nitrogen by about 400,000 tonnes per year (a 30% reduction). The ambitious Baltic Sea Action Plan (BSAP), signed in 2007 by nations surrounding the Baltic, agrees to cut phosphorus and nitrogen inputs further, by about 42% and 18% from present levels, respectively, by 2016. The goal is to achieve "good ecological status" for the marine environment by 2021.

Such action is needed to improve water quality and ecosystem health. Despite current efforts, measurements of water quality have so far shown only small improvements, and the area of hypoxia continues to increase. Models predict that, with time, the BSAP should be able to reduce the hypoxic area — as long as nutrients continue to be reduced as planned. It is vital that this happens.

The Baltic Sea is on the path to a healthier state. It would be a shame if high-profile geoengineering projects were to divert funds or attention from the BSAP. Yet that could happen. The Swedish marine agency has said that its funding for the pilot mixing project in the southern Baltic should help Sweden to meet its BSAP requirements. Creative thinking and technology are a vital part of the mix. But they should be directed at reducing land-based sources of nutrients into the Baltic Sea, not at expensive and potentially harmful schemes to engineer a solution. ■

Daniel J. Conley *is a professor at the GeoBiosphere Science Centre, Department of Geology, Lund University, Sweden. e-mail: daniel.conley@geol.lu.se*

1. Gustafsson, B. G. *et al. AMBIO* http://dx.doi.org/10.1007/s13280-012-0318-x (2012).
2. Meier, H. E. M. *et al. Geophys. Res. Lett.* **38,** L24608 (2011).
3. Stigebrandt, A. & Gustafsson, B. G. *AMBIO* **36,** 280–286 (2007).
4. Conley D. J. *et al. Environ. Sci. Technol.* **43,** 3407–3411 (2009).
5. Kumblad, L., Rydin, E., Sjöö Lillieskiöld, G. & Mörk, E. *Fosforfällning för en förbättrad skärgårdsmiljo: ett mesokosmförsök* (BalticSea2020/Swedish Ecology Consulting, 2011); available at http://go.nature.com/o4x6om (in Swedish).

BREATHING LIFE INTO THE BALTIC

Models predict that the action plan to reduce nutrients that flow into the Baltic Sea should be effective at increasing oxygen levels in the water.

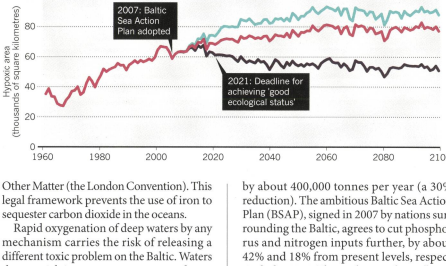

SOURCE: REF. 2

T. STODDART/GETTY

Pork production has risen steadily in Denmark, despite a voluntary halt to using antibiotics to boost growth.

Get pigs off antibiotics

Frank Aarestrup explains how he helped Denmark to cut the use of antibiotics in its livestock by 60%, and calls on the rest of the world to follow suit.

The amount of antibiotics consumed by livestock worldwide is almost double that used by humans, according to some estimates[1,2]. In the United States, for instance, about 300 milligrams of antibiotics are used to produce every kilogram of meat and eggs[3,4]. These drugs are administered not just to treat or to prevent infections. In many countries, they are used to help the animals to grow faster. This is an unsustainable situation. Since many farmers began giving antibiotics to livestock in the late 1940s, people have been infected with strains of bacteria that are resistant to those antibiotics[1,2,5].

To try to combat this dangerous trend, the European Union banned the use of antibiotics for growth in livestock in 2006. The practice continues unabated in the United States, despite a statement from the Food and Drug Administration in April suggesting that farmers should stop voluntarily[6].

Some argue that, without antibiotics, the agricultural industry will collapse. My experience in Denmark proves otherwise. The country is the world's largest exporter of pork, exporting 90% of all it produces, and it did much more than ban the use of antibiotics for growth. It reduced their usage overall and built a comprehensive surveillance system to track and target overuse. It also prohibited veterinarians from profiting from the sale of drugs to farmers — a practice that continues in the United States and in much of Europe.

Since the mid-1990s in Denmark, the use of antimicrobial agents per kilogram of livestock produced has dropped by 60%. And pork production has actually increased by 50% since 1994, before any interventions began.

Any country trying to limit the use of antibiotics in livestock can learn from what my colleagues and I did in Denmark, adjusting what worked there to local needs. Given how difficult it is to control how resistant bacteria behave and spread worldwide, reducing antibiotic use is something we must do for the future health of all — animals and people.

"Vets were making a huge profit selling antibiotics to farmers."

A GROWING PROBLEM

I got involved in helping Denmark to reduce its overuse of antibiotics almost by accident. In September 1994, I was a recently graduated vet, doing my PhD in bovine mastitis and one of its main causes, the bacterium *Staphylococcus aureus*, when I saw some data that worried me. At the annual meeting of the Danish Veterinary Association in Askov, researchers showed an increase in prescriptions for and usage of cheap tetracycline in animals — and a concurrent rise in resistance to the antibiotic among bacteria cultured from animals. These data prompted a heated debate and revealed that many vets were making a huge profit from selling antibiotics to farmers.

At that point, scientists were already concerned about the overuse of antibiotics in livestock. Farmers have been using antibiotics to boost growth since just after the Second World War, when there was a lack of good-quality feed. Experiments at the time showed that animals grew faster when fed low levels of the drugs — although researchers have never fully explained why[1]. The practice spread quickly. As early as the 1960s, scientists began to see the same resistant bacteria in food animals and humans[1,7]. This was no surprise. Bacteria linger in skin and faeces and can easily make their way into meat and onto the hands and kitchen counters of people preparing it. So, starting in the 1970s, countries in Europe[1] began banning the use of antibiotics for growth, particularly those drugs that were being used therapeutically in humans[7].

After some prompting from my collaborator, the German microbiologist Wolfgang Witte, I decided to investigate whether farmers in Denmark prescribed antibiotics to animals purely for growth. I found, to my surprise, that this was common practice. In

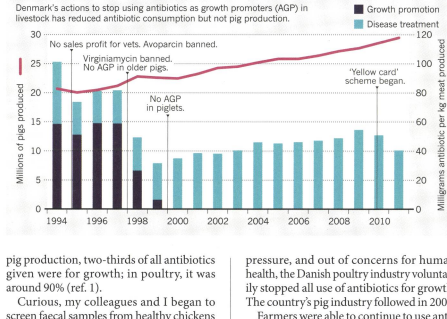

pig production, two-thirds of all antibiotics given were for growth; in poultry, it was around 90% (ref. 1).

Curious, my colleagues and I began to screen faecal samples from healthy chickens and pigs. On 25 January 1995, we isolated for the first time a bacterium that was resistant to one of the growth-promoting antibiotics[8]. Subsequent studies showed a clear relationship between the use of a growth promoter called avoparcin and the widespread occurrence of resistant bacteria[1]. This prompted the Danish government to ban the use of avoparcin to promote growth in livestock. Soon after, in 1997, the EU banned all use of avoparcin.

This became a major story in Denmark, and I began travelling to meetings and taking phone calls from the media and government agencies, all while trying to finish my PhD. Eventually, the director of the institute I was working at, the National Veterinary Laboratory in Copenhagen, asked me to focus on antibiotic resistance full time, including monitoring the ban on avoparcin. This became the foundation of the first comprehensive surveillance system to monitor the use and health effects of antibiotics in livestock.

In 1995, we established DANMAP, the Danish Integrated Antimicrobial Resistance Monitoring and Research Programme (www.danmap.org). This collaboration between vets and human-disease epidemiologists monitors antimicrobial usage and resistance in animals, food products and humans in Denmark. It collects and analyses samples from slaughterhouses, vets and hospitals to track the effects of policy intervention on antibiotic usage and to detect new problems. The United States, Canada, Japan and several countries in Europe now have surveillance programmes that are modelled on DANMAP.

Meanwhile, as scientists found more instances of antibiotic resistance, the Danish government banned another growth promoter, virginiamycin, in 1998. That year, following much media interest and political pressure, and out of concerns for human health, the Danish poultry industry voluntarily stopped all use of antibiotics for growth. The country's pig industry followed in 2000.

Farmers were able to continue to use antibiotics to prevent and treat infections, which provided a back-door route for some of them to obtain inappropriate prescriptions[9]. In 2010, the Danish agriculture ministry began issuing warning letters — dubbed yellow cards — to the pig farmers who had the highest consumption of antibiotics per pig produced. This has led to a reduction in antibiotic use for therapy of almost 25% during the past two years.

Even before Danish farmers cut back on antibiotics, many predicted that the cessation would have a disastrous effect on productivity and the economy. However, in poultry production, it had no negative effects on either the total kilograms of chickens produced per square metre, or the amount of feed used[10]. In pigs, reducing antibiotics had no negative effects on productivity, number of pigs produced per sow, average daily weight gain or the amount of feed needed to produce a kilogram of meat[9]. In fact, pork production has increased steadily in Denmark as farmers have continued to modernize (see 'Bacon boost').

WHAT WORKED

There were three secrets to our success in Denmark. We had data showing that antibiotics were becoming a problem; there was political will to enforce regulations; and there was cross-sector collaboration between farmers, researchers and authorities.

One of the most important steps was the ban. But legal action means nothing without a way to monitor compliance. For example, Danish authorities use DANMAP to target the farms that are using the most antibiotics, or the most dangerous classes of drugs. Some countries' surveillance systems are not comprehensive enough. Data are not available from all animal species, and the systems do not integrate data from humans and animals sufficiently. Some do record antibiotic resistance, but not all of them track usage.

Denmark took another key step that most countries have not yet taken. The government issued legislation in 1995 preventing vets from profiting from selling antibiotics to farmers. The conflict of interest is clear. The more antibiotics farmers use, the more money these vets make. I believe that this decision had a huge impact on the overuse of antibiotics in livestock. Vets in the United States and most of the EU continue to profit from prescribing these drugs.

In my view, it also helped that my scientific colleagues and I were very open about our findings of bacterial resistance. We communicated results in our annual meeting and through regular DANMAP reports, among other methods, even to people who we knew would take issue with what we had to say.

Reducing Denmark's reliance on antibiotics was far from easy. My lab was visited by pharmaceutical executives who did not like what we were finding, and I would be cornered at meetings by people who disagreed with our conclusions. I have even been publicly accused of being paid to produce biased results. Despite such challenges, it has been satisfying to see that Danish farmers and their livestock can thrive without the heavy use of antibiotics. With a little effort, I believe that other countries can and must help their farmers to do the same. ■

Frank Aarestrup *is a professor in microbiology and head of the EU Reference Laboratory for Antimicrobial Resistance and the WHO Collaborating Centre for Antimicrobial Resistance in Foodborne Pathogens at the National Food Institute, Technical University of Denmark, Lyngby, Denmark.*
e-mail: fmaa@food.dtu.dk

1. Aarestrup, F. M. *APMIS Suppl.* **101,** 1–48 (2000).
2. World Health Organization. *The Evolving Threat of Antimicrobial Resistance: Options for Action* (WHO, 2012).
3. Food and Drug Administration. *2010 Summary Report on Antimicrobials Sold or Distributed for Use in Food-Producing Animals* (FDA, 2011); available at http://go.nature.com/mfdtka.
4. FAOSTAT. *Food and Agricultural Commodities Production* (FAO, 2010); available at http://go.nature.com/hzrvqt.
5. Aarestrup, F. M., Wegener, H. C. & Collignon, P. *Expert Rev. Anti. Infect. Ther.* **6,** 733–750 (2008).
6. Food and Drug Administration. *The Judicious Use of Medically Important Antimicrobial Drugs in Food-Producing Animals* (FDA, 2012); available at http://go.nature.com/z1lxxz.
7. Swann, M. M. *Report of the Joint Committee on the Use of Antibiotics in Animal Husbandry and Veterinary Medicine.* (HMSO, 1969).
8. Aarestrup, F. M. *Microb. Drug Resist.* **1,** 255–257 (1995).
9. Aarestrup, F. M., Jensen, V. F., Emborg, H. D., Jacobsen, E. & Wegener, H. C. *Am. J. Vet. Res.* **71,** 726–733 (2010).
10. Emborg, H., Ersbøll, A. K., Heuer, O. E. & Wegener, H. C. *Prev. Vet. Med.* **50,** 53–70 (2001).

SOURCE: REF. 9/WWW.DANMAP.ORG

nature

Nature Awards for Mentoring in Science – The Nordic Countries

For its annual awards for science mentorship in 2012, *Nature* invites nominations of outstanding scientific mentors in the Nordic countries – Denmark, Finland, Iceland, Norway, Sweden and Greenland. Two prizes of €10,000 (or the equivalent local currency) will be awarded, one for a mid-career mentor and one for life-time achievement in mentoring.

Nominations are now open. The closing date for entries is 13 August 2012.

Nominate your mentor today!

nature.com/nature/mentoringawards/nordiccountries

nature publishing group npg

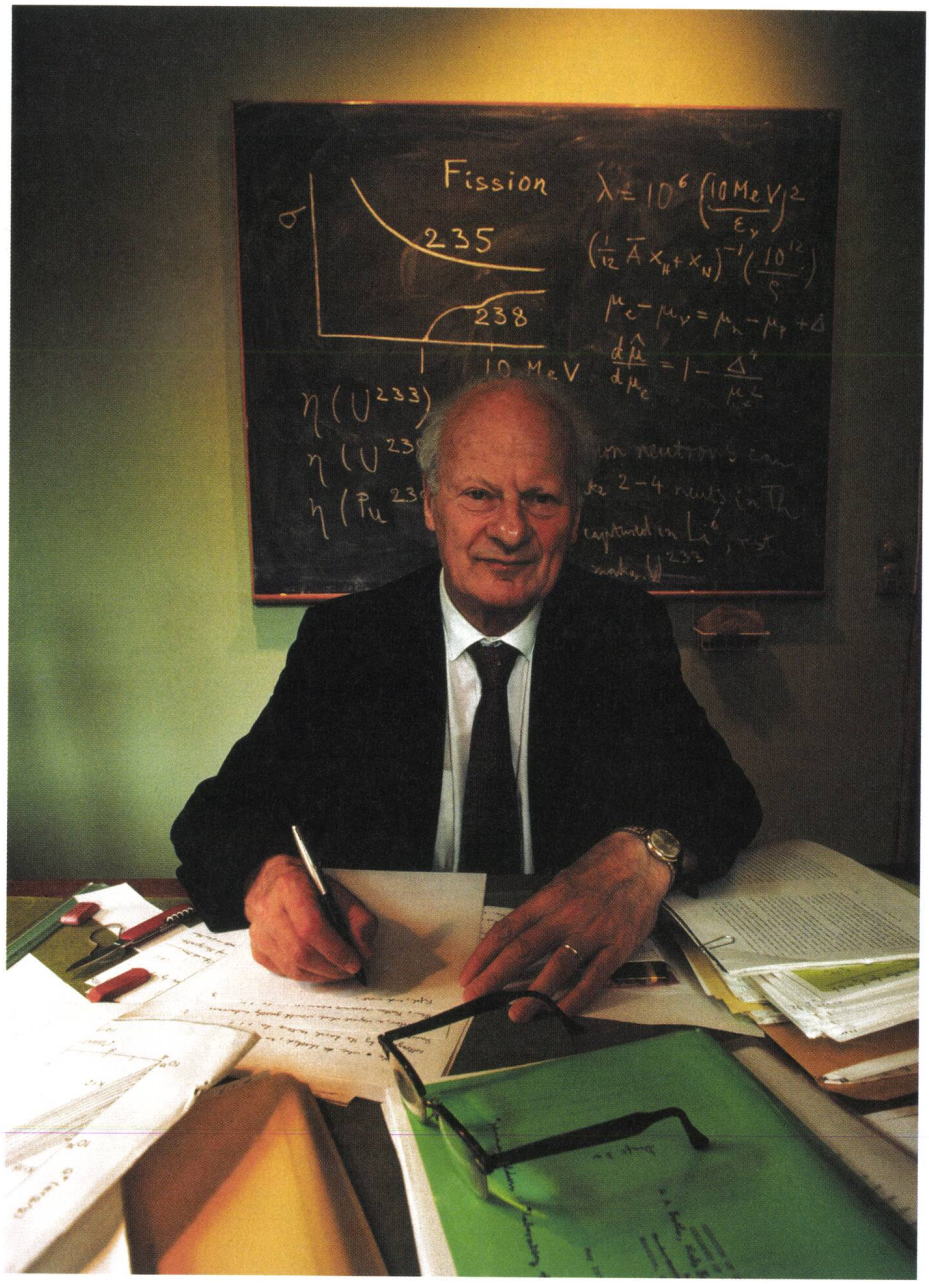

S. BRIMBERG/NATL GEOGRAPHIC/GETTY

Hans Bethe, who won a Nobel prize for his work on stellar energy processes, pictured in 1979.

PHYSICS

A shining life

Frank Close enjoys the life of Hans Bethe, a Manhattan Project veteran who probed the hearts of stars.

Hans Bethe was one of the outstanding scientists of the twentieth century, making seminal contributions to almost all areas of theoretical physics. When he died in 2005, aged 98, he was the last of the generation whose members had, in their youth, established quantum mechanics as the descriptive theory of the atomic world. He was also one of the last veterans of the Manhattan Project.

Nuclear Forces, by the distinguished physicist Silvan Schweber, tells the story of the first three decades of Bethe's life and career, up to the time of his Nobel-prizewinning work on nuclear reactions in stars. But the book offers much more besides, with a history of the development of physics — atomic, solid-state and nuclear — in the first third of the twentieth century, and of the institutions in which Bethe worked.

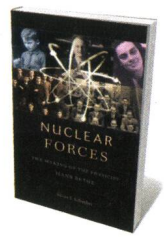

Nuclear Forces: The Making of the Physicist Hans Bethe
SILVAN S. SCHWEBER
Harvard University Press: 2012. 518 pp. £25.95, $35.00

Schweber's analysis of the physics is the book's great strength. Readers conversant with Schrödinger's equation will find it deeply informative. But this is not a book for the faint-hearted, and at times it is hard to determine its target readership. For example, although the concept of the electronvolt is spelled out in some detail, elsewhere we are assured, without further amplification, that "By virtue of the finite range of nuclear forces only the L = 0, s-wave phase shift contributes to the cross section".

Bethe himself sometimes disappears for pages on end as the author provides background. One section covers the history of Cornell University in Ithaca, New York, where Bethe settled. Another explores Jewish intellectualism in German science and the experience of being a Jew in Germany in the 1930s, which were the environments in which Bethe developed. These digressions enrich our understanding of who Bethe really was, and of his milieu.

The complicated role of women in Bethe's life comes through well. His letters revealed that he loved his mother dearly, but that she managed to destroy his potential nuptials with the scientist Hilde Levi. Levi worked in physicist Niels Bohr's institute in Copenhagen, and she and Bethe had planned to marry in 1934. His mother's "continual battering" wore him down and a few days before the wedding, Bethe called it off.

Bohr disapproved, and never subsequently invited Bethe to the annual conferences he hosted in Copenhagen. Schweber notes that Bethe never visited Bohr's institute after he moved to the United States in 1935, although he did go to Europe to see his parents.

Schweber's careful research offers a postscript to this tale. He showed Levi a draft of the relevant chapter, and she told him that Bethe had been prepared to go through with the wedding. It was his mother who had forced the issue by sending a telegram to Levi "stating that the engagement was being broken. Hans's letter to Hilde came thereafter." Later, Schweber reveals, Bethe's mother almost thwarted him again when he set out to marry Rose Ewald, who became his companion for more than 60 years.

NATURE.COM
To read about physicist Edward Teller, see:
go.nature.com/idfuh9

Bethe's long friendship with the great German theoretical physicist Rudi Peierls also comes to life in *Nuclear Forces*. Between 1933 and 1934, Bethe spent a year in Manchester, UK, staying with Peierls' family. In a letter to Arnold Sommerfeld, his mentor, Bethe offers a portrait of a place and an era, remarking that his coal-dust-covered window was cleaned in the spring, after which he could see the rest of the campus "on days when there was no fog".

That year with Peierls was in Bethe's opinion the most productive of his career. He became enamoured of nuclear physics; met Patrick Blackett, an experimental physicist known for his work on cosmic rays; spent time in Bristol, UK. He then moved to Cornell for good. Had someone had the initiative, or daring, to create a position for him in Britain, the course of theoretical physics on two continents might have been very different.

Having settled in the United States, Bethe went to the Washington Conferences on Theoretical Physics every year from 1935 until 1937. He decided not to take part in 1938, because the subject was energy production in stars and "he wasn't interested in that problem". At the urging of fellow émigré Edward Teller, he finally went, and what he heard led him to discover the CNO cycle in stars, in which reactions between protons and nuclei convert carbon sequentially into nitrogen and oxygen and back to carbon, liberating energy. And he identified the dominant processes that power the Sun. At first, the editor of *Physical Review* was not enthused by the CNO article. The resultant delay in publishing proved fortunate for Bethe: it enabled him to win the New York Academy of Science's US$500 prize for an unpublished work on stellar energy. The same work was later instrumental in him winning the Nobel Prize in Physics.

"At first, the editor of Physical Review *was not enthused."*

There is no mention of the legendary story of a romantic walk under the stars, on which Bethe tried to woo Ewald by commenting that at that moment, he was probably the only person on Earth who understood why stars shine. None too impressed, she reportedly replied, "That's nice."

Nuclear Forces does tell a similar story, in which a woman comments on how beautifully the stars shine and her companion proudly responds, "I've known since last night why they shine". The speaker was the atomic physicist Fritz Houtermans, whose early work was part of Bethe's inspiration. Whichever version you prefer, it is a good story. ■

Frank Close *is a professor of theoretical physics at the University of Oxford, UK. e-mail: f.close1@physics.ox.ac.uk*

Books in brief

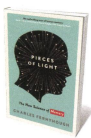

Pieces of Light: The New Science of Memory
Charles Fernyhough PROFILE BOOKS *352 pp. £14.99 (2012)*
We are our memories, says psychologist and writer Charles Fernyhough. Without them, we would be "lost to ourselves". Fernyhough deftly guides us through memory's many facets, from types (autobiographical, episodic, semantic, explicit, implicit, working) to mental mapping, trauma, sense associations such as the smell of fresh paint or a bar from Bach, and the evocative stories of his aged grandmother. Often using himself as a test case, he adds context with research and snippets from a raft of great writers. A thoughtful study of how we make sense of ourselves.

The Violinist's Thumb And Other Lost Tales of Love, War, And Genius, as Written by Our Genetic Code
Sam Kean DOUBLEDAY *416 pp. £20 (2012)*
In this successor to *The Disappearing Spoon* (Little, Brown, 2010), his bestseller on the periodic table, science writer Sam Kean explores the complexities of heredity. The broad focus on DNA allows dazzling diversions: Niccolò Paganini's eponymous thumb; the supersaturation of polar-bear livers with vitamin A; the case of Tsutomu Yamaguchi, who survived both Hiroshima and Nagasaki to live to 93; the key contributions to the field by Dominican nun and chemist Miriam Michael Stimson among others; and much more.

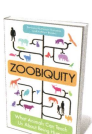

Zoobiquity: What Animals Can Teach Us About Health and the Science of Healing
Barbara Natterson-Horowitz and Kathryn Bowers KNOPF *320 pp. £17.23 (2012)*
Medically, how different are humans from other animals? Cardiologist Barbara Natterson-Horowitz began to probe the divide after learning that emperor tamarins can get stress-related capture myopathy — identical to the human heart condition takotsubo cardiomyopathy. With science journalist Kathryn Bowers, she covers case studies of conditions common across species, such as cancer and heart attacks, and calls for physicians and veterinarians to share data.

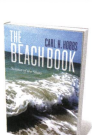

The Beach Book: Science of the Shore
Carl H. Hobbs COLUMBIA UNIVERSITY PRESS *192 pp. £41.50 (2012)*
With 44% of humans living 150 kilometres from a coast, according to United Nations figures, the sea's pull is undeniable. Marine scientist Carl Hobbs peels back the façade of sun and surf to explore the science of the strand. He examines in turn the shore itself, wind, waves, tides, sediments, barrier islands and tidal inlets, sand dunes and salt marshes, sea-level rise, erosion and storms. Fascinating phenomena — from surf beat, edge waves and beach cusps to the dunes known as barchans — bob through this crisply written guide to ecology and geology at the edge.

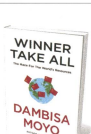

Winner Take All: The Race for the World's Resources
Dambisa Moyo ALLEN LANE *272 pp. £20 (2012)*
Economist Dambisa Moyo, whose hard-hitting *Dead Aid* (Penguin, 2010) criticized 'top-down' aid, pulls no punches in this investigation of China's global 'shopping spree' for resources. Moyo interweaves history into her analysis of the economic implications of China's ascendancy as trade partner and commodities buyer; its influence on markets and resource prices; and the social and political impacts of its investments. There may, she says, be a demographic brake on the resource rush — but commodity crises and wars cannot be ruled out.

C. CAMPBELL/N. MCGOWAN

In *Loitering Theatre*, artists used airborne cameras to film hidden parts of Dublin.

CITIES

Metropolitan mash-up

Anthony King enters a parallel city that teems with hackers innovating for the public good.

Embrace your inner hacker. That is the exhortation of the exhibition *Hack the City* at the Science Gallery in Dublin. Here, science, technology and art mingle in an exploration of how urban spaces and systems such as WiFi networks can be mashed up, recreated and subverted for the public good.

With 70% of the world's population predicted to be living in cities by 2050, the pressure to ensure that these are sustainable, equitable environments is growing. In *Hack the City*, Dublin is the test case for workshops and exhibits probing issues ranging from urban-dwellers' authority, autonomy and ownership to their freedom of expression and social bonds. The timing is apt: during the exhibition's run, Dublin will host the Euroscience Open Forum 2012, a gathering of scientists and policy-makers from across Europe.

The gallery is eager to distinguish between malicious 'cracking' and hacking. The hacking ethos, argues lead curator Teresa Dillon, is about citizens sharing resources and wresting back control from planners and commercial interests. A hacker, she explains, is "a craftsperson who looks at a particular system, identifies weaknesses and creates alternative solutions for their own and others' benefit". Apple co-founder Steve Jobs was an early hero of the hacking community.

'Hacklab' workshops will introduce visitors to crowdsourced science, data manipulation, environmental monitoring and more. For example, 'Sensing the City' is a series of citizen-science experiments that will run in late July and early August. Researchers from IBM and Dublin's Trinity College will offer lessons on how to map urban biodiversity and track waste to create a greener city. Other workshops and projects will show visitors how to turn their phones into noise-measuring devices and explore traffic-noise maps, or to make computer measurements of air pollution.

> *"Hacking is about citizens sharing resources and wresting back control from commercial interests."*

Berlin-based artists Julian Oliver and Danja Vasiliev will showcase Newstweek. This is an innocuous-looking wall plug that, placed in a WiFi hotspot, enables you to alter any news being read on nearby wireless devices such as smart phones. The plug answers faster and more frequently than other hosts, and can route all localized traffic through itself. The stunt shows how a strictly media-defined reality is vulnerable to manipulation, say the artists.

Hack the City
Science Gallery, Dublin. Until 8 September 2012.

Euroscience Open Forum 2012
Dublin. 11–15 July 2012.

A loaded issue in modern cities is the freedom to gather in open public spaces. In the ongoing 'Uncommon Land' project, artist Eilis Murphy explores the creeping privatization of those spaces. In May, for example, she called together a flash mob of 35. Armed with cameras, the crowd shot more than 1,300 images and 50 minutes of video, starting in the privately owned Mayor Square, where photography is banned, and finishing in Commons Street, one of the few remaining publicly owned streets in Dublin's International Financial Services Centre. A distillation of the images is exhibited, and will eventually be uploaded to Google Maps.

'The Sentient City Survival Kit', by architect and artist Mark Shepard, is a collection of artefacts for a near-future city in which retail could invade privacy through item tagging and data-skimming. Shepard offers 'his and hers' bras and boxer shorts that vibrate to alert the wearer to hidden radio frequency identification (RFID) tag readers nearby.

'Loitering Theatre', by film-maker and digital-rights expert Caroline Campbell and visual artist Nina McGowan, turns the tables on urban surveillance. They used iPad-controlled quadcopters — small, rotor-powered aircraft — with cameras on the front to film normally inaccessible views of Dublin. Examples include Facebook's un-signposted European headquarters, and houses hidden behind hoardings in the development wastelands, where, Campbell explains, an elderly lady saved her garden of lilies from the property boom. They hope that this visual information will catalyse ideas on how to improve the Dublin cityscape.

And in a robotic 'hack' of the city's physicality, the small spidery-armed, insect-shaped robots in artist Jérôme Abel's 'Chimères Orchestra' tap out rhythms in the gallery and the Temple Bar area. Abel's schematics and codes will be available online, so anyone can duplicate and modify them.

The hacking ethos has inspired people across the disciplines, from open-source publishers to amateur biohackers practising garage biology. This exhibition is a paean to hacker culture and a call to arms for the rest of us to harness our powers of invention to push our cities in the directions we want them to go. ■

Anthony King *is a writer based in Dublin. E-mail: anthonyjking@gmail.com*

FICTION

Ray Bradbury, an appreciation

Astronomer and author **David Brin** celebrates the legacy of a literary titan whose life-long pursuit of new horizons changed the face of science fiction.

Brilliant science fiction can ignite scientific ambition. After the death of Ray Bradbury on 5 June, thousands of researchers must have reflected on the inspirational power of his works. The author of *The Martian Chronicles* (1950), *The Illustrated Man* (1951) and *Fahrenheit 451* (1953) died in Los Angeles at the age of 91, ruminating and planning stories until the end.

Bradbury was the last living member of the 'BACH quartet' — made up of himself, Isaac Asimov, Arthur C. Clarke and Robert Heinlein. In the 1950s and 1960s these men pulled science fiction from its pulp-magazine ghetto into the hardcover best-seller lists. Asimov, Clarke and Heinlein helped to shatter barriers, establishing the legitimacy of literature that explores plausible tomorrows. But it was Bradbury who made clear to everyone that science fiction can be an art form combining boldness and broad horizons with beauty.

Often, when an author of future-oriented fiction achieves mainstream literary acclaim, there is a temptation to announce, "I don't write sci-fi," as if dropping the label will ensure escape from the ghetto. But when Bradbury said that, he meant the opposite. He wrote mostly fantasy, horror and suspense because, he once told me, "I can't do science, but that's my loss." He never learned to drive and for most of his life avoided aeroplanes, but Bradbury's works had a major influence on space travel and exploration. He became a fixture on television, interviewed whenever some epochal milestone — such as the first Moon landing — was achieved.

In his 1950 breakthrough anthology, *The Martian Chronicles*, rocket ships are taken for granted. The book omits any technical details. The rockets are simply marvellous conveyances that deliver the characters to a frontier where awe mixes with terror and unquenchable hope. Bradbury's doomed Martians are more than just surrogates for native, colonized peoples. They are also humanity's complex and flawed elder siblings on the ladder of wisdom, instructing in spite of their fatal errors.

Readers loved the rockets, but the characters taught us about balance and cost.

Bradbury's great novel, *Fahrenheit 451*, took up a very different tradition: the self-preventing prophecy. The author wrought a tale of book-burning and political correctness gone wild that filled readers first with shock, then with determination to thwart that possible future. He thus joined the ranks of authors such as George Orwell, whose *Nineteen Eighty-four* (1949) and other works frightened millions into taking action through politics and daily life. Again, it was not futuristic technology that made *Fahrenheit 451* effective. The book is, instead, a potent example of what Albert Einstein called the *Gedankenexperiment*, or thought experiment — the essence of good science fiction.

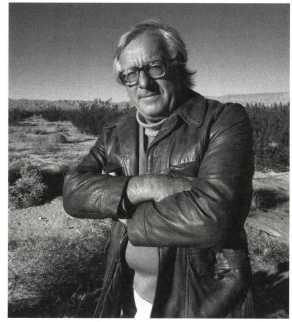

T. KORCOY/SYGMA/CORBIS

Ray Bradbury helped to relaunch science fiction as art form.

Ray Douglas Bradbury was born in 1920, in Illinois. When he was 13, his family moved to Los Angeles, California, where he remained for the rest of his life. Among many early influences on a fertile young imagination was the fact — very exciting to a child — that one of his ancestresses had been tried as a witch in Salem, Massachusetts, in the late seventeenth century. He often described the lasting impressions left by the films of early-twentieth-century horror actor Lon Chaney Senior, and the occasion when a stage magician shocked Bradbury's nose with an electric sword, commanding him to "live forever!" A child of the Depression, Bradbury nurtured his love of writing in free public libraries and while hawking newspapers on street corners.

Like many authors who followed, Bradbury started out writing stories for mimeographed fan publications of the 1940s, climbing gradually upwards while honing his craft. His skills later took him to Hollywood, where he scripted films such as John Huston's *Moby Dick* (1956) and the US television series *Ray Bradbury Theater* (1985–92), while raising four daughters and penning one luminous book after another.

Bradbury's stories and novels often plunged into dark themes. There is satanic-huckster villainy in *Something Wicked This Way Comes* (1962), and the 1954 short story *All Summer in a Day* starkly reveals how basic the tendency toward cruelty is, and that childhood is neither pure nor innocent. His scientific readers forgave things such as his water-drenched Venus and untechnological plot-drivers, including monsters and childhood terrors under the bed.

Could anyone reconcile this chain of chillers with Bradbury's self-proclaimed optimism? He himself did. Human beings are fretful creatures, he said. Our worries often cause us to shine light in dismal corners, and thus help us to do better. To be better.

In fact, Bradbury had a lot to say about a human trait he despised: cynicism. His word for it was treason. Treason against a world — and humanity — that had, in his view, improved enormously over the course of a generation in terms of technological achievements, and in ethics and behaviour. The racism, sexism and class prejudice that our ancestors took for granted may not have been eliminated, but society had at least succeeded in pushing them into ignominy.

Ray Bradbury's writing danced along the boundaries between mystery, sci-fi, horror and fantasy. What mattered to him most was the direction we are heading: forwards, propelled by ever-growing knowledge and the will to peer even farther. ■

David Brin *is an astronomer and author of 15 novels translated into more than 20 languages. His latest novel is* Existence. *e-mail: david.brin@gmail.com*

NATURE.COM
For *Nature*'s online special on science fiction, visit:
go.nature.com/mqc2jd

JAMES DUNCAN DAVIDSON/TED

Imogen Heap produces music with gestures, thanks to Tom Mitchell's glove technology.

Q&A Tom Mitchell

The sound catcher

Tom Mitchell uses engineering and computing to enable people to play and sample live music using gestures. With the latest version of his co-creation 'The Gloves' about to debut at TEDGlobal 2012 in Edinburgh, UK, he talks about adaptive musical interaction.

How do 'The Gloves' work?

The team combined data gloves to measure finger flexion, inertial devices to measure orientation and optical sensors to measure position. Gestures enable a range of tasks. You can 'catch' your voice by singing into your hand, where a microphone records and loops phrases. Opening the hand allows a synthesizer to be played; percussive gestures trigger drums. Reaching for the sky adds reverb; the heavy-metal sign adds distortion.

How did you start to work with Imogen Heap?

I met Imogen at a wedding, and started helping her to use technology in performances. She would manipulate audio using keyboards, drum pads and controllers. Then she met Elena Jessop at the Massachusetts Institute of Technology in Cambridge, who had invented a glove to freeze the timbre of a singing voice. Imogen wanted the audience to relate her actions to the production of music, and asked for a live music system reliant on gestures. The result, she says, lets her perform more fluidly; it is also faster and more intuitive than using a keyboard or computer to compose.

What is your 'evolutionary' approach to audio synthesis'?

I wanted to build an algorithm to reproduce a target sound, such as a cello, voice or sound effect. I used an optimization method modelled on Darwinian natural selection. My program synthesizes sounds, selects those that most closely match the target then recombines and mutates their 'genes' to engender the next generation, advancing towards an optimal solution.

Does that come into your gestural work?

I have plans for experiments that will allow users to describe a timbre using gestures, which can be matched using evolutionary synthesis, allowing 'sound sculpting'.

How did you become interested in electronics and music?

I rejected classical music training but was drawn to machines. In the 1980s, I wrote accompaniments for my sister, a pianist, using a Spectrum computer. I borrowed equipment from electronic-music artist Tom Jenkinson (later recording as Squarepusher), who exploited his equipment's idiosyncrasies by using a hacked cassette machine to simulate a multitrack recorder, or a mixing console to create feedback loops. I built Musical Instrument Digital Interface (MIDI) programs to control synthesizers. Pursuing electronic engineering at university, I studied audio sampling and synthesis, and completed a doctorate combining music and computer science.

TEDGlobal 2012
Edinburgh International Conference Centre, UK. 25–29 June 2012.

What other controllers would you like to see?

We've come a long way since the theremin, the first electronic gestural music controller. Examples from recent years include the Eigen Harp and Karlax, whose sensor-driven interfaces resemble traditional instruments. I would like to see a move away from garments and sensors that constrain movement; camera-based devices have pushed things forward. I can't wait to get my hands on Leap by Leap Motion: a device that allows you to control a computer with fine hand and finger movements. It would be nice for people to be able to program their own systems using any gestures, and I look forward to interfaces as adaptive and versatile as touch screens.

Could this technology be put to other uses?

Yes. The gestural-interface system that we are working on could have applications in animation, gaming and robotics. At the Bristol Robotics Laboratory, based at the University of Western England, where I also work, a similar arrangement is used to design systems that let a robot understand human gestures meaning 'pass me that spanner' and so on.

What is next for you?

I have been helping to expand the capabilities of 'The Gloves' to allow Imogen to write and perform a song from scratch. The system made its debut for the release this year of the song *MeTheMachine*, as part of Imogen's *Heapsongs* series. I am working on machine-learning techniques for synthesis matching and gesture identification and looking at developing the gloves commercially. I've started working on the sonification of chemical reactions and quantum-mechanics simulations, and am collaborating with x-io Technologies in Bristol to build a commercial interface for multimedia interaction.

Is there a future for old-fashioned musical instruments?

Certainly. They are being augmented with sensors that exploit the musicians' 'spare bandwidth' — communicative gestures that don't produce sound. Dan Overholt's Overtone Violin uses sonar and glove-mounted accelerometers, among other sensors. To paraphrase David Wessel, a professor of music at the University of California, Berkeley, instruments should reward quickly, but allow scope for virtuosity. ■

INTERVIEW BY JASCHA HOFFMAN

ILLUSTRATION: NICK HIGGINS (ORIGINAL PHOTO: TIM WARD)

Correspondence

Carson no 'beacon of reason' on DDT

We disagree with Rob Dunn's view that Rachel Carson's 1962 book on human environmental impacts, *Silent Spring*, still stands as a "beacon of reason" (*Nature* **485,** 578–579; 2012).

The insecticide DDT (dichlorodiphenyltrichloroethane) was arguably the most successful chemical ever synthesized to control malaria and other insect-borne diseases. However, *Silent Spring* led to a US ban on DDT use in 1972.

Carson branded DDT as dangerous because of its effects at high doses on experimental rodents and birds. But it was already known that humans experienced no ill effects after consuming 35 milligrams of DDT daily for two years — a dose 1,000 times higher than that received from agricultural exposure. Thousands of pesticides occur naturally in fruit and vegetables and are consumed daily. Around half of these also cause cancer at high doses in rodent tests (B. N. Ames and L. S. Gold *Mutat. Res.* **447,** 3–13; 2000).

DDT is an organohalogen and is concentrated in the food chain, as are many of the organohalogens naturally synthesized by marine and land organisms; some are also found in breast milk (G. W. Gribble *Chemosphere* **52,** 289–297; 2003). But persistence does not equate to harm.

Carson claimed that insect resistance would quickly reduce DDT's effectiveness. But DDT is largely a mosquito repellent, not a toxicant. Repellent resistance has not yet emerged, whereas toxicant resistance is widespread.

Contrary to Dunn's claims and Carson's predictions, the bald eagle had become rare long before DDT, and American robins increased during the 1960s.

At the time of the DDT ban in 1972, 1 billion people were almost malaria-free. Within a few years, malaria cases had risen 10–100-fold. Over 40 years, estimates suggest that there have been 60 million to 80 million premature and unnecessary deaths, mainly children, as a result of misguided fears based on poorly understood evidence.

Tony Trewavas* *University of Edinburgh, UK. trewavas@ed.ac.uk*
**On behalf of 11 co-signatories (see go.nature.com/2hfmok).*

Help to survey the use of smart drugs

We call on *Nature* readers to help us to achieve the highest possible response from students in the United Kingdom or Ireland to a survey on the use of pharmacological drugs for cognitive enhancement (see www.thesmartdrugstudy.com).

In 2007, *Nature* urged academic institutions to address the ethical and regulatory challenges associated with the use of psychotropic drugs that improve cognitive performance in the healthy — notably medications for attention-deficit hyperactive disorder (ADHD) and narcolepsy (*Nature* **450,** 320; 2007). The following year, an informal global survey by *Nature* suggested that as many as one in five academics used cognition-enhancing drugs for non-medical reasons (*Nature* **452,** 674–675; 2008).

Outside the United States and Germany, empirical evidence on the use of cognitive enhancers is sparse (for a review, see C. I. Ragan, I. Bard & I. Singh *Neuropharmacology*; in the press). UK policy discussions have relied mainly on ambiguous US data.

Our survey, in collaboration with the UK Independent Scientific Committee on Drugs, will provide a comprehensive analysis of the use of pharmacological cognitive enhancers by students in the broader context of their substance use. We shall use the results to assess prevalence, concerns, frequency and motivation, and sources and pricing. We will also analyse the perceived effects and side effects, perceptions of social coercion and regulatory measures, and correlation with self-reported ADHD symptoms.

Imre Bard, Ilina Singh *London School of Economics & Political Science, London, UK. i.a.singh@lse.ac.uk*

Less lactation may explain cancer rise

Your Outlook supplement on breast cancer (*Nature* **485,** S49–S66; 2012) does not mention the protective effect of breastfeeding. In most populations, this seems to be even stronger than that conferred by regular exercise (*Nature* **485,** S62–S63; 2012), especially when lactation is extended over several children (S. Ip *et al. Evid. Rep. Technol. Assess.* **153,** 1–186; 2007).

Genetic factors and early puberty both play a part in development of the disease. But these cannot fully account for the increasing incidence of breast cancer in the developed world, given that the genetic make-up of populations is unlikely to have changed much over the past few decades and puberty now starts only slightly earlier.

One change is that Western families have become smaller, so total breastfeeding over a mother's lifetime has declined. Oestrogen exposure, normally suppressed during lactation, is therefore effectively prolonged, increasing the likelihood of developing some types of breast tumour.

Anne Marie Oudesluys-Murphy *Leiden University Medical Centre, Leiden, the Netherlands. h.m.oudesluys-murphy@lumc.nl*

Limit consumption to preserve habitats

Consumption by wealthy nations is driving environmentally hostile production in the developing world, which can threaten species and their habitats (see, for example, M. Lenzen *et al. Nature* **486,** 109–112; 2012). But balancing this unsustainable ecological debt won't be straightforward.

Although consumption-curbing policies in wealthy nations are urgently needed, their potential for adverse effects on the development of poor countries must be taken into account. Changes in demand through international trade could compromise many livelihoods, holding back sustainable development.

Governments in the developing world can help by strengthening their regulations to eliminate environmentally damaging production techniques, with technical and financial assistance from rich nations if necessary.

In summary, possible solutions should consider the interests and needs of both developed and developing nations (see, for example, the latest United Nations report on economic development in Africa; go.nature.com/qjmusf).

Marco Sakai *Sustainability Research Institute, University of Leeds, UK. ee08masd@leeds.ac.uk*

Clue to an ancient cosmic-ray event?

It is tempting to speculate that the ancient text of the *Anglo-Saxon Chronicle* might offer a clue to the cause of the mysterious, dramatic cosmic-ray event in AD 774 (F. Miyake *et al. Nature* **486,** 240–242; 2012).

A chronicle entry for the same year (see go.nature.com/wwkw5j) hints at the presence of a supernova largely hidden behind a dust cloud, which would scatter and absorb all light bar a trickle of red. The resulting supernova remnant would be invisible.

The entry notes: "This year also appeared in the heavens a red crucifix, after sunset; the Mercians and the men of Kent fought at Otford; and wonderful serpents were seen in the land of the South-Saxons."

Jonathon Allen *University of California, Santa Cruz, California, USA. jokallen@ucsc.edu*

Andrew Fielding Huxley

(1917–2012)

Biophysicist who showed how nerves carry electrical signals and muscles contract.

Andrew Fielding Huxley made three crucial discoveries in physiology and biophysics. For establishing how ions carry electrical signals in nerves, he shared the Nobel prize with Alan Hodgkin and John Eccles in 1963. He also described how molecular motors enable muscles to shorten and exert force and how electrical activity triggers the contraction of muscle fibres.

Huxley died on 30 May at the age of 94. He grew up in Cambridge, UK, in a prominent academic and literary dynasty. To his immense pride, his grandfather, the anatomist Thomas Henry Huxley, 'Darwin's bulldog', had defended Charles Darwin in early debates about evolution. Andrew's half-brothers were *Brave New World* author Aldous and evolutionary biologist Julian Huxley.

Andrew Huxley obtained his undergraduate degree in physiology from the University of Cambridge, UK, in 1938. His research was interrupted by the Second World War, during which he applied himself to developing radar and gunnery. After the war, he did not bother with a doctorate: it is said that no one felt competent to serve on his awarding committee. But to his students, who knew him as Prof, Huxley's formidable intellect was made less daunting by his warmth, modesty and enthusiasm. His marriage to the delightful Richenda Pease resulted in six children.

Huxley first encountered the squid giant axon in 1939, working with Hodgkin at the Laboratory of the Marine Biological Association in Plymouth, UK, and resumed work on it after the war. This large nerve fibre provided the keys to understanding the electrical activity that excites biological cells, which had been a mystery since the eighteenth-century experiments of Luigi Galvani and Alessandro Volta in muscle excitability and electricity.

Huxley and Hodgkin's collaboration with biophysicist Bernard Katz yielded the sodium theory of the action potential. Published in 1952, this work showed that the axon membrane can, within a millisecond, switch from being permeable to potassium ions to being permeable to sodium ions instead, causing a voltage spike termed the action potential. The inflow of sodium ions initiates and reinforces the impulse as it carries a signal along the axon, from a fingertip to the spinal cord to the brain, for example.

Hodgkin and Huxley measured the kinetics and voltage dependence of these permeability changes and expressed them as equations, which Huxley evaluated using a mechanical calculator. Their formulation still provides the framework for our understanding of electrical activity in the nervous system and throughout the body. It presaged the discovery of the sodium and potassium channels central to brain activity and is also the basis for our understanding of the heartbeat, cardiac arrhythmias and many drugs.

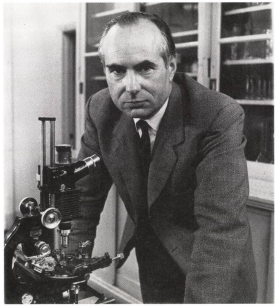

HULTON-DEUTSCH COLLECTION/CORBIS

Huxley turned next to muscle contraction, reviving a boyhood interest in mechanical devices and optical microscopy. He built a two-beam interference microscope and used it to discover how muscle produces force and shortens, and how electrical signals activate contraction.

In 1954, with Rolf Niedergerke (who also died this year), Huxley published the 'sliding-filament' hypothesis, which showed that myosin and actin protein filaments slide relative to one other as muscles shorten. The filaments are propelled by myosin molecular motors that 'walk' along the actin, attaching and detaching. Huxley's ideas underpin a host of molecular motors and cell-motility mechanisms, which are important in the cardiovascular and neurological systems and cancer.

Huxley's second pivotal microscopic observation, published in 1958, showed how voltage differences across the surface membranes of muscle fibres are transmitted deep within the cell along transverse tubules spaced periodically along the fibre. We now know that the signal stimulates the release of calcium ions, which activate the contraction system. Hundreds of similar signal cascades that result in the inward spread of electrical or hormonal excitation have since been discovered in endocrinology, neuroscience and immunology.

Huxley held prominent academic positions — as head of physiology at University College London (beginning in 1960), president of the Royal Society (1980–85), president of the British Science Association (1976–77) and master of Trinity College, Cambridge (1984–90). His management style was meticulous, and at times considered too exacting.

Many of his concerns resonate today: the funding of research and faculty in times of scarcity, industry–university partnerships, the free dissemination of results and England's role in international scientific programmes. Like his grandfather, he spoke strongly for the evaluation of scientific results solely on their merits, and he opposed the suppression of studies on the basis of their unpopularity or for political contingencies.

As postdoctoral fellows in Huxley's laboratory, we had much contact with Prof over the years, although we did not share many publications. He had a strict attitude towards authorship and listed himself only if his contribution was high, but he was always interested and helpful. He had little patience for those who were unprepared, but for those who were, his views were a gold mine.

Andrew Huxley inspired generations of scientists with his careful, imaginative technique and his clear vision. His uses of new instrumentation and the interplay between experimental tests and quantitative models are ideals to be emulated. ■

Yale E. Goldman *and* **Clara Franzini-Armstrong** *are at the Pennsylvania Muscle Institute, and* **Clay M. Armstrong** *is in the Department of Physiology, at the Perelman School of Medicine, University of Pennsylvania, Philadelphia, Pennsylvania 19104, USA.*
e-mail: goldmany@yahoo.com

RESEARCH

NEW ONLINE

Papers published this week at Nature.com/nature

NEWS & VIEWS *SRGAP2*, the gene that made human brains bigger and better **p.481**

LETTER The thousands of isotopes that exist beyond the nuclear comfort zone **p.509**

LETTER How ungainly early tetrapods shuffled their way onto dry land **p.523**

PUBLISHED 24 JUNE 2012

EVOLUTION

New genes from unlikely beginnings

De novo gene birth has occurred in many lineages during evolution but how protein-coding genes emerge in non-functional sequences remains unclear. Anne-Ruxandra Carvunis *et al.* observe in yeast that hundreds of species-specific non-genic transcripts are differentially translated upon stress. These translation events seem to act as a reservoir of adaptive potential on a continuum ranging from non-genic sequences to genes.

Proto-genes and *de novo* gene birth
A-R Carvunis *et al.*
doi:10.1038/nature11184

ECOLOGY

Laws of species distribution

The increase of species richness with area is one of the few known law-like biodiversity patterns. This study assembles species–area and endemics–area relationships for 12,000 bird, mammal and amphibian species across the continents. The data reveal a connection between the size of species' geographic ranges and the spatial 'scaling' of biodiversity that yields a single species–area curve for all taxa and continents. The relationship between area and number of endemic species exhibits similar universality. These findings have important implications for conservation strategies at times of habitat loss.

Universal species–area and endemics–area relationships at continental scales
D Storch *et al.*
doi:10.1038/nature11226

NEUROSCIENCE

Human dorsal anterior cingulate cortex neurons mediate ongoing behavioural adaptation
S A Sheth *et al.*
doi:10.1038/nature11239

PUBLISHED 27 JUNE 2012

PALAEONTOLOGY

A stirring in the woods

Australopithecus sediba is a two-million-year-old hominin from South Africa, related to other *Australopithecus* and early *Homo* species. Using a combination of stable isotope analysis, dental microwear patterns and analysis of plant microfossils extracted from dental calculus, thos paper shows that *A. sediba*'s diet consisted mostly of tree leaves, fruit and bark, suggesting that the species lived in a woodland rather than in a savanna habitat.

The diet of *Australopithecus sediba*
A G Henry *et al.*
doi:10.1038/nature1 1185

EVOLUTIONARY PHYSIOLOGY

Jury out on 'cold' dinosaurs

One case used to argue against endothermy or warm-bloodedness in dinosaurs is the presence of 'lines of arrested growth' in their bone histology, indicating seasonal slowdown of growth. This was considered characteristic of ectothermy, as seen in reptiles and amphibians. Here Meike Köhler *et al.* present a study of wild ruminants — large endothermic mammals — living in climates from the tropical to polar. In all of the animals studied, there is evidence for arrested growth during the unfavourable season. This precludes the use of lines of arrested growth as an argument in support of ectothermy in dinosaurs.

Seasonal bone growth and physiology in endotherms shed light on dinosaur physiology
M Köhler *et al.*
doi:10.1038/nature11264

A bone for all seasons
K Padian
doi:10.1038/nature11382

EVOLUTIONARY PHYSIOLOGY

Muscles stretch back a long way

Structural similarities between striated (skeletal) muscles in bilaterian animals such as humans and insects and non-bilaterians such as jellyfish, suggest a common origin. This phylogenomic study shows that core muscle proteins are present in unicellular organisms, such as sponges, that do not have true muscles. The data support a convergent model for the evolution of striated muscle, in which new proteins are added to the ancient contractile apparatus during independent evolution of cnidarian and bilaterians.

Independent evolution of striated muscles in cnidarians and bilaterians
P R H Steinmetz *et al.*
doi:10.1038/nature11180

ECOLOGY

Atmospheric CO_2 forces abrupt vegetation shifts locally, but not globally
S I Higgins & S Scheiter
doi:10.1038/nature11238

ORGANIC CHEMISTRY

Direct and highly regioselective and enantioselective allylation of β-diketones
W A Chalifoux *et al.*
doi:10.1038/nature11189

Reactions at the end of a tether
S Roesner & V K Aggarwal
doi:10.1038/nature11381

IMMUNOLOGY

Biophysical mechanism of T-cell receptor triggering in a reconstituted system
J R James & R D Vale
doi:10.1038/nature11220

MEDICAL RESEARCH

Myocardial infarction accelerates atherosclerosis
P Dutta *et al.*
doi:10.1038/nature11260

BRIEF COMMUNICATIONS ARISING

Arising from 'Reduced methane growth rate explained by decreased Northern Hemisphere microbial sources' by F M Kai et al. Nature ***476,*** *194–197 (2011)*

No inter-hemispheric $\delta^{13}CH_4$ trend observed
I Levin *et al.*
doi:10.1038/nature11175

***Reply* —** Kai *et al.*
doi:10.1038/nature11176

NATURE PODCAST

On the latest podcast, H5N1's five big unknowns, controversial geoengineering efforts in the Baltic Sea, an *Australopithecus* species that had a 'woodland' diet of berries, bark and leaves, and news from the Rio+20 Earth Summit.

nature.com/nature/podcast

SOLAR PHYSICS

Swirls in the corona

Observations made by NASA's Solar Dynamics Observatory have been used to identify signatures of a conduit through which energy could be transported from the surface of the Sun into its corona. SEE LETTER P.505

STEPHEN J. BRADSHAW

SDO/NASA

Figure 1 | The halo effect. Wedemeyer-Böhm *et al.*[1] have discovered swirling motions of gas in the solar corona, which is seen here in an image taken by the Atmospheric Imaging Assembly instrument on board NASA's Solar Dynamics Observatory. These motions of coronal gas seem to be connected to swirling gas at the Sun's surface.

The Sun's outer atmosphere is called the corona (Fig. 1). It can be observed by eye during solar eclipses, when the Moon blocks the bright disk of the Sun, as a wispy halo of gas. One of the most surprising properties of the corona is that it is hundreds of times hotter than the surface of the Sun. To understand how this can be so, we must discover the source of the energy that heats the corona, how that energy is transported into the corona and how it is dissipated. For example, do waves of energy surge away from the surface and travel along magnetic-field lines to the corona? Or do these field lines behave more like elastic bands, becoming twisted and tangled by surface flows, then snapping and reconnecting? On page 505 of this issue, Wedemeyer-Böhm *et al.*[1] present results that may shed light on this puzzle.

The high temperatures associated with the Sun's corona have made explaining its existence one of the most long-standing problems in astrophysics. In 1869, William Harkness and Charles Young, while independently making observations of the corona during an eclipse, discovered a spectral emission line at 530.3 nanometres in the green part of the visible spectrum, and yet no known chemical emitted a spectral line at this wavelength. The mystery of this line's provenance persisted for 70 years before the combined efforts of Walter Grotrian and Bengt Edlén identified a highly charged state of iron (Fe^{13+}) as responsible (see, for example, ref. 2).

Their discovery provoked a further question. An iron atom in the corona can be stripped of 13 electrons when each one is knocked out of its bound orbit by colliding with a free electron. The energy needed by the free electron to release the thirteenth bound electron corresponds[3] to a gas temperature of 2 million kelvin. The surface temperature of the Sun is a 'mere' 5,800 kelvin. How could the corona be more than 300 times hotter than this? It is a measure of the difficulty of this question that its answer has eluded scientists for longer than the 70 years that it took to solve the original problem.

One challenge has been to detect visible signatures of the transport of mass and energy to the corona that can be unambiguously linked to the mechanisms that have been proposed to create and sustain it. Wedemeyer-Böhm and colleagues' results may offer one such signature. The authors have analysed observations made by the Atmospheric Imaging Assembly[4] on board NASA's space-based Solar Dynamics Observatory, and have detected vortex-like flows, or 'swirls', of coronal gas at temperatures of around 1 million kelvin. It is known that vortex flows of gas at the Sun's surface arise through thermal convection in the layer below. By identifying a coronal counterpart to these swirls, Wedemeyer-Böhm *et al.* have found evidence that the surface and coronal vortices are connected.

Visually, the entire structure resembles a super-tornado. The connection between these swirling layers is provided by the Sun's magnetic field. The field lines pass through the surface of the Sun, where they are forced to follow the swirling motions of the gas, and extend into the corona. The tension in the field lines transmits the swirling motions from the surface into the corona, where the gas is forced to follow the field; swirling gas at the surface then gives some of its energy to drive swirling gas in the corona. The field lines are not perfectly vertical, and the vortex flow gives rise to a centrifugal force that accelerates gas along the field lines, so that it follows a spiral trajectory up into the corona.

In summary, Wedemeyer-Böhm *et al.* have observed connected swirls of gas, at temperatures from a few thousand to more than

1 million kelvin, that are signatures of mass and energy transport from the surface of the Sun into the corona. The authors have calculated that the swirling motions can transport sufficient energy to satisfy the heating requirements of the corona, and they have connected them with a known energy source — the convective motions of the Sun's interior, which are in turn driven by the heat generated in nuclear reactions at the core.

Wedemeyer-Böhm and colleagues' findings apply to the quiet (non-flaring) Sun. But it is less clear what role the authors' proposed energy-transport mechanism has in sunspots (areas of intense magnetic activity that are cooler, and hence darker, than the typical surface temperature of the Sun), and in the active regions overlying sunspots. In these regions, the energy requirements for heating are greater and the magnetic field is strong enough to inhibit the convection associated with the surface swirling motions. In addition, it is not known how the transported energy can be dissipated as heat in the corona. The authors have identified 14 super-tornadoes, from which they estimate that a total of slightly more than 10,000 are continuously present in the quiet Sun — although more observed cases would be necessary for greater confidence in this number. Nonetheless, the great potential of these results for contributing towards a resolution of the coronal heating problem will encourage the pursuit of related investigations. ■

Stephen J. Bradshaw *is in the Department of Physics and Astronomy, William Marsh Rice University, Houston, Texas 77005, USA.*
e-mail: stephen.bradshaw@rice.edu

1. Wedemeyer-Böhm, S. *et al. Nature* **486,** 505–508 (2012).
2. Grotrian, W. *Naturwissenschaften* **27,** 214 (1939).
3. Dere, K. P. *et al. Astron. Astrophys.* **498,** 915–929 (2009).
4. Lemen, J. R. *et al. Solar Phys.* **275,** 17–40 (2012).

AGEING

A healthy diet for stem cells

Understanding how a low calorie intake slows ageing could revolutionize the way that we treat age-related diseases. One potential key to such treatments could be to enhance the local environment of stem cells. SEE ARTICLE P.490

FRESNIDA J. RAMOS & MATT KAEBERLEIN

Decreased calorie ingestion, without malnutrition, extends lifespan and promotes healthy ageing in many animals[1]. Although the mechanisms behind these effects are still being determined, calorie restriction may act, at least in part, by preserving the functions of stem cells — cells that are capable of self-renewal and that have the potential to develop into organ-specific cell types[2–4]. Two studies, one by Yilmaz *et al.*[5] on page 490 of this issue and another by Cerletti *et al.*[6] in *Cell Stem Cell*, shed light on how calorie restriction could influence longevity and health in adult mice. Although one paper focused on intestinal tissue and the other on muscle, both conclude that the beneficial effects of calorie restriction on stem-cell function are mediated by changes in the cells' microenvironment, the stem-cell niche.

A central player in calorie restriction is the protein mTOR (ref. 7). In association with other proteins, mTOR forms two complexes known as mTORC1 and mTORC2. The mTORC1 complex acts in a signalling pathway that regulates many cellular functions[8], including translation of messenger RNAs into proteins, the activity of mitochondria (the cell's powerhouses), and autophagy (a process by which cells dismantle and recycle their own components). Calorie restriction inhibits mTORC1 activity, and experimental inhibition of the mTORC1 pathway extends lifespan in yeast, worms, flies and mice[7]. Rapamycin — a drug that inhibits mTORC1 — also promotes longevity in several organisms, including middle-aged mice[9]. These findings have led to speculation that rapamycin could mimic calorie restriction and slow the progression of age-related maladies in humans[10].

Yilmaz *et al.*[5] provide convincing evidence that the preservation of intestinal stem cells (ISCs) by calorie restriction is a direct result of reduced mTORC1 signalling. Interestingly, it is not the mTORC1 pathway within the ISCs that seems to be the most important. Instead, the dietary intervention inhibits mTORC1 signalling in adjacent specialized cells termed Paneth cells; this results in changes to the local microenvironment that improve ISC function and that lead to increased numbers of both ISCs and Paneth cells.

When the authors cultured ISCs with Paneth cells that had been obtained from calorie-restricted animals, the ISCs were more likely to form organoid bodies — 'mini-organs' that contain stem cells and other cell types typical of intestinal epithelial tissue — than when they were cultured with Paneth cells from non-restricted animals. The researchers further showed that mTORC1-mediated regulation of the *Bst1* gene, which encodes a protein that promotes cell proliferation in bone marrow, is essential for these effects. Accordingly, calorie restriction increased *Bst1* expression in Paneth cells.

Taking a similar approach, Cerletti *et al.*[6] found that calorie restriction increased the number and the regenerative potential of skeletal-muscle stem cells (MSCs, also known as satellite cells) in both young and aged mice. After three months on a reduced-calorie diet, the animals had more MSCs per muscle fibre than did control mice. Moreover, the treated animals' MSCs showed enhanced regenerative capacity when transplanted into the injured muscles of untreated animals. Therefore, calorie restriction seems to exert at least some of its effects on MSC function directly. Such effects may be mediated by alterations in mitochondrial activity. Mitochondria use oxygen to generate energy, and the authors observed that MSCs from calorie-restricted mice had more mitochondria and a higher oxygen consumption rate than did MSCs from control animals.

Similarly to Yilmaz and colleagues' observations with ISCs, calorie restriction also influenced MSC function indirectly by promoting a more favourable stem-cell environment. This is evidenced by the fact that MSCs isolated from control mice showed enhanced muscle engraftment when transplanted into calorie-restricted animals. Cerletti *et al.* propose that reduced inflammation — a hallmark of calorie restriction — may be crucial for enabling MSCs to efficiently regenerate damaged tissue. Although the authors did not test this hypothesis, reduced activity of mTORC1 (which is known to modulate inflammation) might also underlie this aspect of enhanced MSC function following calorie restriction.

Taken together, the two studies indicate that preserving and enhancing stem-cell function in multiple tissues is one of the ways in which calorie restriction slows the ravages of ageing. The studies also suggest that short-term calorie restriction or fasting, or compounds such as rapamycin that target mTORC1, might enhance the efficacy of stem-cell therapies. Rapamycin-derived drugs are already in use to prevent organ rejection in transplant patients, to reduce undesirable cell proliferation after angioplasty (a surgical procedure for repairing or unblocking a blood vessel), and as a treatment for some forms of cancer[7]. Thus, inhibition of mTORC1 may have dual protective effects — preventing aberrant cell multiplication associated with disease, and improving the ability of stem cells to repair and to maintain tissues.

Important questions remain, however. Both

studies examined only relatively short-term calorie restriction, and whether dietary intervention at a young age will confer protection against age-related disease later in life remains uncertain. It will also be important to determine the extent to which mTORC1 inhibition can match the effects of calorie restriction. Yilmaz *et al.* showed that treating mice with rapamycin for a week was sufficient to increase the abundance of ISCs. Furthermore, they observed that Paneth cells from rapamycin-treated mice stimulated ISCs (which had been isolated from rapamycin-treated or untreated animals) to form organoid bodies *in vitro*, just as those from calorie-restricted animals did.

Will rapamycin have similar effects on other adult stem cells, or on their niches? Although this remains to be tested in MSCs, mTORC1 is known to influence the function of haematopoietic (blood-forming) stem cells[11]. In mouse models of autoimmune disease, defects in haematopoietic stem cells are at least partly due to increased mTORC1 activity, and rapamycin treatment can increase the numbers of bone-marrow cells and partly restore haematopoietic activity in these animals.

In spite of these open questions, the studies by Yilmaz *et al.* and Cerletti *et al.* emphasize the vital role of the stem-cell niche for the response of stem cells to calorie restriction. Moreover, they support the hypothesis that appropriate regulation of mTORC1 signalling could be crucial for maintaining stem-cell function during ageing. ■

Fresnida J. Ramos *and* **Matt Kaeberlein** *are in the Department of Pathology, University of Washington, Seattle, Washington 98195, USA.* **M.K.** *is also at the Institute of Aging Research, Guangdong Medical College, Dongguan 523808, China.*
e-mail: kaeber@uw.edu

1. Fontana, L., Partridge, L. & Longo, V. D. *Science* **328**, 321–326 (2010).
2. Chen, J., Astle, C. M. & Harrison, D. E. *Exp. Hematol.* **31**, 1097–1103 (2003).
3. Lee, J., Duan, W., Long, J. M., Ingram, D. K. & Mattson, M. P. *J. Mol. Neurosci.* **15**, 99–108 (2000).
4. Mair, W., McLeod, C. J., Wang, L. & Jones, D. L. *Aging Cell* **9**, 916–918 (2010).
5. Yilmaz, O. H. *et al. Nature* **486**, 490–495 (2012).
6. Cerletti, M., Jang, Y. C., Finley, L. W. S., Haigis, M. C. & Wagers, A. J. *Cell Stem Cell* **10**, 515–519 (2012).
7. Stanfel, M. N., Shamieh, L. S., Kaeberlein, M. & Kennedy, B. K. *Biochim. Biophys. Acta* **1790**, 1067–1074 (2009).
8. Zoncu, R., Efeyan, A. & Sabatini, D. M. *Nature Rev. Mol. Cell Biol.* **12**, 21–35 (2011).
9. Harrison, D. E. *et al. Nature* **460**, 392–395 (2009).
10. Kaeberlein, M. *Bioessays* **32**, 96–99 (2010).
11. Chen, C., Liu, Y., Liu Y. & Zheng, P. *J. Clin. Invest.* **120**, 4091–4101 (2010).

ORGANIC CHEMISTRY

Directors extend their reach

Controlling the positions at which chemical groups attach to benzene rings is vital for the synthesis of materials and medicines. A reaction that targets a normally inaccessible position takes chemists closer to this goal. SEE LETTER P.518

MATTHEW O. KITCHING & VICTOR SNIECKUS

In 1865, the German chemist Friedrich August Kekulé proposed that benzene has a ring-like molecular structure, allegedly after a dream containing the vivid visual metaphor of a serpent seizing its own tail[1]. Ever since then, aromatic molecules — those that contain benzene or benzene-like rings of atoms — have fuelled the imagination of organic chemists. From aspirin to Viagra, Kevlar to car seats, and polystyrenes to sunscreens, aromatic rings decorated with other chemical groups are now an intrinsic part of life. Yet despite the prevalence of such compounds, 'regioselective' reactions that allow groups to be placed at specific positions on benzene rings are often difficult to achieve. On page 518 of this issue, Yu and colleagues[2] report a conceptually new method for attaching groups at the '*meta*-position' of electron-rich benzene rings, in which a metal catalyst is guided to this difficult-to-access position.

The root of the regioselectivity problem is taught to chemistry students in their first organic chemistry course at university, in studies of classical electrophilic aromatic-substitution reactions — the most widely used reactions for attaching groups to benzene rings. To explain further, let us begin with some basic terminology. In a benzene ring, the carbon atoms on either side of the point of attachment of a chemical group are said to be in the *ortho*-positions; the next two around the ring are in the *meta*-positions; and the carbon atom on the other side of the ring from the attached group is in the *para*-position (Fig. 1a). If a group attached to benzene releases electrons to the aromatic ring, that group promotes the attachment of electrophilic groups (those that are attracted to electron-rich regions of molecules) at the *ortho*- and/or *para*-positions of the ring, with varying degrees of selectivity.

Although such reactions have been extremely useful, the inherent lack of control of *ortho*- versus *para*-selectivity can lead to an unwelcome mixture of isomeric products. Furthermore, when both electron-releasing and electron-withdrawing groups are attached to benzene, the electronic 'tug-of-war' between them often makes it difficult to predict where electrophilic groups will attach to the ring, so that the actual outcome can be found only through experimentation. Other widely used methods for functionalizing (attaching groups to) aromatic molecules, such as nucleophilic aromatic substitution and vicarious nucleophilic substitution[3], are similarly subject to these strong electronic effects.

Powerful approaches have been evolved that enable impressively selective *ortho*-functionalization of benzene rings; these include directed *ortho*-metalation reactions[4,5] and directed C–H activation strategies[6]. In such processes, a group attached to the ring guides an incoming base (in the case of metalations) or a metal catalyst (in C–H activations) to the neighbouring position (Fig. 1b). The directing groups in both of these processes are attached either directly to the aromatic ring or through a linker, and they usually contain electron-rich atoms that chelate (bind to) the base or the metal catalyst. Processes in which reactive sites are 'walked' around the ring, and in which groups are attached sequentially at the *ortho*-, *meta*- and *para*-positions of a directing group, are particularly valuable examples of multiple directed *ortho*- metalations[7].

By comparison, selective *meta*-functionalization of electron-rich aromatic rings has proved more challenging. Resourceful approaches have been developed for specific cases[8–10], but with the possible exception of seminal work from Matthew Gaunt's group[11,12], a general solution to this problem has not been found.

On the basis of a previous study[13] demonstrating that the geometrically linear nitrile (CN) group can chelate metal atoms 'end-on', Yu and co-workers[2] offer a fresh approach to *meta*-functionalization (Fig. 1c). They designed special linkers to connect nitrile groups to aromatic rings. The linkers allow the nitrile to chelate a metal in such a way that the metal can 'grab' hydrogen atoms from *meta*-positions, enabling other groups to be attached there. The authors demonstrated that both the nitrile group and the bulkiness of the linkers were essential for success, supporting their chelation-control model.

Yu and colleagues obtained the most impressive results with a benzyl ether linker (Fig. 1d), which enabled bulky di- and tri-substituted alkenes (compounds in which two or three groups are attached to a carbon–carbon double bond) to be attached to the *meta*-position of a benzene ring. Such substrates are difficult to use in *ortho*-directed C–H activation

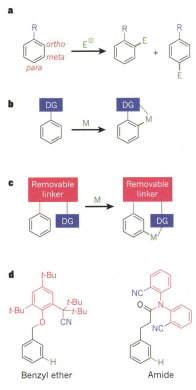

Figure 1 | Site-selective reactions of benzene. **a**, When a benzene ring has a chemical group (R) attached, the carbon atoms in the ring are defined as being in the *ortho*-, *meta*- and *para*-positions, depending on their relationship to the point of attachment. If R is an electron-donating group, classical reactions of benzene rings attach electrophiles (E$^+$, compounds that are attracted to electron-rich regions of molecules) to the *ortho*- and/or *para*-positions, which can lead to undesirable mixtures of isomeric products. **b**, In directed *ortho*-metalation reactions and C–H activation reactions, a 'directing' group (DG) guides metal atoms (M) only to the *ortho*-position; the broken line indicates the directing effect. The metal is then displaced by a different group to form a final product (not shown). For *ortho*-metalation, M is lithium or magnesium; for *ortho*-C–H activation, M is palladium, copper, rhodium, ruthenium or iridium. **c**, Yu and colleagues[2] have designed benzene-containing systems in which removable linker units bear groups that guide metal atoms to the *meta*-position. M is palladium. **d**, The first of their linkers attaches to benzene through an oxygen atom; the resulting compound is known as a benzyl ether. The second linker attaches through an amide bond (N–CO). Nitrile groups (CN) act as the directing groups in both cases. The carbon–hydrogen bond activated in the authors' reactions is shown in green. *t*-Bu is a tertiary butyl group, $C(CH_3)_3$.

reactions, presumably because the directing group blocks the approach of bulky alkenes. In Yu and colleagues' reactions, however, more space is available around the *meta*-position, allowing reactions with these large alkenes to occur.

Having demonstrated that their innovative reaction works with a reasonable range of substrates, the authors went on to solve the problem of how to remove the linkers[14] once *meta*-functionalization has occurred. This is necessary because molecules used as pharmaceuticals or materials do not have such linker groups in their structures. The researchers found that the benzyl ether can be removed by reacting it with hydrogen, whereas the other linker (an amide; Fig 1d) can be removed by treating it with a base in water. In the latter case, the cleaved linker survives the removal conditions, allowing it to be reclaimed and reused, further adding to the value of this approach for *meta*-functionalization. Yu and colleagues demonstrated the synthetic usefulness of their method by *meta*-functionalizing a derivative of the drug baclofen, opening up the possibility of using the technique to make analogues of other known drugs and so to generate new, potentially biologically active molecules.

Although the preliminary nature of these results prevents any definitive analysis, a comparison with Gaunt's *meta*-functionalization technique[11,12] is appropriate and valuable. The huge size of Yu and colleagues' linkers is a current drawback, because it limits the practicality and scalability of the method compared with Gaunt's procedure — although this issue will undoubtedly be addressed by the researchers. On the other hand, Gaunt's method requires reagents (hypervalent iodine compounds) that need to be prepared in advance, whereas Yu and colleagues' process uses more easily available alkenes.

Such criticisms, however, should not detract from both groups' great achievements: the development of powerful methods for the *meta*-functionalization of electron-rich aromatic rings. These methods open up many opportunities for the synthesis of aromatic compounds, and perhaps also of heteroaromatic compounds — benzene-like compounds that incorporate nitrogen, oxygen and sulphur atoms in their rings. Yu and colleagues' chelation-driven approach to obtaining *meta*-selective reactions will undoubtedly be eagerly pursued in the hope of developing other ways to selectively functionalize aromatic molecules. ■

Matthew O. Kitching *and* **Victor Snieckus** *are in the Department of Chemistry, Queen's University, Kingston, Ontario K7L 3N6, Canada.*
e-mails: victor.snieckus@chem.queensu.ca; matthew.kitching@chem.queensu.ca

1. Benfey, O. T. *J. Chem. Educ.* **35**, 21–23 (1958).
2. Leow, D., Li, G., Mei, T.-S. & Yu, J.-Q. *Nature* **486**, 518–522 (2012).
3. Makosza, M. *Synthesis* **15**, 2341–2356 (2011).
4. Snieckus, V. *Chem. Rev.* **90**, 879–933 (1990).
5. Macklin, T. & Snieckus, V. in *Handbook of C–H Transformations* (ed. Dyker, G.) 106–119 (Wiley-VCH, 2005).
6. Chen, X., Engle, K. M., Wang, D.-H. & Yu, J.-Q. *Angew. Chem. Int. Edn* **48**, 5094–5115 (2009).
7. Mills, R. J., Taylor, N. J. & Snieckus, V. *J. Org. Chem.* **54**, 4372–4385 (1989).
8. Akai, S., Peat, A. J. & Buchwald, S. L. *J. Am. Chem. Soc.* **120**, 9119–9125 (1998).
9. Mkhalid, I. A. I., Barnard, J. H., Marder, T. B., Murphy, J. M. & Hartwig, J. F. *Chem. Rev.* **110**, 890–931 (2010).
10. Andrikopoulos, P. C. *et al. Angew. Chem. Int. Edn* **44**, 3459–3462 (2005).
11. Phipps, R. J. & Gaunt, M. J. *Science* **323**, 1593–1597 (2009).
12. Duong, H. A., Gilligan, R. E., Cooke, M. L., Phipps, R. J. & Gaunt, M. J. *Angew. Chem. Int. Edn* **50**, 463–466 (2011).
13. Schwarz, H. *Acc. Chem. Res.* **22**, 282–287 (1989).
14. Rousseau, G. & Breit, B. *Angew. Chem. Int. Edn* **50**, 2450–2494 (2011).

PHARMACOLOGY

A false sense of non-self

A drug used for HIV treatment can alter the set of antigens that activates T cells of the immune system, thereby triggering life-threatening reactions against the body's own proteins. SEE LETTER P.554

ELLIS L. REINHERZ

The drug abacavir can be an effective treatment for HIV but it is also associated with an autoimmune response in 5–10% of patients[1]. These hypersensitivity reactions, which include fever, rash and gastrointestinal problems, mandate immediate drug cessation to prevent the emergence of life-threatening symptoms. It has previously been reported[2,3] that abacavir hypersensitivity syndrome occurs in patients who express one particular major histocompatibility complex (MHC) class I protein, and genetic screening for this protein variant is an effective way to avoid this adverse drug reaction[4]. In an elegant study on page 554 of this issue, Illing *et al.*[5] reveal the molecular basis of this response, showing that abacavir alters the repertoire of antigens that activate the immune system.

T cells are immune cells that allow the body to distinguish abnormal or foreign cells from normal cells. The ability of T cells to discriminate between 'self' and 'non-self' is endowed by surface-bound T-cell receptors (TCRs)[6]. In any mammal, there are millions to billions of T cells, each with a slightly different

TCR structure that confers a unique antigen-binding specificity. However, TCRs recognize antigens only when these are bound to MHC receptors on the surface of other cells. These MHC molecules display an array of antigen peptides that provides a snapshot of the cell's internal composition. Aberrant cellular processes, such as viral infection, are reflected by alterations in the antigens that are displayed. When a T cell recognizes a variant peptide (one derived from a viral protein, for example), cellular signalling pathways are initiated that cause the T cell to proliferate and to differentiate. When activated in this manner, T cells called $CD8^+$ T cells eliminate the cells expressing these abnormal antigens[7] (Fig. 1a). T cells are able to detect a variant peptide even if just a few copies are present among the hundreds of thousands of normal self peptides that are displayed by the cell-surface MHC receptors[8].

In humans, the MHC molecules are called HLA proteins, and different people express versions encoded by different gene variants (alleles). In general, peptides associate with HLA molecules by inserting parts of their amino-acid residues into a set of six binding pockets (termed A–F) in the HLA[9]. The structure of these pockets is highly allele-specific, thereby dictating peptide-binding preferences for each HLA molecule. Illing *et al.* show that abacavir binds directly to the F pocket of one of these proteins, HLA-B*57:01, but that the drug does not bind to the closely related molecule HLA-B*57:03, which is not linked to abacavir hypersensitivity.

Illing and colleagues also reveal that the binding of abacavir to HLA-B*57:01 alters the F pocket's binding preference for side chains of the amino acids tryptophan or phenylalanine, so as to include those of the amino acids isoleucine and leucine. By determining the amino-acid sequences of almost 2,500 HLA-B*57:01-bound peptides, the researchers demonstrated an enormous shift in peptide presentation: 20–25% of the peptides bound by the HLA molecule following drug treatment differed from those that bound beforehand. The authors observed no such drug-induced change in the peptides that bound to HLA-B*57:03.

These data imply that HLA-B*57:01 and abacavir form a complex before the HLA molecules are loaded with peptides inside the cell, thereby altering the pool of self peptides that are bound to the HLA and displayed on the cell surface for $CD8^+$ T-cell recognition. This shift in the specific HLA-associated cell-surface-peptide display leads to the activation of different $CD8^+$ T cells (Fig. 1b). However, the authors detected no obvious skewing towards a single $CD8^+$ T-cell population, or clone, being activated by the altered range of peptides. Instead, they observed responses by many different $CD8^+$ T cells (polyclonality). This is in keeping with a previous study[10] that revealed broad-scale activation of $CD8^+$ T cells as the cellular basis of abacavir hypersensitivity reactions.

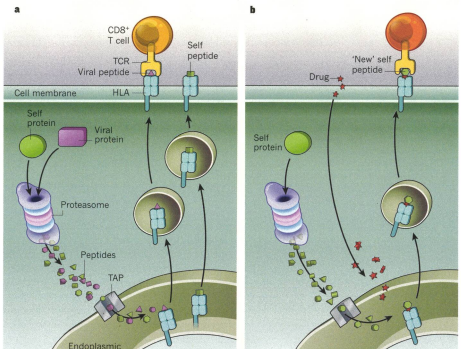

Figure 1 | Mistaken identity. a, In the cytoplasm of most human cells, self proteins and foreign proteins, such as those from a virus that has infected a cell, are cleaved into multiple peptides by a complex called the proteasome. A subset of these peptides is then carried by TAP proteins to an organelle called the endoplasmic reticulum. Here, an even more limited set of peptides are loaded onto HLA molecules, which are transported to the cell surface. These surface-displayed HLA–peptide complexes are recognized by T-cell receptors (TCRs) on the surface of immune cells called T cells. Any T cells with TCRs that recognize HLA–self-peptide complexes are destroyed during T-cell development, such that only T cells with TCRs specific for foreign antigens survive. **b**, Illing *et al.*[5] show that the anti-HIV drug abacavir binds to a specific HLA molecule and alters its peptide-binding characteristics, causing the HLA molecule to load and display a new range of peptides on the cell surface. Because this repertoire includes self peptides that were not displayed during T-cell development, the immune system contains some T cells that can recognize these antigens and launch an immune attack against the cell.

To examine the structural cause of the change in bound peptides, the authors refolded the HLA-B*57:01 protein in the presence of abacavir and a self peptide that binds to the HLA molecule only after drug treatment. They then compared the X-ray crystallographic structure of the resulting HLA-B*57:01–self-peptide complex with that of a different HLA-B*57:01–self-peptide complex that forms in the absence of abacavir. The researchers found that part of the drug, the cyclopropyl moiety, protrudes into the HLA molecule's F pocket, reducing the pocket's size, which accounts for its preferred binding of smaller amino acids following drug exposure. The structures also revealed that abacavir binds to the two amino-acid residues that are unique to the HLA-B*57:01 molecule, thereby explaining the drug's allele specificity.

This shift in the bound-peptide repertoire is a plausible explanation for drug-induced hypersensitivity. As T cells develop in the thymus, TCRs are randomly generated by a process of gene rearrangement. A mechanism referred to as negative selection[11] ensures that any developing T cell expressing a receptor that strongly recognizes self peptides bound to self-MHC molecules is destroyed, whereas T cells that lack self-reactivity but that have the potential to recognize foreign antigens survive.

Some self peptides are never encountered during T-cell development but can be exposed during pathological conditions[10] — when this occurs, a situation of 'mistaken identity' can arise, in which the self peptides are perceived as foreign by the immune system. For example, the eye is an immune privileged site, such that some ocular proteins are hidden from the immune system. However, if these proteins are released into the body — as occurs following a traumatic eye injury — T cells are activated, leading to inflammation in both the injured and uninjured eyes. This condition, referred to as sympathetic ophthalmia, can result in catastrophic blindness. It seems that the autoimmune response associated with abacavir treatment stems from a similar effect — the exposure of self peptides attached to HLA-B*57:01 that are

not normally associated with this molecule leads T cells to perceive these self peptides as foreign.

This false sense of non-self is not restricted to abacavir. Illing *et al.* show that the anti-convulsive drug carbamazepine, which is associated with hypersensitivity responses in patients with the *HLA-B*15:02* allele, also binds to that HLA molecule and alters its set of associated peptides. The awareness engendered by this study is likely to result in many more examples of known drug–HLA associations[12] being linked to similar auto-immune mechanisms. If so, it may become desirable to screen patients for their HLA alleles before choosing drugs for treatment. By extension, it is possible that organ-specific drug-metabolism processes might limit the altered HLA–peptide display to specific cell types, and thus limit the resulting immune reaction to certain organs, such as the liver, kidneys or bone marrow.

Finally, it is worth considering that environmental toxins and other chemicals could also interact with HLA molecules. The genes that encode HLA are extremely variable — at the last count, there were 4,269 different HLA (-A,-B and -C) variants referred to as MHC class I molecules[13]. This diversity is believed to have evolved owing to the selection pressures imposed by infectious pathogens[14], but it also seems to afford ample opportunity for HLA interactions with drugs and other molecules. Similar drug interactions undoubtedly exist for the other class of HLA molecules (MHC class II, with -DR, -DP and -DQ types) that binds peptides recognized by $CD4^+$ T cells. The field of pharmacogenetics is going to expand and, in so doing, redefine our understanding of the basis of many forms of autoimmunity. ■

Ellis L. Reinherz *is in the Harvard Medical School and Dana-Farber Cancer Institute, Boston, Massachusetts 02115, USA.*
e-mail: ellis_reinherz@dfci.harvard.edu

1. Hetherington, S. *et al. Clin. Ther.* **23,** 1603–1614 (2001).
2. Mallal, S. *et al. Lancet* **359,** 727–732 (2002).
3. Hetherington, S. *et al. Lancet* **359,** 1121–1122 (2002).
4. Mallal, S. *et al. N. Engl. J. Med.* **358,** 568–579 (2008).
5. Illing, P. T. *et al. Nature* **486,** 554–558 (2012).
6. Kim, S. T. *et al. Front. Immunol.* **3,** 76 (2012).
7. Smith, K. A. *Science* **240,** 1169–1176 (1988).
8. Sykulev, Y., Joo, M., Vturina, I., Tsomides, T. J. & Eisen, H. N. *Immunity* **4,** 565–571 (1996).
9. Madden, D. R, Gorga, J. C., Strominger, J. L. & Wiley, D. C. *Nature* **353,** 321–325 (1991).
10. Chessman, D. *et al. Immunity* **28,** 822–832 (2008).
11. von Boehmer, H. *Immunol. Today* **13,** 454–458 (1992).
12. Alfirevic, A. & Pirmohamed, M. *Pharmaceuticals* **4,** 69–90 (2011).
13. Robinson, J., Mistry, K., McWilliam, H., Lopez, R., Parham, P. & Marsh, S. G. *Nucleic Acids Res.* **39,** D1171–D1176 (2011).
14. Doherty, P. C. & Zinkernagel, R. M. *Lancet* **305,** 1406–1409 (1975).

NEUROSCIENCE

Genes and human brain evolution

Several genes were duplicated during human evolution. It seems that one such duplication gave rise to a gene that may have helped to make human brains bigger and more adaptable than those of our ancestors.

DANIEL H. GESCHWIND & GENEVIEVE KONOPKA

The decoding of the human and chimpanzee genomes was heralded as an opportunity to truly understand how changes in DNA resulted in the evolution of our cognitive features. However, more than a decade and much detective work later, the functional consequences of such changes have proved elusive, with a few exceptions[1,2]. Now, writing in *Cell*, Dennis *et al.*[3] and Charrier *et al.*[4] describe the evolutionary history and function of the human gene *SRGAP2* and provide evidence for molecular and cellular mechanisms that may link the gene's evolution with that of our brain*.

It was already known that *SRGAP2* is involved in brain development[5] and that humans have at least three similar copies of the gene, whereas non-human primates carry only one[6]. However, the study of duplicated, or very similar, segments of DNA is hampered by the fact that most human cells carry two sets of chromosomes (one inherited from each parent), which makes it difficult to distinguish duplicated copies from the different parental forms of the gene. To circumvent this problem, Dennis *et al.*[3] searched for copies of *SRGAP2* in the genome of a hydatidiform mole — an abnormal, non-viable human embryo that results from the fusion of a sperm with an egg that has lost its genetic material; it therefore has chromosomes derived from a single parent.

The authors showed that humans carry four non-identical copies (named *A*–*D*) of *SRGAP2* at different locations on chromosome 1. By comparing the genes' sequences with that of the *SRGAP2* gene from the orang-utan and chimpanzee, the authors estimated that *SRGAP2* was duplicated in the human lineage about 3.4 million years ago, resulting in *SRGAP2A* (the ancestral version that we share with other primates) and *SRGAP2B*. Further duplications of *SRGAP2B* gave rise to *SRGAP2C* about 2.4 million years ago and to *SRGAP2D* about 1 million years ago (Fig. 1a).

Dennis *et al.* found that *SRGAP2B* and *SRGAP2D* are expressed at much lower levels, and are more prone to sequence variations among humans, than are the *A* and *C* copies. They therefore suggest that *SRGAP2C* might have played a major part in the emergence of the *Homo* lineage 2 million to 3 million years ago, when human brain specializations (such as those leading to the development of language, social cognition and problem solving) were probably evolving.

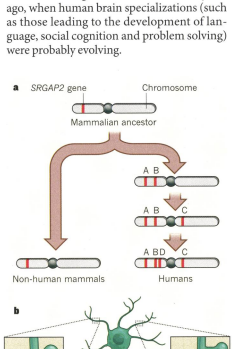

Figure 1 | Evolution and function of a human gene. a, Dennis *et al.*[3] and Charrier *et al.*[4] detail how the *SRGAP2* gene, which is found as a single copy in the genomes of most mammals, was duplicated three times during the evolution of human ancestors to give rise to four similar versions of the gene, named *A*–*D*. **b,** Charrier *et al.* demonstrate that the 'ancestral' version, *SRGAP2A*, stimulates the maturation of dendritic spines (protuberances) on the surfaces of neurons, whereas *SRGAP2C* promotes an increased number of immature spines in humans. This development might have contributed to the evolution of human cognitive abilities.

*This News & Views article was published online on 20 June 2012.

In a complementary study, Charrier and colleagues[4] investigated the role of the *SRGAP2* genes in the development of spines — not those that permit us to walk upright, but dendritic spines. These are small protrusions from the surface of neurons that have an important role in the transmission of nerve impulses. Previous studies had documented the fact that humans have greater numbers and densities of dendritic spines than other primates and rodents[7,8], but the molecular mechanisms driving this feature were unknown. By studying cells from genetically modified mice and human brain tissue, the authors show that *SRGAP2A* promotes the maturation of spines and slows down the migration of neurons within the developing cerebral cortex, whereas the human-specific *SRGAP2C* has opposite effects and so favours the formation of further spines (Fig. 1b). These results suggest that the emergence of *SRGAP2C* could have contributed to expansion of the cortex and increase in spine numbers in human ancestors, and therefore to the evolution of brain function and plasticity (the ability to alter neural connections in response to new experiences).

Interestingly, Dennis *et al.* studied a group of young patients who had developmental disorders, and identified a few individuals — out of several thousand — who had DNA duplications or deletions that affected *SRGAP2A* or *SRGAP2C*. Although such numbers are too small to be statistically significant, they indicate that mutations in *SRGAP2A* and *SRGAP2C* could be linked to disease. This hypothesis is consistent with previous suggestions that the evolution of a bigger and more complex brain in the human lineage was accompanied by an increased susceptibility to neurological disorders[9].

Taken together, the findings reported by Dennis *et al.* and Charrier *et al.* significantly add to the current working version of the human genome, and provide an example of how human-specific gene duplications can modulate brain function. They also give functional context to the long-known prolonged immaturity of the developing human brain (a process known as neoteny)[10,11]. By slowing spine maturation and promoting neuronal migration, *SRGAP2C* might allow the environment to have a more protracted influence on brain development than is possible during the shorter brain maturation times seen in other mammals, providing additional malleability.

Furthermore, Charrier *et al.* demonstrate how evolutionary hypotheses derived from the comparative genomics of humans and other primates can be tested in cell culture and animal models. This elegant work provides a launching point for unravelling a more detailed mechanistic understanding of the role of human-specific duplicated genes in brain development, and of their potential contribution to brain evolution and neurodevelopmental disorders. ■

Daniel H. Geschwind *is in the Department of Neurology and the Semel Institute, David Geffen School of Medicine at UCLA, University of California, Los Angeles, Los Angeles, California 90095-1761, USA.*
Genevieve Konopka *is in the Department of Neuroscience, University of Texas Southwestern Medical Center, Dallas, Texas 75390-9111, USA.*
e-mails: dhg@ucla.edu; genevieve.konopka@utsouthwestern.edu

1. Konopka, G. *et al. Nature* **462,** 213–217 (2009).
2. Enard, W. *et al. Cell* **137,** 961–971 (2009).
3. Dennis, M. Y. *et al. Cell* **149,** 912–922 (2012).
4. Charrier, C. *et al. Cell* **149,** 923–935 (2012).
5. Guerrier, S. *et al. Cell* **138,** 990–1004 (2009).
6. Sudmant, P. H. *et al. Science* **330,** 641–646 (2010).
7. Elston, G. N., Benavides-Piccione, R. & DeFelipe, J. *J. Neurosci.* **21,** RC163 (2001).
8. Benavides-Piccione, R., Ballesteros-Yañez, I., DeFelipe, J. & Yuste, R. *J. Neurocytol.* **31,** 337–346 (2002).
9. Preuss, T. M., Cáceres, M., Oldham, M. C. & Geschwind, D. H. *Nature Rev. Genet.* **5,** 850–860 (2004).
10. Petanjek, Z. *et al. Proc. Natl Acad. Sci. USA* **108,** 13281–13286 (2011).
11. Somel, M. *et al. Proc. Natl Acad. Sci. USA* **106,** 5743–5748 (2009).

CANCER

Pinprick diagnostics

Rare tumour cells with mutations that confer drug resistance can go undetected by standard testing procedures, according to two studies, which show that such mutations can be detected in patients' blood. SEE LETTERS P.532 AND P.537

EDUARDO VILAR & JOSEP TABERNERO

Some tumours carry mutations that confer resistance to specific drugs, precluding the use of these drugs in patients with these mutations. However, drug resistance can arise even when a tumour does not seem to meet these criteria. In this issue, Misale *et al.*[1] (page 532) and Diaz *et al.*[2] (page 537) report that a commonly acquired drug resistance in colorectal cancer can be explained by rare tumour cells that have mutations in a particular gene, *KRAS*, and that outgrow susceptible cancer cells during drug exposure. Excitingly, the two research groups demonstrate that they can detect this mutation in the tumour DNA that circulates freely in a patient's bloodstream. Their findings highlight the potential for blood samples to be used in the diagnosis and monitoring of cancers, thereby reducing the need for more-invasive procedures such as tumour biopsies.

Patients with colorectal cancers are often treated with drugs that target epidermal growth factor receptor (EGFR), a signalling protein that activates cellular proliferation. A key predictor of a person's suitability for anti-EGFR therapy is whether their cancerous cells contain a mutated form of *KRAS*; the KRAS protein functions downstream of EGFR, such that cells with overactive KRAS will not respond to anti-EGFR therapies. The use of *KRAS* mutations for predicting the effectiveness of anti-EGFR treatment is an example of successful, although imperfect, biomarker development in oncology, and also demonstrates how an understanding of cancer biology should inform drug development at an early stage of the process.

However, the majority of patients who are selected for anti-EGFR therapy develop secondary resistance to the drug within 5–11 months. One of the main challenges in colorectal cancer research is to uncover the molecular mechanisms involved in this acquired resistance. An essential question is whether the resistance mechanisms derive from new mutation events or from existing clones — rare (and undetected) mutation-carrying cells that are present in the tumour at the start of treatment.

Results obtained by Misale *et al.* and Diaz *et al.* using *in vitro* experiments and mathematical models suggest that secondary resistance to anti-EGFR therapy is a fait accompli, because of the presence of *KRAS*-mutant clones in tumours that initially seem to express only wild-type *KRAS*. Both papers also present data from colorectal cancer patients whose tumours were classified, by biopsy, as *KRAS* wild-type at the initiation of therapy, but in whom the authors detected *KRAS*-mutant clones following treatment with either of two anti-EGFR drugs, cetuximab or panitumumab. These clinical studies were made possible by the use of 'liquid biopsies' in which circulating tumour DNA (ctDNA) was extracted from the serum of the patients' blood. The ctDNA was then studied using an ultrasensitive mutation-detection method called the BEAMing assay[3]. In both studies, the mutant clones were identified before drug resistance could be detected using standard tumour-imaging techniques.

These findings suggest that the same biological mechanism (in this case, *KRAS* mutation) can drive both primary and secondary drug

resistance, and that secondary resistance can arise when tumours are genetically heterogeneous, such that some cells can acquire a growth advantage during treatment. However, this idea contrasts with another mechanism for secondary resistance that has been reported recently, involving a mutation in EGFR that impairs cetuximab binding but that seems to be absent in pre-existing tumour-cell subpopulations[4]. Another of Misale and colleagues' observations is also at odds with the existing-clone hypothesis. In their experimental models, Misale *et al.* report examples of resistance arising from mutations in codon 146 of the *KRAS* gene (a codon is a string of three DNA bases that codes for an amino acid). However, the typical sites of *KRAS* mutations in tumour samples are codons 12 and 13, and codon-146 mutations have been described in less than 5% of colorectal tumours[5]. These unusual mutations are more suggestive of resistance arising from an adaptive response of tumour cells, in which novel mutations accumulate over time, rather than from clonal selection linked to tumour heterogeneity.

It is becoming clear that the existing strategies used to select therapies on the basis of a tumour's genetic status are suboptimal. The existence of heterogeneous tumours and the evolution of diverse cancer-cell populations over the course of the disease, especially under the selection pressure of local and systemic treatment, need to be taken into account in both individual treatment strategies and drug development[6]. We anticipate that tumour heterogeneity will be a recurring theme in future oncology research aimed at improving therapeutics.

The schematic representation of tumour heterogeneity as a branched tree, an idea borrowed from the field of ecology, is a realistic approximation of the evolution of a cancer[7]. Following this theme, therapeutic approaches could be likened to a gardener's toolkit — by targeting selected cellular pathways, certain branches of the tree will be 'pruned'. This pruning will provide selection pressures that favour the growth of cells that are present in very low abundance, which will shift the behaviour of the tumour from that determined by the mutations present in the pruned branches to that specified by the biology of the now-dominant cell populations (Fig. 1). Nonetheless, greater understanding of the proliferative dynamics of cell clones, and of the interactions between them, is needed for such strategies to be successful. The complexity of these interactions is exemplified by the fact that although only 0.4–17% of the mutated alleles detected by Misale *et al.* in patients with anti-EGFR-resistant tumours involved the *KRAS* gene, the whole tumour became resistant to therapy.

Major challenges for the accurate assessment of tumour heterogeneity include gaining access to tissue and the question of appropriate sampling. Currently, biomarker-driven

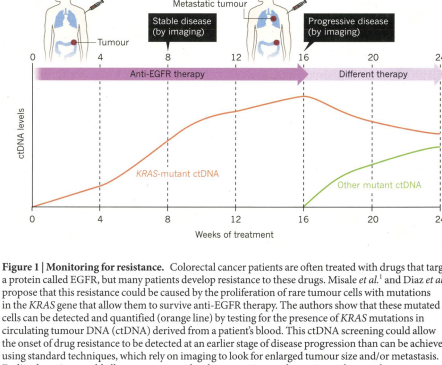

Figure 1 | Monitoring for resistance. Colorectal cancer patients are often treated with drugs that target a protein called EGFR, but many patients develop resistance to these drugs. Misale *et al.*[1] and Diaz *et al.*[2] propose that this resistance could be caused by the proliferation of rare tumour cells with mutations in the *KRAS* gene that allow them to survive anti-EGFR therapy. The authors show that these mutated cells can be detected and quantified (orange line) by testing for the presence of *KRAS* mutations in circulating tumour DNA (ctDNA) derived from a patient's blood. This ctDNA screening could allow the onset of drug resistance to be detected at an earlier stage of disease progression than can be achieved using standard techniques, which rely on imaging to look for enlarged tumour size and/or metastasis. Earlier detection would allow treatment with a drug targeting an alternative pathway to be commenced sooner. However, it is likely that the tumour will also contain rare cells that harbour mutations conferring resistance to this second drug, and that these cells will, in turn, become more prevalent (green line).

therapeutic decisions rely mostly on testing biopsied samples of primary tumours that have been stored since the initial diagnosis, or biopsies from new metastatic sites. However, single biopsies are inadequate. Primary tumours and their metastases are connected by a mixture of different tissues, including cancer cells and supporting structures such as stroma and blood vessels. Moreover, as has been reported[8] in renal-cell cancer, common alterations in cancer-causing genes may differ in different regions of the tumour. Therefore, a single cancerous site and a single tumour biopsy will probably not provide a representative picture of the tumour landscape.

As has previously been suggested[9], these sampling problems could be eliminated by the use of blood biopsies to study genomic alterations in ctDNA. The virtues of this approach include its low invasiveness, the ease of obtaining samples at different time points, and the lack of spatial sampling bias. However, we still need a better understanding of the contribution of each dynamic cell population in a heterogeneous tumour to ctDNA. Furthermore, assays are required that can interrogate mutations in several genes at the same time, which represents a technical challenge because the total amount of ctDNA and its quality are both relatively low. In one recent attempt[10], researchers used next-generation DNA-sequencing technology, instead of BEAMing, to simultaneously screen ctDNA from patients with ovarian cancer for the presence of mutations in seven cancer-related genes. Such emerging mutation-detection platforms will raise standards for interrogating heterogeneous cancer-cell populations. Applications of this technique are likely to expand from the early diagnosis of secondary mutations that could lead to drug resistance, as demonstrated by Misale *et al.* and Diaz *et al.*, to include metastasis monitoring, diagnosis of relapse after surgery, and the early detection of individuals at risk of developing cancer. ■

Eduardo Vilar *is in the Department of Clinical Cancer Prevention, the University of Texas M. D. Anderson Cancer Center, Houston, Texas 77030, USA.* **Josep Tabernero** *is in the Department of Medical Oncology, Vall d'Hebron University Hospital and Vall d'Hebron Institute of Oncology (VHIO), Universitat Autònoma de Barcelona, 08035 Barcelona, Spain.*
e-mails: evilar@mdanderson.org; jtabernero@vhebron.net

1. Misale, S. *et al. Nature* **486,** 532–536 (2012).
2. Diaz, L. A. Jr *et al. Nature* **486,** 537–540 (2012).
3. Diehl, F. *et al. Nature Methods* **3,** 551–559 (2006).
4. Montagut, C. *et al. Nature Med.* **18,** 221–223 (2012).
5. Edkins, S. *et al. Cancer Biol. Ther.* **5,** 928–932 (2006).
6. Marusyk, A., Almendro, V. & Polyak, K. *Nature Rev. Cancer* **12,** 323–334, (2012).
7. Yap, T. A., Gerlinger, M., Futreal, P. A., Pusztai, L. & Swanton, C. *Sci. Transl. Med.* **4,** 127ps10 (2012).
8. Gerlinger, M. *et al. N. Engl. J. Med.* **366,** 883–892 (2012).
9. Diehl, F. *et al. Nature Med.* **14,** 985–990 (2008).
10. Forshew, T. *et al. Sci. Transl. Med.* **4,** 136ra68 (2012).

nature

28 June 2012 / Vol 486 / Issue No. 7404

Publication policies, author guidelines and information

This is a summary of *Nature*'s guide to authors, publication policies and other author information, available in full on the web via our main author information page at www.nature.com/nature/authors.

Getting published in *Nature*

Please read www.nature.com/nature/authors/get_published before finalizing any original scientific research manuscripts you intend to submit. This section explains *Nature*'s editorial criteria, and how manuscripts are handled by the editors after submission and before acceptance for publication.

Formatting guide

Please read www.nature.com/nature/authors/gta before finalizing and submitting your contribution. This section provides instructions for preparing, formatting and writing all types of contribution published by *Nature*.

Publication policies

This section, at www.nature.com/authors, describes *Nature*'s conditions of publication, including policies on authorship; competing financial interests; duplicate publication; prepublicity and embargoes; materials and data availability; research on animal (including human) subjects; referees; corrections, retractions, errata and addenda to published papers; the complaints procedure and refutations; and copyright/licence to publish. All contributions, for whatever section of the journal, are considered for publication and published on the condition that authors agree to these policies.

Submissions

These sections, at www.nature.com/nature/authors/submissions, contain our online service for presubmission enquiries and submission and tracking of Articles, Letters and Review-type manuscripts. Authors should read the formatting guide before using this service. Authors who cannot submit online can submit by post, but *Nature* strongly recommends the online service. **Authors must not submit by both methods.** Authors experiencing operational difficulty in using the online submission service can send an enquiry to mtshelp@nature.com, with a brief explanation of the problem.

Editorial contacts and author services

This section, at www.nature.com/nature/about/contact, provides the addresses of *Nature*'s editorial offices; names of editorial staff; and contact details for advice, reprints, permissions, press office (press@nature.com), and other author-related contact information, including postal addresses for mailed submissions. Short biographies of editors are also available at www.nature.com/nature/about/editors.

Final submissions

This section, at www.nature.com/nature/authors/submissions/final, applies only if an Article or Letter has been accepted in principle for publication and the author has been asked by the editor for a final version. Authors will need to upload electronic files of the text, production-quality figures and supplementary information (if any) to our database. Authors must include a completed manuscript checklist and all relevant signed forms and declarations as requested by the editor.

Short version of guide to authors

See www.nature.com/nature/authors for full version. Contributors not used to *Nature*'s format are advised to read some papers in published issues before submission, to familiarize themselves with *Nature*'s style. *Nature*'s main formats for original research are Articles and Letters.

ARTICLES are original reports whose conclusions represent a substantial advance in understanding of an important problem and have immediate, far-reaching implications. They do not normally exceed **5 pages** of *Nature* and have **no more than 50** references. (One page of undiluted text is about 1,300 words.)

Articles have a summary for readers outside the discipline, separate from the main text and containing no references, of up to 150 words. The summary does not contain numbers, abbreviations, acronyms or measurements unless essential. It contains a brief account of the background and rationale of the work, followed by a statement of the main conclusions, introduced by the phrase 'Here we show' or its equivalent.

The Article itself typically has about 3,000 words of text, beginning with up to 500 words of referenced text expanding on the background to the work, followed by a concise, focused account of the findings, and ending with one or two short paragraphs of discussion. The text can contain a few short subheadings consisting of about 20 but no more than 40 characters (including spaces) each.

LETTERS are short reports of original research focused on an outstanding finding whose importance means that it will be of interest to scientists in other fields. They do not normally exceed **4 pages** of *Nature*, and have **no more than 30** references. They begin with a **fully referenced paragraph** of not more than 300 words, aimed at readers in other disciplines. This paragraph contains a summary of the background and rationale for the work, followed by a one-sentence statement of the main conclusions introduced by the phrase 'Here we show' or its equivalent, and ending with two to three sentences describing the implications in context.

The main text which follows is typically up to 1,500 words long. This text can, if the author requires, start with a further brief paragraph of introductory material. A description of the research then follows. Any discussion at the end of the text should be as succinct as possible.

FIGURES in both Articles and Letters are as small as possible: Articles typically have 5 or 6 figures, Letters typically have 3 or 4 figures. Legends and/or methods are additional to the main text. Methods Summaries (which are published in print only) are no longer than 300 words; Methods sections (which are published online) can be up to 1,000 words; legends should not exceed 100 words each and start with a one-sentence title for the figure, followed by a brief explanation of the parts and symbols.

See www.nature.com/nature/authors/gta/others.html for details of other types of contribution to *Nature*, including Brief Communications Arising; Reviews and Perspectives (presubmission enquiries to reviewsandinsights@nature.com); and Correspondence (submit to corres@nature.com).

See Authors and Referees @ NPG (www.nature.com/authors) for details of Nature journals' publication policies, author and referee services, author benefits and for links to Nautilus and Peer to Peer blogs.

ARTICLE

doi:10.1038/nature11131

Dimensionality of consumer search space drives trophic interaction strengths

Samraat Pawar[1], Anthony I. Dell[1,2] & Van M. Savage[1,3,4]

Trophic interactions govern biomass fluxes in ecosystems, and stability in food webs. Knowledge of how trophic interaction strengths are affected by differences among habitats is crucial for understanding variation in ecological systems. Here we show how substantial variation in consumption-rate data, and hence trophic interaction strengths, arises because consumers tend to encounter resources more frequently in three dimensions (3D) (for example, arboreal and pelagic zones) than two dimensions (2D) (for example, terrestrial and benthic zones). By combining new theory with extensive data (376 species, with body masses ranging from 5.24×10^{-14} kg to 800 kg), we find that consumption rates scale sublinearly with consumer body mass (exponent of approximately 0.85) for 2D interactions, but superlinearly (exponent of approximately 1.06) for 3D interactions. These results contradict the currently widespread assumption of a single exponent (of approximately 0.75) in consumer–resource and food-web research. Further analysis of 2,929 consumer–resource interactions shows that dimensionality of consumer search space is probably a major driver of species coexistence, and the stability and abundance of populations.

Understanding how physical differences between habitats, such as differences in precipitation, temperature and spatial dimensionality, affect trophic interactions is key to predicting stability and diversity in ecological systems[1–6]. By assuming a simple relationship between consumption rate (energy acquisition) and metabolic rate (energy use), most studies assume that per-capita consumption rates scale with consumer body size (m) to an exponent of approximately 0.75, irrespective of taxon, environment or dimensionality[7–13]. Consequently, mass-specific production rates[6,14] scale as $m^{-0.25}$, including biomass flow rate and per-link trophic interaction strengths in food webs[10,11,13,15,16]. Deviations from quarter-power scaling can arise for at least two reasons. First, foraging is constrained by traits, such as length of locomotory appendages or visual acuity, that do not scale directly with metabolic rate[8,17–20]. Second, species interactions in the field do not occur under the idealized conditions at which metabolic and ingestion rates are usually measured, in which individuals are not foraging, growing or reproducing[8,18,19]. Therefore, consumption-rate scaling may be more closely tied to field or maximal metabolic rate (exponent greater than 0.85), rather than resting metabolic rate (exponent of approximately 0.75)[8,21].

From a biomechanical perspective, both non-metabolic and metabolic constraints on consumption rate should depend on the habitat's spatial dimensionality because it strongly influences the energetic costs of locomotion (for example, to overcome gravity)[18,19] and the probability either of a consumer detecting a resource or vice versa[17,20]. Indeed, over two decades ago, habitat dimensionality was proposed as a major factor driving food-web structure and ecosystem dynamics[1,4,22]. Subsequent studies have further elucidated the effects of habitat dimensionality[3,6,23–25]. Notably, previous models suggest that grazers (one type of consumer; Fig. 1 and Supplementary Fig. 1) are constrained by how resources are distributed in space[3,24,25]. These studies are foundational, but do not apply to the full diversity of foraging strategies and interactions in natural communities.

Here we show that shifting focus from dimensionality of the habitat[3,4,6,23–25] to the dimensionality of each trophic interaction yields a new, mechanistic theory for trophic interaction strengths (Figs 1 and 2). Our approach allows both 2D and 3D interactions within the same habitat to be considered, and can be applied to the wide range of foraging strategies found in nature (Fig. 1 and Supplementary Fig. 1). To test our predictions, we compiled a data set that contains a per-capita consumption rate of 255 consumer–resource interactions covering 230 species, 12 orders of magnitude in body size, and aquatic (189 interactions) as well as terrestrial (66 interactions) habitats (Methods).

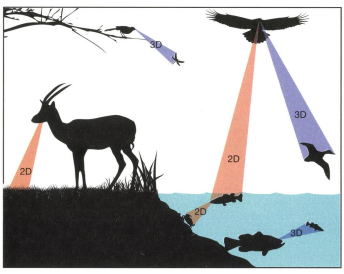

Figure 1 | Consumer–resource interactions can be classified by dimensionality. If the consumer searches for resources (by flying, swimming, or sitting and waiting) on habitat surfaces (for example, on the water surface, benthos or in grassland), the interaction is 2D, and if it searches habitat volume, the interaction is 3D. A consumer or resource may be involved in both 2D and 3D interactions, corresponding to different consumer–resource combinations and foraging strategies.

[1]Department of Biomathematics, David Geffen School of Medicine, University of California, Los Angeles, California 90095-1766, USA. [2]School of Marine and Tropical Biology, James Cook University, Townsville QLD 4811, Australia. [3]Department of Ecology & Evolutionary Biology, University of California, Los Angeles, California 90095, USA. [4]Santa Fe Institute, 1399 Hyde Park Road, Santa Fe, New Mexico 87501, USA.

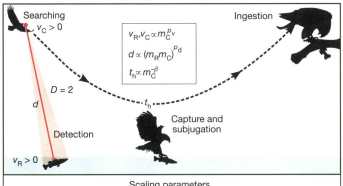
Searching
$v_C > 0$
Ingestion
$v_R m_C^{p_v}$
$d \propto (m_R m_C)^{p_d}$
$t_h \propto m_C^{\beta}$
$D = 2$
d
t_h
Capture and subjugation
Detection
$v_R > 0$
Scaling parameters
m_R, m_C = Resource (R) and consumer (C) body masses
$k_{RC} = m_R/m_C$ = Body mass ratio
β = Exponent for handling time (t_h)
p_v = Exponent for consumer or resource velocity (v_R, v_C)
p_d = Exponent for consumer–resource reaction distance (d)
D = Interaction dimensionality (2 or 3)

Figure 2 | Model for scaling of search and consumption rate with body size. This model (2D active capture is shown here) can also be used to predict search and consumption rates for grazing and sit-and-wait foraging strategies (Supplementary Information).

Empirical patterns

Using our comprehensive data set, we first demonstrate strong empirical differences between 2D and 3D interactions in the scaling of search and consumption rate with consumer body size (Fig. 3). When resources are scarce, more closely resembling field conditions, the observed scaling exponent for consumption rate in 3D interactions (1.06 ± 0.06 (95% confidence intervals)) is significantly higher than in 2D (0.85 ± 0.05) (likelihood ratio test, $P < 0.001$) (Fig. 3a, c). These scaling exponents are significantly higher than the currently used exponent of 0.75 (one-sample F-test $P < 0.01$). Furthermore, apart from organisms that are much smaller than a honeybee (weighing less than 3×10^{-4} kg, where 2D and 3D scaling lines would intersect), 3D consumption rates are higher than in 2D (Fig. 3a, b). For a 1-kg organism, 3D consumption rate is ten times higher than in 2D (6.30 ± 3.01 versus 0.63 ± 0.24 mg s^{-1}) (Fig. 3a, b).

When resources are abundant, typical of laboratory conditions, consumption rates still scale more steeply (1.00 ± 0.06 versus 0.85 ± 0.05) and show higher baseline values in 3D than 2D (19.95 ± 11.00 versus 3.16 ± 1.30 mg s^{-1} for a 1-kg organism) (Fig. 3c, d). Thus, even at high resource densities at which searching for resources is expected to be less constraining, dimensionality remains important. The canonical 0.75 scaling exponent for consumption rate is excluded from the 95% confidence intervals of the observed scaling exponents under all conditions (Fig. 3).

We also analysed the scaling of search rates. The rate at which a consumer searches for a resource limits consumption rates when resources are scarce (Figs 1, 2 and 3e, f). For active-capture and grazing foragers, search rate (area/time or volume/time) is the speed at which a consumer moves through the landscape to find food, whereas for sit-and-wait foragers, it is the speed at which resources move through the consumer's attack space (Figs 1 and 2). We find that search rates have a scaling exponent of 1.05 ± 0.08 in 3D and 0.68 ± 0.12 in 2D (Fig. 3e, f), indicating that differences in consumption-rate scaling are primarily driven by differences in search rate. This result is a key validation of our model below.

A mechanistic model for search rate

Our empirical analysis reveals that search- and consumption-rate scaling vary systematically with the dimensionality of search space (that is, interaction dimensionality). We now present a model that

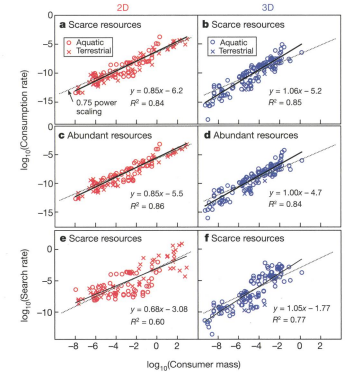

Figure 3 | Effect of interaction dimensionality on scaling of search and consumption rate. a–d, Scaling of per-capita consumption rate (kg s^{-1}) with consumer body mass (kg) at different resource densities. **e**, **f**, Scaling of search rate (m^2 s^{-1} in 2D, and m^3 s^{-1} in 3D). See Table 1 for sample sizes. Solid black lines were fitted using OLS regression (see Methods). Exponents in all panels except **e** are significantly different from the canonical 0.75 value (dotted line). Consumption-rate scaling shows less variance than search rate, possibly because consumers choose resources that maximize biomass consumption rate (product of search rate, resource density and resource mass; equation (4)), thus minimizing scatter.

predicts these empirical patterns by focusing on three key components of search rate: relative velocity, reaction distance and handling time[13,17,26] (Fig. 2). Relative velocity (v_r) is the rate at which consumer–resource pairs converge across the landscape, and it is the root-mean-square of their body velocities. A potential encounter occurs when either the resource or consumer comes within the distance (d) at which one can detect and react to the other. Because each individual moving through the landscape maintains a search space enclosed by a surface with radius d, we can derive (Supplementary Information) that the search rate (α) increases with dimensionality (D):

$$\alpha = s_D v_r d^{D-1} \quad (1)$$

where $s_D = 2$ in 2D and π in 3D. Based on biomechanical principles, we obtained predictions for the scaling exponents p_v and p_d (of v_r and d, respectively; Fig. 2), and validated them empirically using another, independent data set that we compiled (Table 1 and Supplementary Information). Using these, we predict:

$$\alpha = \alpha_0 m_C^{p_v + 2p_d(D-1)} f(k_{RC}) \quad (2)$$

where m_C is consumer body mass. For active foraging, the constant α_0 is $2v_{R0}d_0$ in 2D and $\pi v_{R0}d_0^2$ in 3D. The function $f(k_{RC})$ isolates dependence of α on consumer–resource size ratio k_{RC} (that is, m_R/m_C (where m_R is resource body mass)) from its direct dependence on consumer mass. Both α_0 and $f(k_{RC})$ vary weakly with foraging strategy (Supplementary Information). To relate equation (2) directly to previous studies by expressing it solely in terms of consumer mass, we determine how k_{RC} scales with consumer mass using our consumption-rate data set. Substituting this scaling together with values for p_v and p_d (Table 1) into equation (2) gives:

Table 1 | Empirical and predicted scaling exponents of consumption rate and its components with interaction dimensionality (*D*)

D	Search and consumption rate ($n = 255$)			Consumption-rate components				
	Search rate (scarce resources)	Consumption rate		Relative velocity ($n = 21$)	Reaction distance ($n = 39$)	Handling time ($n = 78$)	Resource mass ($n = 255$)	Resource density ($n = 255$)
		Scarce resources	Abundant resources					
2D	**0.68** ± 0.12* (0.63)	**0.85** ± 0.05 (0.78)	**0.85** ± 0.05 (0.78)	0.26 ± 0.04* (0.27)	0.21 ± 0.08 (0.33)	−1.02 ± 0.08 (−0.75)	0.73 ± 0.10	−0.79 ± 0.08
3D	**1.05** ± 0.08* (1.03)	**1.06** ± 0.06 (1.16)	**1.00** ± 0.06 (1.16)	0.26 ± 0.04* (0.27)	0.20 ± 0.06 (0.33)	−1.1 ± 0.07 (−0.75)	0.92 ± 0.08	−0.86 ± 0.07

For search and consumption rate, if the 3D exponent is significantly larger than 2D as predicted (likelihood ratio test), both are shown in bold. There are no predicted exponents for resource mass and resource density scaling because they depend upon experimental design (Supplementary Information). Steeper than predicted exponents of handling time may arise because pursuit and subjugation scale with maximal rather than resting metabolic rate[9,11].

* Empirical exponent is statistically indistinguishable ($P = 0.05$ for all significance tests) from the predicted value (in parentheses).

$$\begin{aligned} \alpha &\approx \alpha_{2D} m_C^{0.63} \text{ in 2D} \\ \alpha &\approx \alpha_{3D} m_C^{1.03} \text{ in 3D} \end{aligned} \tag{3}$$

where α_{2D} and α_{3D} are dimension-specific constants. These exponents match our empirical results extremely well (Fig. 3e, f and Table 1). Even if the weak contribution of $f(k_{RC})$ (Supplementary Information) to the scaling is ignored, the predicted search rate exponents ($p_y + 2p_d(D-1)$) would be 0.68 in 2D and 1.06 in 3D. These exponents are extremely close to the empirical estimates of 0.68 ± 0.12 in 2D and 1.05 ± 0.08 in 3D (Table 1; Fig. 3).

Predictions for consumption rate

The product of search rate, α, and resource density, x_R (individuals per area or volume), yields encounter rate. Consumption rate is constrained by this encounter rate and by handling time; that is, the duration of time to pursue, subdue and ingest each resource (Fig. 2). Together, these components give a saturating per-capita biomass consumption rate (c) (Holling's type II functional response[27]) in terms of spatial dimension (D):

$$c = \frac{\alpha m_R x_R}{1 + h_t \alpha m_R x_R} = \frac{s'_D v_t d^{D-1} m_R x_R}{1 + h_t s'_D v_t d^{D-1} m_R x_R} \tag{4}$$

Here, m_R is the average mass of the resource, $x_R m_R$ is resource biomass density, and t_h is conventional handling time divided by resource mass (Supplementary Information 1.4). The constant s'_D includes a roughly constant attack success probability. Our results are robust to changes in this probability for resource items common in the consumer's diet (Supplementary Information).

With scarce resources ($x_R \to x_{R,min}$) the second term in the denominator of equation (4) becomes much smaller than 1, and thus $c \approx \alpha x_R m_R$. Substituting the scaling for α (equation (2)) gives:

$$c = \alpha_0 m_C^{p_y + 2p_d(D-1)} f(k_{RC}) x_R m_R \tag{5}$$

To convert this into a scaling relationship solely with consumer mass, we use our functional response data set (Supplementary Information) to quantify the scaling of x_R and m_R with consumer mass (Table 1). Substituting these along with the previously determined scaling of size ratio (k_{RC}) in equation (5) gives:

$$\begin{aligned} c &\approx c_{2D} m_C^{0.78} \text{ in 2D} \\ c &\approx c_{3D} m_C^{1.16} \text{ in 3D} \end{aligned} \tag{6}$$

where c_{2D} and c_{3D} are dimension-specific constants. Equation (6) predicts the steeper and superlinear scaling that is empirically observed in 3D for consumption rate (Fig. 3a, b and Table 1). Note that the scaling of consumption rate, c, closely matches the scaling of search rate, α (compare equations (3) and (6)). The existing small difference arises because of the weak scaling of the product ($x_R m_R$) of resource density and mass with consumer mass (Table 1 and Supplementary Information).

When resources are unlimited ($x_R \to \infty$), the term $s'_D v_t d^{D-1} x_R m_R$ dominates both the numerator and denominator of equation (4), resulting in a value of 1. Consequently, search and detection become instantaneous, and consumption rate depends only on mass-specific handling rate ($1/t_h$) (Fig. 2):

$$c = t_{h,0}^{-1} m_C^{\beta} \tag{7}$$

where β is the scaling exponent of the consumer's whole-body metabolic rate and $t_{h,0}$ is a body-temperature and metabolic-state-dependent constant. We find that mass-specific handling time, t_h, scales as 1.1 ± 0.07 in 3D and 1.02 ± 0.08 in 2D (Supplementary Information). However, the observed consumption-rate scaling in 2D is 0.85 ± 0.05, and is 1.00 ± 0.06 in 3D, both closer to predictions for scarce rather than unlimited resources (Table 1). Therefore, even when functional responses seem to saturate and resources are considered abundant, consumption rate does not scale like handling time, and must therefore continue to be constrained by search dimensionality. This also explains why most previous studies have reported 0.75 power scaling of consumption rate[7,8,19]. The data in these previous studies are actually maximal ingestion rates collected from sedentary individuals that are provided with unlimited resources[7,8,19]. Our data, for both scarce and abundant resources, are more representative of field conditions because they are extracted from functional response data.

Although our theory predicts that α_{3D} and c_{3D} are larger than α_{2D} and c_{2D}, respectively (Supplementary Information), the magnitude of the observed difference is much larger than predicted (Fig. 3). One explanation is that most 3D interactions are aquatic, and most 2D interactions are terrestrial. The energetic cost for swimming is about ten times lower than for running[18,19], probably increasing encounter rates for non-directed movement. This difference could elevate the intercept (but not exponent), contributing to the observed ten times larger baseline consumption rates in 3D. Nevertheless, 2D aquatic and 2D terrestrial interactions scale similarly (Fig. 3a–c), indicating other differences between pelagic (3D) and benthic (2D) aquatic zones, and highlighting the need for further study.

Dimensionality and trophic interaction strengths

By deriving the scaling of search rate (α), a fundamental parameter in consumer–resource and food-web models, we have provided a mechanistic basis for linking interaction dimensionality with trophic interaction strengths, which are proportional to $\alpha x_R m_R / m_C$ (refs 11, 13, 15, 16, 28, 29). In contrast to current theories, our results show that scaling of trophic interaction strength can deviate substantially from $m_C^{-0.25}$. Specifically, if resource size (m_R) and resource density (x_R) are decoupled from consumer size, consumption rate scales like search rate (equation (3)), and thus interaction strength scales as $\alpha x_R m_R / m_C \propto m_C^{-0.32}$ in 2D, and $m_C^{0.05}$ in 3D. Even when m_R and x_R scale with consumer mass (Table 1 and Supplementary Fig. 2), trophic interaction strengths scale as $m_C^{-0.15}$ (2D) or $m_C^{0.06}$ (3D) when resources are scarce, and as $m_C^{-0.15}$ (2D) or m_C^{0} (3D) when resources are abundant. This variation in the scaling of trophic interaction strengths implies that consumer–resource dynamics are likely to be constrained by interaction dimensionality.

Implications for population dynamics

By incorporating our scaling equations for α (equation (3)) into a population dynamics model (Methods), we now show that dimensionality can affect populations in three fundamental ways. First, 3D interactions allow a larger range of viable consumer–resource body-size

combinations than in 2D, primarily because 3D consumption rates scale more steeply and have higher baseline values. Depending upon baseline carrying capacity (K_0, defined as maximal biomass density for a 1 kg organism; Supplementary Information), the majority of 2,929 species pairs from seven communities fall within our predicted coexistence domains (Fig. 4a), with upper and lower limits of observed size ratios closely matching predicted extinction boundaries. In 2D, when K_0 ranges from 0.01 to 1 ($kg^{0.75}\ m^2$) the predicted coexistence domains contain 88.8% to 99.8% of the empirical data. In 3D, when K_0 ranges from 3 to 300 ($kg^{0.75}\ m^3$), 74.3% to 99.8% of the data are within the predicted domain (we explain below why carrying capacity is typically higher in 3D than 2D). Thus, interaction dimensionality may explain why consumer–resource interactions with larger size ratios (for example, filter feeding[30]) and larger consumers are more common in pelagic environments compared to benthic or terrestrial environments[1,8,31] (Fig. 4a).

Second, because strong trophic interactions can destabilize communities[15,16,28,29], communities dominated by 3D interactions (for example, pelagic or aerial habitats) may be inherently unstable. Indeed, we find that persistent consumer–resource boom–bust dynamics are more likely in 3D than in 2D (Fig. 4b and Supplementary Fig. 3). In nature, these instabilities may be partly offset by larger regions of coexistence that are possible in 3D (Fig. 4a) or by negative consumer density dependence[3,24]. Nevertheless, our results are consistent with empirical observations that pelagic communities appear less stable than terrestrial communities[5]. They also suggest that 3D aquatic ecosystems may experience more frequent top-down regulation than 2D terrestrial ecosystems[32,33].

Third, we predict that population densities across consumer–resource pairs scale with body size more steeply in 3D (exponent of −1.12) than 2D (exponent of −0.76) (Fig. 4c). Only 2D scaling matches Damuth's −0.75 rule, which was derived from data on terrestrial mammals (that is, 2D consumers)[14,34]. Thus, for a given carrying capacity (maximal abundance of resources), steeper size–abundance scaling of consumers in 3D habitats relative to 2D habitats should be expected, and this helps to explain deviations from Damuth's rule in local communities[6,14,34–36].

In our population model, we assume resource carrying capacities scale with a 0.75 exponent (Supplementary Information), as expected when food supply to resources is unlimited (equation (7))[26]. For example, maximal abundance of primary producers in 2D (for example, terrestrial plants) and 3D (for example, pelagic phytoplankton) should scale as metabolic rate (that is, Damuth's rule) irrespective of dimensionality, which is well supported empirically[6,8,37,38]. Future studies should incorporate potential differences in scaling of carrying capacity across trophic levels. We also assume higher baseline carrying capacities (K_0) in 3D than 2D (Fig. 4a) because pelagic (3D) phytoplankton have 2–3 orders of magnitude higher turnover rates than terrestrial plants and form a less variable and more nutritious autotroph base than plants in 2D terrestrial ecosystems such as grasslands[6,32,39]. This is an important difference between habitats because it helps to explain the potential advantage of 3D interactions. If resources had the same numbers (but not densities) in 2D and 3D habitats (for example, 1 kg m^{-2} and 1 kg m^{-3}), resources would probably be too sparse for a 3D search space to be advantageous.

The consequences of interaction dimensionality for population dynamics may also be mediated by other abiotic differences between aquatic and terrestrial habitats. For example, 2D habitats such as benthic zones may have a greater potential for prey refuges than 3D habitats such as pelagic zones. Structural complexity reduces consumer search rates, potentially resulting in type III functional responses instead of type I or II (refs 30, 40). We find no significant propensity for type III functional responses in 2D relative to 3D in our data set (Supplementary Information), probably because laboratory experiments typically use habitats that are simpler than real habitats. Even if type III responses are more common in 2D, results for the effects of dimensionality on consumer–resource population dynamics remain qualitatively unchanged (Supplementary Information). Nevertheless, an important future direction will be to understand how habitat complexity affects search and consumption rates. Synthesizing our model with previous work on fractal dimensionality of resource dispersion[3,22,25] should be an important step in this direction. Perception of structural complexity also scales with body size[3]. Grasslands may be structurally simple for a bison, but complex for a nematode.

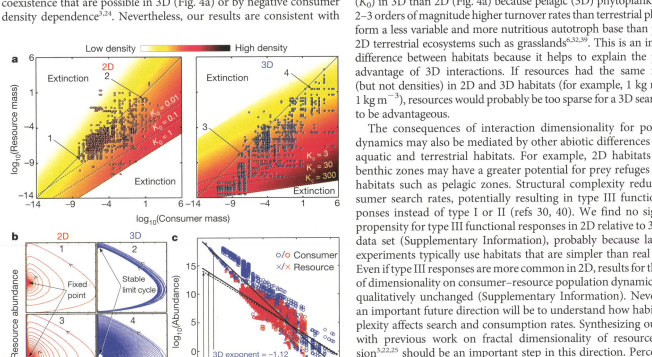

Figure 4 | Effects of interaction dimensionality on consumer–resource dynamics. a, Intensity map of logarithm of total consumer–resource equilibrium densities, ranging from coexistence at high (dark) to low (yellow) densities, or extinction (white). Black dots are real 2D (n = 1,627) and 3D (n = 1,302) consumer–resource pairs (Supplementary Table 8). Consumer and resource sizes are equal along the diagonal line. Lower extinction boundaries (dashed lines) correspond to different baseline carrying capacities (K_0); the outermost boundary corresponds to empirical estimates. Predicted 2D coexistence regions that lack observed species pairs probably represent undersampling of interactions for the smallest consumers (for example, micro predators) and largest consumers (for example, large mammalian herbivores)[31]. **b,** Comparison of population dynamics of two 2D (1 and 2 in **a**) and two 3D (3 and 4 in **a**) species pairs. **c,** Scaling of equilibrium abundance across all 3D (blue) and 2D (red) consumer–resource pairs plotted in **a**. The variation and discrete appearance of the data arises mainly because a consumer may feed on multiple resource species of different sizes and vice versa.

Conclusion

Our study provides new and more accurate scaling relationships for consumer–resource interactions[11,16,31], gives novel insights into consumer–resource dynamics, and offers a mechanistic model that incorporates dimensionality and foraging strategy into food-web dynamics. Our results help to explain why aquatic environments generally show higher energy fluxes and lower stability than terrestrial environments[5], why they often show inverted biomass pyramids[5,32], and why larger consumers have a relative advantage in pelagic (3D) versus terrestrial (2D) environments[1,6]. Predicting strengths of pair-wise trophic interactions is key to understanding higher-order effects, including indirect interactions and polyphagy[5,28,29]. Our model for pairwise interactions should provide a starting point for studying how the effects of dimensionality propagate through entire community food-webs. Studying communities with mixtures of 2D and 3D interactions will

be particularly revealing in this context. We conclude that interaction dimensionality is a critical factor driving consumer–resource dynamics. A better understanding of the effects of dimensionality will lead to better predictions of food-web and ecosystem dynamics, and how these complex systems might respond to environmental change.

METHODS SUMMARY

Functional response data were compiled from the literature (Supplementary Table 5). Interaction dimensionality was assigned according to consumer search space (Fig. 1). The minimum resource density in each study was classified as scarce, and the density corresponding to the maximum consumption rate was classified as abundant. The search rate (a) in each functional response was calculated at each scarce density by dividing the associated consumption rate (c) by the associated density. The scaling of a is our fundamental theoretical result (equation (2)) and is based on derived scalings for v_r, d and t_h. We verified predicted scalings of these components by compiling an additional data set of 136 interactions between 157 taxa. To move from predicted scaling exponents of α (equation (3)) to predictions for scaling exponents of c (equation (4)), we calculated the scaling of resource number density (x_R) and mass (m_R) across studies in the functional response database. All exponents were estimated using ordinary least squares regression (OLS) of log trait value versus log body mass. Major axis regression yields steeper exponents than OLS but does not qualitatively alter our results. We also tested for robustness of predictions to realistic variation in body velocity scaling. All data were standardized to 15 °C using the Boltzmann–Arrhenius model[30,14]. For population dynamics we used the Rosenzweig–MacArthur model for the rate of change in time, t, for the resource ($R = x_R m_R$) and consumer ($C = x_C m_C$) biomass densities[13,26]:

$$\frac{\mathrm{d}R}{\mathrm{d}t} = rR\left(1-\frac{R}{K}\right) - \frac{(\alpha/m_C)RC}{1+h_0\alpha R}$$

$$\frac{\mathrm{d}C}{\mathrm{d}t} = \frac{e(\alpha/m_C)RC}{1+h_0\alpha R} - zC$$

Here, r is the resource's intrinsic biomass production rate, K is resource's biomass carrying capacity, z is the consumer's biomass loss rate, e is the consumer's biomass conversion efficiency, and t_h is the resource mass-specific handling time. Size scaling for α and t_h were based on our results, and that for r, z and K were based on previous work[8,9,14]. We tested robustness of our results by varying model structure between the Rosenzweig-MacArthur model and the Lotka–Volterra predator–prey model, and also by using a type III instead of a type II functional response.

Received 13 December 2011; accepted 3 April 2012.
Published online 30 May 2012.

1. Cohen, J. E. & Fenchel, T. Marine and continental food webs: three paradoxes? *Phil. Trans. R. Soc. Lond. B* **343,** 57–69 (1994).
2. Savage, V. M., Webb, C. T. & Norberg, J. A general multi-trait-based framework for studying the effects of biodiversity on ecosystem functioning. *J. Theor. Biol.* **247,** 213–229 (2007).
3. Ritchie, M. E. *Scale, Heterogeneity, and the Structure and Diversity of Ecological Communities*. Vol. 112 (Princeton Univ. Press, 2009).
4. Briand, F. & Cohen, J. E. Environmental correlates of food-chain length. *Science* **238,** 956–960 (1987).
5. Rip, J. M. K. & McCann, K. S. Cross-ecosystem differences in stability and the principle of energy flux. *Ecol. Lett.* **14,** 733–740 (2011).
6. Cyr, H., Peters, R. H. & Downing, J. A. Population density and community size structure: comparison of aquatic and terrestrial systems. *Oikos* **80,** 139–149 (1997).
7. Farlow, J. O. A consideration of the trophic dynamics of a late Cretaceous large-dinosaur community (Oldman formation). *Ecology* **57,** 841–857 (1976).
8. Peters, R. H. *The Ecological Implications of Body Size*. (Cambridge Univ. Press, 1983).
9. Brown, J. H., Gillooly, J. F., Allen, A. P., Savage, V. M. & West, G. B. Toward a metabolic theory of ecology. *Ecology* **85,** 1771–1789 (2004).
10. Otto, S. B., Rall, B. C. & Brose, U. Allometric degree distributions facilitate food-web stability. *Nature* **450,** 1226–1229 (2007).
11. Berlow, E. L. *et al.* Simple prediction of interaction strengths in complex food webs. *Proc. Natl Acad. Sci. USA* **106,** 187–191 (2009).
12. Lewis, H. M., Law, R. & McKane, A. J. Abundance-body size relationships: the roles of metabolism and population dynamics. *J. Anim. Ecol.* **77,** 1056–1062 (2008).
13. Yodzis, P. & Innes, S. Body size and consumer resource dynamics. *Am. Nat.* **139,** 1151–1175 (1992).
14. Savage, V. M., Gillooly, J. F., Brown, J. H., West, G. B. & Charnov, E. L. Effects of body size and temperature on population growth. *Am. Nat.* **163,** 429–441 (2004).
15. Brose, U., Williams, R. J. & Martinez, N. D. Allometric scaling enhances stability in complex food webs. *Ecol. Lett.* **9,** 1228–1236 (2006).
16. Brose, U. Body-mass constraints on foraging behaviour determine population and food-web dynamics. *Funct. Ecol.* **24,** 28–34 (2010).
17. McGill, B. J. & Mittelbach, G. G. An allometric vision and motion model to predict prey encounter rates. *Evol. Ecol. Res.* **8,** 691–701 (2006).
18. Alexander, R. M. *Principles of Animal Locomotion*. (Princeton Univ. Press, 2003).
19. Schmidt-Nielsen, K. *Scaling, Why is Animal Size so Important?* (Cambridge Univ. Press, 1984).
20. Jetz, W., Carbone, C., Fulford, J. & Brown, J. H. The scaling of animal space use. *Science* **306,** 266–268 (2004).
21. Weibel, E. R., Bacigalupe, L. D., Schmitt, B. & Hoppeler, H. Allometric scaling of maximal metabolic rate in mammals: muscle aerobic capacity as determinant factor. *Respir. Physiol. Neurobiol.* **140,** 115–132 (2004).
22. Holling, C. S. Cross-scale morphology, geometry, and dynamics of ecosystems. *Ecol. Monogr.* **62,** 447–502 (1992).
23. Whitehead, H. & Walde, S. J. Habitat dimensionality and mean search distances of top predators: implications for ecosystem structure. *Theor. Popul. Biol.* **42,** 1–9 (1992).
24. Witting, L. The body mass allometries as evolutionarily determined by the foraging of mobile organisms. *J. Theor. Biol.* **177,** 129–137 (1995).
25. Milne, B. T., Turner, M. G., Wiens, J. A. & Johnson, A. R. Interactions between the fractal geometry of landscapes and allometric herbivory. *Theor. Popul. Biol.* **41,** 337–353 (1992).
26. Weitz, J. S. & Levin, S. A. Size and scaling of predator-prey dynamics. *Ecol. Lett.* **9,** 548–557 (2006).
27. Holling, C. S. Some characteristics of simple types of predation and parasitism. *Can. Entomol.* **91,** 385–398 (1959).
28. Laska, M. S. & Wootton, T. J. Theoretical concepts and empirical approaches to measuring interaction strength. *Ecology* **79,** 461–476 (1998).
29. Pawar, S. Community assembly, stability and signatures of dynamical constraints on food web structure. *J. Theor. Biol.* **259,** 601–612 (2009).
30. Jeschke, J. M., Kopp, M. & Tollrian, R. Consumer-food systems: why type I functional responses are exclusive to filter feeders. *Biol. Rev. Camb. Phil. Soc.* **79,** 337–349 (2004).
31. Brose, U. *et al.* Consumer–resource body-size relationships in natural food webs. *Ecology* **87,** 2411–2417 (2006).
32. Shurin, J. B., Gruner, D. S. & Hillebrand, H. All wet or dried up? Real differences between aquatic and terrestrial food webs. *Proc. R. Soc. B* **273,** 1–9 (2006).
33. Chase, J. M. Are there real differences among aquatic and terrestrial food webs? *Trends Ecol. Evol.* **15,** 408–412 (2000).
34. Damuth, J. Population density and body size in mammals. *Nature* **290,** 699–700 (1981).
35. Reuman, D. C. *et al.* Allometry of body size and abundance in 166 food webs. *Adv. Ecol. Res.* **41,** 1–44 (2009).
36. Leaper, R. & Raffaelli, D. Defining the abundance body-size constraint space: data from a real food web. *Ecol. Lett.* **2,** 191–199 (1999).
37. Cermeño, P., Maranon, E., Harbour, D. & Harris, R. P. Invariant scaling of phytoplankton abundance and cell size in contrasting marine environments. *Ecol. Lett.* **9,** 1210–1215 (2006).
38. Belgrano, A., Allen, A. P., Enquist, B. J. & Gillooly, J. F. Allometric scaling of maximum population density: a common rule for marine phytoplankton and terrestrial plants. *Ecol. Lett.* **5,** 611–613 (2002).
39. Field, C. B., Behrenfeld, M. J., Randerson, J. T. & Falkowski, P. Primary production of the biosphere: integrating terrestrial and oceanic components. *Science* **281,** 237–240 (1998).
40. Vucic-Pestic, O., Rall, B. C., Kalinkat, G. & Brose, U. Allometric functional response model: body masses constrain interaction strengths. *J. Anim. Ecol.* **79,** 249–256 (2010).

Supplementary Information is linked to the online version of the paper at www.nature.com/nature.

Acknowledgements We thank the authors who contributed data (Supplementary Tables 5–8), and P. Amarasekare, J. H. Brown, E. Economo, A. Mikheyev, C. Estrada, C. Johnson, M. Johnson and K. Lafferty for helpful discussions and comments. S.P., A.I.D. and V.M.S. were supported by University of California, Los Angeles Biomathematics start-up funds and by the US National Science Foundation Division of Environmental Biology award 1021010. The data reported in this paper are available in the Supplementary Information online.

Author Contributions S.P., A.I.D. and V.M.S. contributed equally to this work. All authors discussed the results and commented on the manuscript.

Author Information Reprints and permissions information is available at www.nature.com/reprints. The authors declare no competing financial interests. Readers are welcome to comment on the online version of this article at www.nature.com/nature. Correspondence and requests for materials should be addressed to S.P. (samraat@ucla.edu).

ARTICLE

doi:10.1038/nature11163

mTORC1 in the Paneth cell niche couples intestinal stem-cell function to calorie intake

Ömer H. Yilmaz[1,2]*, Pekka Katajisto[2]*, Dudley W. Lamming[2], Yetis Gültekin[1,2], Khristian E. Bauer-Rowe[2], Shomit Sengupta[2], Kivanc Birsoy[2], Abdulmetin Dursun[1], V. Onur Yilmaz[2], Martin Selig[1], G. Petur Nielsen[1], Mari Mino-Kenudson[1], Lawrence R. Zukerberg[1], Atul K. Bhan[1], Vikram Deshpande[1] & David M. Sabatini[2]

How adult tissue stem and niche cells respond to the nutritional state of an organism is not well understood. Here we find that Paneth cells, a key constituent of the mammalian intestinal stem-cell (ISC) niche, augment stem-cell function in response to calorie restriction. Calorie restriction acts by reducing mechanistic target of rapamycin complex 1 (mTORC1) signalling in Paneth cells, and the ISC-enhancing effects of calorie restriction can be mimicked by rapamycin. Calorie intake regulates mTORC1 in Paneth cells, but not ISCs, and forced activation of mTORC1 in Paneth cells during calorie restriction abolishes the ISC-augmenting effects of the niche. Finally, increased expression of bone stromal antigen 1 (*Bst1*) in Paneth cells—an ectoenzyme that produces the paracrine factor cyclic ADP ribose—mediates the effects of calorie restriction and rapamycin on ISC function. Our findings establish that mTORC1 non-cell-autonomously regulates stem-cell self-renewal, and highlight a significant role of the mammalian intestinal niche in coupling stem-cell function to organismal physiology.

Mammalian tissue-specific stem cells maintain tissue homeostasis by undergoing either self-renewing or differentiation divisions that generate more stem cells or restricted progenitors, respectively[1]. Stem cells often require cues from their microenvironment or 'niche' to regulate their fates. Caloric restriction, an intervention in which caloric intake is reduced while maintaining adequate nutrition, promotes longevity in diverse organisms, possibly by preserving stem and progenitor cell function[2,3]. In mice, calorie restriction promotes the generation of new neurons from neural progenitors and prevents the decline of haematopoietic stem-cell numbers and function in certain strains of mice with age[2,4–7]. These findings raise the question of how caloric restriction mediates these effects on stem cells, and whether the mammalian stem-cell niche is involved.

We have investigated this question in the rapidly renewing mammalian small intestine. The intestine is organized into crypts that contain the stem cells and the rapidly dividing transient amplifying cells, and villi composed primarily of post-mitotic absorptive enterocytes. In response to fasting and re-feeding, the intestine undergoes structural alterations such as changes in villi length, crypt depth and cell turnover, indicating that organismal physiology may modify intestinal progenitor function[8,9]. Recent studies have begun to define the identity of intestinal stem cells as well as their interaction with their Paneth cell niche[10–15]. Although no single marker identifies the entire ISC pool, Lgr5 is expressed by a majority of ISCs throughout the intestinal tract[13,15]. $Lgr5^+$ ISCs (also called crypt base columnar cells) can self-renew and differentiate for the life of the organism, and they reside at the base of crypts sandwiched between Paneth cells[13,16]. Loss of Paneth cells *in vivo* leads to reduced numbers of $Lgr5^+$ ISCs, whereas the addition of Paneth cells to *in vitro* cultures markedly increases the potential of $Lgr5^+$ ISCs to form multipotent, self-renewing organoid bodies reminiscent of 'mini-intestines'[14]. Thus, Paneth cells constitute a critical component of the stem-cell niche both *in vivo* and *in vitro*[13,14].

Calorie restriction increases stem and niche cell numbers

To assess the effects of calorie restriction on intestinal homeostasis, we calorically restricted mice for 4–28 weeks, which is sufficient to observe many of the metabolic phenotypes of calorie restriction[17–19]. Consistent with previous reports, calorically restricted mice had a $19.7 \pm 5.8\%$ loss in body mass compared to *ad libitum* fed counterparts (Supplementary Fig. 1a)[20]. In calorically restricted mice the small intestine was morphologically normal (Supplementary Fig. 1f), with no change in crypt density (Supplementary Fig. 1d), intestinal length (Supplementary Fig. 1c), or apoptotic cell frequency (Supplementary Fig. 3). However, it did have reduced mass (1.8 ± 0.4 versus 1.4 ± 0.2 g; Supplementary Fig. 1b) with villi that were 15% shorter and possessed fewer enterocytes (Supplementary Fig. 1e, f). Calorie restriction did not affect the frequency of chromogranin A^+ enteroendocrine cells, but mildly reduced that of alcian $blue^+$ secretory goblet cells (Supplementary Fig. 2a, b). To address how calorie restriction influenced the frequency of ISCs, we performed *in situ* hybridization for olfactomedin 4 (Olfm4), a recently described marker that is co-expressed by $Lgr5^+$ ISCs[21]. Calorie restriction led to a 35% increase in $Olfm4^+$ primitive intestinal progenitors compared to those in *ad libitum* fed mice (Fig. 1a and Supplementary Fig. 7a). Notably, calorie restriction also caused a commensurate increase in cryptdin 4^+ Paneth cells (Fig. 1a and Supplementary Fig. 7b), which we confirmed by morphological examination of 1-μm-thick tissue sections (Supplementary Fig. 4a) and by electron microscopy (Supplementary Fig. 4b). These findings lead to two intriguing conclusions: first, calorie restriction promotes the preservation and self-renewal of ISCs (increased $Olfm4^+$ ISCs) at the expense of differentiation (shorter villi with fewer mature

[1]Department of Pathology, Massachusetts General Hospital and Harvard Medical School, Boston, Massachusetts 02114, USA. [2]Whitehead Institute for Biomedical Research, Boston, Massachusetts 02142; Department of Biology, MIT, Cambridge, Massachusetts 02139; Howard Hughes Medical Institute, MIT, Cambridge, Massachusetts 02139; Broad Institute of Harvard and MIT, Seven Cambridge Center, Cambridge, Massachusetts 02142; The David H. Koch Institute for Integrative Cancer Research at MIT, Cambridge, Massachusetts 02139, USA.
*These authors contributed equally to this work.

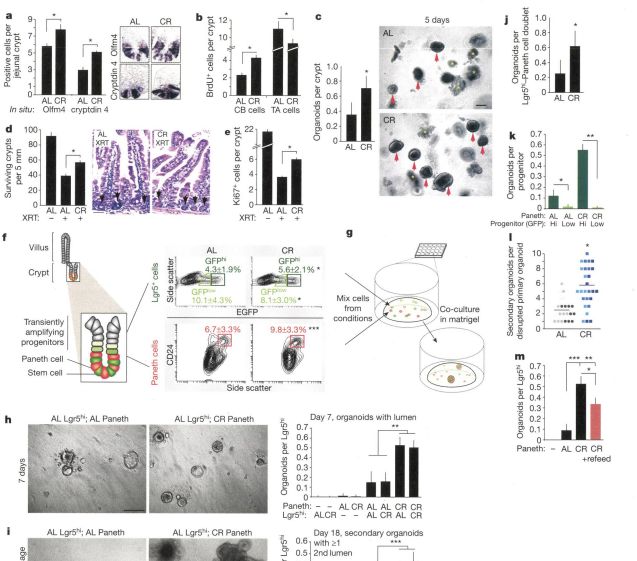

Figure 1 | Calorie restriction augments the capacity of Paneth cells to boost ISC function. a, Olfm4$^+$ ISCs and cryptdin 4$^+$ Paneth cells were increased in calorie-restricted (CR) mice (*in situ* hybridization, proximal jejunum, $n = 3$). AL, *ad libitum* fed. **b**, Crypt base columnar cells (CB cells) showed a twofold increase in BrdU incorporation and transient amplifying cells revealed a reduction after a 4-h pulse in calorie-restricted mice ($n = 3$). **c**, Calorie-restricted crypts were twofold more capable of forming organoids ($n = 8$). Representative *ad libitum* fed and calorie-restricted organoids are shown at 5 days (red arrowhead marks organoids and yellow asterisk indicates aborted crypts). **d**, **e**, Calorie restriction increased the number of surviving (**d**) and proliferating (**e**, Ki67$^+$) crypts after ionizing irradiation-induced (XRT) damage ($n = 3$ for **d** and **e**). **f**, Schematic demonstrating dark-green Lgr5^{hi} ISCs, red Paneth cells and light-green EGFP^{low} progenitors. Calorie restriction increased ISCs (dark green) and Paneth cells (red) by 1.5-fold, and reduced EGFP^{low} (light green) progenitors by 20% (calorie restriction, $n = 27$; *ad libitum*, $n = 26$). **g**, Schematic illustrating the mixing of ISCs with Paneth cells in matrigel. **h**, Organoid formation per Lgr5^{hi} ISCs co-cultured with Paneth cells from calorie-restricted mice was significantly increased ($n = 5$). **A** representative image of primary organoids at day 7 is shown. **i**, Dissociated organoids derived from calorie-restricted Paneth cells gave rise to larger secondary organoids at day 18 ($n = 5$). **j**, Sorted ISC–Paneth cell doublets plated at clonal density (50–100 doublets per 30 µl droplet of matrigel) demonstrated that calorie-restricted doublets had nearly threefold more organoid potential ($n = 3$). **k**, EGFP^{low} progenitors harboured little organoid potential ($n = 4$). **l**, Subcloning of individual calorie-restricted Paneth-derived organoids gave rise to threefold more secondary organoids (27 organoids from 3 independent mice per condition were analysed, shades of grey or blue denote separate mice). **m**, Paneth cells isolated from mice that had been on calorie restriction, but were returned to an *ad libitum* diet for 3 days, also retained an augmented capacity to promote organoid formation ($n = 3$). (Unless otherwise indicated, in all panels: values are mean; error bars indicate s.d.; scale bars are 50 µm; $*P < 0.05$; $**P < 0.01$; $***P < 0.001$.)

enterocytes); second, ISCs and their Paneth cells increase in tandem, raising the possibility that the Paneth cell niche may coordinate ISC adaptation to calorie restriction.

The fact that calorie restriction augmented ISC numbers while reducing the total number of differentiated enterocytes indicated that calorie restriction enhances the proliferation of ISCs while reducing the proliferation of more differentiated progenitors (transient amplifying cells). To test this possibility, we assessed incorporation of 5-bromodeoxyuridine (BrdU) into ISCs and transient amplifying cells. After a 4-h pulse of BrdU, crypts of calorie-restricted mice

had nearly twofold as many $BrdU^+$ ISCs compared to crypts of *ad libitum* fed mice (4.3 ± 0.3 versus 2.4 ± 0.2, Fig. 1b and Supplementary Fig. 1g, h). However, calorie restriction decreased the number of $BrdU^+$ cells in the larger pool of transient amplifying cells (11.0 ± 0.9 versus 9.4 ± 0.5; Fig. 1b), indicating that output and migration into the villi from this compartment may also be reduced. Indeed, calorie-restricted mice 24 h after a single dose of BrdU had fewer absolute numbers of BrdU-labelled cells in the villi compared to *ad libitum* fed controls (14.5 ± 1.5 versus 19.0 ± 1.7; Supplementary Fig. 1i, j). However, there was no significant difference in the percentage of $BrdU^+$ villous enterocytes, indicating that in calorie-restricted mice, transient amplifying cells generate fewer progeny for shorter, less cellular villi (Supplementary Fig. 1k). These data demonstrate that calorie restriction alters the coupling between stem cell and transient amplifying cell proliferation *in vivo*.

Calorie restriction promotes intestinal regeneration

Because calorie restriction increased the frequency and proliferation of ISCs, we asked whether it also promotes the regeneration of the small intestinal epithelium. We tested the potential of isolated crypts, independent of intestinal stem cell markers, to form clonal, multipotent organoid bodies that posses all intestinal cell types *in vitro*[22] (Supplementary Fig. 5). Crypts from calorie-restricted mice were nearly twofold more likely to form organoid bodies than those from *ad libitum* fed controls (Fig. 1c). These data indicate that calorie restriction leads to an increase in stem-cell activity per crypt, as only stem cells are capable of self-renewing and differentiating into the various cell types that are required for organoid body formation and maintenance.

To ask whether calorie restriction also augments crypt regeneration *in vivo*, we used the clonogenic microcolony assay for testing ISC activity[23]. In *ad libitum* and calorie-restricted mice exposed to lethal doses of radiation and examined 72 h later, calorie restriction significantly increased the number of surviving and regenerating crypts and $Ki67^+$ intestinal progenitors per unit length of intestine (Fig. 1d, e). These data are consistent with our *in vivo* and *in vitro* data showing that calorie restriction increases the number and regenerative capacity of ISCs.

Calorie restriction enhances ISC function via the niche

To understand how calorie restriction affects the frequency and function of ISCs and their Paneth cell niche, we performed calorie restriction experiments on *Lgr5-EGFP-IRES-creERT2* knock-in mice, which allow isolation by flow cytometry of Lgr5–$EGFP^{hi}$ ISCs and their daughter, more differentiated $EGFP^{low}$ cells[16]. Compared to *ad libitum* fed controls, calorie restriction increased the frequency of Lgr5–$EGFP^{hi}$ ISCs ($5.6 \pm 2.1\%$ versus $4.3 \pm 1.9\%$; Fig. 1f) and Paneth cells ($9.8 \pm 3.3\%$ versus $6.7 \pm 3.3\%$; Fig. 1f and Supplementary Figs 8 and 9) by 1.5-fold. The frequency of the much larger pool of $EGFP^{low}$ differentiated progenitors, however, was lower in calorie-restricted mice ($8.1 \pm 3.0\%$ versus $10.1 \pm 4.3\%$; Fig. 1f). These data corroborate the phenotypic expansion of ISCs and Paneth cells detected with the Olfm4 and cryptdin 4 markers, respectively (Fig. 1a, and Supplementary Fig. 7a, b), and suggest that although calorie restriction expands the pool of ISCs it leads to a reduction of more differentiated progenitors. Thus, calorie restriction has opposing effects on the numbers of stem cells and their immediate progeny, shifting the equilibrium towards stem-cell self-renewal.

The enhanced regenerative activity of crypts in calorie-restricted mice led us to ask whether ISCs respond to calorie restriction autonomously or non-autonomously through the Paneth cell. To test this, we combined ISCs and Paneth cells isolated from calorie-restricted and *ad libitum* fed mice and assayed their ability to form organoid bodies in culture (Fig. 1g). Consistent with previous studies[14,22], neither Lgr5–$EGFP^{hi}$ ISCs nor Paneth cells established organoid bodies on their own, but, when co-cultured, 15% of ISCs did generate organoid bodies (Fig. 1g, h). Notably, Paneth cells isolated from calorie-restricted mice were significantly more likely than those from *ad libitum* fed controls to promote organoid body formation when mixed with ISCs (Fig. 1h), and this augmentation persisted even after 7 months of calorie restriction (Supplementary Fig. 6). In contrast, calorie restriction had neither a direct effect on ISC function (as calorie-restricted and *ad libitum* ISCs behaved similarly) nor did it boost the potential of $EGFP^{low}$ progenitors to form organoid bodies (Fig. 1h, k). Ruling out the possibility that the enhanced regeneration caused by calorie-restricted Paneth cells resulted from an increase in their ability to home and attach to ISCs in culture, ISC–Paneth cell doublets isolated from calorie-restricted mice had a threefold increase in their capacity to form organoid bodies compared to those from *ad libitum* fed mice (Fig. 1j). Not only did calorie-restricted Paneth cells promote primary organoid body formation, these organoids gave rise to more and larger secondary organoid bodies, even when individually subcloned (Fig. 1i, l). Thus, individual organoid bodies from calorie-restricted Paneth cells posses a greater ability to self-renew (Fig. 1l). The fact that Lgr5–$EGFP^{hi}$ ISCs form more organoid bodies when co-cultured with calorie-restricted Paneth cells indicates that most Lgr5–$EGFP^{hi}$ cells harbour stem-cell potential when exposed to the appropriate niche signals (Fig. 1h, k).

Calorie intake activates mTORC1 in the niche

Because the mTORC1 kinase is a major sensor of the organismal nutritional state, we asked whether calorie restriction mediates its effects on Paneth cells through mTORC1 (ref. 24). Consistent with this, overnight fasting decreased phosphorylation of S6 (pS6), a marker of mTORC1 activity in the intestine (Fig. 2a). Interestingly, feeding or insulin activated mTORC1 in Paneth cells but not in ISCs in a rapamycin-sensitive fashion (Fig. 2a). We confirmed these findings in sorted Paneth cells (>95% $lysozyme^+$; Fig. 2b) and found that pS6 expression was induced in the Paneth cells of fasted mice by insulin administration. Similarly in immunoblots from isolated crypts of calorie-restricted mice, phosphorylation of S6 and S6K1, the latter being a direct substrate of mTORC1, was diminished (Fig. 2c). These data indicate that Paneth cells may modulate ISC function by sensing the organismal nutritional status through mTORC1.

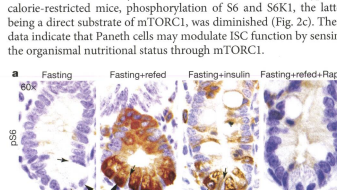

Figure 2 | Nutritional regulation of mTORC1 in Paneth cells. a, Overnight fasted mice treated without or with rapamycin (Rapa) were refed for 5 h and intestinal sections immunostained for phospho-S6 (pS6). Refeeding or administration of insulin activates mTORC1 in Paneth cells (arrowheads) but not ISCs (arrows, $n = 3$–5, scale bar = 20 μm). **b**, Similar results were observed in preparations of sorted Paneth cells that were confirmed to be greater than 95% positive for the Paneth cell marker lysozyme ($n = 3$). pS6 was reduced in sorted Paneth cells from fasted mice and was induced 20 min after injection with insulin. **c**, Immunoblots of isolated crypts from calorie-restricted mice show reduced phosphorylation of known mTORC1 substrates phospho-S6K1 (pS6K1) and pS6.

Niche mTORC1 mediates calorie restriction effects

To address whether reduced mTORC1 signalling in Paneth cells enhances ISC function in response to calorie restriction, we generated mice in which the expression of *Rheb2* (an mTORC1 activator) can be induced by doxycycline from the ubiquitously expressed *Col1a1* (also called *Col1a1*) promoter (*Rheb*-tg, using the human *RHEB2* coding sequence) (Fig. 3a, b). In mice fasted overnight, induction of *Rheb2* was sufficient to reactivate mTORC1 signalling in Paneth cells (Fig. 3c, d). Notably, *Rheb2* induction during calorie restriction blocked the increase in clonogenicity per crypt (Fig. 3e) normally caused by calorie restriction, prevented isolated Paneth cells from enhancing organoid formation when cultured with ISCs (Fig. 3f), and abolished the increase in Olfm4$^+$ ISC and cryptdin 4$^+$ Paneth cell numbers observed in calorie restriction *in vivo* (Supplementary Fig. 7a, b). To confirm that persistent mTORC1 activity negates the increase in Paneth cell frequency observed under calorie restriction, *Tsc1*—a negative regulator of mTORC1—was excised using *Tsc1*$^{loxp/loxp}$; *Rosa26-creERT2* mice. The excision of *Tsc1* during calorie restriction (similar to Rheb2 induction) prevented the increase in Paneth cell frequency as assessed by flow cytometry (Supplementary Fig. 7c). Thus, persistent mTORC1 activity during calorie restriction is sufficient to prevent Paneth cells in calorie-restricted mice from promoting ISC function (Fig. 3e, f and Supplementary Fig. 7a–c).

As constitutive activation of mTORC1 abrogated the effects of calorie restriction, we asked whether inhibition of mTORC1 with rapamycin mimics the effects of calorie restriction. Indeed, administration of rapamycin for 4 weeks to mice increased the frequency of ISCs and Paneth cells by more than 1.5-fold (Fig. 3g, h), and crypts isolated from mice treated for just 1 week with rapamycin were as capable of forming organoid bodies as those from mice on calorie restriction (Fig. 3i). Furthermore, rapamycin increased the clonogenicity of crypts irrespective of whether they were isolated from adult intestines expressing or lacking *Rictor*, a necessary and specific component of mTORC2 (Fig. 3k)[25]. These data indicate that rapamycin mediates this enhancement in crypt clonogenicity by inhibiting mTORC1 and does so independently of mTORC2.

Like calorie restriction, rapamycin acts non-autonomously because when Paneth cells isolated from rapamycin-treated mice were mixed with ISCs from control or rapamycin-treated mice, they caused a prominent increase in the formation of primary and subcloned

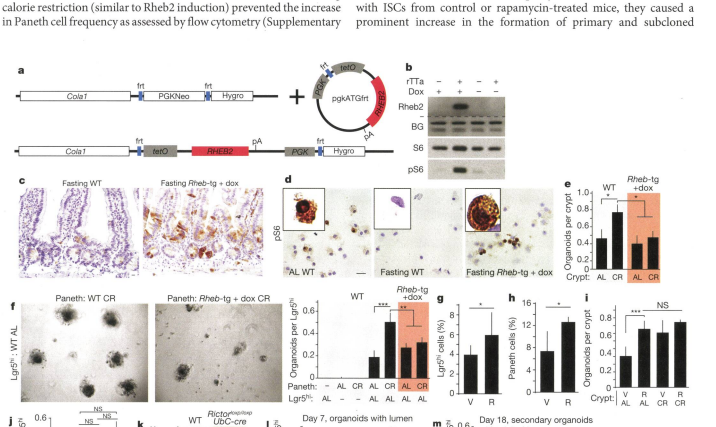

Figure 3 | mTORC1 signalling in Paneth cells mediates the effects of calorie restriction on ISC function. **a**, Schematic of the Tet-ON human *RHEB2* transgene (*Rheb*-tg). **b**, Doxycycline (dox) induced Rheb2 protein and S6 phosphorylation in the liver (background band, BG). **c**, **d**, Fasted *Rheb*-tg mice demonstrated increased immunostaining of pS6 in intestinal epithelium (**c**) and in isolated Paneth cells (**d**) upon doxycycline injection. WT, wild type. **e**, **f**, Induction of *Rheb2* from the start of calorie restriction abrogated the enhancement in organoid formation per crypt ($n = 3$) (**e**) and per Lgr5^{hi} ISC co-cultured with Paneth cells ($n = 5$) (**f**). **g**, **h**, Four weeks of rapamycin (R) ($n = 13$) increased the *in vivo* frequency of Lgr5^{hi} ISCs (**g**) and Paneth cells (**h**) compared to vehicle (V) ($n = 14$) as measured by flow cytometry. **i**, **j**, Organoid potential of intestinal crypts ($n = 3$) (**i**) and *ad libitum* fed Lgr5^{hi} ISCs with Paneth cells ($n = 5$) (**j**) from rapamycin, calorie restricted, or calorie-restricted and rapamycin-treated mice. NS, not significant. **k**, Rapamycin increased crypt organoid formation in Rictor-deleted *Rictor*$^{flox/flox}$*UBC-creERT2* mice ($n = 3$) to a similar extent as in wild-type (WT) mice. **l**, Organoid formation of Lgr5^{hi} ISCs combined with Paneth cells from rapamycin-treated mice was significantly increased in comparison to Paneth cells from vehicle-treated mice ($n = 5$). **m**, Dissociated primary organoids derived from rapamycin-treated Paneth cells gave rise to more secondary organoids ($n = 5$). (Unless otherwise indicated, in all panels: values are mean; error bars indicate s.d.; scale bars are 20 μm; $^*P < 0.05$, $^{**}P < 0.01$; $^{***}P < 0.001$.)

secondary organoid bodies (Fig. 3j, l, m). Moreover, rapamycin treatment and calorie restriction did not have additive effects on either the ability of crypts (Fig. 3i) or Paneth cells (Fig. 3j, l) to form organoid bodies, indicating that calorie restriction mediates many of its effects by reducing mTORC1. These data, together with the finding that calorie restriction and rapamycin have non-additive effects (Fig. 3i, j), demonstrate that calorie restriction and rapamycin indirectly promote ISC function and do so by reducing mTORC1 signalling in Paneth cells.

Calorie restriction boosts *Bst1* levels in Paneth cells

Several observations indicate that calorie restriction and rapamycin induce a state in Paneth cells that is quite stable. For example, Paneth cells taken from calorie-restricted or rapamycin-treated mice maintain their augmented capacity to promote ISC self-renewal even when placed in nutrient-rich media that should activate mTORC1 (Figs 1h and 3l). Similarly, Paneth cells isolated from mice that had been on calorie restriction, but were returned to an *ad libitum* diet for 3 days, also retain an enhanced capacity to promote ISC function in the organoid assay (Fig. 1m). To gain a mechanistic insight into how calorie restriction mediates its effects in Paneth cells, we undertook gene expression profiling of Paneth cells isolated by flow cytometry from *ad libitum* fed and calorie-restricted mice ($n = 3$ and 4, respectively). Calorie restriction significantly changed the expression of 401 genes ($P < 0.01$), including 57 that encode cell-surface or secreted proteins; however, there were no changes in pathways previously implicated in mediating the Paneth cell and ISC interaction, such as Wnt or Notch (Fig. 4a, b and Supplementary Table 1)[14].

Of the genes upregulated by calorie restriction, we focused on *Bst1* because its expression in bone marrow stromal cells promotes the proliferation of haematopoietic progenitors[26]. Bst1 is an ectoenzyme that converts NAD+ to cyclic ADP ribose (cADPR), a paracrine effector that enters responder cells via nucleoside transporters to activate calcium signalling and promote proliferation. Calorie restriction increased *Bst1* mRNA and protein expression in Paneth cells and caused a shift in its SDS–PAGE mobility, indicative of protein processing (Fig. 4b–d). Notably, although the addition of cADPR to crypt culture boosted the organoid-forming potential of crypts in *ad libitum* fed mice, it did not augment the ability of crypts in calorie-restricted mice to form organoids (Fig. 4e). Lastly, we asked whether *Bst1* was necessary to mediate the effects of calorie restriction in the organoid formation assay (Fig. 4f, g). Indeed, knockdown of *Bst1* mRNA with two independent functional siRNAs abrogated the enhanced capacity of crypts in calorie-restricted mice to form organoids, and the addition of exogenous cADPR was sufficient to rescue the loss of Bst1. These data demonstrate that calorie restriction, in an mTORC1-regulated manner, induces *Bst1* in Paneth cells, that *Bst1* is necessary to mediate many of the effects of calorie restriction, and that cADPR substitutes for *Bst1* in the organoid assay.

Discussion

Our data favour a model in which the mammalian intestinal stem-cell niche couples organismal nutritional status to stem-cell function. Reduced calorie intake leads to more ISC self-renewal (expansion of phenotypic ISCs *in vivo*), an accompanying increase in the ISC niche, and to an increase in ISC function and regeneration *in vivo* and *in vitro*. Although it is unclear why calorie restriction increases ISC numbers and function, one possibility is that in low calorie conditions it may be advantageous for ISCs to shift the balance slightly towards self-renewal while reducing the pool and proliferation of more differentiated transient amplifying cells. Preserving or increasing the stem-cell pool may better prepare the intestine for rapid regeneration once nutrients become available and so enable organisms to adapt to periods of prolonged famine interspersed with times of abundant food.

Non-cell-autonomous mechanisms also orchestrate intestinal remodelling in the *Drosophila* mid-gut, highlighting the importance of the stem-cell niche as a sensor of organismal physiology in diverse species[27]. Fasting in *Drosophila* diminishes ISC numbers whereas refeeding markedly expands them. In contrast, we find that calorie

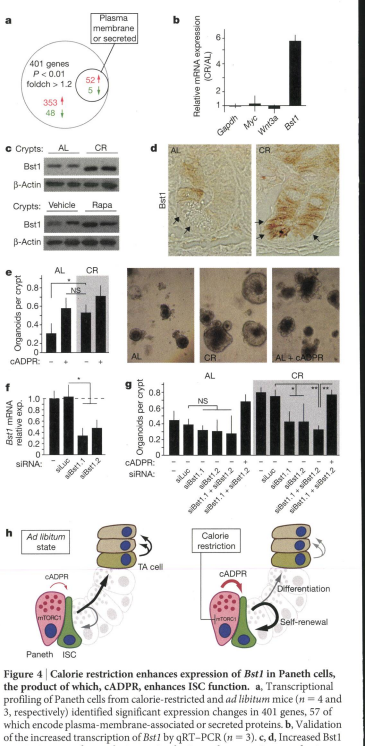

Figure 4 | Calorie restriction enhances expression of *Bst1* in Paneth cells, the product of which, cADPR, enhances ISC function. **a**, Transcriptional profiling of Paneth cells from calorie-restricted and *ad libitum* mice ($n = 4$ and 3, respectively) identified significant expression changes in 401 genes, 57 of which encode plasma-membrane-associated or secreted proteins. **b**, Validation of the increased transcription of *Bst1* by qRT–PCR ($n = 3$). **c**, **d**, Increased Bst1 protein in crypts from calorie-restricted mice and rapamycin-treated mice detected via immunoblotting (**c**) and in calorie-restricted Paneth cells by immunostaining (**d**). **e**, Exogenous cADPR increased the organoid forming potential of crypts of *ad libitum* fed mice to an extent similar to that of crypts of calorie-restricted mice ($n = 3$). **f**, **g**, Inhibition of *Bst1* by short interfering RNA (siRNA)-mediated knockdown ($n = 3$) (**f**) abrogated the enhanced potential of crypts from calorie-restricted mice to form organoids ($n = 3$) (**g**). **h**, A model of intestinal adaptation to calorie restriction by non-cell-autonomous regulation of ISC self-renewal. Calorie restriction attenuates mTORC1 activity in the Paneth cells, resulting in increased expression of *Bst1*, whose paracrine product cADPR promotes ISC self-renewal. TA, transient amplifying. $*P < 0.05$; $**P < 0.01$; $***P < 0.001$. Values are means and error bars indicate s.d.

restriction in the murine intestine preserves the numbers of ISCs, but reduces the numbers and output of transient amplifying cells. Flexible intestinal adaptation in the fly gut occurs by direct modulation of ISCs, the only cells capable of proliferation, whereas in the murine intestine such adaptation can be achieved by differentially regulating ISCs and the larger, more proliferative pool of transient amplifying cells. In both systems, however, ISCs respond to organismal demands in part by niche signals.

Calorie restriction mediates many of its effects on ISCs by reducing mTORC1 signalling in the ISC niche, emphasizing the importance of non-cell-autonomous mechanisms in intestinal adaptation and regeneration. Moreover, our data raise the possibility that the use of mTORC1 inhibitors or Bst1 mimetics, such as US Food and Drug Administration (FDA)-approved drugs like rapamycin or cADPR, respectively, may have an application in improving intestinal regeneration and function in patients. It remains to be determined whether persistent mTORC1 activity in the ISC niche accounts for intestinal atrophy in intestinal diseases, and whether calorie restriction or rapamycin treatment can improve intestinal regeneration in these patients.

METHODS SUMMARY

The *Rheb2* transgenic mouse was produced as described previously[28] using the human *RHEB2* coding sequence. Mice used in this study include *Lgr5-EGFP-IRES-creERT2*, *Rosa26-creERT2*, *UbiquitinC-creERT2* (all obtained from the Jackson Laboratory), $Rictor^{loxp}$, and TSC^{loxp}. All were maintained on a C57BL/6 background. Calorie restriction was achieved by providing individual or paired mice with a daily portion of a chow diet fortified with vitamins and minerals amounting to 60% of the daily food intake of their *ad libitum* counterparts[30]. All mice used in calorie restriction experiments were between the ages of 10–28 weeks and were killed before their daily feeding. Intestinal crypts and ISCs were isolated and cultured as adapted from refs 14, 22. Unless otherwise indicated, data are presented as means ± s.d. and two-tailed Student's *t*-tests were used to assess statistical significance ($*P < 0.05$, $**P < 0.01$, $***P < 0.001$).

Full Methods and any associated references are available in the online version of the paper at www.nature.com/nature.

Received 17 October 2011; accepted 28 April 2012.
Published online 20 May 2012.

1. Simons, B. D. & Clevers, H. Strategies for homeostatic stem cell self-renewal in adult tissues. *Cell* **145,** 851–862 (2011).
2. Nakada, D., Levi, B. P. & Morrison, S. J. Integrating physiological regulation with stem cell and tissue homeostasis. *Neuron* **70,** 703–718 (2011).
3. McCay, C. M., Maynard, L. A., Sperling, G. & Barnes, L. L. The Journal of Nutrition: Retarded growth, life span, ultimate body size and age changes in the albino rat after feeding diets restricted in calories. *Nutr. Rev.* **33,** 241–243 (1975).
4. Bondolfi, L., Ermini, F., Long, J. M., Ingram, D. K. & Jucker, M. Impact of age and caloric restriction on neurogenesis in the dentate gyrus of C57BL/6 mice. *Neurobiol. Aging* **25,** 333–340 (2004).
5. Ertl, R. P., Chen, J., Astle, C. M., Duffy, T. M. & Harrison, D. E. Effects of dietary restriction on hematopoietic stem-cell aging are genetically regulated. *Blood* **111,** 1709–1716 (2008).
6. Chen, J., Astle, C. M. & Harrison, D. E. Hematopoietic senescence is postponed and hematopoietic stem cell function is enhanced by dietary restriction. *Exp. Hematol.* **31,** 1097–1103 (2003).
7. Yilmaz, O. H., Kiel, M. J. & Morrison, S. J. SLAM family markers are conserved among hematopoietic stem cells from old and reconstituted mice and markedly increase their purity. *Blood* **107,** 924–930 (2006).
8. Dunel-Erb, S. *et al.* Restoration of the jejunal mucosa in rats refed after prolonged fasting. *Comp. Biochem. Physiol. A* **129,** 933–947 (2001).
9. Altmann, G. G. Influence of starvation and refeeding on mucosal size and epithelial renewal in the rat small intestine. *Am. J. Anat.* **133,** 391–400 (1972).
10. Zhu, L. *et al.* Prominin 1 marks intestinal stem cells that are susceptible to neoplastic transformation. *Nature* **457,** 603–607 (2009).
11. Sangiorgi, E. & Capecchi, M. R. Bmi1 is expressed *in vivo* in intestinal stem cells. *Nature Genet.* **40,** 915–920 (2008).
12. Breault, D. T. *et al.* Generation of mTert-GFP mice as a model to identify and study tissue progenitor cells. *Proc. Natl Acad. Sci. USA* **105,** 10420–10425 (2008).
13. Barker, N. *et al.* Identification of stem cells in small intestine and colon by marker gene *Lgr5*. *Nature* **449,** 1003–1007 (2007).
14. Sato, T. *et al.* Paneth cells constitute the niche for Lgr5 stem cells in intestinal crypts. *Nature* **469,** 415–418 (2011).
15. Takeda, N. *et al.* Interconversion between intestinal stem cell populations in distinct niches. *Science* **334,** 1420–1424 (2011).
16. Snippert, H. J. *et al.* Intestinal crypt homeostasis results from neutral competition between symmetrically dividing Lgr5 stem cells. *Cell* **143,** 134–144 (2010).
17. Hempenstall, S., Picchio, L., Mitchell, S. E., Speakman, J. R. & Selman, C. The impact of acute caloric restriction on the metabolic phenotype in male C57BL/6 and DBA/2 mice. *Mech. Ageing Dev.* **131,** 111–118 (2010).
18. Cohen, D. E., Supinski, A. M., Bonkowski, M. S., Donmez, G. & Guarente, L. P. Neuronal SIRT1 regulates endocrine and behavioral responses to calorie restriction. *Genes Dev.* **23,** 2812–2817 (2009).
19. Spindler, S. R. Rapid and reversible induction of the longevity, anticancer and genomic effects of caloric restriction. *Mech. Ageing Dev.* **126,** 960–966 (2005).
20. Kalaany, N. Y. & Sabatini, D. M. Tumours with PI3K activation are resistant to dietary restriction. *Nature* **458,** 725–731 (2009).
21. van der Flier, L. G. *et al.* Transcription factor achaete scute-like 2 controls intestinal stem cell fate. *Cell* **136,** 903–912 (2009).
22. Sato, T. *et al.* Single Lgr5 stem cells build crypt-villus structures *in vitro* without a mesenchymal niche. *Nature* **459,** 262–265 (2009).
23. Marsh, V. *et al.* Epithelial Pten is dispensable for intestinal homeostasis but suppresses adenoma development and progression after Apc mutation. *Nature Genet.* **40,** 1436–1444 (2008).
24. Sengupta, S., Peterson, T. R., Laplante, M., Oh, S. & Sabatini, D. M. mTORC1 controls fasting-induced ketogenesis and its modulation by ageing. *Nature* **468,** 1100–1104 (2010).
25. Sarbassov, D. D. *et al.* Prolonged rapamycin treatment inhibits mTORC2 assembly and Akt/PKB. *Mol. Cell* **22,** 159–168 (2006).
26. Podesta, M. *et al.* Concentrative uptake of cyclic ADP-ribose generated by BST-1+ stroma stimulates proliferation of human hematopoietic progenitors. *J. Biol. Chem.* **280,** 5343–5349 (2005).
27. O'Brien, L. E., Soliman, S. S., Li, X. & Bilder, D. Altered modes of stem cell division drive adaptive intestinal growth. *Cell* **147,** 603–614 (2011).
28. Beard, C., Hochedlinger, K., Plath, K., Wutz, A. & Jaenisch, R. Efficient method to generate single-copy transgenic mice by site-specific integration in embryonic stem cells. *Genesis* **44,** 23–28 (2006).

Supplementary Information is linked to the online version of the paper at www.nature.com/nature.

Acknowledgements This work was supported by the National Institutes of Health (CA103866 and CA129105 to D.M.S.), the Koch Institute (Initiator award to D.M.S.), Ellison Medical Foundation (D.M.S.), the Warshaw Institute from the Massachusetts General Hospital (Ö.H.Y.), and the Center for the study of Inflammatory Bowel Disease from the Massachusetts General Hospital (Ö.H.Y. and D.M.S.), and fellowship support from the NCI (T32CA092216 to the Department of Pathology at the MGH to Ö.H.Y.), the Academy of Finland and the Foundations' Post Doc Pool (P.K.), the NIH (1F32AG032833-01A1 to D.W.L.) and Jane Coffin Childs Medical Fund (K.B.). We thank P. Wisniewski and C. Araneo of the Whitehead flow cytometry core facility, the Whitehead Genome Technology Core and Bioinformatics and Research Computing, S. Holder for histology and help with special stains, K. Ottina for laboratory management, and A. Hutchins for animal husbandry and genotyping. D.M.S. is an investigator of the Howard Hughes Medical Institute.

Author Contributions Ö.H.Y. and P.K. designed and performed all experiments and data analyses with input from D.M.S. S.S. generated the *Rheb2* transgenic mice. D.W.L., K.B., V.D., A.K.B., M.M.-K. and L.R.Z. participated in design and interpretation of experiments. Y.G., V.O.Y., A.D. and K.E.B.-R. performed and interpreted all of the immunohistochemistry and *in situ* hybridization under the guidance of Ö.H.Y. M.S. and G.P.N. performed electron microscopy and helped with its interpretation. Ö.H.Y. wrote the paper with help from P.K. and D.M.S.

Author Information Microarray data have been deposited in the GEO database under accession number GSE37209. Reprints and permissions information is available at www.nature.com/reprints. The authors declare no competing financial interests. Readers are welcome to comment on the online version of this article at www.nature.com/nature. Correspondence and requests for materials should be addressed to D.M.S. (sabatini@wi.mit.edu).

ARTICLE

doi:10.1038/nature11142

A map of nucleosome positions in yeast at base-pair resolution

Kristin Brogaard[1], Liqun Xi[2], Ji-Ping Wang[2] & Jonathan Widom[1,3]‡

The exact positions of nucleosomes along genomic DNA can influence many aspects of chromosome function. However, existing methods for mapping nucleosomes do not provide the necessary single-base-pair accuracy to determine these positions. Here we develop and apply a new approach for direct mapping of nucleosome centres on the basis of chemical modification of engineered histones. The resulting map locates nucleosome positions genome-wide in unprecedented detail and accuracy. It shows new aspects of the *in vivo* nucleosome organization that are linked to transcription factor binding, RNA polymerase pausing and the higher-order structure of the chromatin fibre.

Nucleosomes distort and occlude the genomic DNA from access to most DNA-binding proteins, and their exact positions affect the structure of the chromatin fibre[1]. Even single base-pair shifts of the position of a nucleosome can change chromatin configurations[2] and protein binding kinetics[3–5]. A map of nucleosome positions at single-base-pair resolution is necessary to understand fully a wide range of biological processes including RNA polymerase activity[6–8], transcription-factor binding kinetics[4,5,9,10], DNA replication[11,12], centromere structure[13–15] and gene splicing[16–18].

The most commonly used method for nucleosome mapping relies on treatment of chromatin with micrococcal nuclease (MNase) to digest DNA sequences not protected by the histone core. The nucleosome positions are indirectly inferred by the centres of undigested DNA sequence fragments. Although this method has provided insights into our understanding of nucleosomes, it is imprecise because of large variability of read lengths, transient unwrapping of nucleosomes, MNase sequence preferences and interference of other DNA-binding proteins[19–23]. Thus, a different approach is required to measure nucleosome locations with greater accuracy.

A chemical approach to mapping nucleosomes

We developed a new, genome-wide mapping approach that directly determines nucleosome centre positions with single-base-pair resolution. It derives from earlier work in which localized hydroxyl radicals were used to map reconstituted mononucleosomes centre positions[24,25]. In *Saccharomyces cerevisiae* we introduced a unique cysteine into histone H4 at position 47 (H4S47C) to covalently attach a sulphhydryl-reactive, copper-chelating label, *N*-(1,10-phenanthroline-5-yl)iodoacetamide. This cysteine mutation positions the label in close proximity to the DNA backbone and at sites symmetrically flanking the nucleosome centre (Fig. 1a). Log-phase yeast was collected and permeabilized immediately[26–29]. The label was subsequently introduced to the cells, where it reacts with the cysteines present in histone H4. Addition of copper and hydrogen peroxide catalyses the formation of short-lived hydroxyl radicals that react with and cleave the DNA backbone (Supplementary Methods). This strategy leads to a highly specific cleavage of the DNA backbone at sites that symmetrically flank the nucleosome centre[24,25]. On an agarose gel, a DNA banding pattern forms only when the reaction includes the sulphhydryl-reactive label, copper, H_2O_2 and the H4S47C mutant yeast, where the smallest fragment corresponds to DNAs between the centres of neighbouring nucleosomes (Fig. 1b).

We purified and sequenced the lowest molecular weight DNA band from the agarose gel (Fig. 1b) in six independent experiments (four with single-end and two with paired-end parallel sequencing), and produced a map of 105 million cleavages on each DNA strand (Figs 1c and 2a). The cleavage peaks on opposite DNA strands show two important correlations: a separation by either +2 or −5 nucleotides (with the 5′ to 3′ direction defined as positive) (Fig. 2b). This pattern is expected if cleavage occurs mainly at positions −1 (primary site) and +6 (secondary site) relative to the nucleosome centre (Fig. 1c), similar to that described for reconstituted mononucleosomes[24,25] (Supplementary Methods). The dominance and sharpness of these peaks show that the chemical maps contain high-resolution nucleosome positioning information.

We defined the nucleosome centres by identifying the characteristic pattern of chemical cleavages genome-wide (Supplementary Methods). We first trained a single-template model and then a four-template model to represent the average cleavage pattern at eight nucleotide positions centred around the primary and secondary sites (Supplementary Table 1). The four-template model accounts for four principal distinct cleavage patterns associated with nucleotide composition at positions −3/+3 and outperforms the single-template model (Supplementary Fig. 1a–c). The templates were built into a Bayesian deconvolution algorithm to calculate the nucleosome centre positioning (NCP) score at every genomic location. A larger NCP score means more cleavages observed in positions that conform to primary and secondary site configuration, thus indicating more well-positioned nucleosomes. Nucleosome centres were defined on the basis of the magnitude of the NCP score-to-noise ratio (Fig. 2a and Supplementary Fig. 1d).

Comparing two independent chemical mapping experiments, the resulting nucleosome positions are extremely consistent (Fig. 2c). Hence we combined the six independent data sets and produced a final unique map of 67,543 nucleosomes (Supplementary Methods), allowing two neighbouring nucleosomes to overlap by no more than 40 base pairs (bp) (occupying 79.9% of the genome, Supplementary Table 2); and a redundant map of 351,264 nucleosomes (allowing nucleosomes to overlap arbitrarily) by including all positions whose

[1]Department of Molecular Biosciences, Northwestern University, Evanston, Illinois 60208, USA. [2]Department of Statistics, Northwestern University, Evanston, Illinois 60208, USA. [3]Department of Chemistry, Northwestern University, Evanston, Illinois 60208, USA.
‡Deceased.

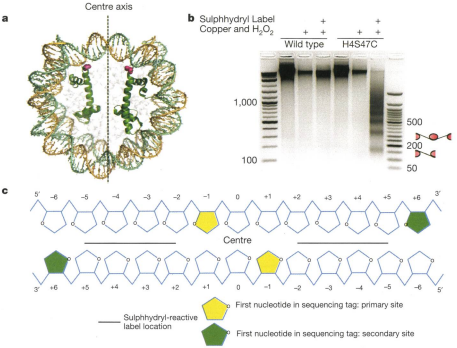

Figure 1 | Mapping nucleosome centres by site-specific chemical cleavage. **a**, Nucleosome structure, highlighting histone H4 (green) and residue serine 47 (pink), which is mutated to a cysteine where the sulphhydryl-reactive label covalently binds. **b**, Ethidium-bromide-stained agarose gel showing the chemical mapping results in a DNA banding pattern, which occurs only when the reaction includes (indicated by '+') the sulphhydryl-reactive label, copper, H_2O_2 and the H4S47C mutant yeast. The cartoons adjacent to the agarose gel illustrate mapping successive nucleosome centres produced the banding pattern. **c**, Locations of dominant hydroxyl radical cleavages relative to the nucleosome centre (base pair 0).

NCP score-to-noise ratio exceeded the smallest ratio value from the unique map (Supplementary Table 3). The chemical map shows general accordance with published MNase maps (MNase 1 (ref. 30) and MNase 2 (ref. 31)) of nucleosome positions, establishing that the chemical mapping technique does map nucleosome centres (Fig. 2a, d and Supplementary Fig. 2a, b). All analyses (unless indicated) presented in the main text use the unique set of nucleosomes. Important conclusions drawn from the unique map were confirmed using the redundant map, and results are presented separately in Supplementary Fig. 12.

The current chemical data show unbalanced cleavage patterns between the two strands at nucleosomes flanking long linkers including nucleosome-free regions upstream of transcription start sites (TSSs) (Supplementary Fig. 3a). As only the densest portion of the lowest molecular mass DNA fragment (~125–200 bp) was isolated from the agarose gel, DNA fragments spanning longer linkers were selected against (Fig. 1b). We confirmed this by isolating and sequencing DNA fragments of higher molecular mass (~200–500 bp) produced from one chemical mapping experiment (Supplementary Methods). The resulting data recovered the expected symmetric cleavage pattern at nucleosomes flanking the nucleosome-free regions (Supplementary Fig. 3b), and confirmed that failure to map nucleosomes because of consecutive long linkers is not a concern in the current data (Supplementary Fig. 3c). The cleavage asymmetry is not problematic for defining nucleosome centres, as one strand can still give a local maximum positioning score in our Bayesian deconvolution approach.

Nucleosome overlap and base composition

The chemical map shows detail of competing preferential nucleosome positions genome-wide. The redundant map suggests that in a population of cells nucleosomes often maintain several overlapping positions, creating closely clustered cleavage sites (Supplementary Fig. 4a, b). These sites were deconvoluted to yield locations and relative abundance of overlapping nucleosomes. Strikingly, overlapping nucleosomes are predominantly spaced by integral multiples of the DNA helical repeat (~10 bp) (Fig. 2e and Supplementary Fig. 4b). This result accords with ~10-bp periodic cleavage endpoints in MNase maps[32,33] and clarifies that MNase cleavage periodicities reflect several nucleosome positions instead of an artefact of the MNase itself[32]. This overlapping positioning of nucleosomes could be a consequence of the population or dynamic average, or even the co-existence of overlapping nucleosomes on the same DNA molecule[34]. By shifting in 10-bp steps (one helical turn), nucleosomes can maintain the local chromatin three-dimensional structure, while sampling several positions.

Nucleosomes *in vivo* are enriched for particular DNA sequence motifs at particular points along the nucleosomal DNA, most notably ~10-bp periodic occurrences of AA/TT/AT/TA dinucleotides that are favoured when the DNA backbone (minor groove) faces inwards towards the histone core, and CC/CG/GC/GG dinucleotides when the DNA backbone faces outwards[27,35,36]. These signals are seen in the chemical map with a period of 10.3 bp, and are far stronger than what was seen from MNase maps (Figs 3a, b and Supplementary Fig. 5a), suggesting that imprecision in the MNase maps degrades the sequence alignment. The ~0.2-bp difference between the dinucleotide periodicity and the classical helix repeat length (that is, 10.5 bp (ref. 37)) implies that DNAs probably over-stretch by 1–2 bp to accommodate the packing constraints of nucleosome structures in the chromatin fibre[1]. The strength of dinucleotide signal increases with the NCP score-to-noise ratio, suggesting that stronger dinucleotide sequence features are associated with positioning of more stable nucleosomes (Fig. 3a).

These dinucleotide signals are average features of the aggregated nucleosomes in the unique set, and of the overlapping nucleosomes (Supplementary Fig. 5b). The unique nucleosomes show an average of 40–50% occurrence rate of AA/TT/AT/TA at peak positions while lacking a dominant AA/TT/AT/TA bias at the edges of the nucleosomes observed in MNase maps (Fig. 3b)[19,21]. The preferences of nucleotide five-base polymers from the chemical map agree well with those measured by MNase, including the strong negative preference of nucleosomes for A/T-rich pentanucleotides[38,39]. However, both the

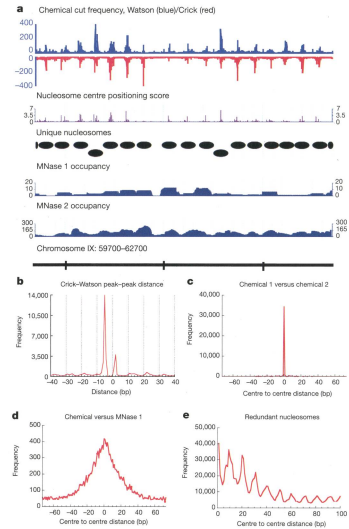

Figure 2 | Raw data, defined nucleosomes and pairwise comparison of nucleosome maps. **a**, Screenshot of raw data, nucleosome centre positioning score (NCP score), defined unique nucleosomes and two MNase maps (MNase 1 (ref. 30) and MNase 2 (ref. 31)). **b**, Crick–Watson cleavage peak–peak distances showing two dominant distances: +2 and −5 nucleotides. **c**, Distances between the nearest nucleosome centres in two independent chemical maps and **d**, in the combined chemical map compared with the MNase 1 map. **e**, Distance between nucleosome centres in the redundant map showing preferential spacing of multiples of ~10 bp.

nucleosome and linker regions are less strongly biased against A/T pentanucleotides in the chemical map than in the MNase maps (Fig. 3c), indicating that MNase preferentially degrades A/T-rich nucleosomes.

Intriguingly we noted a high frequency of occurrences (~0.6) of an A at position −3, and its symmetry-related T at position +3 relative to the nucleosome centre (Supplementary Figs 6 and 7). This high frequency has been observed in previous *in vitro* nucleosome positioning studies, with a frequency of 0.5 at these two locations[40]. Nucleosomes lacking both A(−3) and T(+3) (10% of the unique set) show similar but slightly weaker dinucleotide preference patterns compared with those having one or two of these nucleotides (Supplementary Fig. 5c). However, we cannot exclude the possibility that the chemical map might present a minor bias favouring an A(−3) or a T(+3) on top of the true preference of these nucleotides.

Global features of the nucleosome map

The high-resolution chemical map allows for more accurate conclusions about global nucleosome features. We defined the nucleosome

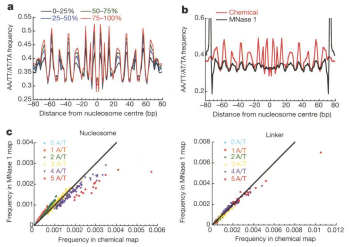

Figure 3 | Nucleosome sequence preferences. **a**, Position-dependent frequencies of AA/TT/AT/TA dinucleotides in the chemical map, by quartiles of NCP score-to-noise ratio. **b**, Comparison of dinucleotide frequency between the chemical map and the MNase 1 map. The chemical map shows significantly stronger AA/TT/AT/TA dinucleotide signals, suggesting an improved centre alignment of nucleosomal DNA. **c**, Pentanucleotide preferences of nucleosomes (left) and linker DNA regions (right) in the chemical map compared with the MNase 1 map, coloured by numbers of A or T nucleotides.

occupancy score at any given location as the total NCP scores in the ±73-bp region after correction for cleavage asymmetry on the two strands and controlling for signal-to-noise ratio as done in the redundant map (Supplementary Methods). The chemical map reproduces the well-known strong depletion of nucleosomes immediately upstream of the TSS[41] exposing the binding sites of regulatory proteins, with ordered nucleosomes extending downstream over the protein coding sequence, and much weaker ordering upstream of the TSS (Fig. 4a). The average occupancy curve within 1,000 bp of TSS is highly consistent with that from the MNase map ($r = 0.98$, Fig. 4a), suggesting the chemical map can provide a reasonable measure of nucleosome occupancy. Substantial nucleosome depletion is shown at the ends of the open reading frames (Fig. 4a), implying that nucleosome depletion at 3′ gene ends[20] is not an artefact of MNase digestion, but a real phenomenon. For transfer RNA (tRNA) genes, which are highly transcribed by RNA polymerase III and have their promoters inside the gene bodies[42], the upstream nucleosomes are strongly ordered whereas the gene body regions are nucleosome-depleted (Fig. 4a). No particular ordering of nucleosomes was observed relative to exon–intron or intron–exon boundaries (Supplementary Fig. 8a). We also observed strong ordering of nucleosomes on both sides of autonomously replicating sequences (ARS), and at centromere start (start of centromere DNA element I (CDEI)) and end (end of centromere DNA element III (CDEIII)) sites (Supplementary Fig. 8a, b). For the centromere sites, the nucleosome centres are highly localized at several specific positions, as shown by the sharp spikes of NCP score. Thus, the locations of the unique centromeric nucleosomes seem to be positioned relative to the exact locations of other key centromere-specific DNA-binding proteins.

An important unresolved problem concerns the role of DNA sequence features in positioning nucleosomes in protein-coding regions. Nucleosomes can be classified, with +1 referring to a nucleosome covering the start of the coding sequence, and +2 … +n for each successive nucleosome downstream. Nucleosomes of all classes (not only evident in the −1 and +1 class[43]) show strong AA/TT/AT/TA patterns with periodicity ranging from 10.20 to 10.26 bp, at which the amplitude of transform differs by no more than 5% between any two classes (Fig. 4b, Supplementary Fig. 9 and Supplementary Methods). Separate analysis using MNase data shows a similar but weaker periodic pattern, comparable across different classes (Fig. 4b

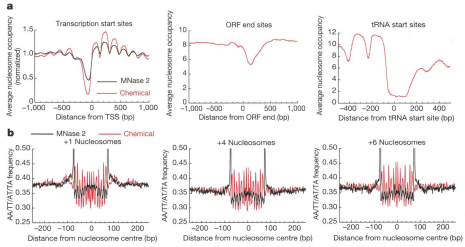

Figure 4 | Genome-wide features of nucleosome positions. a, Genome-wide average nucleosome occupancy across all sites in the chemical map plotted relative to TSSs (3,017 in total[43]), open reading frame (ORF) ends (centre) and tRNA start sites (right). **b**, AA/TT/AT/TA dinucleotide frequency within nucleosomes for nucleosome classes +1, +4 and +6 from the chemical map and the MNase 2 map.

and Supplementary Fig. 9). This suggests that DNA sequence features have an important role in detailed positioning of nucleosomes. A recent *in vitro* study[44] postulates an ATP-facilitated positioning, suggesting that chromatin complexes may use ATP to override DNA-intrinsic positioning and drive directional packaging of nucleosomes against a 5′ barrier at the 5′ ends of genes and to a lesser extent at the 3′ ends. Future studies are needed to understand the exact relationship of DNA sequence features and ATP in nucleosome positioning *in vivo*.

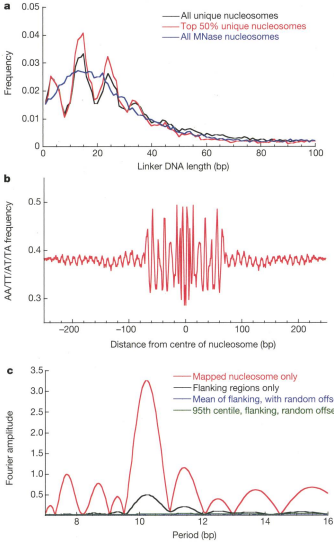

Chromatin structure and nucleosome spacing

The length of free DNA between two neighbouring nucleosomes (linker length) is a crucial determinant in the structure and compaction of the chromatin fibre and is directly related to the regulation of DNA-associated cellular processes[2,45,46]. The linker length distribution has a median of 23 bp (for linkers $\leq$ 100 bp) and shows a non-random pattern with a set of strong peaks at lengths equal to 3, 15, 24, 34 and 44 bp, differing by multiples of the DNA helical repeat (Fig. 5a and Supplementary Fig. 10). If we add 1 or 2 bp uniformly to each linker length to account for over-stretching of nucleosome DNAs, the linker length will follow a form of $10.41n + 4.6$ bp or $10.47n + 5.5$ bp (for integer n) respectively by Fourier analysis (for linker lengths $\leq$ 60 bp). The actual over-stretching varies across nucleosomes, which may alter details of the linker length distribution.

The non-random spacing of nucleosomes is also explicitly shown in the genomic DNA sequence. The periodicity of AA/TT/AT/TA motifs extends from the aligned unique nucleosomes to flanking regions beyond one nucleosome repeat length (Fig. 5b) with a period of 10.26 bp and a phase offset that accords with nucleosome spacing of $\sim 10n + 5$ bp, confirming the direct analyses above and previous findings[47] (Fig. 5c and Supplementary Methods). This suggests that given a nucleosome somewhere in the genome, the next nucleosome down the chain probably starts at approximately the opposite face of the double helical DNA, creating an open zigzag intrinsic chromatin structure, consistent with the two-start architecture of the 30 nm fibre[48].

Nucleosomes and DNA-binding proteins

We also examined the spatial relationships between nucleosomes and other high-resolution genomic features critical to genetic regulation.

Figure 5 | Nucleosome spacing and higher-order chromatin structures. a, Linker length distribution for all ~67,000 unique nucleosomes (black), for the top 50% of nucleosomes with highest NCP score-to-noise ratio (red) and for ~45,000 MNase 2 unique nucleosomes (blue). **b**, AA/TT/AT/TA frequency in the genomic DNA flanking the nucleosomes. **c**, Fourier transform of AA/TT/AT/TA signals in the unique nucleosomes (red), in downstream flanking regions (black), and the mean (blue) and 95th centile (green) of transform in the flanking regions after permuting the phase offset between the flanking region and the mapped nucleosome (Supplementary Methods).

Functional transcription-factor-binding sites, defined as sites that are conserved and occupied *in vivo*[49], were frequently contained inside mapped nucleosomes (Figs 6a, b, top and Supplementary Fig. 11a). This observation signifies that in a population of cells at any moment, some cells lack a nucleosome and have a bound factor, whereas other cells lack the bound transcription factor and have the nucleosome instead, or some cells might have transcription factor bound to the edge of the nucleosomes while the latter are partly unwrapped. More remarkably, within the nucleosome, transcription factor sites are strongly enriched at highly specific sites where the nucleosome sequence preferences best match those of the transcription factor; thus they can be predicted, given a position weight matrix for the transcription factor (Fig. 6a). Similarly, for the Hermes transposase, another sequence-specific DNA-binding protein, the transposon integration sites occur periodically through the nucleosome (Fig. 6b; bottom, and Supplementary Fig. 11b) at locations predictable by the transposase sequence specificity, demonstrating a type of multiplexing of genomic information.

Nucleosomes also influence elongation by RNA polymerase II (RNAP), with a recent genome-wide analysis showing enhanced pausing by RNAP predominantly within the first half of the nucleosome[8]. The chemical map shows enhanced pause sites across the full length of nucleosomes, suggesting that DNA downstream of the RNAP can remain wrapped even after RNAP has progressed far inside the nucleosome. However, we cannot exclude the possibility that this observation is complicated by the population average of nucleosomes from different locations within clusters. Notably, the RNAP pause sites do not occur at random locations in the nucleosome: rather, they occur periodically, at the DNA helical repeat (Fig. 6c and Supplementary Fig. 11b), indicating that RNAP stalls preferentially at specific locations relative to the nucleosome rotational position. The locations at which RNAP pauses are best reflected in a *dst1-Δ* strain that lacks the ability for RNAP to backtrack. Strikingly, in this mutant, RNAP pause sites again appear periodically, but at locations that are systematically displaced by ~5 bp: that is, by half of a DNA helical turn relative to the wild-type pause sites (Supplementary Fig. 11c). In the *dst1-Δ* strain, the RNAP has the greatest probability of pausing at locations where the DNA backbone faces out, away from the histones. This suggests that RNAP pauses at sites where further forward motion requires rotation around the DNA backbone, creating a steric clash between the polymerase and the histones. Conversely, the backtracking RNAP is most likely to pause at locations in the nucleosome at which the backbone faces inwards towards the histones (with maximal steric clash between histone and RNAP). In this situation, at the initiation of transcription, the first few forward steps will reduce this clash, as the polymerase rotates away from the histone surface.

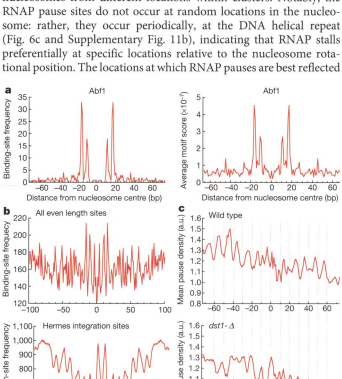

Figure 6 | High-resolution nucleosome centre positions relative to genomic features. a, Frequency of functional Abf1 sites (left) and the average motif score calculated using position weight matrix for Abf1 (right) relative to nucleosome centres. **b**, Frequency of all even-length functional transcription-factor-binding sites (top) and Hermes transposon integration sites (bottom) relative to the nucleosome centres. **c**, Frequencies of RNA polymerase II pause sites mapped inside nucleosomes +2 to +4 relative to the nucleosome centres, for wild-type yeast cells (top) and *dst1-Δ* yeast cells (lacking polymerase backtracking ability; bottom).

Conclusions and prospects

We developed a new method for mapping nucleosome centres in yeast with unprecedented consistency and accuracy. The resulting map shows significantly stronger dinucleotide signals in nucleosome DNAs than MNase maps. These signals are present and comparable in nucleosomes spanning entire protein-coding regions, demonstrating an important role of the DNA sequence features in detailed positioning and spacing of nucleosomes genome-wide. The observed linker length distribution suggests that the genome prefers an organized local chromatin structure. The exact locations of nucleosomes are associated with diverse biological phenomena, including the exact locations of transcription-factor-binding sites, transposon integration sites and RNAP pausing. We anticipate that this map will shed more light on many other genetic processes, including DNA replication, recombination, mutation, repair and genome evolution, because of the intimate relationship between nucleosome locations and these diverse processes.

METHODS SUMMARY

We genetically engineered *S. cerevisiae* to contain a cysteine at position 47 in histone H4. Cells grown to mid-log phase were collected, permeabilized and labelled with *N*-(1,10 phenanthroline-5-yl)iodoacetamide. The label covalently bound to the cysteine and allowed for copper chelation. Copper chloride, mercaptopropionic acid and hydrogen peroxide were added sequentially, creating hydroxyl radicals that cleaved the nucleosomal DNA at sites flanking the centre. After the mapping reaction, the genomic DNA was purified from the cells and run on an agarose gel. The lowest molecular mass DNA fragment (~150–200 bp) was purified and prepared for high-throughput parallel sequencing.

Received 23 September 2011; accepted 11 April 2012.
Published online 3 June 2012.

1. Richmond, T. J. & Davey, C. A. The structure of DNA in the nucleosome core. *Nature* **423,** 145–150 (2003).
2. Kosiver, E. F., Fuller, C. J., Straight, A. F. & Spakowitz, A. J. Local geometry and elasticity in compact chromatin structure. *Biophys. J.* **99,** 3941–3950 (2010).
3. Li, G. & Widom, J. Nucleosomes facilitate their own invasion. *Nature Struct. Mol. Biol.* **11,** 763–769 (2004).
4. Raveh-Sadka, T., Levo, M. & Segal, E. Incorporating nucleosomes into thermodynamic models of transcription regulation. *Genome Res.* **19,** 1480–1496 (2009).
5. Mao, C., Brown, C. R., Griesenbeck, J. & Boeger, H. Occlusion of regulatory sequences by promoter nucleosomes *in vivo*. *PLoS ONE* **6,** e17521 (2011).
6. Li, B., Carey, M. & Workman, J. L. The role of chromatin during transcription. *Cell* **128,** 707–719 (2007).
7. Petesch, S. J. & Lis, J. T. Rapid, transcription-independent loss of nucleosomes over a large chromatin domain at Hsp70 loci. *Cell* **134,** 74–84 (2008).
8. Churchman, L. S. & Weissman, J. S. Nascent transcript sequencing visualizes transcription at nucleotide resolution. *Nature* **469,** 368–373 (2011).
9. Owen-Hughes, T. & Workman, J. L. Experimental analysis of chromatin function in transcription control. *Crit. Rev. Eukaryot. Gene Expr.* **4,** 403–441 (1994).
10. Li, G., Levitus, M., Bustamante, C. & Widom, J. Rapid spontaneous accessibility of nucleosomal DNA. *Nature Struct. Mol. Biol.* **12,** 46–53 (2005).
11. Lipford, J. R. & Bell, S. P. Nucleosomes positioned by ORC facilitate the initiation of DNA replication. *Mol. Cell* **7,** 21–30 (2001).
12. Dorn, E. S. & Cook, J. G. Nucleosomes in the neighborhood: new roles for chromatin modifications in replication origin control. *Epigenetics* **6,** 552–559 (2011).

13. Tachiwana, H. *et al.* Crystal structure of the human centromeric nucleosome containing CENP-A. *Nature* **476,** 232–235 (2011).
14. Cole, H. A., Howard, B. H. & Clark, D. J. The centromeric nucleosome of budding yeast is perfectly positioned and covers the entire centromere. *Proc. Natl Acad. Sci. USA* **108,** 12687–12692 (2011).
15. Dalal, Y., Furuyama, T., Vermaak, D. & Henikoff, S. Structure, dynamics, and evolution of centromeric nucleosomes. *Proc. Natl Acad. Sci. USA* **104,** 15974–15981 (2007).
16. Beckmann, J. S. & Trifonov, E. N. Splice junctions follow a 205-base ladder. *Proc. Natl Acad. Sci. USA* **88,** 2380–2383 (1991).
17. Schwartz, S., Meshorer, E. & Ast, G. Chromatin organization marks exon-intron structure. *Nature Struct. Mol. Biol.* **16,** 990–995 (2009).
18. Tilgner, H. *et al.* Nucleosome positioning as a determinant of exon recognition. *Nature Struct. Mol. Biol.* **16,** 996–1001 (2009).
19. Dingwall, C., Lomonossoff, G. P. & Laskey, R. A. High sequence specificity of micrococcal nuclease. *Nucleic Acids Res.* **9,** 2659–2673 (1981).
20. Fan, X. *et al.* Nucleosome depletion at yeast terminators is not intrinsic and can occur by a transcriptional mechanism linked to 3′-end formation. *Proc. Natl Acad. Sci. USA* **107,** 17945–17950 (2010).
21. Hörz, W. & Altenburger, W. Sequence specific cleavage of DNA by micrococcal nuclease. *Nucleic Acids Res.* **9,** 2643–2658 (1981).
22. Chung, H. R. *et al.* The effect of micrococcal nuclease digestion on nucleosome positioning data. *PLoS ONE* **5,** e15754 (2010).
23. Zhang, Y. *et al.* Intrinsic histone-DNA interactions are not the major determinant of nucleosome positions *in vivo*. *Nature Struct. Mol. Biol.* **16,** 847–852 (2009).
24. Flaus, A., Luger, K., Tan, S. & Richmond, T. J. Mapping nucleosome position at single base-pair resolution by using site-directed hydroxyl radicals. *Proc. Natl Acad. Sci. USA* **93,** 1370–1375 (1996).
25. Flaus, A. & Richmond, T. J. Base-pair resolution mapping of nucleosome positions using site-directed hydroxy radicals. *Methods Enzymol.* **304,** 251–263 (1999).
26. Yager, T. D., McMurray, C. T. & van Holde, K. E. Salt-induced release of DNA from nucleosome core particle. *Biochemistry* **28,** 2271–2281 (1989).
27. Widom, J. Role of DNA sequence in nucleosome stability and dynamics. *Q. Rev. Biophys.* **34,** 269–324 (2001).
28. Thåström, A., Bingham, L. M. & Widom, J. Nucleosomal locations of dominant DNA sequence motifs for histone–DNA interactions and nucleosome positioning. *J. Mol. Biol.* **338,** 695–709 (2004).
29. Teif, V. B. & Rippe, K. Predicting nucleosomes positions on the DNA: combining intrinsic sequence preferences and remodeler activities. Predicting nucleosome positions on the DNA. *Nucleic Acids Res.* **37,** 5642–5655 (2009).
30. Field, Y. *et al.* Distinct modes of regulation by chromatin encoded through nucleosome positioning signals. *PLoS Comput. Biol.* **4,** e1000216 (2008).
31. Floer, M. *et al.* A RSC/nucleosome complex determines chromatin architecture and facilitates activator binding. *Cell* **141,** 407–418 (2010).
32. Cockell, M., Rhodes, D. & Klug, A. Location of the primary sites of micrococcal nuclease cleavage on the nucleosome core. *J. Mol. Biol.* **170,** 423–446 (1983).
33. Albert, I. *et al.* Translational and rotational settings of H2A.Z nucleosomes across the *Saccharomyces cerevisiae* genome. *Nature* **446,** 572–576 (2007).
34. Engeholm, M. *et al.* Nucleosomes can invade DNA territories occupied by their neighbors. *Nature Struct. Mol. Biol.* **16,** 151–158 (2009).
35. Wang, J. P. & Widom, J. Improved alignment of nucleosome DNA sequences using a mixture model. *Nucleic Acids Res.* **33,** 6743–6755 (2005).
36. Segal, E. *et al.* A genomic code for nucleosome positioning. *Nature* **442,** 772–778 (2006).
37. Travers, A. A. & Klug, A. The bending of DNA in nucleosomes and its wider implications. *Phil. Trans. R. Soc. Lond. B* **317,** 537–561 (1987).
38. Segal, E. & Widom, J. What controls nucleosome positions? *Trends Genet.* **25,** 335–343 (2009).
39. Segal, E. & Widom, J. Poly(dA:dT) tracts: major determinants of nucleosome organization. *Curr. Opin. Struct. Biol.* **19,** 65–71 (2009).
40. Thåström, A., Lowary, P. T. & Widom, J. Measurement of histone-DNA interaction free energy in nucleosomes. *Methods* **33,** 33–44 (2004).
41. David, L. *et al.* A high-resolution map of transcription in the yeast genome. *Proc. Natl Acad. Sci. USA* **103,** 5320–5325 (2006).
42. Schramm, L. & Hernandez, N. Recruitment of RNA polymerase III to its target promoters. *Genes Dev.* **16,** 2593–2620 (2002).
43. Mavrich, T. N. *et al.* A barrier nucleosome model for statistical positioning of nucleosomes throughout the yeast genome. *Genome Res.* **18,** 1073–1083 (2008).
44. Zhang, Z. *et al.* A packaging mechanism for nucleosome organization reconstituted across a eukaryotic genome. *Science* **332,** 977–980 (2011).
45. Lohr, D. & van Holde, K. E. Organization of spacer DNA in chromatin. *Proc. Natl Acad. Sci. USA* **76,** 6326–6330 (1979).
46. Routh, A., Sandin, S. & Rhodes, D. Nucleosome repeat length and linker histone stoichiometry determine chromatin fiber structure. *Proc. Natl Acad. Sci. USA* **105,** 8872–8877 (2008).
47. Wang, J. P. *et al.* Preferentially quantized linker DNA lengths in *Saccharomyces cerevisiae*. *PLoS Comput. Biol.* **4,** e1000175 (2008).
48. Dorigo, B. *et al.* Nucleosome arrays reveal the two-start organization of the chromatin fiber. *Science* **306,** 1571–1573 (2004).
49. MacIsaac, K. D. *et al.* An improved map of conserved regulatory sites for *Saccharomyces cerevisiae*. *BMC Bioinformatics* **7,** 113 (2006).

Supplementary Information is linked to the online version of the paper at www.nature.com/nature.

Acknowledgements We dedicate this paper to J.W., who guided this project. We thank R. Holmgren, A. Matouschek, B. Meyer, R. Phillips, E. Segal and O. Uhlenbeck for comments and discussions. We are grateful to Northwestern University's Genomic Core for all sequencing completed for this project. The work was supported by National Institutes of Health grants T32GM00806 (to K.B.), R01GM058617 (to J.W.), R01GM075313 (to J.-P.W.) and U54CA143869 (to J.W.).

Author Contributions K.B. did all the experimental work. L.X. and J.-P.W. developed the algorithm and performed the analyses. K.B., J.-P.W. and J.W. wrote the paper. J.W. directed the project.

Author Information Sequence data are deposited in National Center for Biotechnology Information Gene Expression Omnibus database under accession number GSE36063. Reprints and permissions information is available at www.nature.com/reprints. The authors declare no competing financial interests. Readers are welcome to comment on the online version of this article at www.nature.com/nature. Correspondence and requests for materials should be addressed to J.-P.W. (jzwang@northwestern.edu).

LETTER

doi:10.1038/nature11161

The signature of orbital motion from the dayside of the planet τ Boötis b

Matteo Brogi[1], Ignas A. G. Snellen[1], Remco J. de Kok[2], Simon Albrecht[3], Jayne Birkby[1] & Ernst J. W. de Mooij[1,4]

The giant planet orbiting τ Boötis (named τ Boötis b) was amongst the first extrasolar planets to be discovered[1]. It is one of the brightest exoplanets and one of the nearest to us, with an orbital period of just a few days. Over the course of more than a decade, measurements of its orbital inclination have been announced[2] and refuted[3], and have hitherto remained elusive[4–8]. Here we report the detection of carbon monoxide absorption in the thermal dayside spectrum of τ Boötis b. At a spectral resolution of ~100,000, we trace the change in the radial velocity of the planet over a large range in phase, determining an orbital inclination of 44.5° ± 1.5° and a mass 5.95 ± 0.28 times that of Jupiter, demonstrating that atmospheric characterization is possible for non-transiting planets. The strong absorption signal points to an atmosphere with a temperature that is decreasing towards higher altitudes, in contrast to the temperature inversion inferred for other highly irradiated planets[9,10]. This supports the hypothesis that the absorbing compounds believed to cause such atmospheric inversions are destroyed in τ Boötis b by the ultraviolet emission from the active host star[11].

We observed τ Boötis for three sessions of 6 h each during the nights of 1, 8 and 14 April 2011, using the Cryogenic Infrared Echelle Spectrograph (CRIRES[12]) at the Nasmyth A focus of the Very Large Telescope UT1, located at the European Southern Observatory (ESO) on Cerro Paranal, Chile. Targeting the planet almost continuously between orbital phase (φ) 0.37 and 0.63, we collected 452 spectra at a resolution of $R \approx 100{,}000$ in the wavelength range 2,287–2,345 nm, centred on the 2–0 R-branch of carbon monoxide (CO). We used the ESO CRIRES data pipeline for the basic data reduction and the extraction of the one-dimensional spectra. We subsequently extracted the signal of the planet using purpose-built algorithms, similar to those used for high-dispersion transit spectroscopy of HD 209458b[13], which are described in detail in Supplementary Information section 2. The most critical step in this analysis is the removal of telluric features caused by the Earth's atmosphere, which completely dominate our spectra. This can be achieved without destroying the planetary signature only because the signal from the planet moves significantly in wavelength during our observations, owing to its large change in radial velocity along the orbit.

We cross-correlated each of the 452 extracted and processed spectra with a CO template (described in Supplementary Information section 5.1), and subsequently aligned and combined all the cross-correlation functions, assuming a range of values for the maximum orbital radial velocity of the planet, K_P. Figure 1 shows the combined cross-correlation signal as function of K_P, corresponding to a wide range in orbital inclinations. We detect a 6σ absorption signal at $K_P = 110.0 \pm 3.2\ \mathrm{km\ s^{-1}}$, at a systemic velocity of $-16.4\ \mathrm{km\ s^{-1}}$, which is within the uncertainties of that of the host star[14], τ Boötis. The distributions of the values of the cross-correlated time series for points in the planet trail (the position of the planet in velocity space as function of time) and out of the planet trail are shown in Fig. 2. A detailed discussion of the noise properties of the cross-correlated time series and of the significance level of this detection is presented in Supplementary Information section 3. Figure 3 shows the radial velocity trail of the planet in CO over the full phase range of our observations. Combining the measured K_P with the maximum radial velocity of the host star, $K_S = 0.4664 \pm 0.0033\ \mathrm{km\ s^{-1}}$ (see Supplementary Information section 4), yields a star/planet mass ratio of 235.8 ± 7.1. With a host stellar mass[15] of $M_S = 1.34 \pm 0.05\ M_{Sun}$ we derive a planetary mass of $M_P = 5.95 \pm 0.28\ M_{Jup}$. In addition, using Kepler's third law, we determine a planetary orbital inclination of $i = 44.5^\circ \pm 1.5^\circ$. Note that orbital solutions to the long-term monitoring of the radial velocity variations of the host star show a modest preference[16] for a slightly eccentric orbit with eccentricity $e = 0.023 \pm 0.015$. However, the combination of our planetary radial velocity data and a reanalysis of the stellar data in the literature shows no evidence for an eccentric orbit (see Supplementary Information section 4). We therefore adopt a circular orbit for τ Boötis b in our analysis.

Spectro-polarimetric observations[14,17] of τ Boötis show that the host star exhibits strong differential rotation, with a period P_{rot} ranging

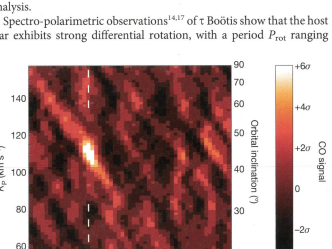

Figure 1 | CO signal in the dayside spectrum of the extrasolar planet τ Boötis b. Shown is a colour scale plot of the carbon monoxide signal as function of heliocentric (systemic) velocity (V_{sys}) on the x axis, and the maximum radial velocity of the planet, K_P, on the left-hand y axis. The latter translates to an orbital inclination, as indicated by the scale on the right-hand y axis. Lighter colours indicate CO in absorption. A clear signal at the 6.2σ level is visible at the systemic velocity of τ Boötis ($-16.4\ \mathrm{km\ s^{-1}}$), as indicated by the vertical dashed line, for a maximum orbital radial velocity of the planet of $K_P = 110.0 \pm 3.2\ \mathrm{km\ s^{-1}}$. This corresponds to an orbital inclination $i = 44.5^\circ \pm 1.5^\circ$ and to a planetary mass of $M_P = 5.95 \pm 0.28\ M_{Jup}$. The signal is obtained by cross-correlating a template spectrum of CO lines with the CRIRES/VLT spectra, which were each shifted in wavelength using the planet's ephemeris assuming a particular value of K_P. This to compensate for the changing Doppler effect caused by the change in the planet's radial velocity over the large range in phase. The significance of the signal and the properties of the cross-correlated noise are discussed in Supplementary Information.

[1]Leiden Observatory, Leiden University, Postbus 9513, 2300RA Leiden, The Netherlands. [2]SRON, Sorbonnelaan 2, 3584 CA Utrecht, The Netherlands. [3]Department of Physics, and Kavli Institute for Astrophysics and Space Research, Massachusetts Institute of Technology, Cambridge, Massachusetts 02139, USA. [4]Department of Astronomy and Astrophysics, University of Toronto, 50 St George Street, Toronto, Ontario M5S 3H4, Canada.

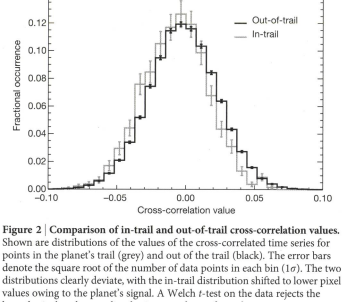

Figure 2 | Comparison of in-trail and out-of-trail cross-correlation values. Shown are distributions of the values of the cross-correlated time series for points in the planet's trail (grey) and out of the trail (black). The error bars denote the square root of the number of data points in each bin (1σ). The two distributions clearly deviate, with the in-trail distribution shifted to lower pixel values owing to the planet's signal. A Welch t-test on the data rejects the hypothesis that the two distributions are drawn from the same parent distribution at the 6σ level.

from 3.0 to 3.9 days from the equator to the poles. It indicates that the stellar rotation at intermediate latitudes is synchronized with the planet's orbital period ($P = 3.312$ days). If we assume that the stellar rotation axis is aligned with the normal to the orbital plane of the planet, the projected rotational velocity[16] of the star, $v\sin(i) \approx 15\,\mathrm{km\,s^{-1}}$, combined with a stellar radius[15] of $R_S = 1.46 \pm 0.05\ R_{\mathrm{Sun}}$ and our measurement of i, indeed corresponds to a stellar rotational period of $P_{\mathrm{rot}} = 3.3$ days, matching the planet's orbital period. Therefore, in addition to synchronization, it suggests that the orbital plane and the plane of stellar rotation are not significantly misaligned. We point out that a large fraction of the hot Jupiters around hot stars ($T_{\mathrm{eff}} > 6{,}250$ K) such as τ Boötis, whose orbital alignment can be measured via the Rossiter-McLaughlin effect, exhibit strong misalignments[18,19].

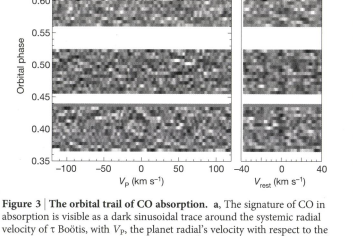

Figure 3 | The orbital trail of CO absorption. a, The signature of CO in absorption is visible as a dark sinusoidal trace around the systemic radial velocity of τ Boötis, with V_p, the planet radial's velocity with respect to the systemic velocity, changing from $+80\,\mathrm{km\,s^{-1}}$ at phase 0.37, to $-80\,\mathrm{km\,s^{-1}}$ at phase 0.63. In **b**, the data are shifted to the reference frame of τ Boötis b, after subtracting the planet's radial velocity computed assuming a circular orbit and a system inclination of 44.5°: here the planet's signal is recovered as a dark vertical trace around the planet's rest-frame velocity of $v_{\mathrm{rest}} = 0\,\mathrm{km\,s^{-1}}$. A comparison between the observed trail and artificially generated data with the same noise properties is shown in Supplementary Fig. 4.

However, most of the massive planets ($M_P > 3M_{\mathrm{Jup}}$) are found in more aligned orbits[20], and τ Boötis b does not break this trend.

Our observations at high spectral resolution are only sensitive to narrow spectral features, because of the particular data reduction necessary to remove the telluric contamination. Owing to the high opacity at the wavelengths of molecular transitions, these narrow features probe the atmosphere at lower pressures than the surrounding continuum. The probed pressures are directly linked to the volume mixing ratio (VMR) of CO, but the depth of the absorption features in the emitted planetary spectrum depends on the relative temperatures at the altitudes at which the continuum and CO lines are formed. This means that there is a strong degeneracy between the temperature–pressure (T-p) profile of the planet's atmosphere, and the VMR of CO. We compare our data with a range of models, in order to constrain the CO abundance and the T-p profile (see Supplementary Information section 5.2). We obtain a lower limit to the CO VMR by using the adiabatic lapse rate ($\mathrm{d}T/\mathrm{d}\log_{10}(p) \approx 1{,}000$ K at these temperatures), which is the maximum temperature gradient of a planet's atmosphere before it becomes unstable to convection. An additional uncertainty is that the size of τ Boötis b is unknown, because it is a non-transiting planet. Because the average radius of the 17 transiting hot Jupiters currently known[21] with $3M_{\mathrm{Jup}} < M_P < 9M_{\mathrm{Jup}}$ is $1.15R_{\mathrm{Jup}}$, we assume this value for the planet. When we set the temperature of the atmospheric layer in which the continuum is formed to $T = 2{,}000$ K (near the expected dayside equilibrium temperature for a planet without energy redistribution to the nightside), and use an adiabatic lapse rate, we require a CO VMR of 10^{-3} to match the observed signal. If we assume a temperature of $T = 1{,}650$ K for the continuum photospheric layer (near the dayside equilibrium temperature for a planet with perfect redistribution of energy to its nightside), under similar adiabatic conditions, a CO VMR of 10^{-4} is required. Note that this result is consistent with the metallicity of the host star, which corresponds to a CO VMR of $\sim 10^{-3}$. We do not detect spectral features from methane or water vapour above a significance of 2σ, and we use our atmospheric models to derive upper limits to the relative abundances of these molecules; we find $\mathrm{VMR}(CH_4)/\mathrm{VMR}(CO) < 1$ and $\mathrm{VMR}(H_2O)/\mathrm{VMR}(CO) < 5$ at the 90% confidence level.

Photometric observations of hot Jupiters with the Spitzer Space Telescope have been interpreted as suggestive of atmospheric thermal inversions, characterized by molecular features in emission rather than in absorption, of which HD 209458b is the best-studied example. These inversions are probably fuelled by absorption of stellar radiation in a high-altitude absorbing layer. In such a model, a thermal inversion is more likely to occur in the most highly irradiated planets, for which indeed some evidence exists[22]. The planet τ Boötis b is more strongly irradiated than HD 209458b. However, it is clear that τ Boötis b does not exhibit a strong thermal inversion over the pressure range probed by our observations, because we see the CO signal in absorption. Although the exact pressure range probed depends on the CO abundance, the inversion layer invoked to explain the emission spectrum of HD 209458b encompasses such a wide range in atmospheric pressures that it is evident that τ Boötis b does not have an HD 209458b-type thermal inversion. Interestingly, the host star of τ Boötis b exhibits a high level of chromospheric activity, and it has been recently suggested that hot Jupiters orbiting active stars are less likely to have thermal inversions[11] because the strong ultraviolet radiation that accompanies chromospheric activity destroys the absorbing compound at high altitude, which would otherwise be responsible for the thermal inversion.

These observations show that high-resolution spectroscopy from the ground is a valuable tool for detailed analysis of the temperature structure and molecular content of exoplanet atmospheres. The technique that we used not only reveals its potential for transmission spectroscopy[13], but also for dayside spectroscopy, meaning that atmospheric characterization is no longer constrained to transiting planets alone. Detection of different molecular bands will further constrain the relative molecular abundances and T-p profiles. In addition, tracing the

signal along the orbit will reveal the planet's phase function, which is linked to its global atmospheric circulation. Measuring this for different molecules may reveal changes between a planet's morning and evening spectrum driven by photochemical processes. Furthermore, molecular line profiles, in both dayside and transmission spectra, can potentially show the effects of a planet's rotational velocity, and unveil whether these hot Jupiters are indeed tidally locked.

Received 17 November 2011; accepted 24 April 2012.

1. Butler, R. P., Marcy, G. W., Williams, E., Hauser, H. & Shirts, P. Three new "51-Pegasi-type" planets. *Astrophys. J.* **474,** L115–L118 (1997).
2. Collier Cameron, A., Horne, K., Penny, A. & James, D. Probable detection of starlight reflected from the giant planet orbiting τ Boötis. *Nature* **402,** 751–755 (1999).
3. Collier Cameron, A., Horne, K., James, D., Penny, A. & Semel, M. in *Proceedings of IAU Symposium 202: Planetary Systems in the Universe* (eds Penny, A. J., Artymowicz, P., Lagrange, A.-M. & Russell, S.) 75–77 (Astronomical Society of the Pacific, 2004).
4. Leigh, C., Collier Cameron, A., Horne, K., Penny, A. & James, D. A new upper limit on the reflected starlight from τ Bootis b. *Mon. Not. R. Astron. Soc.* **344,** 1271–1282 (2003).
5. Charbonneau, D., Noyes, R. W., Korzennik, S. G., Nienson, P. & Jha, S. An upper limit on the reflected light from the planet orbiting the star τ Bootis. *Astrophys. J.* **522,** L145–L148 (1999).
6. Wiedemann, G., Deming, D. & Bjoraker, G. A sensitive search for methane in the infrared spectrum of τ Bootis. *Astrophys. J.* **546,** 1068–1074 (2001).
7. Lucas, P. W. *et al.* Planetpol polarimetry of the exoplanet systems 55 Cnc and τ Boo. *Mon. Not. R. Astron. Soc.* **393,** 229–244 (2009).
8. Rodler, F., Kürster, M. & Henning, T. τ Boötis b: hunting for reflected starlight. *Astron. Astrophys.* **514,** A23 (2010).
9. Burrows, A., Budaj, J. & Hubeny, I. Theoretical spectra and light curves of close-in extrasolar giant planets and comparison with data. *Astrophys. J.* **678,** 1436–1457 (2008).
10. Fortney, J. J., Lodders, K., Marley, M. S. & Freedman, R. S. A unified theory for the atmospheres of the hot and very hot Jupiters: two classes of irradiated atmospheres. *Astrophys. J.* **678,** 1419–1435 (2008).
11. Knutson, H. A., Howard, A. W. & Isaacson, H. A correlation between stellar activity and hot-Jupiter emission spectra. *Astrophys. J.* **720,** 1569–1576 (2010).
12. Kaeufl, H. U. *et al.* CRIRES: a high resolution infrared spectrograph for ESO's VLT. *Proc. SPIE* **5492,** 1218–1227 (2004).
13. Snellen, I. A., de Kok, R. J., de Mooij, E. J. W. & Albrecht, S. The orbital motion, absolute mass and high-altitude winds of exoplanet HD 209458b. *Nature* **465,** 1049–1051 (2010).
14. Donati, J.-F. *et al.* Magnetic cycles of the planet-hosting star τ Bootis. *Mon. Not. R. Astron. Soc.* **385,** 1179–1185 (2008).
15. Takeda, G. *et al.* Structure and evolution of nearby stars with planets. II. Physical properties of ~1000 cool stars from the SPOCS catalog. *Astrophys. J. Suppl. Ser.* **168,** 297–318 (2007).
16. Butler, R. P. *et al.* Catalog of nearby exoplanets. *Astrophys. J.* **646,** 505–522 (2006).
17. Catala, C., Donati, J.-F., Shkolnik, E., Bohlender, D. & Alecian, E. The magnetic field of the planet-hosting star τ Bootis. *Mon. Not. R. Astron. Soc.* **374,** L42–L46 (2007).
18. Winn, J. N., Fabrycky, D., Albrecht, S. & Johnson, J. A. Hot stars with hot Jupiters have high obliquities. *Astrophys. J.* **718,** L145–L149 (2010).
19. Johnson, J. A. *et al.* HAT-P-30b: a transiting hot Jupiter on a highly oblique orbit. *Astrophys. J.* **735,** 24–31 (2011).
20. Hébrard, G. *et al.* Observation of the full 12-hour-long transit of the exoplanet HD 80606b. Warm-Spitzer photometry and SOPHIE spectroscopy. *Astron. Astrophys.* **516,** A95 (2010).
21. Schneider, J., Dedieu, C., Le Sinader, P., Savalle, R. & Zolotukhin, I. Defining and cataloguing exoplanets: the exoplanet.eu database. *Astron. Astrophys.* **532,** A79 (2011).
22. Knutson, H. A., Charbonneau, D., Burrows, A., O'Donovan, F. T. & Mandushev, G. Detection of a temperature inversion in the broadband infrared emission spectrum of TrES-4. *Astrophys. J.* **691,** 866–874 (2009).

Supplementary Information is linked to the online version of the paper at www.nature.com/nature.

Acknowledgements We thank the ESO support staff of the Paranal Observatory for their help during the observations. This work is based on observations collected at the European Southern Observatory (186.C-0289). S.A. acknowledges support by a Rubicon fellowship from the Netherlands Organisation for Scientific Research (NWO), and by NSF grant no. 1108595.

Author Contributions M.B. led the observations and data analysis, and co-wrote the manuscript. I.A.G.S. conceived the project, contributed to the analysis and co-wrote the manuscript. R.J.d.K. constructed the planet atmosphere models. S.A. conducted the MCMC orbital analysis. J.B., E.J.W.d.M., R.J.d.K. and S.A. discussed the analyses, results and commented on the manuscript.

Author Information Reprints and permissions information is available at www.nature.com/reprints. The authors declare no competing financial interests. Readers are welcome to comment on the online version of this article at www.nature.com/nature. Correspondence and requests for materials should be addressed to M.B. (brogi@strw.leidenuniv.nl).

LETTER

doi:10.1038/nature11202

Magnetic tornadoes as energy channels into the solar corona

Sven Wedemeyer-Böhm[1,2], Eamon Scullion[1], Oskar Steiner[3], Luc Rouppe van der Voort[1], Jaime de la Cruz Rodriguez[4], Viktor Fedun[5] & Robert Erdélyi[5]

Heating the outer layers of the magnetically quiet solar atmosphere to more than one million kelvin and accelerating the solar wind requires an energy flux of approximately 100 to 300 watts per square metre[1–6], but how this energy is transferred and dissipated there is a puzzle and several alternative solutions have been proposed. Braiding and twisting of magnetic field structures, which is caused by the convective flows at the solar surface, was suggested as an efficient mechanism for atmospheric heating[7]. Convectively driven vortex flows that harbour magnetic fields are observed[8–10] to be abundant in the photosphere (the visible surface of the Sun). Recently, corresponding swirling motions have been discovered[11] in the chromosphere, the atmospheric layer sandwiched between the photosphere and the corona. Here we report the imprints of these chromospheric swirls in the transition region and low corona, and identify them as observational signatures of rapidly rotating magnetic structures. These ubiquitous structures, which resemble super-tornadoes under solar conditions, reach from the convection zone into the upper solar atmosphere and provide an alternative mechanism for channelling energy from the lower into the upper solar atmosphere.

Chromospheric swirls are seen as narrow rotating rings (or ring fragments) in the core of the singly ionized calcium (Ca II) 854.2-nm absorption line that is formed in the chromosphere (Fig. 1b–d). Their diameters are typically of the order of 1,500 km, which is thousands of times larger than the diameters of terrestrial tornadoes. Swirls appear dark in the spectral line core images and have Doppler shifts corresponding to upward (line-of-sight) velocities of typically 4 km s^{-1}, with even larger peak values (Fig. 1d, Dopplergram). We detect a corresponding response in the atmospheric layers above the chromosphere by using the 30.4-nm (He II), 17.1-nm (Fe IX), 19.3-nm (Fe XII and Fe XXIV) and 21.1-nm (Fe XIV) channels of the SDO/AIA[12] (Figs 1d and 2c). We found 14 swirls with an average lifetime of 12.7 ± 4.0 min during a 55-min-long observation sequence on 8 May 2011 (Fig. 2a and Supplementary Table 1). Statistically, there were 3.8 swirls in each 1′ × 1′ field at all times, resulting in there always being approximately 1.1 × 10^4 swirls on the solar surface (Fig. 1a). In view of the observational limitations, this number must be understood as a lower limit.

An exemplary swirl is illustrated in Fig. 1c, d. The chosen wavelength channels of CRISP and AIA effectively map the atmospheric layers with increasing height. The fact that we find a signal at the same

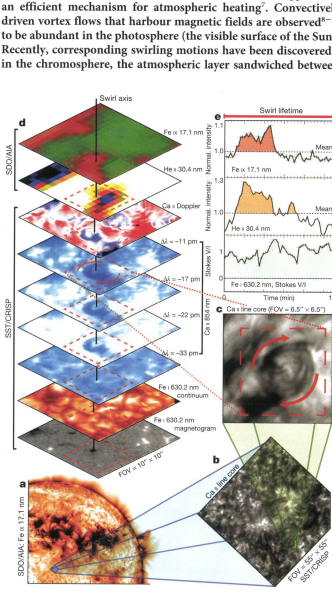

Figure 1 | Observation of a swirl event and its coronal counterpart. Co-aligned and co-temporal solar observations made on 8 May 2011 using the Atmospheric Imaging Assembly (AIA) on board NASA's space-based Solar Dynamics Observatory (SDO) (cadence, 12 s; image scale, 0.6″ per pixel) and the Crisp Imaging Spectropolarimeter (CRISP) on the ground-based, Swedish 1-m Solar Telescope (cadence, 14 s; 47 line positions across the Ca II 854.2-nm spectral line of the infrared triplet; image scale, 0.06″ per pixel). **a**, Part of the full-disk AIA Fe IX 17.1-nm channel with the field of view (FOV) of CRISP at the centre of the solar disk (blue box, 55″ × 55″). **b**, Corresponding CRISP image in the Ca II 854.2-nm line core. **c**, Close-up of the region with a chromospheric swirl. **d**, Layered atmosphere from the photosphere (bottom panel: magnetogram, Fe I 630.2-nm continuum), through the chromosphere (Dopplergram, Ca II 854.2 nm) and the transition region (He II 30.4 nm) to the low corona (top: Fe IX 17.1 nm). The visible radiation of the lower solar atmosphere is compared with high-resolution imaging of the extreme-ultraviolet radiation components. Here it is revealed that tornado-like swirls (**c**), previously only observed in the chromosphere, have a signal in the spectral lines formed in the hot solar corona (**e**). The line-of-sight component of the magnetic field (**e**, bottom) reveals the unipolar nature of the rotating structure. The concurrent transition region (**e**, middle) and low normalized coronal intensity (**e**, top) reveal radiative emission during the lifetime of the swirl, thus implying heating. See Supplementary Movie 1.

[1]Institute of Theoretical Astrophysics, University of Oslo, PO Box 1029 Blindern, N-0315 Oslo, Norway. [2]Center of Mathematics for Applications, University of Oslo, PO Box 1053 Blindern, N-0316 Oslo, Norway. [3]Kiepenheuer Institute for Solar Physics, Schöneckstrasse 6–7, D-79104 Freiburg, Germany. [4]Department of Physics and Astronomy, Uppsala University, Box 516, SE-75120 Uppsala, Sweden. [5]Solar Physics and Space Plasma Research Centre, School of Mathematics and Statistics, University of Sheffield, Hicks Building, Hounsfield Road, Sheffield S3 7RH, UK.

location in each subsequent co-aligned layer implies that these layers are connected by a coherent structure (visualized by the swirl axis in Fig. 1d). The enhanced normalized intensities in the 30.4-nm and 17.1-nm channels, integrated across the swirl region (Fig. 1d, dashed boxes), shows that this event channels energy into the transition region and low corona (Fig. 1e). A signal in the 30.4-nm channel is found for all 14 swirls. Four of them also show co-aligned emission in the AIA channels at 19.3 and 21.1 nm, which implies that the vertical extents of the individual swirls vary (Fig. 2b and Supplementary Table 1).

We found that at exactly the same spatial position as each swirl, there is at least one or often several bright points in the corresponding Fe I continuum intensity, which maps the photospheric surface (Fig. 1d). These bright points are the observational signature of the footpoints of magnetic flux concentrations as seen in the simultaneously recorded magnetogram (Fig. 1d). The time series of the magnetograms (Fig. 1e, bottom) shows that the magnetic polarity and total magnetic flux are conserved during the lifetime of the swirls, which makes it unlikely that magnetic reconnection occurred. The observations also strongly suggest that swirls are connected to magnetic field structures that couple the layers of the solar atmosphere from the photosphere to the corona. This conclusion is further supported by the fact that the cross-section of the swirl feature increases with height, which is a fundamental property of expanding magnetic structures[13].

The solar surface is characterized by horizontally divergent flow fields in the bright granular plasma updrafts, which converge into the dark network of intergranular lanes. There the cooled plasma sinks down again into the solar interior. In particular, at the vertices of the lanes the conservation of angular momentum of an initially weak, net angular motion of the inflowing plasma results in the formation of vortex flows. This 'bathtub effect'[14] is observed in a wide variety of hydrodynamical systems, for example in tornadoes in Earth's atmosphere[15]. The predicted vortex flows are commonly observed in the

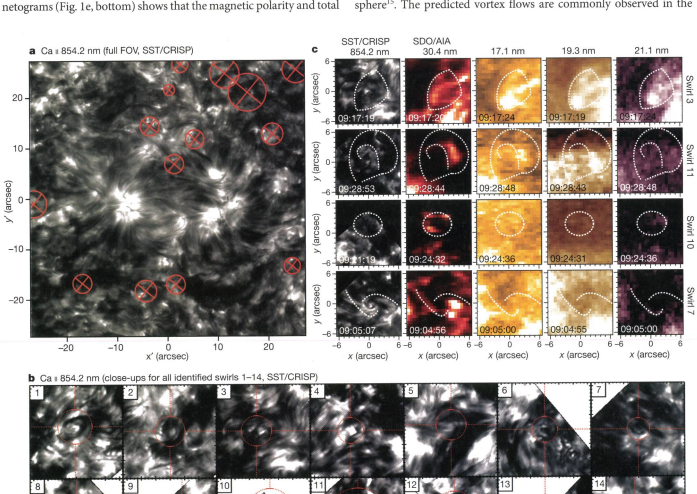

Figure 2 | Detected swirl events in the solar observations on 8 May 2011. **a**, Field of view of SST/CRISP at the centre of the solar disk (spatial coordinates x' and y' refer to the de-rotated image), with all identified swirls marked with crosses and circles on top of an exemplary image in the Ca II 854.2-nm spectral line core. The size of the circles represents the area attributed to the individual swirls. **b**, Close-ups (field of view 13″ × 13″) of the Ca II 854.2-nm line core maps for each of the 14 swirls (Supplementary Movie 2). **c**, Comparison of the Ca II images, and the SDO/AIA channels at 30.4, 17.1, 19.3 and 22.2 nm for four selected examples labelled on right. Swirl 3 is the hottest event with the strongest emission in the swirl centre in the 21.1-nm channel. There is also strong emission in the swirl ring fragments in all SDO/AIA channels. Swirl 11 is the largest in terms of spatial area, and the swirl arc (outlined with white contours in the Ca II map) contains hot components in all SDO channels. The hottest (21.1-nm) signal is sourced to the leading edge of the front of the swirl arc. Swirl 10 reveals a distinct ring formation in the 30.4-nm SDO channel and weaker signal in the other SDO maps. We detect a propagating signal in the ring formed in the 30.4-nm SDO channel, which occurs in unison with the swirl arc in the Ca II map. Likewise, with swirl 7 we observe the swirl structure in the ring in all four SDO channels. Swirl 1 is shown in more detail in Fig. 1. See Supplementary Table 1.

solar photosphere on various spatial scales ranging from over several thousand kilometres[8] down to 1,000 km and smaller[9,10]. Photospheric vortex flows have also been found in high-resolution numerical simulations of the solar atmosphere[16–20], including those presented here. Despite the apparent similarities between previously observed photospheric vortex flows[8,9] and chromospheric swirls, the formation of chromospheric swirls is most likely related to the convective motions on even smaller spatial scales.

We validate this hypothesis with a detailed analysis of simulations carried out with the three-dimensional, radiative magnetohydrodynamics codes CO^{5}BOLD[21] (Fig. 3) and BIFROST[22] (Supplementary Fig. 1). The generated granular flows reorganize the magnetic field, which is essentially advected passively under the conditions of the low photosphere in quiet Sun regions. The result of this reorganization is a complex magnetic field topology where footpoints are concentrated in the intergranular downflow lanes in the form of knots and sheets (Fig. 3a, e). This process generates high magnetic field strengths, in excess of 0.1 T, in the lane vertices where the vortex flows are found. It has been observed directly that such small-scale magnetic concentrations are continuously dragged by vortex motions[23,24]. Consequently, the bathtub effect causes the footpoints of magnetic field structures to rotate.

The magnetic field itself effectively couples the different layers of the solar atmosphere and transfers the rotation of the footpoints into the upper layers (Fig. 1d). Whereas the magnetic footpoints are forced to follow the photospheric flow field, the situation is reversed in the layers above. There the magnetic pressure dominates over the gas pressure, such that the plasma motion is forced to follow the magnetic field. This process, which is probably also responsible for the 'solar cyclones' observed on larger spatial scales[25], is characteristic in our numerical simulations. A close-up of an exemplary region with a chromospheric swirl is shown in Fig. 3. The magnetic field lines (Fig. 3a, b, red lines) are concentrated in the photospheric footpoints (Fig. 3e) and expand in the atmosphere above, where the field stays largely vertically aligned.

Driven by the overshoot of granular flows into the photosphere and by the omnipresent 5-min oscillations at the solar surface, gas moves up and down throughout the photosphere and the chromosphere. At the location of a swirl, the matter following the rotating field lines is effectively forced into spiral trajectories (Fig. 3a, b, blue–green lines) as the field expands with height. This small-scale, tornado-like vortex structure is easily detected as a ring of increased horizontal velocity at chromospheric heights (Fig. 3c) and also as confined regions of enhanced vorticity (Fig. 3d). The diameter of the rotating flux structure increases with height in the atmosphere, owing to the decrease in the gas pressure that balances the magnetic pressure in the structure. The structure is thus much narrower in the photosphere than in the less dense chromosphere and rotates approximately as a rigid body (Fig. 3f).

The simulations provide a realistic description of the solar atmosphere, which is validated by a detailed comparison of corresponding synthetic intensity maps with the observations (Supplementary Fig. 2). The excellent agreement regarding the pattern in the line core maps and also the Doppler shifts confirms that chromospheric swirls are indeed the observational tracers of rotating magnetic flux structures. The analysed CO^{5}BOLD model contains 11 additional smaller examples. A similar swirl signature is found in numerical simulations with BIFROST (Supplementary Fig. 1).

The fast rotation of the magnetic flux structures generates a centrifugal force that moves the contained plasma outwards along the slanted magnetic field lines (Fig. 3a, b). The rotation axis of the swirl, and with it the whole structure, is tilted and twisted and changes with height and time. The axis of the example shown in Fig. 3 is inclined with respect to

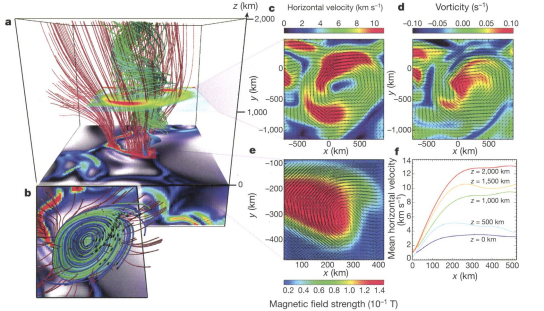

Figure 3 | Numerical model of a swirl event produced with CO^{5}BOLD. **a**–**e**, The displayed close-up region (**a**) is part of the evolved model, which has an overall horizontal size of 8,000 km × 8,000 km and extends vertically from 2,400 km below the surface to the top of the chromosphere at an altitude of 2,000 km. The initial magnetic field was vertical and homogeneous, with a field strength of 5 mT. Periodic lateral boundary conditions and an open lower boundary condition were used, whereas the top boundary has transmitting hydrodynamic and radiative boundary conditions. The three-dimensional geometry of the region around the swirl is visualized with VAPOR[26] from the side (**a**) and from the top (**b**). Next to the (photospheric) surface at $z = 0$ km (grey plane with granulation pattern and overlaid magnetic field strength), the magnetic field lines are plotted as red lines. The plasma flows along and co-rotates with the magnetic field, resulting in spiral trajectories (blue–green streamlines following the velocity field). The swirl is clearly seen in the horizontal velocity (**c**) and the vorticity (**d**) in horizontal cross-sections at a height of $z = 1{,}000$ km (middle chromosphere). The arrows map the horizontal flow field. The bathtub effect is clearly visible in the close-up (**e**) of the magnetic footpoint in the intergranular lane ($z = 0$ km). The resulting rotation is mediated to the chromosphere above by the magnetic field, which effectively couples the atmospheric layers. It produces a rotating funnel in the chromosphere. The corresponding radial velocity profiles (**f**) show that the structures undergo quasi-rigid-body rotation within a cut-off radius, which increases with height. See Supplementary Movie 3.

the vertical by an angle mostly between 10° and 20°. Gas parcels can thus be effectively accelerated upwards in the inclined flux structure, against gravity. The observations indeed show the greatest upward velocity to be in the outer, ring-like regions of swirls, where the centrifugal forces are strongest (Supplementary Fig. 2d, h).

Furthermore, torsional Alfvén waves[26,27] that are generated by the vortex flow in the photosphere and chromosphere propagate upwards and direct part of the associated Poynting flux vertically[28]. The analysed swirl has a net Poynting flux component parallel to the swirl axis that amounts to $1.4 \times 10^4\,\mathrm{W\,m^{-2}}$ measured over the effective swirl area at the top of the model (Supplementary Fig. 3). We estimate a net positive Poynting flux of $440\,\mathrm{W\,m^{-2}}$ averaged over the computational box (Supplementary Notes). This energy flux is delivered at the transition region and, thus, at the boundary to the low corona, where it could be transformed into a substantial heating contribution and emission of radiation, accounting for the signals that we observed with SDO/AIA (Figs 1d and 2c). There the related Alfvén waves generate current sheets when interacting with pre-existing magnetic fields, or potentially cascade to the high-frequency waves[29] needed to drive the fast solar wind from coronal holes. The discovery of this process demonstrates that the energy that reaches the transition region is generated by vortex driving of the magnetic footpoints on small spatial scales at the top of the convection zone, and is then channelled into the outer solar atmosphere by magnetic fields.

Received 7 February; accepted 24 April 2012.

1. Parker, E. Dynamical theory of the solar wind. *Space Sci. Rev.* **4,** 666–708 (1965).
2. Priest, E. *et al.* Nature of the heating mechanism for the diffuse solar corona. *Nature* **393,** 545–547 (1998).
3. Schrijver, C. *et al.* Large-scale coronal heating by the small-scale magnetic field of the Sun. *Nature* **394,** 152–154 (1998).
4. De Pontieu, B. *et al.* Chromospheric Alfvénic waves strong enough to power the solar wind. *Science* **318,** 1574–1577 (2007).
5. Cirtain, J. *et al.* Evidence for Alfvén waves in solar X-ray jets. *Science* **318,** 1580–1582 (2007).
6. McIntosh, S. *et al.* Alfvénic waves with sufficient energy to power the quiet solar corona and fast solar wind. *Nature* **475,** 477–480 (2011).
7. Parker, E. Nanoflares and the solar X-ray corona. *Astrophys. J.* **330,** 474–479 (1988).
8. Brandt, P., Scharmer, G., Ferguson, S., Shine, R. & Tarbell, T. Vortex flow in the solar photosphere. *Nature* **335,** 238–240 (1988).
9. Bonet, J., Márquez, I., Sánchez Almeida, J., Cabello, I. & Domingo, V. Convectively driven vortex flows in the Sun. *Astrophys. J.* **687,** L131–L134 (2008).
10. Bonet, J. *et al.* SUNRISE/IMaX observations of convectively driven vortex flows in the Sun. *Astrophys. J.* **723,** L139–L143 (2010).
11. Wedemeyer-Böhm, S. & Rouppe van der Voort, L. Small-scale swirl events in the quiet Sun chromosphere. *Astron. Astrophys.* **507,** L9–L12 (2009).
12. Lemen, J. *et al.* The Atmospheric Imaging Assembly (AIA) on the Solar Dynamics Observatory (SDO). *Sol. Phys.* **275,** 17–40 (2012).
13. Tu, C.-Y. *et al.* Solar wind origin in coronal funnels. *Science* **308,** 519–523 (2005).
14. Nordlund, Å. Solar convection. *Sol. Phys.* **100,** 209–235 (1985).
15. Bethlinj, L., Andersen, A. & Fabre, D. Structure of a steady drain-hole vortex in a viscous fluid. *J. Fluid Mech.* **656,** 177–188 (2010).
16. Stein, R. & Nordlund, Å. Simulations of solar granulation. I. General properties. *Astrophys. J.* **499,** 914–933 (1998).
17. Steiner, O. *et al.* Detection of vortex tubes in solar granulation from observations with SUNRISE. *Astrophys. J.* **723,** L180–L184 (2010).
18. Shelyag, S., Keys, P., Mathioudakis, M. & Keenan, F. Vorticity in the solar photosphere. *Astron. Astrophys.* **526,** A5 (2011).
19. Moll, R., Cameron, R. & Schüssler, M. Vortices in simulations of solar surface convection. *Astron. Astrophys.* **533,** A126 (2011).
20. Kitiashvili, I., Kosovichev, A., Mansour, N. & Wray, A. Excitation of acoustic waves by vortices in the quiet Sun. *Astrophys. J.* **727** L50. (2011).
21. Freytag, B. *et al.* Simulations of stellar convection with CO^{5}BOLD. *J. Comput. Phys.* **231,** 919–959 (2012).
22. Gudiksen, B. *et al.* The stellar atmosphere simulation code Bifrost. Code description and validation. *Astron. Astrophys.* **531,** A154 (2011).
23. Balmaceda, L., Vargas Domínguez, S., Palacios, J., Cabello, I. & Domingo, V. Evidence of small-scale magnetic concentrations dragged by vortex motion of solar photospheric plasma. *Astron. Astrophys.* **513,** L6 (2010).
24. Attie, R., Innes, D. & Potts, H. Evidence of photospheric vortex flows at supergranular junctions observed by FG/SOT (Hinode). *Astron. Astrophys.* **493,** L13–L16 (2009).
25. Zhang, J. & Liu, Y. Ubiquitous rotating network magnetic fields and extreme-ultraviolet cyclones in the quiet Sun. *Astrophys. J.* **741,** L7 (2011).
26. Jess, D. *et al.* Alfvén waves in the lower solar atmosphere. *Science* **323,** 1582–1585 (2009).
27. Fedun, V., Shelyag, S., Verth, G., Mathioudakis, M. & Erdélyi, R. MHD waves generated by high-frequency photospheric vortex motions. *Ann. Geophys.* **29,** 1029–1035 (2011).
28. van Ballegooijen, A., Asgari-Targhi, M., Cranmer, S. & DeLuca, E. Heating of the solar chromosphere and corona by Alfvén wave turbulence. *Astrophys. J.* **736,** 3 (2011).
29. Cranmer, S., van Ballegooijen, A. & Edgar, R. Self-consistent coronal heating and solar wind acceleration from anisotropic magnetohydrodynamic turbulence. *Astrophys. J.* **171** (suppl.), 520–551 (2007).
30. Clyne, J., Mininni, P., Norton, A. & Rast, M. Interactive desktop analysis of high resolution simulations: application to turbulent plume dynamics and current sheet formation. *N. J. Phys.* **9,** 301 (2007).

Supplementary Information is linked to the online version of the paper at www.nature.com/nature.

Acknowledgements We acknowledge discussions with R. Hammer, M. Carlsson, V. Hansteen and S. McIntosh. M. Carlsson and B. Gudiksen are thanked for providing BIFROST simulation data and input on its analysis. This work was supported by the Research Council of Norway including computing time through the Programme for Supercomputing (Notur). R.E. acknowledges M. Keray for encouragement and is also grateful to the NSF, Hungary. R.E. and V.F. also acknowledge the support received from the Science and Technology Facilities, UK. The Swedish 1-m Solar Telescope is operated on the island of La Palma by the Institute for Solar Physics of the Royal Swedish Academy of Sciences in the Spanish Observatorio del Roque de los Muchachos of the Instituto de Astrofísica de Canarias. We thank the Computational Information Systems Laboratory at the National Center for Atmospheric Research for providing the VAPOR analysis tool.

Author Contributions S.W.-B. and E.S. produced and analysed the data with help from all authors. O.S., V.F. and R.E. gave advice on the data analysis, aspects of the physical interpretation and the applied numerical methods. J.d.l.C.R. and L.R.v.d.V. contributed to the collection and preparation of the observational data and its comparison with numerical data. All authors discussed the results and contributed to and commented on the manuscript.

Author Information Reprints and permissions information is available at www.nature.com/reprints. The authors declare no competing financial interests. Readers are welcome to comment on the online version of this article at www.nature.com/nature. Correspondence and requests for materials should be addressed to S.W.-B. (svenwe@astro.uio.no).

LETTER

doi:10.1038/nature11188

The limits of the nuclear landscape

Jochen Erler[1,2], Noah Birge[1], Markus Kortelainen[1,2,3], Witold Nazarewicz[1,2,4], Erik Olsen[1,2], Alexander M. Perhac[1] & Mario Stoitsov[1,2]‡

In 2011, 100 new nuclides were discovered[1]. They joined the approximately 3,000 stable and radioactive nuclides that either occur naturally on Earth or are synthesized in the laboratory[2,3]. Every atomic nucleus, characterized by a specific number of protons and neutrons, occupies a spot on the chart of nuclides, which is bounded by 'drip lines' indicating the values of neutron and proton number at which nuclear binding ends. The placement of the neutron drip line for the heavier elements is based on theoretical predictions using extreme extrapolations, and so is uncertain. However, it is not known how uncertain it is or how many protons and neutrons can be bound in a nucleus. Here we estimate these limits of the nuclear 'landscape' and provide statistical and systematic uncertainties for our predictions. We use nuclear density functional theory, several Skyrme interactions and high-performance computing, and find that the number of bound nuclides with between 2 and 120 protons is around 7,000. We find that extrapolations for drip-line positions and selected nuclear properties, including neutron separation energies relevant to astrophysical processes, are very consistent between the models used.

Only 288 of the several thousand nuclides, or isotopes, known to inhabit the nuclear landscape are either stable or practically stable (that is, have half-lives longer than the expected life of the Solar System). These 288 nuclides form the 'valley of stability' (Fig. 1). By moving away from this valley, by adding nucleons, we enter the vast territory of short-lived radioactive nuclei, which disintegrate by emitting β- and α-particles or split into smaller parts through spontaneous fission. Nuclear existence ends at the drip lines, where there is no longer enough binding energy to prevent the last nucleons from escaping the nucleus. As indicated in Fig. 1, the proton-rich border of the nuclear territory has been experimentally delineated up to protactinium[2] (proton number, $Z = 91$). The neutron-rich boundary is known only up to oxygen ($Z = 8$) because of the long distance separating the valley of stability from the neutron drip line[3]. The superheavy nucleus with $Z = 118$ and $A = 294$ (ref. 4) marks the current limit of nuclear charge and mass. The borders of the superheavy region are unknown and difficult to predict because competition between Coulomb and shell effects can cause voids and exotic topologies to form (compare with section 4 of ref. 5).

Today, about 3,000 nuclides are known[2,3] (see also http://www.nscl.msu.edu/~thoennes/2009/discovery.htm). Experimental exploration of very neutron-rich nuclei is extremely challenging because of the very low production rates in studies involving the fragmentation of stable nuclei, and the separation and identification of the products. It is anticipated that the next generation of radioactive ion-beam facilities will have high-power beams and highly efficient and selective fragment separators with which to delineate most of the neutron drip line up to mass number $A \approx 100$ (ref. 6).

The primary factor that determines the particle stability—and drip line—of a nuclide is its separation energy[7]: the amount of energy needed to remove from it a single neutron (S_{1n}) or proton (S_{1p}) or two neutrons (S_{2n}) or protons (S_{2p}). In terms of the binding energy, $B(Z,N)$, where N denotes the neutron number, the one-neutron and two-neutron separation energies are $S_{1n}(Z,N) = B(Z,N-1) - B(Z,N)$ and $S_{2n}(Z,N) = B(Z,N-2) - B(Z,N)$, respectively; analogous relationships apply to protons. If the separation energy is positive, the nucleus is stable to nucleon emission; conversely, if the separation energy is negative, the nucleus is unstable. The drip line is reached when $S_{1n} \approx 0$ (one-neutron drip line) or $S_{2n} \approx 0$ (two-neutron drip line). The drip-line position is strongly affected by nucleonic superfluidity[7], which makes nuclei with even numbers of nucleons more bound than their odd-nucleon-number neighbours. In terms of the chemical potential, λ_n, and odd–even energy difference (or pairing gap), Δ_n, the separation energies can be written[8] as $S_{1n} \approx -\lambda_n - \Delta_n$ (for odd N) and $S_{2n} \approx -2\lambda_n$ (for even N). Although the negative chemical potential guarantees that an even-N system is bound, this is not true if N is odd: $S_{1n} > 0$ only if $\lambda_n < -\Delta_n$. The helium isotopes provide evidence for the impact of pairing on nuclear existence: the even–even isotopes ^{4}He, ^{6}He and ^{8}He are bound whereas ^{5}He, ^{7}He and ^{9}He are not. Consequently, the one-nucleon drip line is reached earlier than the two-nucleon drip line, and the region of nuclear existence has a ragged border that zigzags between odd- and even-particle species. Because the aim of this study is to estimate the maximum extent of nuclear binding, we focus on even–even nuclei and two-neutron separation energies.

The quest for the limits of nuclear binding is closely connected to the question about the origin of elements in the universe. The astrophysical rapid proton capture and rapid neutron capture processes, which are responsible for the generation of many heavy elements, operate very close to the drip lines[9]; hence, the structure of very exotic, weakly bound nuclei directly impacts the way the elements are produced in stars.

From the theoretical point of view, the description of weakly bound superfluid complex nuclei is a demanding task as it requires the understanding and control of three crucial aspects of the nuclear many-body problem: interaction, pairing and coupling to the low-lying particle continuum[10,11]. For such a task, the microscopic tool of choice is the nuclear density functional theory (DFT) based on the self-consistent mean-field approach[12]. The main ingredient of the nuclear DFT is the effective interaction between nucleons represented by the energy density functional (EDF), which depends on total (neutron-plus-proton) and isovector (neutron-minus-proton) densities and currents. Because the coupling constants of the nuclear EDF cannot yet be computed by *ab initio* methods, it is customary to use optimization techniques to adjust them to carefully selected experimental data[13–15] (primarily on nuclei near the valley of stability). The resulting uncertainties in model parameters can be used to estimate statistical errors of calculated quantities, especially when it comes to extrapolations into unexplored regions (for example towards the neutron drip line)[14]. However, to estimate systematic model errors, resulting from different theoretical assumptions and/or different optimization protocols, it is necessary to compare a variety of models and parameterizations. In this way, it is possible to assess the robustness of theoretical predictions and estimate theoretical uncertainties. The

[1]Department of Physics and Astronomy, University of Tennessee, Knoxville, Tennessee 37996, USA. [2]Physics Division, Oak Ridge National Laboratory, Oak Ridge, Tennessee 37831, USA. [3]Department of Physics, PO Box 35 (YFL), University of Jyväskylä, FI-40014 Jyväskylä, Finland. [4]Institute of Theoretical Physics, Warsaw University, PL-00681 Warsaw, Poland.
‡Deceased.

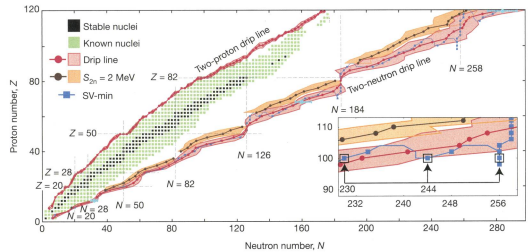

Figure 1 | Nuclear even–even landscape as of 2012. Map of bound even–even nuclei as a function of Z and N. There are 767 even–even isotopes known experimentally[2,3] both stable (black squares) and radioactive (green squares). Mean drip lines and their uncertainties (red) were obtained by averaging the results of different models. The two-neutron drip line of SV-min (blue) is shown together with the statistical uncertainties at $Z = 12$, 68 and 120 (blue error bars). The $S_{2n} = 2$ MeV line is also shown (brown) together with its systematic uncertainty (orange). The inset shows the irregular behaviour of the two-neutron drip line around $Z = 100$.

application of modern optimization and statistical methods, together with high-performance computing, has revolutionized nuclear DFT during recent years.

In our study, we use quasi-local Skyrme functionals[13] in the particle–hole channel augmented by the density-dependent, zero-range pairing term. The commonly used Skyrme EDFs reproduce total binding energies with a root mean square error of the order of 1–4 MeV (refs 15, 16), and the agreement with the data can be significantly improved by adding phenomenological correction terms[17]. The Skyrme DFT approach has been successfully tested over the entire chart of nuclides on a broad range of phenomena, and it usually performs quite well when applied to energy differences (such as S_{2n}), radii and nuclear deformations. Other well-calibrated mass models include the microscopic–macroscopic finite-range droplet model (FRDM)[18], the Brussels–Montreal Skyrme–HFB models based on the Hartree–Fock–Bogoliubov (HFB) method[17] and Gogny force models[19,20].

Figure 2 illustrates the difficulties with theoretical extrapolations towards drip lines. Shown are the S_{2n} values for the isotopic chain of even–even erbium isotopes predicted with different EDF, SLy4[21], SV-min[13], UNEDF0[15], UNEDF1[22], and with the FRDM[18] and HFB-21[17] models. In the region for which experimental data are available, all models agree and well reproduce the data. However, the discrepancy between various predictions steadily grows when moving away from the region of known nuclei, because the dependence of the effective force on the neutron-to-proton asymmetry (neutron excess) is poorly determined. In the example considered, the neutron drip line is

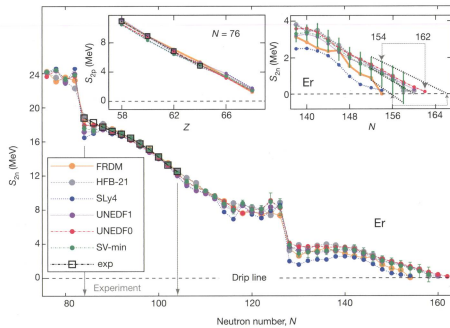

Figure 2 | Calculated and experimental two-neutron separation energies of even–even erbium isotopes. Calculations performed in this work using SLy4, SV-min, UNEDF0 and UNEDF1 functionals are compared to experiment[2] and FRDM[18] and HFB-21[17] models. The differences between model predictions are small in the region where data exist (bracketed by vertical arrows) and grow steadily when extrapolating towards the two-neutron drip line ($S_{2n} = 0$). The bars on the SV-min results indicate statistical errors due to uncertainty in the coupling constants of the functional. Detailed predictions around $S_{2n} = 0$ are illustrated in the right inset. The left inset depicts the calculated and experimental two-proton separation energies at $N = 76$.

predicted to be between $N = 154$ (FRDM) and $N = 162$ (UNEDF0); that is, the model-dependent 'error bar' is appreciable. This is not the case for the proton-rich boundary. The calculated values of S_{2p} at $N = 76$ are shown in the left inset of Fig. 2. Because the proton drip line lies relatively close to the valley of stability owing to the repulsive electrostatic interaction between protons, and because the proton continuum is effectively shifted up in energy as a result of the confining effect of the Coulomb barrier, the associated extrapolation error is small and all the models we used are in excellent agreement with experiment.

As discussed earlier, in addition to systematic errors, calculated observables are also subject to statistical errors due to uncertainties in EDF parameters[13,14]. Fig. 2 shows how the statistical error in S_{2n} predicted with the SV-min EDF propagates with N. The gradual growth of error bars when approaching the neutron drip line is primarily caused by the isovector coupling constants of the functional that are not well constrained by the current data[14]. The resulting statistical error in the position of the neutron drip line can be obtained by extrapolating the error band of calculated values towards $S_{2n} = 0$ (indicated by dotted lines in the right inset of Fig. 2). In the case of SV-min and erbium isotopes, the statistical uncertainty corresponds to $N = 156$–166.

To assess the current status of theoretical predictions for the limits of nuclear binding and provide a benchmark for future improvements, we carried out large-scale DFT calculations[16,23] of global nuclear properties using six Skyrme EDFs (SkM*[24], SkP[25], SLy4[21], SV-min[13], UNEDF0[15] and UNEDF1[22]) and covering a wide range of even–even nuclei of up to 120 protons and 300 neutrons. The summary of our survey is presented in Fig. 1. The dashed grey gridlines show the magic numbers known around the valley of stability (20, 28, 50, 82 and 126) as well as the predicted regions of stability in superheavy nuclei[6] around $N = 184$ and 258. The mean neutron and proton drip lines and associated systematic uncertainties have been obtained by averaging the predictions of individual models (given in tabular form in Supplementary Information). We also show the two-neutron drip line of SV-min together with its statistical error bars at $Z = 12$, 68, and 120. As can be seen, the statistical error generally falls into the band of systematic uncertainty.

As expected, the theoretical error in the position of the neutron drip line grows steadily with distance from the valley of stability. Yet the overall consistency of model predictions is greater than initially anticipated. This is particularly true for $N \leq 50$ and N around 60, 126 and 184, where the error band is small. In particular, the recently discovered isotope ^{40}Mg (ref. 26) is predicted to be neutron-bound by all our models. Also, the neutron-rich isotopes ^{26}O and ^{28}O are consistently calculated to lie inside the neutron drip line. Experimental searches have so far provided no evidence[3] for the existence of ^{26}O and ^{28}O, and configuration interaction calculations[27] have attributed this anomalous behaviour to the repulsive three-body force. If a similar effect is observed in heavier nuclei, where DFT calculations are believed to be more reliable, this may suggest systematic modifications of the isovector-density-dependent interactions of EDF. As illustrated in Supplementary Fig. 1, the predictions of the FRDM and HFB-21 models generally fall within our uncertainty band.

As seen in Fig. 1, the two-neutron drip line has a complicated zigzag pattern in some regions. The inset shows the irregular behaviour of the two-neuron drip line predicted by SV-min at around $Z = 100$. Although the primary drip line is located at $N = 230$, neutron binding reappears around $N = 242$ and then again at $N = 256$, giving rise to a secondary and a tertiary drip line. Such behaviour is due to the presence of shell effects at neutron closures that tend to lower binding energy along the localized bands of stability[16]. The phenomenon of re-entrant binding is predicted in several areas of the neutron drip line, for example at around $Z = 60$ ($N = 132$ and 140), 70 ($N = 182$) and 100 ($N = 258$). (For more examples, see Supplementary Information and also refs 16–20.)

The astrophysical rapid neutron capture process (r-process) is expected to proceed along a path of constant neutron separation energies, fairly close to the neutron drip line[2]. Fig. 1 shows the $S_{2n} = 2$ MeV line, together with its uncertainty band, corresponding to the very neutron-rich r-process path. (Such theoretical data can be used in future r-process simulations to estimate uncertainties of element abundances related to theoretical uncertainties of separation energies; on request, we can provide uncertainties for other values of S_{2n} and S_{1n}.) Again, the DFT predictions seem fairly robust, especially around the neutron magic numbers where the separation energies change rapidly. Finally, there is a great deal of consistency between models regarding the position of the two-proton drip line, with the calculated systematic uncertainty usually not exceeding $\Delta Z = 2$. The nuclides ^{42}Cr, ^{48}Ni and ^{54}Zn, which are known[3] to be two-proton unstable, are firmly predicted as such, as are the α-emitters ^{166}Pt, ^{172}Hg and ^{186}Po.

To assess how model dependent DFT extrapolations are when it comes to observables other than the separation energy, in Supplementary Figs 2–4 we show the mass and isovector quadrupole deformations and differences between radii of neutron and proton distributions (neutron skins) predicted in our models. Despite the fact that these quantities are greatly influenced by shell effects, global patterns predicted by various EDFs are fairly similar.

The intermodel consistency of our results allows us to address the question of the number of isotopes inhabiting the nuclear landscape. According to our Skyrme DFT mass tables, the numbers of particle-bound even–even nuclei with $2 \leq Z \leq 120$ are 2,333 in the SkM* model, 2,042 in SkP, 1,928 in SLy4, 2,116 in SV-min, 2,209 in UNEDF0 and 2,219 in UNEDF1. Adding the odd-mass and odd–odd neighbours, we predict that $6{,}900 \pm 500_{\mathrm{syst}}$ nuclei with $Z \leq 120$ are bound to proton and neutron emission. To put things in perspective, the total number of nuclides known experimentally is slightly more than 3,000 (refs 1, 2). Although the majority of rare isotopes inhabiting the outskirts of the nuclear landscape are unlikely to be seen, their properties impact astrophysical processes and, hence, the matter around us. The road to understanding those exotic species takes us through reliable nuclear simulations with quantified uncertainties, and this study represents a step in this direction. In the long term, of particular importance is the development of novel nuclear energy density functionals that reproduce both bulk nuclear properties and spectroscopic data. Work along these lines is in progress[15,22].

The experimental range of the nuclear landscape is fluid: new rare isotopes are being added to it every year. As experiment advances, increasingly more-quantitative models of the atomic nucleus are being developed with the aid of high-performance computing. In this context, the theoretical range of the chart of nuclides is continually changing, and our predictions should be viewed as specific to 2012.

METHODS SUMMARY

The calculations were carried out within the nuclear DFT framework[16,23]. The Skyrme functionals SkM*[24], SkP[25], SLy4[21], SV-min[13], UNEDF0[15] and UNEDF1[22] were used in the particle–hole channel, and a density-dependent pairing force of the mixed type[28] was used in the pairing channel. The self-consistent HFB equations of the nuclear DFT were solved with the code HFBTHO[29] as further optimized in refs 15, 22. The code solves the nonlinear HFB equations in configuration space by expanding self-consistent eigenstates in a large basis of the deformed harmonic oscillator. The axial symmetry and parity of nuclear mean fields are imposed to reduce the dimension and complexity of the problem. (The effect of triaxial and reflection-asymmetric ground-state deformations on particle drip lines is expected to be minor[30].) The single-particle basis consisted of the harmonic oscillator states originating in the 20 major oscillator shells (see Supplementary Fig. 5 and Supplementary Information for more discussion). To restore approximately the particle number symmetry broken in HFB, we used the variant of the Lipkin–Nogami scheme in ref. 16. The large-scale mass tables were computed using the JAGUAR and KRAKEN Cray XT5 supercomputers housed at Oak Ridge National Laboratory.

The Skyrme energy functional with a pairing term is parameterized by up to 14 coupling constants. To assess better the systematic error, we used functionals having distinct characteristics. SkM* was developed with a focus on surface energy

and fission barriers; SkP aimed at a simultaneous description of the mean field and pairing; SLy4 was optimized with a bias on neutron-rich nuclei and properties of neutron matter; SV-min was adjusted to a variety of data on spherical nuclei, including diffraction radii and surface thickness; UNEDF0 was developed by considering data on spherical and deformed nuclei; and the data set of UNEDF1 also considered excitation energies of fission isomers.

Received 28 February; accepted 2 May 2012.

1. Thoennessen, M. & Sherrill, B. From isotopes to the stars. *Nature* **473,** 25–26 (2011).
2. National Nuclear Data Center. Evaluated Nuclear Structure Data File. http://www.nndc.bnl.gov/ensdf/.
3. Thoennessen, M. Reaching the limits of nuclear stability. *Rep. Prog. Phys.* **67,** 1187–1232 (2004).
4. Oganessian, Yu Ts. *et al.* Synthesis of the isotopes of elements 118 and 116 in the ^{249}Cf and ^{245}Cm + ^{48}Ca fusion reactions. *Phys. Rev. C* **74,** 044602 (2006).
5. Nazarewicz, W. *et al.* Theoretical description of superheavy nuclei. *Nucl. Phys. A* **701,** 165–171 (2002).
6. Rare Isotope Science Assessment Committee. *Scientific Opportunities with a Rare-Isotope Facility in the United States* (Natl Acad. Press, 2007).
7. Brink, D. M. & Broglia, R. A. *Nuclear superfluidity: pairing in finite systems* (Cambridge Univ. Press, 2005).
8. Beiner, M., Lombard, R. J. & Mas, D. Self-consistent calculations of ground state properties for unstable nuclei. *Nucl. Phys. A* **249,** 1–28 (1975).
9. Langanke, K. & Wiescher, M. Nuclear reactions and stellar processes. *Rep. Prog. Phys.* **64,** 1657–1701 (2001).
10. Dobaczewski, J. *et al.* Shell structure of exotic nuclei. *Prog. Part. Nucl. Phys.* **59,** 432–445 (2007).
11. Matsuo, M. & Nakatsukasa, T. Open problems in nuclear structure near drip lines. *J. Phys. G* **37,** 064017 (2010).
12. Bender, M., Heenen, P.-H. & Reinhard, P.-G. Self-consistent mean-field models for nuclear structure. *Rev. Mod. Phys.* **75,** 121–180 (2003).
13. Klüpfel, P. *et al.* Variations on a theme by Skyrme: a systematic study of adjustments of model parameters. *Phys. Rev. C* **79,** 034310 (2009).
14. Reinhard, P.-G. & Nazarewicz, W. Information content of a new observable: The case of the nuclear neutron skin. *Phys. Rev. C* **81,** 051303(R) (2010).
15. Kortelainen, M. *et al.* Nuclear energy density optimization. *Phys. Rev. C* **82,** 024313 (2010).
16. Stoitsov, M. V. *et al.* Systematic study of deformed nuclei at the drip lines and beyond. *Phys. Rev. C* **68,** 054312 (2003).
17. Gorely, S., Chamel, N. & Pearson, J. M. Further explorations of Skyrme-Hartree-Fock-Bogoliubov mass formulas. XII. Stiffness and stability of neutron-star matter. *Phys. Rev. C* **82,** 035804 (2010).
18. Möller, P. *et al.* Nuclear ground-state masses and deformations. *At. Data Nucl. Data Tables* **59,** 185–381 (1995).
19. Gorely, S., Hilaire, S., Girod, M. & Peru, S. First Gogny-Hartree-Fock-Bogoliubov nuclear mass model. *Phys. Rev. Lett.* **102,** 242501 (2009).
20. Delaroche, J.-P. *et al.* Structure of even-even nuclei using a mapped collective Hamiltonian and the D1S Gogny interaction. *Phys. Rev. C* **81,** 014303 (2010).
21. Chabanat, E. *et al.* A Skyrme parametrization from subnuclear to neutron star densities Part II. Nuclei far from stabilities. *Nucl. Phys. A* **635,** 231–256 (1998); erratum **643,** 441 (1998).
22. Kortelainen, M. *et al.* Nuclear energy density optimization: large deformations. *Phys. Rev. C* **85,** 024304 (2012).
23. Stoitsov, M., Nazarewicz, W. & Schunck, N. Large-scale mass table calculations. *Int. J. Mod. Phys. E* **18,** 816–822 (2009).
24. Bartel, J. *et al.* Towards a better parametrisation of Skyrme-like effective forces: a critical study of the SkM force. *Nucl. Phys. A* **386,** 79–100 (1982).
25. Dobaczewski, J., Flocard, H. & Treiner, J. Hartree-Fock-Bogolyubov description of nuclei near the neutron-drip line. *Nucl. Phys. A* **422,** 103–139 (1984).
26. Baumann, T. *et al.* Discovery of ^{40}Mg and ^{42}Al suggests neutron drip-line slant towards heavier isotopes. *Nature* **449,** 1022–1024 (2007).
27. Otsuka, T. *et al.* Three-body forces and the limit of oxygen isotopes. *Phys. Rev. Lett.* **105,** 032501 (2010).
28. Dobaczewski, J., Nazarewicz, W. & Stoitsov, M. V. Nuclear ground-state properties from mean-field calculations. *Eur. Phys. J. A* **15,** 21–26 (2002).
29. Stoitsov, M. V. *et al.* Axially deformed solution of the Skyrme–Hartree–Fock–Bogolyubov equations using the transformed harmonic oscillator basis. The program HFBTHO (v1.66p). *Comput. Phys. Commun.* **167,** 43–63 (2005).
30. Möller, P. *et al.* Axial and reflection asymmetry of the nuclear ground state. *At. Data Nucl. Data Tables* **94,** 758–780 (2008).

Supplementary Information is linked to the online version of the paper at www.nature.com/nature.

Acknowledgements This work was supported by the Office of Nuclear Physics, US Department of Energy, and by the Academy of Finland.

Author Contributions Theoretical calculations were performed by J.E., M.K. and M.S. The data were analysed by N.B., J.E., W.N., E.O. and A.M.P. The manuscript was prepared by J.E. and W.N. All authors contributed to this work, discussed the results and conclusions, and commented on the manuscript.

Author Information Reprints and permissions information is available at www.nature.com/reprints. The authors declare no competing financial interests. Readers are welcome to comment on the online version of this article at www.nature.com/nature. Correspondence and requests for materials should be addressed to W.N. (witek@utk.edu)

LETTER

doi:10.1038/nature11222

Fractal morphology, imaging and mass spectrometry of single aerosol particles in flight

N. D. Loh[1], C. Y. Hampton[1], A. V. Martin[2], D. Starodub[1], R. G. Sierra[1], A. Barty[2], A. Aquila[2,3], J. Schulz[2,3], L. Lomb[4], J. Steinbrener[4], R. L. Shoeman[4], S. Kassemeyer[4], C. Bostedt[5], J. Bozek[5], S. W. Epp[6,7], B. Erk[6,7], R. Hartmann[8], D. Rolles[4,6], A. Rudenko[6,7], B. Rudek[6,7], L. Foucar[4,6], N. Kimmel[9,10], G. Weidenspointner[9,10], G. Hauser[9,10], P. Holl[8], E. Pedersoli[11], M. Liang[2], M. M. Hunter[12], L. Gumprecht[2], N. Coppola[3], C. Wunderer[13], H. Graafsma[13], F. R. N. C. Maia[14], T. Ekeberg[15], M. Hantke[15], H. Fleckenstein[2], H. Hirsemann[13], K. Nass[2,16], T. A. White[2], H. J. Tobias[17], G. R. Farquar[12], W. H. Benner[12], S. P. Hau-Riege[12], C. Reich[8], A. Hartmann[8], H. Soltau[8], S. Marchesini[18], S. Bajt[13], M. Barthelmess[13], P. Bucksbaum[1], K. O. Hodgson[1], L. Strüder[9,10], J. Ullrich[6,7], M. Frank[12], I. Schlichting[4,6], H. N. Chapman[7,16] & M. J. Bogan[1]

The morphology of micrometre-size particulate matter is of critical importance in fields ranging from toxicology[1] to climate science[2], yet these properties are surprisingly difficult to measure in the particles' native environment. Electron microscopy requires collection of particles on a substrate[3]; visible light scattering provides insufficient resolution[4]; and X-ray synchrotron studies have been limited to ensembles of particles[5]. Here we demonstrate an *in situ* method for imaging individual sub-micrometre particles to nanometre resolution in their native environment, using intense, coherent X-ray pulses from the Linac Coherent Light Source[6] free-electron laser. We introduced individual aerosol particles into the pulsed X-ray beam, which is sufficiently intense that diffraction from individual particles can be measured for morphological analysis. At the same time, ion fragments ejected from the beam were analysed using mass spectrometry, to determine the composition of single aerosol particles. Our results show the extent of internal dilation symmetry of individual soot particles subject to non-equilibrium aggregation, and the surprisingly large variability in their fractal dimensions. More broadly, our methods can be extended to resolve both static and dynamic morphology of general ensembles of disordered particles. Such general morphology has implications in topics such as solvent accessibilities in proteins[7], vibrational energy transfer by the hydrodynamic interaction of amino acids[8], and large-scale production of nanoscale structures by flame synthesis[9].

Complex airborne particulate matter, with particle mobility diameters less than 2.5 μm, efficiently enters the human lungs, and also constitutes the second most important contribution to current global warming[10]. Among such particulate matter, the morphology and composition of carbonaceous soot has been extensively studied[11]: the fractal morphology and coagulation of soot in atmospheric water or ice particles modifies their radiative properties in the atmosphere[2,11–14], which in turn affects atmospheric energy balance[15], and hence climate[16].

The fractal properties of soot have been estimated from two-dimensional projections obtained from electron microscopy[3], often requiring prior information such as the amount of overlap between monomer units, or whether the expected fractal dimension is less than or greater than two[3]. More recently, morphology has also been extracted from structure factors estimated from transmission electron micrographs[17]. Electron microscopy, however, requires that particles first adhere to substrates, which may alter the conformation of larger particles and encourage agglomeration absent in the aerosol phase. Substrate-bound measurements may also lead to systematic biases in the projections from electron micrographs, especially for asymmetric particles that may roll around to maximize substrate contact[3].

Light scattering experiments, by contrast, can probe the *in situ* morphology of particles in flight. Scattering experiments performed with optical lasers on randomly oriented soot particles in flight[18] have revealed low-resolution morphology for single micrometre-size particles[4]. However, interpreting the optical scattering from such particles is complicated because the Born scattering approximation does not strictly apply[11]. Moreover, optical measurements are particularly restrictive for fractal morphology of micrometre-size soot, as these measurements are limited to scaling exponents occupying only about a decade of length scales. High-resolution, *in situ* fractal morphology has been performed on soot aggregates using X-rays from synchrotrons[5], but these light sources do not supply sufficient incident intensity to measure the morphology of single aggregates.

X-ray free-electron lasers (XFELs) provide sufficient photons, in a single pulse lasting less than 100 fs, to measure X-ray diffraction at high resolution from individual soot particles in flight. Our experiment was carried out at the CFEL-ASG Multi-Purpose (CAMP) instrument[19] at the Atomic, Molecular and Optical Science beam line[20] of the Linac Coherent Light Source (LCLS), with a setup (Fig. 1) similar to that used in previous work[21,22]. Individual X-ray pulses of less than 150 fs, containing ~10^{12} photons of 1.0 nm wavelength, were focused to 10 μm^2, and intercepted a jet of aerosolized particulate matter at the machine repetition rate of 60 Hz. Single-particle diffraction patterns were captured on X-ray detectors[18] to a maximum full-period resolution of 13 nm at the corner of the detector (see Supplementary Information for details).

Diffraction imaging can be used to produce images of isolated nanoparticle morphology[21–25]. Figure 2a–d shows reconstructions of airborne microclusters of polystyrene spheres, revealing connectivity between individual monomers (monomer radii between 44 and 75 nm). Sphere monomers exhibit tenuous connectivity in certain microclusters (Fig. 2c, d), whereas clusters of ellipsoidal nanoparticles (Fig. 2e, f) tend to stack more efficiently. This trend has been observed in previous studies[23,24] and is related to monomer–monomer contact area, adhesion strength, and hence packing efficiency. The open structures in our

[1]PULSE Institute, SLAC National Accelerator Laboratory, 2575 Sand Hill Road, Menlo Park, California 94025, USA. [2]Center for Free-Electron Laser Science, DESY, Notkestraße 85, 22607 Hamburg, Germany. [3]European XFEL GmbH, Albert-Einstein-Ring 19, 22761 Hamburg, Germany. [4]Max-Planck-Institut für medizinische Forschung, Jahnstrasse 29, 69120 Heidelberg, Germany. [5]Linac Coherent Light Source, LCLS, SLAC National Accelerator Laboratory, 2575 Sand Hill Road, Menlo Park, California 94025, USA. [6]Max Planck Advanced Study Group, Center for Free-Electron Laser Science (CFEL), Notkestraße 85, 22607 Hamburg, Germany. [7]Max-Planck-Institut für Kernphysik, Saupferchekweg 1, 69117 Heidelberg, Germany. [8]PNSensor GmbH, Otto-Hahn-Ring 6, 81739 München, Germany. [9]Max-Planck-Institut Halbleiterlabor, Otto-Hahn-Ring 6, 81739 München, Germany. [10]Max-Planck-Institut für extraterrestrische Physik, Giessenbachstraße, 85741 Garching, Germany. [11]Sincrotrone Trieste, Microscopy Section, 34149 Trieste, Italy. [12]Lawrence Livermore National Laboratory, 7000 East Avenue, Mail Stop L-211, Livermore, California 94551, USA. [13]Photon Science, DESY, Notkestraße 85, 22607 Hamburg, Germany. [14]National Energy Research Scientific Computing Center (NERSC), 1 Cyclotron Road, Berkeley, California 94720, USA. [15]Laboratory of Molecular Biophysics, Department of Cell and Molecular Biology, Uppsala University, Husargatan 3 (Box 596), SE-751 24 Uppsala, Sweden. [16]University of Hamburg, Luruper Chaussee 149, 22761 Hamburg, Germany. [17]Cornell University, Division of Nutritional Sciences, Savage Hall, Ithaca, New York 14853, USA. [18]Advanced Light Source, Lawrence Berkeley National Laboratory, Berkeley, California 94720, USA.

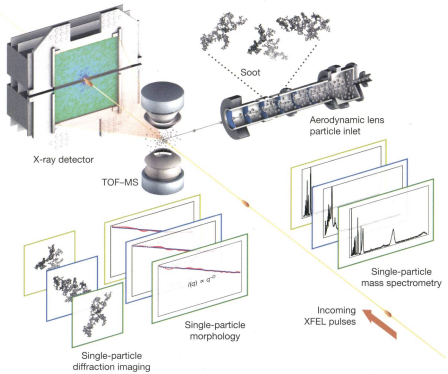

Figure 1 | Schematic of concurrent imaging, morphology and spectroscopy of single soot particles in flight. Coherent XFEL pulses (orange) were made to intersect a particle stream, producing a diffraction pattern and ion fragments whenever a pulse and a particle coincided. Diffraction patterns were measured on a pnCCD (p–n-junction charge-coupled device) X-ray detector, and ion fragments were captured by a time-of-flight mass spectrometer (TOF-MS), both of which operated at the pulse repetition rate of 60 Hz.

sphere clusters differ considerably from the close packing in aerosol-assisted colloidal microclusters[26], indicating the presence of non-equilibrium processes in our system.

Reconstructed electron density maps of structurally complex particles such as soot and soot–salt mixtures show more complex morphology (Fig. 2g, h). For these larger, random particles the relationship between their growth and their morphology is more easily established from the statistics of spatial correlations within each particle, which in turn can be obtained directly from its diffraction intensities. The diffraction patterns in Fig. 2 contain substantial signal to the edge of the detector, indicating the potential to resolve spatial correlations down to tens of nanometres for particles larger than those in Fig. 2, as larger particles scatter more photons under similar illumination conditions. Soot belongs to a class of disordered particles called mass fractals, which show dilation symmetry over a considerable range of length scales. This symmetry is revealed through power laws of their scattering intensity, $S(q) \propto q^{-D}$, where q is the spatial frequency and D is the particle's fractal dimension[11,27]. To minimize

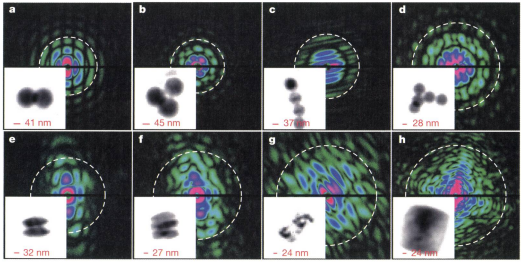

Figure 2 | Diffraction patterns of self-assemblies of particles in flight, and reconstructions of their electron densities. a–d, Polystyrene spheres with radii of 70 nm (**a**, **b**) and 44 nm (**c**, **d**). **e**, **f**, Ellipsoidal nanoparticles. **g**, A spark-generated soot particle. **h**, A salt–soot mixture. Electron density maps were averaged from ten independent, randomly initialized phase-retrieval reconstructions. Red scale bars in the insets also correspond to the full-period resolutions of the respective reconstructions (white circles in the diffraction patterns). The wavelength of incident radiation was 1.0 nm. Resolution computation is discussed in the Methods Summary.

finite-size and monomer shape effects, this power-law scaling is most evident for spatial frequencies $R_g^{-1} < q < a^{-1}$, where R_g is the particle's radius of gyration and a the average monomer radius (see Supplementary Fig. 3). Dilation symmetry in mass fractals indicates a scale-invariance in their aggregation kinetics, which is also observed in computer simulations of aggregation models for single particles in the aerosol phase[28].

Fractal morphology measures a particle's elastic scattering intensity $S(q)$, which is obtained from an angular average of its three-dimensional diffraction intensities. However, we collected only two-dimensional diffraction patterns, and hence were restricted to the angular average of a particle's two-dimensional scattering intensities, sampled on the surface of the Ewald sphere, $I(q)$. Nevertheless, even in the presence of modestly anisotropic external fields it is unlikely for numerous tumbling, aggregating sub-clusters to experience simultaneously a constant anisotropy in their body-fixed coordinate system throughout the entire aggregation process. Under this assumption, the ensemble of polydisperse sub-clusters attached to each aggregate should appear rotationally symmetric, and the Ewald sphere sample $I(q)$ should approach $S(q)$ for spatial frequencies q equal to the inverse length of these sub-clusters. This applies only to sufficiently small sub-clusters within sufficiently large aggregates.

The single-particle diffraction intensities $I(q)$ of the seventeen largest airborne soot aggregates showed a distinct non-integer power-law decay between 170 and 20 nm (Fig. 3), consistent with expectations of mass fractals. Although measurements on soot particles are frequently compared to diffusion-limited cluster–cluster aggregated mass fractals[11], we measured an average fractal dimension of 2.3 ± 0.3, closer to that of mass fractals that show internal restructuring[20]. Such high fractal dimensions were also previously observed in transmission electron micrographs of large soot particles prepared in the cluster-dense regime[28]. Our data established that such dense fractal aggregates also exist in the aerosol phase, free from substrate-initiated agglomeration. There was also considerable variability in our soot's measured fractal dimensions. While this variation could arise from sampling view-dependent diffraction measurements, the relatively small modulations in $I(q)$ suggest ample view-averaging at the scale of sub-clusters in the range 170–20 nm within each soot particle. Hence, this sizable variation in fractal dimension may reflect a genuine fluctuation in our manufactured soot, or in the manner in which it was delivered into the XFEL interaction region, or both. The Fig. 3 inset plots our measured fractal morphology against our soot size estimates, demonstrating the possibility of ascertaining such a relationship with our methods. Such a relationship can be used to detect changes in the growth of these particles over a considerable range of length scales.

Focused X-ray pulses from XFELs typically destroy the particle being imaged, giving rise to energetic ejected ions that can be analysed using time-of-flight mass spectrometry (TOF-MS) to determine the particle's elemental composition (details in Supplementary Information). We correlated simultaneous TOF-MS and X-ray diffraction data from 208 aggregates, as shown in Fig. 4a. The presence of salt and carbonaceous soot in the TOF-MS data corresponds well with the scattering features simultaneously captured in the complementary diffraction patterns (Fig. 4b–e). Despite each particle's absorption of large doses of ionizing radiation, signal intensity corresponding to the mass-to-charge ratio (m/z) of large $[Na(NaCl)]^+$ and $[Na(NaCl)_2]^+$ molecular fragments were observed in the TOF-MS spectra in Fig. 4a. The presence of large ions may be due to particles illuminated in the periphery of the X-ray focus, leading to incomplete ionization.

Fractals are suitable candidates for damage studies using XFELs, which can help in optimizing X-ray pulse parameters for diffraction imaging of single biomolecules. Morphology measurements on mass fractals with a small variance in fractal dimension can potentially resolve the extent of damage inflicted by diffraction imaging with XFELs; one expects dilation symmetry in mass fractals preserved down to length scales unaffected by radiation damage. When combined with mass spectrometry, one could identify changes in features of the spectra of ejected ions, such as the width and shape of spectral lines in Fig. 4a, as a function of X-ray pulse length and energy.

The intense, femtosecond X-ray pulses provided by XFELs provide sufficient diffraction signal to resolve single aggregates from the ensemble *in situ*, opening the door to new means of morphological study of aerosol dynamics in their native environment. We observed considerable variation in the fractal dimension of individual soot aggregates, as well as the extent of dilation symmetry. Combination of morphology with mass spectrometry further enriches our measurement of the ensemble, and allows particles of different elemental composition to be separated. Significantly, we observe a fractal dimension of 2.3 ± 0.3 for soot aggregates *in situ*, a value that suggests in-flight restructuring beyond diffusion-limited cluster–cluster aggregation. The substantial variability in the fractal dimension may indicate non-uniform aggregation rates, and/or spatial variations in aggregation conditions and air/carbon ratio. Further studies to resolve these connections will have implications for combustion efficiencies and climate modelling, which can now include effects due to polydispersities in the ensemble measured from *in situ* single-particle morphology.

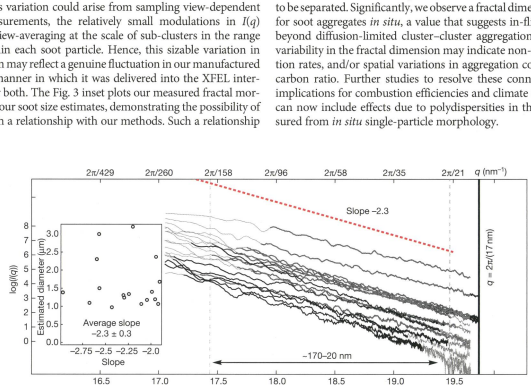

Figure 3 | Fractal morphology of micrometre-sized soot aggregates. We show the unnormalized $I(q)$ of 17 of our largest spark-generated soot particles. The slopes of distinctly linear regions in the log–log plot of $I(q)$ (darkened segments) is the negative of each particle's fractal dimension, showing a range of dilation symmetry (170–20 nm) common to these particles. The inset shows these slopes, plotted against the respective particle sizes.

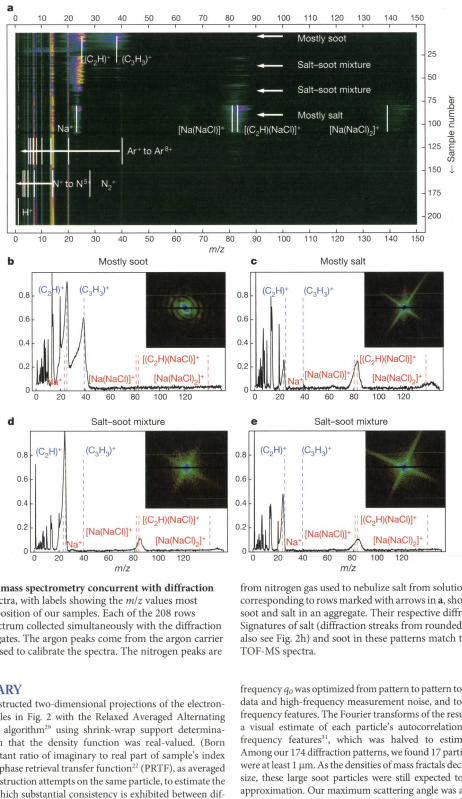

Figure 4 | Time-of-flight mass spectrometry concurrent with diffraction imaging. a, TOF-MS spectra, with labels showing the m/z values most compatible with the composition of our samples. Each of the 208 rows represents a TOF-MS spectrum collected simultaneously with the diffraction pattern from single aggregates. The argon peaks come from the argon carrier gas for the soot, and are used to calibrate the spectra. The nitrogen peaks are from nitrogen gas used to nebulize salt from solution. **b**–**e**, Four typical spectra corresponding to rows marked with arrows in **a**, showing various admixtures of soot and salt in an aggregate. Their respective diffraction patterns are inset. Signatures of salt (diffraction streaks from rounded facets of salt agglomerates; also see Fig. 2h) and soot in these patterns match those in the corresponding TOF-MS spectra.

METHODS SUMMARY

Phase retrieval. We reconstructed two-dimensional projections of the electron-density functions of particles in Fig. 2 with the Relaxed Averaged Alternating Reflections phase-retrieval algorithm[29] using shrink-wrap support determination[30] and the assumption that the density function was real-valued. (Born approximation holds; constant ratio of imaginary to real part of sample's index of refraction.) We used the phase retrieval transfer function[22] (PRTF), as averaged over ten independent reconstruction attempts on the same particle, to estimate the maximum resolution for which substantial consistency is exhibited between different reconstructions. The full-period resolution in these reconstructions was determined from the point at which each particle's PRTF falls below 0.5.

Soot aggregates. In approximately 70 min, we collected 174 diffraction patterns of spark-generated single soot particles at low carrier-gas flow rates, to suppress the coincidence of multiple soot particles in the X-ray interaction region. None of these 174 patterns was expected to contain multiple soot particles, assuming that particles arrive randomly and uniformly at the XFEL pulse interaction region (empirically verified in our experiment).

To estimate the size of the soot particles, we multiplied their respective diffraction patterns by band-pass filters of the form $q^4\exp(-(q-q_0)^4)$, where the spatial frequency q_0 was optimized from pattern to pattern to reduce the effects of missing data and high-frequency measurement noise, and to isolate each particle's high-frequency features. The Fourier transforms of the results were calculated to obtain a visual estimate of each particle's autocorrelation support from these high-frequency features[31], which was halved to estimate each particle's length. Among our 174 diffraction patterns, we found 17 particles whose longest diameters were at least 1 μm. As the densities of mass fractals decrease with increasing particle size, these large soot particles were still expected to satisfy the Born scattering approximation. Our maximum scattering angle was approximately 4.3°, meaning that our intensities sampled a mildly curved Ewald sphere section, which was accounted for in averaging of $I(q)$.

Received 16 September 2011; accepted 9 May 2012.

1. Zereini, F. & Wiseman, C. L. S. *Urban Airborne Particulate Matter* (Springer, 2010).
2. Jacobson, M. Z. Strong radiative heating due to the mixing state of black carbon in atmospheric aerosols. *Nature* **409,** 695–697 (2001).
3. Wentzel, M. *et al.* Transmission electron microscopical and aerosol dynamical characterization of soot aerosols. *J. Aerosol Sci.* **34,** 1347–1370 (2003).
4. Berg, M. J. *et al.* Two-dimensional Guinier analysis: application of single aerosol particles in-flight. *Opt. Express* **18,** 23343–23352 (2010).

5. Braun, A. *et al.* X-ray scattering and spectroscopy studies on diesel soot from oxygenated fuel under various engine load conditions. *Carbon* **43,** 2588–2599 (2005).
6. Emma, P. *et al.* First lasing and operation of an angstrom-wavelength free-electron laser. *Nature Photon.* **4,** 641–647 (2010).
7. Balafas, J. S. & Dewey, T. G. Multifractal analysis of solvent accessibilities in proteins. *Phys. Rev. E* **52,** 880–887 (1995).
8. Granek, R. Proteins as fractals: role of the hydrodynamic interaction. *Phys. Rev. E* **83,** 020902(R) (2011).
9. Beaucage, G. *et al.* Probing the dynamics of nanoparticle growth in a flame using synchrotron radiation. *Nature Mater.* **3,** 370–373 (2004).
10. Ramanathan, V. & Carmichael, G. Global and regional climate changes due to black carbon. *Nature Geosci.* **1,** 221–227 (2008).
11. Sorensen, C. M. Light scattering by fractal aggregates: a review. *Aerosol Sci. Technol.* **35,** 648–687 (2001).
12. Nelson, J. Test of a mean field theory for the optics of fractal clusters. *J. Mod. Opt.* **36,** 1031–1057 (1989).
13. Moffet, R. C. & Prather, K. A. In situ measurements of the mixing state and optical properties of soot with implications for radiative forcing estimates. *Proc. Natl Acad. Sci. USA* **106,** 11872–11877 (2009).
14. Zhang, R. *et al.* Variability in morphology, hygroscopicity, and optical properties of soot aerosols during atmospheric processing. *Proc. Natl Acad. Sci. USA* **105,** 10291–10296 (2008).
15. Nelson, J. Fractality of soot smoke: implications for the severity of nuclear winter. *Nature* **339,** 611–613 (1989).
16. Jacobson, M. Z. Effects of externally-through-internally-mixed soot inclusions within clouds and precipitation on global climate. *J. Phys. Chem. A* **110,** 6860–6873 (2006).
17. Dhaubhadel, R. *et al.* Hybrid superaggregate morphology as a result of aggregation in a cluster-dense aerosol. *Phys. Rev. E* **75,** 011404 (2006).
18. Puri, R. *et al.* Aerosol dynamic processes of soot aggregates in a laminar ethene diffusion flame. *Combust. Flame* **92,** 320–333 (1993).
19. Strüder, L. *et al.* Large-format, high-speed, X-ray pnCCDs combined with electron and ion imaging spectrometers in a multipurpose chamber for experiments at 4th generation light sources. *Nucl. Instr. Meth. A* **614,** 483–496 (2010).
20. Bozek, J. D. AMO instrumentation for the LCLS x-ray FEL. *Eur. Phys. J. Spec. Top.* **169,** 129–132 (2009).
21. Bogan, M. J. *et al.* Aerosol imaging with a soft x-ray free electron laser. *Aerosol Sci. Technol.* 44, i–vi (2010).
22. Seibert, M. M. *et al.* Single mimivirus particles intercepted and imaged with an x-ray laser. *Nature* **470,** 78–81 (2011).
23. Bogan, M. J. *et al.* Single-particle coherent diffractive imaging with a soft x-ray free electron laser: towards soot aerosol morphology. *J. Phys. B* **43,** 194013 (2010).
24. Bogan, M. J. *et al.* Single-shot femtosecond x-ray diffraction from randomly oriented ellipsoidal nanoparticles. *Phys. Rev. Spec. Topics* **13,** 094701 (2010).
25. Bogan, M. J. *et al.* Single particle x-ray diffractive imaging. *Nano Lett.* **8,** 310–316 (2008).
26. Cho, Y.-S. *et al.* Complex colloidal microclusters from aerosol droplets. *Langmuir* **23,** 12079–12085 (2007).
27. Martin, J. E. & Hurd, A. J. Scattering from fractals. *J. Appl. Cryst.* **20,** 61–78 (1987).
28. Meakin, P. Fractal aggregates. *Adv. Colloid Interf. Sci.* **28,** 249–331 (1988).
29. Luke, D. R. Relaxed averaged alternating reflections for diffraction imaging. *Inverse Probl.* **21,** 37–50 (2005).
30. Marchesini, S. *et al.* X-ray image reconstruction from a diffraction pattern alone. *Phys. Rev. B* **68,** 140101(R) (2003).
31. Fienup, J. R. *et al.* Reconstruction of the support of an object from the support of its autocorrelation. *J. Opt. Soc. Am.* **72,** 610–624 (1982).

Supplementary Information is linked to the online version of the paper at www.nature.com/nature.

Acknowledgements Experiments were carried out at the Linac Coherent Light Source, a national user facility operated by Stanford University on behalf of the US Department of Energy (DOE), Office of Basic Energy Sciences. N.D.L., C.Y.H., R.G.S., P.B. and M.J.B. were supported by the AMOS program within the Chemical Sciences, Geosciences, and Biosciences Division of the Office of Basic Energy Sciences, Office of Science, US Department of Energy. M.J.B. acknowledges support by the SLAC Laboratory Directed Research and Development Program. We acknowledge support from the Max Planck Society for funding the development and operation of the CAMP instrument within the ASG at CFEL, the Hamburg Ministry of Science and Research and Joachim Herz Stiftung as part of the Hamburg Initiative for Excellence in Research (LEXI) and the Hamburg School for Structure and Dynamics in Infection, CBST at UC under Cooperative Agreement number PHY 01120999. Lawrence Livermore National Laboratory (LLNL) is operated by Lawrence Livermore National Security, LLC, for the US Department of Energy, National Nuclear Security Administration under Contract DE-AC52-07NA27344. Work by LLNL has been supported, in part, by University of California Laboratory Fee grant 09-LR-05-118036-BARA. We also acknowledge support from the Swedish Research Council, the European Research Council, Knut och Alice Wallenbergs Stiftelse, and the DFG Cluster of Excellence at the Munich Centre for Advanced Photonics. We acknowledge the staff of the LCLS for their support in carrying out these experiments. The Max Planck Advanced Study Group at CFEL acknowledges technical support by R. Andritschke, K. Gärtner, O. Hälker, S. Herrmann, A. Hömke, Ch. Kaiser, K.-U. Kühnel, W. Leitenberger, D. Miessner, D. Pietschner, M. Porro, R. Richter, G. Schaller, C. Schmidt, F. Schopper, C.-D. Schröter, Ch. Thamm, A. Walenta, A. Ziegler and H. Gorke. N.D.L. thanks M. J. Berg, G. Simpson, G. Williams and J. Hajdu for their critique, and G. M. Stewart for rendering the experiment's schematic.

Author Contributions M.J.B. conceived the soot and soot/salt imaging experiments. M.J.B., C.Y.H., D.S., H.N.C., I.S., A.B., W.H.B., S.P.H.-R., S.M., S.B. and M.F. conceived the sphere/nanoparticle imaging experiments. D.S., N.D.L. and M.J.B conceived the fractal dimension determination. C.B. and J.B. built and managed the AMO beamline at LCLS, where the experiments were performed. C.Y.H., A.V.M., D.S., R.G.S., A.B., A.A., J.S., L.L., R.L.S., S.K., S.W.E., B.E., R.H., D.R., A.R., B.R., L.F., N.K., G.W., G.H., P.H., E.P., M.L., M.S.H., L.G., N.C., C.W., H.G., H.F., H.H., K.N., H.J.T., G.R.F., S.B., M.B., L.S., J.U., P.B. and K.O.H. were responsible for critical preparation leading up to and immediately after the experiment. C.Y.H., L.L., R.L.S., R.G.S., M.L., E.P., H.J.T. and M.J.B. were responsible for sample delivery. A.R., B.R., D.R. and L.F. developed and operated the mass spectrometer. M.L. took the electron micrographs (Supplementary Figs 2 and 3). M.J.B. and R.G.S. characterized and operated the MOUDI particle filter. The CAMP instrument was the responsibility of S.W.E., R.H., D.R., A.R., L.F., N.K., P.H., B.R., B.E., A.H., C.R., G.W., G.H., H.H., C.W., H.G., H.S., J.U., I.S. and L.S., who jointly designed and set up the instrument and/or developed and operated the pnCCD detectors. Efforts to calibrate, align the imaging apparatus and collect data were shared among C.Y.H., D.S., R.G.S., A.B., A.A., J.S., L.L., R.L.S., S.K., C.B., J.B., S.W.E., B.E., R.H., D.R., A.R., B.R., L.F., E.P., M.L., L.G., N.C., H.H., K.N., H.J.T., J.U., M.F., I.S., H.N.C. and M.J.B.. S.K., A.B., K.N. and A.V.M. provided crucial preliminary analysis of the data during the experiment. A.B., A.V.M., A.A. and S.K. processed and analysed the raw data, using software developed by L.F., S.K., A.B., T.A.W. and F.R.N.C.M.. M.J.B., N.D.L., D.S., C.Y.H., A.V.M., A.B., A.A., L.L., J.S., F.R.N.C.M., T.E. and M.H. developed the ideas for analyses. A.V.M. did the phase retrieval reconstructions. N.D.L. and D.S. contributed equally to the fractal morphology and calibration. N.D.L., M.J.B., D.S., A.B., A.V.M., D.R. and I.S. wrote the paper, with input from all co-authors.

Author Information Reprints and permissions information is available at www.nature.com/reprints. The authors declare no competing financial interests. Readers are welcome to comment on the online version of this article at www.nature.com/nature. Correspondence and requests for materials should be addressed to N.D.L. (duaneloh@slac.stanford.edu) or M.J.B. (mbogan@slac.stanford.edu).

LETTER

doi:10.1038/nature11158

Activation of remote *meta*-C–H bonds assisted by an end-on template

Dasheng Leow[1]*, Gang Li[1]*, Tian-Sheng Mei[1] & Jin-Quan Yu[1]

Functionalization of unactivated carbon–hydrogen (C–H) single bonds is an efficient strategy for rapid generation of complex molecules from simpler ones. However, it is difficult to achieve selectivity when multiple inequivalent C–H bonds are present in the target molecule. The usual approach is to use *σ*-chelating directing groups, which lead to *ortho*-selectivity through the formation of a conformationally rigid six- or seven-membered cyclic pre-transition state[1–14]. Despite the broad utility of this approach, proximity-driven reactivity prevents the activation of remote C–H bonds. Here we report a class of easily removable nitrile-containing templates that direct the activation of distal *meta*-C–H bonds (more than ten bonds away) of a tethered arene. We attribute this new mode of C–H activation to a weak 'end-on' interaction[15] between the linear nitrile group and the metal centre. The 'end-on' coordination geometry relieves the strain of the cyclophane-like pre-transition state of the *meta*-C–H activation event. In addition, this template overrides the intrinsic electronic and steric biases as well as *ortho*-directing effects with two broadly useful classes of arene substrates (toluene derivatives and hydrocinnamic acids).

The development of new transformations in which inert C–H bonds react as dormant functional groups holds great promise for expediting organic synthesis by providing unprecedented retrosynthetic disconnections. In this endeavour, controlling the positional selectivity of C–H cleavage in molecules that contain multiple C–H bonds is an outstanding challenge that must be addressed before widespread synthetic applications. Currently, *σ*-chelation-directed metalation of C–H bonds has been used as a powerful means of achieving *ortho*-selectivity[1–6]. Diverse carbon–carbon and carbon–heteroatom bond-forming reactions with broadly useful substrates have recently been developed using Pd(II)[7–9], Rh(III)[10–13], and Ru(II)[14] catalysts. In directed C–H activation, assembly of a conformationally rigid cyclic pre-transition state is required (**I** in Fig. 1a), which introduces two inherent limitations. First, despite extensive and innovative efforts towards remote C–H functionalization reactions[15–18], the difficulties associated with forming a macrocyclic pre-transition state larger than a seven-membered ring generally preclude the activation of remote C–H bonds. Second, the high energy associated with well-defined cyclophane-like pre-transition states prevents *meta*- or *para*-selective C–H activation reactions (**II** in Fig. 1a). Although significant progress has been made in the development of *meta*- and *para*-selective C–H functionalization reactions[19–27], the positional selectivity is largely governed by steric (1,3-substituted arenes)[19,20], or electronically biased (mono-substituted arenes)[20–25] properties of the arene substrates. A generally applicable approach for remote *meta*-C–H activation that controls positional selectivity by overriding the intrinsic electronic

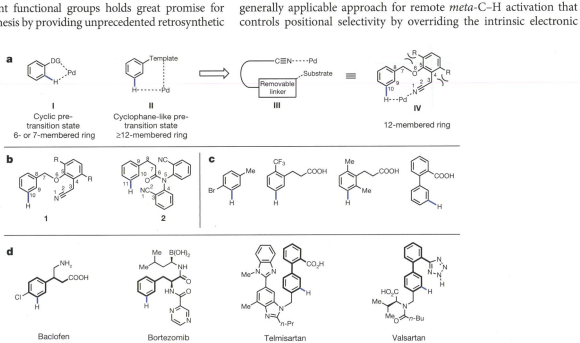

Figure 1 | A template strategy for the activation of distal *meta*-C–H bonds (more than ten bonds away). a, Remote *meta*-C–H activation is a challenge. I: *ortho*-directed C–H activation. DG, directing group. II, III and IV: Remote *meta*-C–H activation using an 'end-on' template. The dotted blue lines divide the arene template into four quadrants. The blue bonds in all figures highlight the targeted C–H bonds. **b**, Templates for toluenes and hydrocinnamic acids. **c**, Unprecedented positional selectivity in C–H activation, overriding electronic and steric biases, and *ortho*-directing effects.. **d**, Structurally related drug molecules (brand names in parentheses).

[1]Department of Chemistry, The Scripps Research Institute, 10550 North Torrey Pines Road, La Jolla, California 92037, USA.
*These authors contributed equally to this work.

and steric properties of arene substrates, especially mono-substituted arenes, has remained a challenge.

Here we report the discovery of a class of nitrile-containing templates that deliver palladium to the vicinity of tethered arene substrates to promote C–H olefination of distal *meta*-C–H bonds with excellent selectivity (Fig. 1). This linear 'end-on' coordinating nitrile group[15] is proposed to accommodate a macrocyclic cyclophane-like pre-transition state, thus overcoming the inherent limitations of traditional directed C–H activation. We demonstrate the generality of this template approach with two categorically different classes of substrates (toluene and hydrocinnamic acid derivatives **1** and **2**) (Fig. 1b). Remarkably, the template overrides the intrinsic electronic and steric biases as well as *ortho*-directing effects of the arene substrates, consistently securing high *meta*-selectivity in most cases (Fig. 1c). This *meta*-selective C–H olefination reaction is also compatible with *ortho*,*ortho*-disubstituted arene and 2-biphenylcarboxylic acid substrates. Both hydrocinnamic and 2-biphenylcarboxylic acids are key structural motifs in many drug molecules, including the $GABA_B$ receptor agonist drug Baclofen (Fig. 1d).

Considering that the major limitations of directed C–H activation arise from the stringent requirement of assembling a rigid cyclic pre-transition state, we began to devise a removable chelating template that would recruit the Pd(II) catalyst through a less rigid assembly involving reversible weak coordination. We suspected that the weakly binding end-on nitrile group would either make the cyclophane-like pre-transition state less strained or would lead to release of the Pd(II) catalyst in the vicinity of the target C–H bond, thereby providing high effective concentration (**III** in Fig. 1a). The latter 'catch and release' scenario would obviate the need to assemble a cyclophane-like pre-transition state all together. Although weak coordination is not as effective as strong coordination in terms of compensating for the entropic cost during the assembly of the pre-transition state, the nitrile-bound Pd(II) centre is more reactive because it is highly electrophilic, which is beneficial for C–H activation. We also anticipated that the linear coordination mode of the nitrile group would be more likely to anchor the palladium to the *meta* position rather than the *ortho* position. In this putative structure, the interaction with the *ortho*-C–H bond would incur high levels of cyclophane ring strain caused by the linear geometry of the nitrile group. Encouragingly, Schwarz's pioneering studies showed that this mode of end-on coordination of alkyl nitriles with Fe(II) in the gas phase can guide the metal to perform remote C–H activation[15].

To put this hypothesis into practice, we engineered a nitrile-containing template in which the substrate was attached through a removable benzyl ether linkage (**IV** in Fig. 1a). At the outset, we hypothesized that the flat arene would help to keep the substrate moiety and nitrile group as coplanar as possible. Given that the plane in which the arene template lies could be spatially divided into four distinct quadrants (see **IV** in Fig. 1a), we further hypothesized that sterically bulky *tert*-butyl groups at the *ortho* positions of the arene template could serve as blocking groups to ensure that the pendant substrate and the nitrile group were kept in the same quadrant to achieve high effective concentration of the Pd(II) catalyst. In our first design, we used a nitrile-containing phenol as the template, which could easily be attached to benzyl bromide to give benzyl ether **3** as the model substrate for testing *meta*-selective C–H activation (Table 1).

Using olefination of **3** as the model reaction[28,29], we extensively screened catalysts, oxidants and solvents (see Supplementary Information) and found that a combination of $Pd(OPiv)_2$ as the catalyst and AgOPiv as the oxidant gave a 15% yield with encouraging levels of *meta*-selectivity (*m*:*p*:*o* = 59:33:8) (Table 1, entries 1–3). To improve the reactivity further via the Thorpe–Ingold effect, we installed two alkyl groups at the α-position adjacent to the nitrile group. Both the yield and the *meta*-selectivity steadily improved with increasing size of the alkyl groups (entries 4–8). The isobutyl-substituted template gave a

Table 1 | Optimization of template

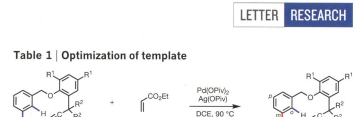

3–10 **11a** **12–19**

Entry	Substrate	R^1	R^2	Yield (%) (mono)	Yield (%) (di)	Selectivity (*meta*:*para*:*ortho*)
1	**3**	*tert*-butyl	H	Trace	0	—
2	**3**	*tert*-butyl	H	4	0	56:26:18
3	**3**	*tert*-butyl	H	15	0	59:33:8
4	**4**	*tert*-butyl	Methyl	60	17	91:7:2
5	**5**	*tert*-butyl	Ethyl	52	16	93:6:1
6	**6**	*tert*-butyl	$-(CH_2)_4-$	50	11	88:7:5
7	**7**	*tert*-butyl	$-(CH_2)_5-$	51	15	91:5:4
8	**8a**	*tert*-butyl	Isobutyl	63	20	95:4:1
9	**9**	H	Isobutyl	—	—	—
10	**10**	Methyl	Isobutyl	39	10	91:8:1

The reaction scheme is shown above the table. Unless otherwise noted, the reaction conditions were as follows: benzyl ethers **3**–**10** (0.05 mmol), olefin **11a** (1.5 equiv.), $Pd(t\text{-}Bu\text{-}val)_2$ (10 mol%), Ag-pivalate (2.1 equiv.), 1,2-dichloroethane (0.5 ml), 90 °C, 18 h. The isolated yield was obtained by silica gel column chromatography. The ratio of *meta*:*para*:*ortho* mono-olefinated products was determined by ^1H NMR analysis of the unpurified reaction mixture; the variance is estimated to be within 5%. For entry 1, O_2 was used as the oxidant instead of Ag-pivalate. For entry 2, $Pd(OAc)_2$ and AgOAc were used instead of $Pd(OPiv)_2$ and AgOPiv respectively and NMR yield was determined by using *o*-xylene as an internal standard. For entry 9, C–H olefination occurred on both the arene substrate and template with a combined yield of approximately 20% yield.

mixture of mono- and di-olefinated products $\mathbf{17a}_{mono}$ and $\mathbf{17a}_{di}$ in 83% combined yield (entry 8). The mono- and di-olefinated products can be readily separated by chromatography. Importantly, the *meta*-selectivity was found to be 95%. We also confirmed through control experiments that the presence of the bulky *tert*-butyl blocking groups on the template was essential for reactivity (entries 9, 10). Replacement of the nitrile by a methyl group also resulted in complete loss of reactivity and selectivity (see Supplementary Information).

With this newly established *meta*-selective C–H olefination procedure in hand, we carried out olefination on a variety of substituted arenes (Fig. 2). *Meta*-substituted arenes were olefinated at the remaining *meta* position with excellent selectivity regardless of the electronic properties of the substituents (**17b**–**g**). With *ortho*-substituted arene substrates, high *meta*-selectivity was also achieved with both an electron-donating methyl group and electron-withdrawing fluoro and bromo groups (**17h**–**j**). Notably, in the absence of the template, the *para*- and *meta*-C–H bonds of these 1,2-substituted arene substrates are often difficult to distinguish, yet the template directed *meta*-C–H activation with high selectivity. For example, *meta*-selective olefination places the newly installed functional group at the position *para* to the bromo group, which is synthetically enabling owing to the diverse reactivities of the bromo group (**17j**). Despite the steric hindrance, *para*-substituted arenes are also olefinated at the *meta*-position in excellent selectivity (**17k**–**n**). In sharp contrast to previously reported *meta*-selective C–H functionalization reactions[21], the template also effectively overrides the electronic effect of bromide or ester groups at the *para* position, affording predominantly the *meta*-olefinated products (**17m**, **17n**). Intriguingly, the template can guide the catalyst to reach and activate the *meta*-C–H bond in a selective manner in the presence of *ortho*,*ortho*-di-fluoro substitution (**17o**). *Meta*-C–H functionalization of *ortho*,*ortho*-disubstituted arenes provides a powerful disconnection for constructing 1,2,3,4-tetrasubstituted arenes. Finally, *meta*-C–H olefination of naphthalene **8p** also proceeded to give **17p** in 79% yield.

We next extensively surveyed the scope of the olefin coupling partners. Olefination with commonly used electron-deficient α,β-unsaturated esters, ketones and phosphonates gave desired products in good yields (**17b$_2$**–**b$_5$**). Given that the lack of reactivity with disubstituted olefins in directed C–H olefination reactions is a significant drawback[28,29], we tested a series of di- or tri-substituted olefins. We were pleased to find that olefination with all of these olefins proceeded

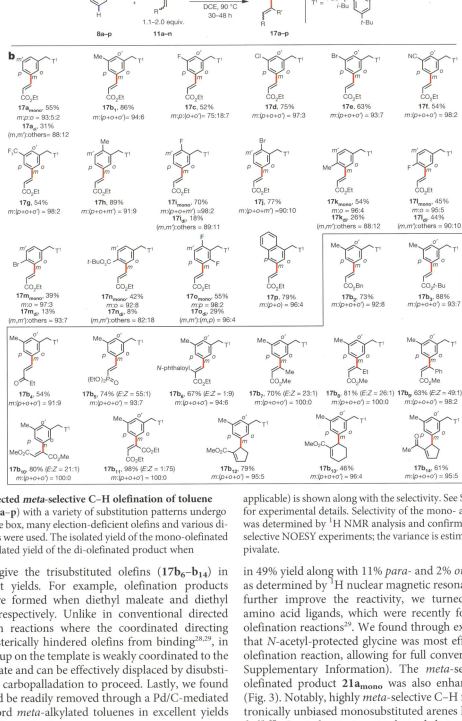

Figure 2 | Template-directed *meta*-selective C–H olefination of toluene derivatives. a, Arenes (**8a–p**) with a variety of substitution patterns undergo facile olefination. **b**, In the box, many electron-deficient olefins and various di- and tri-substituted olefins were used. The isolated yield of the mono-olefinated product (and also the isolated yield of the di-olefinated product when applicable) is shown along with the selectivity. See Supplementary Information for experimental details. Selectivity of the mono- and di-olefinated products was determined by ^{1}H NMR analysis and confirmed by one-dimensional selective NOESY experiments; the variance is estimated to be within 5%. OPiv, pivalate.

stereoselectively[30] to give the trisubstituted olefins (**17b$_6$–b$_{14}$**) in moderate to excellent yields. For example, olefination products **17b$_{10}$** and **17b$_{11}$** were formed when diethyl maleate and diethyl fumarate were used respectively. Unlike in conventional directed *ortho*-C–H olefination reactions where the coordinated directing group could prevent sterically hindered olefins from binding[28,29], in this case the nitrile group on the template is weakly coordinated to the [Pd(II)–Ar] intermediate and can be effectively displaced by disubstituted olefins, allowing carbopalladation to proceed. Lastly, we found that the template could be readily removed through a Pd/C-mediated hydrogenolysis to afford *meta*-alkylated toluenes in excellent yields (see Supplementary Information).

Having demonstrated the concept of using a nitrile-containing end-on template to activate *meta*-C–H bonds that are ten bonds away from the chelating atom, we tested whether this approach would be generally applicable to other broadly useful substrates, after appropriate tuning of the template. Therefore, we used a readily cleavable amide linkage to attach a benzonitrile template to hydrocinnamic acid to form **20a**. Using the established olefination protocol from above (Fig. 2), we screened various reaction parameters with substrate **20a** and observed significant solvent effects, presumably owing to the dramatic influence of the solvent medium on the assembly of the pre-transition state via weak coordination (see Supplementary Information). Olefination of **20a** in hexafluoroisopropanol gave *meta*-olefinated product **21a$_{mono}$** in 49% yield along with 11% *para*- and 2% *ortho*-olefinated products, as determined by ^{1}H nuclear magnetic resonance (NMR) analysis. To further improve the reactivity, we turned to mono-*N*-protected amino acid ligands, which were recently found to accelerate C–H olefination reactions[29]. We found through extensive ligand screening that *N*-acetyl-protected glycine was most effective in promoting the olefination reaction, allowing for full conversion to be achieved (see Supplementary Information). The *meta*-selectivity of the mono-olefinated product **21a$_{mono}$** was also enhanced from 79% to 95% (Fig. 3). Notably, highly *meta*-selective C–H functionalization of electronically unbiased monosubstituted arenes has not been reported so far[19–27]. Control experiments showed that replacement of the nitrile group on the template with a trifluoromethyl group resulted in poor reactivity and selectivity giving a *m*:*p*:*o* 1:1:2 mixture of mono-olefinated products in 38% yield under the optimized conditions.

The efficiency of this template was first demonstrated by the excellent observed reactivity with the electron-deficient *meta*-trifluoromethylarene **20b**. To showcase the power of the template in controlling the *meta*-selectivity, *meta*-methoxy and *ortho*-trifluoromethyl groups were introduced onto the aromatic rings (**20c** and **20d** respectively), two functional groups known to exert strong electronic effects on traditional electrophilic aromatic substitution reactions. Remarkably, excellent *meta*-selectivity was maintained in the olefination of both *meta*-methoxyarene **20c** and *ortho*-trifluoromethylarene **20d** to give **21c**

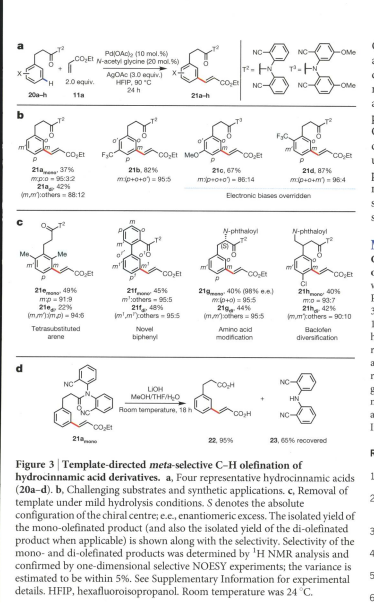

Figure 3 | Template-directed *meta*-selective C–H olefination of hydrocinnamic acid derivatives. **a**, Four representative hydrocinnamic acids (**20a–d**). **b**, Challenging substrates and synthetic applications. **c**, Removal of template under mild hydrolysis conditions. *S* denotes the absolute configuration of the chiral centre; e.e., enantiomeric excess. The isolated yield of the mono-olefinated product (and also the isolated yield of the di-olefinated product when applicable) is shown along with the selectivity. Selectivity of the mono- and di-olefinated products was determined by ^{1}H NMR analysis and confirmed by one-dimensional selective NOESY experiments; the variance is estimated to be within 5%. See Supplementary Information for experimental details. HFIP, hexafluoroisopropanol. Room temperature was 24 °C.

and **21d** respectively, suggesting that the template effectively overrides the electronic effects of both electron-donating and -withdrawing groups. To further demonstrate the potential synthetic applications of this method, we first constructed a sterically encumbered tetrasubstituted arene **21e** via *meta*-selective olefination of the *ortho*,*ortho*-dimethylarene **20e**, in which case the steric hindrance was overcome by the template. Intriguingly, *meta*-selective C–H olefination of biphenyl substrate (**20f**) also proceeded at the remote aryl ring to afford synthetically useful biphenyl **21f** with unprecedented site-selectivity. Importantly, the unnatural chiral amino acid **21g** was also prepared via *meta*-selective olefination of *N*-phthaloyl-protected phenylalanine **20g** without racemization. Both 2-biphenylcarboxylic acid (**20f**) and phenylalanine (**20g**) are key structural motifs in drug molecules such as Micardis and Velcade. Finally, *N*-phthaloyl-protected Baclofen (**20h**) was selectively olefinated at the *meta*-position to give **21h** in 82% yield, providing access to a novel library of molecules of medicinal interest. The reactivity and selectivity patterns observed with **20a–h** have not been reported in previous studies towards *meta*-selective C–H activation[19–21]. To establish scalability, the reaction of **20d** was also run at the 0.5 g (1.2 mmol) scale to give **21d** in 77% yield. The removal of the template in **21a$_{meta}$** was readily accomplished by hydrolysis at room temperature using LiOH as a base to give diacid **22** in 95% yield (Fig. 3).

In summary, we have developed a template approach to activate remote *meta*-C–H bonds of two categorically distinct classes of substrates with high *meta*-selectivity. Template-assisted *meta*-selective C–H activation overrides *ortho*-directing effects as well as electronic and steric biases on the appended arene substrates. The template design is predicated on the weak interaction between Pd(II) and a nitrile group, where the nitrile group coordinates in an end-on fashion and can overcome the difficulties associated with assembling a cyclophane-like pre-transition state. This new strategy for directing remote C–H activation provides a novel route for the preparation of toluene derivatives, hydrocinnamic acids, 2-biphenylcarboxylic acids, unnatural amino acids, and drug molecules with sophisticated substitution patterns that are difficult to access using conventional C–H activation methods. We expect that this end-on nitrile-based template can be structurally modified to suit other classes of synthetically useful arene substrates.

METHODS SUMMARY

General procedure for template-directed *meta*-selective C–H olefination of toluene derivatives. A 15-ml sealed tube (with a Teflon cap) equipped with a magnetic stir bar was charged with substrate (46.1 mg, 0.10 mmol), $Pd(OPiv)_2$ (3.0 mg, 0.010 mmol, 0.10 equiv.), and AgOPiv (62.7 mg, 0.30 mmol, 3.0 equiv.). Ethyl acrylate (16.5 μl, 0.15 mmol, 1.5 equiv.) was added, followed by 1,2-dichloroethane (1.0 ml). The tube was then capped and submerged into a preheated 90 °C oil bath. The reaction was stirred for a total of 42 h and cooled to room temperature. The crude reaction mixture was filtered through a pad of Celite and washed with Et_2O (2 ml × 3). The filtrate was concentrated *in vacuo*, and the resulting residue was purified by column or preparative thin layer chromatography using hexanes/EtOAc as the eluent. The positional selectivity was determined by ^{1}H NMR of the unpurified reaction mixture. Full experimental details and characterization of new compounds can be found in the Supplementary Information.

Received 13 February; accepted 20 April 2012.

1. Hartung, C. G. & Snieckus, V. in *Modern Arene Chemistry* (ed. Astruc, D.) 330–367 (Wiley, 2004).
2. Flemming, J. P., Berry, M. B. & Brown, J. M. Sequential *ortho*-lithiations; the sulfoxide group as a relay to enable *meta*-substitution. *Org. Biomol. Chem.* **6,** 1215–1221 (2008).
3. Ryabov, A. D. Cyclopalladated complexes in organic synthesis. *Synthesis* 233–252 (1985).
4. Kakiuchi, *F. et al.* Catalytic addition of aromatic carbon–hydrogen bonds to olefins with the aid of ruthenium complexes. *Bull. Chem. Soc. Jpn* **68,** 62–83 (1995).
5. Jun, C.-H., Hong, J.-B. & Lee, D.-Y. Chelation-assisted hydroacylation. *Synlett* 1–12 (1999).
6. Colby, D. A., Bergman, R. G. & Ellman, J. A. Rhodium-catalyzed C–C bond formation via heteroatom-directed C–H bond activation. *Chem. Rev.* **110,** 624–655 (2010).
7. Dauguilis, D., Do, H.-Q. & Shabashov, D. Palladium- and copper-catalyzed arylation of carbon–hydrogen bonds. *Acc. Chem. Res.* **42,** 1074–1086 (2009).
8. Lyons, T. W. & Sanford, M. S. Palladium-catalyzed ligand-directed C–H functionalization reactions. *Chem. Rev.* **110,** 1147–1169 (2010).
9. Engle, K. M., Mei, T.-S., Wasa, M. & Yu, J.-Q. Weak coordination as a powerful means for developing broadly useful C–H functionalization reactions. *Acc. Chem. Res.*, (2011).
10. Satoh, T. & Miura, M. Oxidative coupling of aromatic substrates with alkynes and alkenes under rhodium catalysis. *Chem. Eur. J.* **16,** 11212–11222 (2010).
11. Guimond, N., Gorelsky, S. I. & Fagnou, K. Rhodium(III)-catalyzed heterocycle synthesis using an internal oxidant: improved reactivity and mechanistic studies. *J. Am. Chem. Soc.* **133,** 6449–6457 (2011).
12. Rakshit, S., Grohmann, C., Besset, T. & Glorius, F. Rh(III)-catalyzed directed C–H olefination using an oxidizing directing group: mild, efficient, and versatile. *J. Am. Chem. Soc.* **133,** 2350–2353 (2011).
13. Park, S. H., Kim, J. Y. & Chang, S. Rhodium-catalyzed selective olefination of arene esters via C–H bond activation. *Org. Lett.* **13,** 2372–2375 (2011).
14. Ackermann, L. & Pospech, J. Ruthenium-catalyzed oxidative C–H bond alkenylations in water: expedient synthesis of annulated lactones. *Org. Lett.* **13,** 4153–4155 (2011).
15. Schwarz, H. Remote functionalization of C–H and C–C bonds by naked transition-metal ions (*cosi fan tutte*). *Acc. Chem. Res.* **22,** 282–287 (1989).
16. Breslow, R. Biomimetic control of chemical selectivity. *Acc. Chem. Res.* **13,** 170–177 (1980).
17. Das, S., Incarvito, C. D., Crabtree, R. H. & Brudvig, G. W. Molecular recognition in the selective oxygenation of saturated C–H bonds by a dimanganese catalyst. *Science* **312,** 1941–1943 (2006).
18. Li, J.-J., Giri, R. & Yu, J.-Q. Remote C–H bond functionalization reveals the distance-dependent isotope effect. *Tetrahedron* **64,** 6979–6987 (2008).
19. Cho, J.-Y., Tse, M. K., Holmes, D., Maleczka, R. E. Jr & Smith, M. R. III. Remarkably selective iridium catalysts for the elaboration of aromatic C–H bonds. *Science* **295,** 305–308 (2002).

20. Ishiyama, T. *et al.* Mild iridium-catalyzed borylation of arenes. High turnover numbers, room temperature reactions, and isolation of a potential intermediate. *J. Am. Chem. Soc.* **124,** 390–391 (2002).
21. Zhang, Y.-H., Shi, B.-F. & Yu, J.-Q. Pd(II)-catalyzed olefination of electron-deficient arenes using 2,6-dialkylpyridine ligands. *J. Am. Chem. Soc.* **131,** 5072–5074 (2009).
22. Wang, X., Leow, D. & Yu, J.-Q. Pd(II)-catalyzed *para*-selective C–H arylation of monosubstituted arenes. *J. Am. Chem. Soc.* **133,** 13864–13867 (2011).
23. Ueda, K., Yanagisawa, S., Yamaguchi, J. & Itami, K. A general catalyst for the *β*-selective C–H bond arylation of thiophenes with iodoarenes. *Angew. Chem. Int. Edn* **49,** 8946–8949 (2010).
24. Ye, M., Gao, G.-L. & Yu, J.-Q. Ligand-promoted C-3 selective C–H olefination of pyridines with Pd catalysts. *J. Am. Chem. Soc.* **133,** 6964–6967 (2011).
25. Saidi, O. *et al.* Ruthenium-catalyzed *meta*-sulfonation of 2-phenylpyridines. *J. Am. Chem. Soc.* **133,** 19298–19301 (2011).
26. Phipps, R. J. & Gaunt, M. J. A *meta*-selective copper-catalyzed C–H bond arylation. *Science* **323,** 1593–1597 (2009).
27. Duong, H. A., Gilligan, R. E., Cooke, M. L., Phipps, R. J. & Gaunt, M. J. Copper(II)-catalyzed *meta*-selective direct arylation of α-aryl carbonyl compounds. *Angew. Chem. Int. Edn* **50,** 463–466 (2011).
28. Boele, M. D. K. *et al.* Selective Pd-catalyzed oxidative coupling of anilides with olefins through C–H bond activation at room temperature. *J. Am. Chem. Soc.* **124,** 1586–1587 (2002).
29. Wang, D.-H., Engle, K. M., Shi, B.-F. & Yu, J.-Q. Ligand-enabled reactivity and selectivity in a synthetically versatile aryl C–H olefination. *Science* **327,** 315–319 (2010).
30. Gürtler, C. & Buchwald, S. L. A phosphane-free catalyst system for the Heck arylation of disubstituted alkenes: application to the synthesis of trisubstituted olefins. *Chem. Eur. J.* **5,** 3107–3112 (1999).

Supplementary Information is linked to the online version of the paper at www.nature.com/nature.

Acknowledgements We thank The Scripps Research Institute and the NIH (NIGMS, 1 R01 GM084019-03) for their financial support. We also thank the Agency for Science, Technology and Research (A*STAR) in Singapore for a postdoctoral fellowship (to D.L.).

Author Contributions D.L., G.L. and T.-S.M. performed the experiments and analysed the data. D.L., G.L. and J.-Q.Y. designed the templates and developed the reactions. J.-Q.Y. conceived this concept and prepared this manuscript with feedback from D.L. and G.L.

Author Information Reprints and permissions information is available at www.nature.com/reprints. The authors declare no competing financial interests. Readers are welcome to comment on the online version of this article at www.nature.com/nature. Correspondence and requests for materials should be addressed to J.-Q.Y. (yu200@scripps.edu).

LETTER

doi:10.1038/nature11124

Three-dimensional limb joint mobility in the early tetrapod *Ichthyostega*

Stephanie E. Pierce[1,2], Jennifer A. Clack[2] & John R. Hutchinson[1]

The origin of tetrapods and the transition from swimming to walking was a pivotal step in the evolution and diversification of terrestrial vertebrates. During this time, modifications of the limbs—particularly the specialization of joints and the structures that guide their motions—fundamentally changed the ways in which early tetrapods could move[1–4]. Nonetheless, little is known about the functional consequences of limb anatomy in early tetrapods and how that anatomy influenced locomotion capabilities at this very critical stage in vertebrate evolution. Here we present a three-dimensional reconstruction of the iconic Devonian tetrapod *Ichthyostega* and a quantitative and comparative analysis of limb mobility in this early tetrapod. We show that *Ichthyostega* could not have employed typical tetrapod locomotory behaviours, such as lateral sequence walking. In particular, it lacked the necessary rotary motions in its limbs to push the body off the ground and move the limbs in an alternating sequence. Given that long-axis rotation was present in the fins of tetrapodomorph fishes[5–7], it seems that either early tetrapods evolved through an initial stage of restricted shoulder[8,9] and hip joint mobility or that *Ichthyostega* was unique in this respect. We conclude that early tetrapods with the skeletal morphology and limb mobility of *Ichthyostega* were unlikely to have made some of the recently described Middle Devonian trackways[10].

Early tetrapods, and the fish that gave rise to them, were originally interpreted as being terrestrially capable animals with load-bearing fins or limbs[11–13]. Since the 1990s, however, new fossil discoveries and anatomical interpretations have demonstrated that the first limbed vertebrates were primarily aquatic in habit and that limbs evolved before the ability to 'walk' on land[1,2]. More recently, work has suggested that hindlimb-powered locomotion first evolved in sarcopterygian fish, well before the origin of digit-bearing limbs or terrestriality[14]; this model implies that a muscularly supported pelvis and sacrum are not compulsory for fin/limb–substrate interactions[10]. Others have even unconventionally proposed that some early tetrapods may have been more seal-like in their mode of locomotion[3,4], rather than moving in a primitively salamander-like fashion. This apparent conflict surrounding the timing of events that gave rise to modern tetrapod locomotory styles has left our understanding of the evolution of terrestriality uncertain.

To illuminate the evolution of early tetrapod locomotion, we conducted a computer-aided assessment of limb joint mobility in one of the best known Devonian tetrapods, *Ichthyostega*. To achieve this goal, we used micro-computed tomography (μCT) to scan suitable *Ichthyostega* specimens, created a digitally rendered three-dimensional skeletal model (Fig. 1), and quantified maximum range of motion in the shoulder, elbow, hip and knee in three orthogonal planes of movement. To interpret joint mobility in a locomotor context, we compared the data of *Ichthyostega* with those of five morphologically and phylogenetically distinct modern tetrapod analogues with varying joint morphologies and locomotion behaviours. These include a salamander (*Ambystoma tigrinum*), crocodile (*Crocodylus niloticus*), platypus

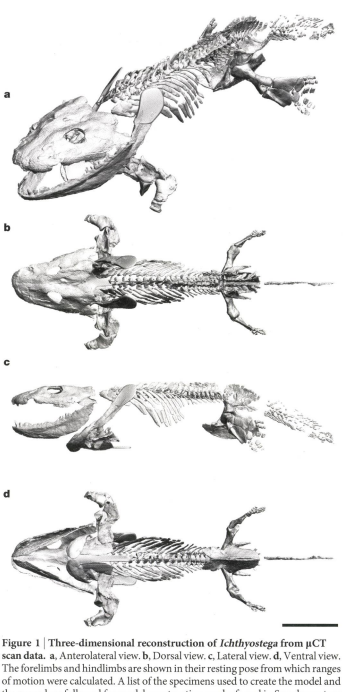

Figure 1 | Three-dimensional reconstruction of *Ichthyostega* from μCT scan data. **a**, Anterolateral view. **b**, Dorsal view. **c**, Lateral view. **d**, Ventral view. The forelimbs and hindlimbs are shown in their resting pose from which ranges of motion were calculated. A list of the specimens used to create the model and the procedure followed for model construction can be found in Supplementary Information, as can a comparison with the most recent two-dimensional reconstruction presented in ref. 4. Scale bar, 10 cm.

[1]Department of Veterinary Basic Sciences and Structure and Motion Laboratory, The Royal Veterinary College, Hawkshead Lane, Hatfield AL9 7TA, UK. [2]University Museum of Zoology, Department of Zoology, University of Cambridge, Downing Street, Cambridge CB2 3EJ, UK.

(*Ornithorhynchus anatinus*), seal (*Halichoerus grypus*) and otter (*Lutra vulgaris*). Moreover, we validated our methodology through dissection and joint manipulation to determine the effect of soft tissues (or lack thereof) on joint mobility (see Supplementary Information).

Data from the hindlimb demonstrate that the hip joint in *Ichthyostega* has a comparable degree of mobility, in terms of flexion/extension and adduction/abduction, to that of the modern tetrapods. However, unlike the modern tetrapods, the hip joint of *Ichthyostega* has a minimal degree of long-axis rotation (pronation/supination) capacity (Fig. 2a, but note that the seal, whose hindlimb is modified as a flipper, has a reduced range of long-axis rotation in comparison with the other modern taxa). When range of mobility is partitioned into positive (increasing angle between limb and girdle) and negative (decreasing angle between limb and girdle) angular movements (Fig. 3a), the hip joint of *Ichthyostega* shows a relatively equal distribution of mobility, with the pattern approaching that seen in the modern tetrapods (see Supplementary Table 5); however, there is somewhat more abduction capacity. In terms of knee joint movements, *Ichthyostega* displays the most restricted mobility in flexion/extension (see Supplementary Table 6), but no discernible differences were recovered for the other two planes of movement, presumably because soft tissues rather than osteology are primary limits on knee mobility, as in many other tetrapods.

The hip joint in *Ichthyostega* forms a condyloid-like articulation with greatly enlarged dorsal and ventral bony buttresses surrounding an anteroventrally-to-posterodorsally elongated acetebulum[13]. In addition to this, the femoral head is boomerang-shaped with a large ventral intertrochanteric fossa enveloping the ventral bony buttress of the acetabulum, forming a locking mechanism. This type of hip

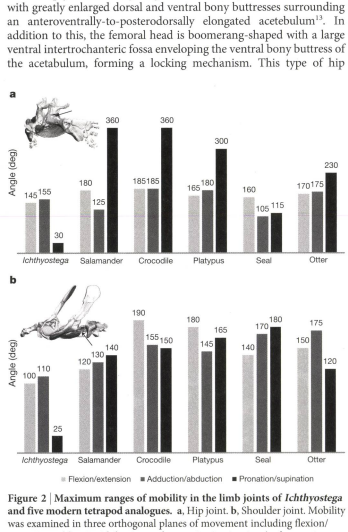

Figure 2 | Maximum ranges of mobility in the limb joints of *Ichthyostega* and five modern tetrapod analogues. a, Hip joint. **b**, Shoulder joint. Mobility was examined in three orthogonal planes of movement including flexion/extension, adduction/abduction and pronation/supination (or long-axis rotation). The most obvious difference between *Ichthyostega* and the modern tetrapods analysed is a distinct lack of long-axis rotation. A validation test of the method used to calculate range of mobility can been found in Supplementary Information.

morphology permits the femur to rock along the primary and secondary axes of the acetabulum but prevents any major long-axis rotary movements. Because the primary axis of the acetabulum (and associated femoral head) in *Ichthyostega* is tilted anteriorly, movement of the hindlimb would have occurred at an angle about 45° from the main horizontal axis of the body. Consequently, the hindlimb would primarily have moved in an anteroventral-to-posterodorsal arc during hip extension and an anterodorsal-to-posteroventral arc during hip adduction (Fig. 3b, c).

The limited range of hip long-axis rotation, in combination with a joint offset of about 45° from the horizontal, implies that the plantar surface of the pes in *Ichthyostega* was unable to contact the substrate. In particular, the femur would have been prevented from attaining a horizontal orientation and the pes would not have been capable of pointing anteriorly, a limb pose conventionally considered plesiomorphic for terrestrial tetrapods[15,16] (see Supplementary Figs 5 and 6). This means that the pelvis could not have been lifted free of the ground and that the hindlimbs were more critical during swimming, with a more passive or stabilizing function during land/substrate movement (analogous to phocid seals[17]). This proposed model of hindlimb movement in *Ichthyostega* is in accordance with the development of broad, paddle-shaped, distal limb bones and expanded pedes[4]. It is also further supported by a reduced range of flexion/extension in the knee, which is an essential component of terrestrial locomotion in living tetrapods[18–21].

With respect to the forelimb, the shoulder joint in *Ichthyostega* has the most restricted range of angular motions in all three planes of movement (Fig. 2b), with the most striking characteristic again being a distinct lack of long-axis rotation (pronation/supination). Partitioning the range of motion into positive and negative angular movements further reveals that the shoulder joint in *Ichthyostega* is primarily restricted to negative angular movements, with the majority of mobility occurring in flexion and adduction (Fig. 3d). In contrast to *Ichthyostega*, the modern tetrapods examined show appreciable shoulder mobility in all three planes of movement (Fig. 2b) and a more equal distribution between positive and negative angular movements (see Supplementary Table 3). Elbow joint mobility in *Ichthyostega* is, as far as can be judged from the ulna articulation, comparable to that in the modern tetrapods. It is relatively flexible in all degrees of freedom and shows a pattern intermediate between more sprawling animals and those that use more upright limb postures (see Supplementary Table 4).

The restricted range of shoulder mobility in *Ichthyostega* is primarily the product of an anteroposteriorly elongated and dorsoventrally flattened glenoid fossa and humeral head[13]. As with the hip, this type of joint morphology produces a condyloid-like joint articulation, permitting flexion/extension and adduction/abduction but preventing humeral long-axis rotation. Further to this, the glenoid fossa in *Ichthyostega* is somewhat twisted along its primary axis, with its anterior portion facing ventrally and its posterior portion facing dorsally. The morphology of the glenoid fossa in *Ichthyostega* guides the forelimb to move in a slight anteroventral-to-posterodorsal plane during shoulder joint flexion, whereas during adduction it directs the forelimb to move in an inclined plane from the vertical, causing the humerus to trend posteriorly (Fig. 3e, f). In addition to joint shape, the pectoral girdle of *Ichthyostega* also has a large bony buttress surrounding the anterodorsal border of the glenoid itself, further restricting movements in extension and abduction.

Given that symmetrical gaits (for example lateral sequence walking, trotting) require a large degree of limb retraction and rotation, in addition to girdle rotation by means of bending of the vertebral column[15,16,18–23], it is unlikely that *Ichthyostega* employed such gaits with its forelimbs. Indeed, the pattern of shoulder joint mobility in *Ichthyostega*, in combination with a rigid pectoral girdle and thorax (due to large overlapping ribs[13]) and terrestrially ineffectual hindlimbs, indicates that the most likely mode of forelimb movement on land/substrate involved synchronous mudskipper-like 'crutching' motions[24]. This

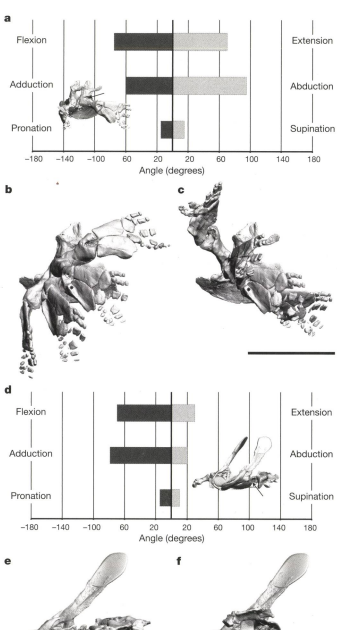

Figure 3 | Partitioned range of mobility in the hip joint and shoulder joint of *Ichthyostega*. **a**, Hip joint mobility partitioned into positive and negative angular movements. **b**, Movement of the hip in flexion/extension. **c**, Movement of the hip in adduction/abduction. **d**, Shoulder joint mobility partitioned into positive and negative angular movements. **e**, Movement of the shoulder in flexion/extension. **f**, Movement of the shoulder in adduction/abduction. Asterisks indicate the resting pose. Specific details of the method used to calculate joint range of mobility are provided in Supplementary Information, as are animations of maximum range of mobility in the shoulder and hip of *Ichthyostega*. Scale bars, 10 cm.

proposed locomotory behaviour for the forelimbs of *Ichthyostega* concurs with previous conjectures[3,4] and is further supported by highly developed elbow extensor musculature (implied by large dorsally extending olecranon processes)[9] attached to a relatively mobile elbow joint. In addition to land/substrate movement, however, the large amount of shoulder adduction and elbow extension in the forelimb of *Ichthyostega* would have enabled both station-holding and lifting of the head out of the water to breathe and potentially feed[25].

On the basis of our study of limb joint mobility, combined with rib and vertebral morphology[4,13], we conclude that *Ichthyostega* could not use 'normal' quadrupedal gaits. The ability to rotate the humerus and femur longitudinally and use symmetrical gaits (for example lateral sequence walking) must have evolved in other early tetrapod species. Given that a similar type of shoulder and/or hip joint morphology presents itself in some other early tetrapod species[2,8,26], limited limb joint mobility—particularly long-axis rotation—may have been more widespread (see Supplementary Information). However, the use of symmetrical gaits, or lack thereof, in other early tetrapods would need to be tested through further three-dimensional investigations of both the limbs and axial skeleton. Nevertheless, long-axis rotation capacity was present in the fins of tetrapodomorph fishes[5–7], indicating that some tetrapods evolved through a phase of restricted shoulder[8,9] and hip joint mobility before acquiring the ability to perform rotary motions and the associated locomotory behaviours that persist in extant taxa.

In addition, our data indicate that the tetrapod forelimb was the first to gain a role in land/substrate locomotion, with the pelvis and hindlimb becoming robust more as a muscular and propulsive adjunct to the tail for swimming and only later being exapted for walking on land (*contra* ref. 14). The divergent functional roles of early tetrapod limbs and the late onset of hindlimb-powered land/substrate locomotion are consistent with both the diminutive pelvic fins of tetrapodomorph fishes compared with their pectoral fins, and with the genetic mechanisms controlling the formation of fin and limb musculature. In particular, studies demonstrate a distinct evolutionary lag between the developmental modes of pectoral and pelvic fin musculature in bony fishes[27,28]. Therefore, in addition to hip joint constraints, it is conceivable that *Ichthyostega* did not yet have the pelvic musculature necessary for hindlimb-driven land/substrate movement, but rather gradually transformed the existing musculature from a more aquatic to a more terrestrial propulsive role.

Given our results, could an *Ichthyostega*-like early tetrapod have produced similar trackways to some of those recently described from the Middle Devonian[10]? All available evidence from limb joint mobility and axial anatomy[4,13] indicates that such animals could not have made symmetrical gait 'foot' prints. In particular, these early tetrapods probably lacked the necessary rotary motions in their limbs (and perhaps lateral flexion of the vertebral column) to push the body off the substrate and progress using alternating limb movements. Maybe as yet unknown tetrapod species (or known taxa that currently lack postcranial material) with different joint mobility and axial anatomy made these traces; available data cannot yet answer this conundrum. Nonetheless, the analysis presented here supports the possibility that *Ichthyostega*-like animals could produce synchronous (parallel) trackways, as our findings indicate that such a trace should consist of a series of bilateral forelimb impressions.

METHODS SUMMARY

Study taxa were medical or μCT scanned depending on size, with settings varying widely. Scan data were segmented in Mimics (Materialise) and reconstructed in the rendering software Autodesk 3D Studio Max. Limb joints were modelled as ball-and-socket joints with three degrees of freedom: adduction/abduction (about the *x* axis), flexion/extension (about the *y* axis) and pronation/supination (that is, long-axis rotation; about the *z* axis). Joint angles were measured in the biomechanical modelling software SIMM (Software for Interactive Musculoskeletal Modeling; Musculographics, Inc.) from an anatomical resting pose that was set to a starting angle of 0°. Maximum range of movement was determined by moving joints in 5° increments until there was either bone-to-bone contact or the joint became disarticulated. Movements in adduction, flexion and pronation were considered to be negative angular movements (decreasing angle between segments) and ranged from a minimum of 0° to a maximum of −180°. Movements in abduction,

extension and supination were considered to be positive angular movements (increasing angle between segments) and ranged from a minimum of 0° to a maximum of +180°.

Full Methods and any associated references are available in the online version of the paper at www.nature.com/nature.

Received 30 January; accepted 3 April 2012.
Published online 23 May 2012.

1. Coates, M. I. & Clack, J. A. Polydactyly in the earliest known tetrapod limbs. *Nature* **347**, 66–69 (1990).
2. Coates, M. I. The Devonian tetrapod *Acanthostega gunnari* Jarvik: postcranial anatomy, basal tetrapod interrelationships and patterns of skeletal evolution. *Trans. R. Soc. Edinb. Earth Sci.* **87**, 363–421 (1996).
3. Clack, J. A. Devonian tetrapod trackways and trackmakers: a review of the fossils and footprints. *Palaeogeogr. Palaeoclimatol. Palaeoecol.* **130**, 227–250 (1997).
4. Ahlberg, P. E., Clack, J. A. & Blom, H. The axial skeleton of the Devonian tetrapod *Ichthyostega*. *Nature* **437**, 137–140 (2005).
5. Andrews, S. M. & Westoll, T. S. The postcranial skeleton of *Eusthenopteron foordi* Whiteaves. *Trans. R. Soc. Edinb.* **68**, 207–329 (1970).
6. Shubin, N. H., Daeschler, E. B. & Jenkins, F. A. Jr The pectoral fin of *Tiktaalik roseae* and the origin of the tetrapod limb. *Nature* **440**, 764–771 (2006).
7. Boisvert, C. A., Mark-Kurik, E. & Ahlberg, P. E. The pectoral fin of *Panderichthys* and the origin of digits. *Nature* **456**, 636–638 (2008).
8. Shubin, N. H., Daeschler, E. B. & Coates, M. I. The evolution of the tetrapod humerus. *Science* **304**, 90–93 (2004).
9. Ahlberg, P. E. Humeral homology and the origin of the tetrapod elbow: a reinterpretation of the enigmatic specimens ANSP 21350 and GSM 104536. *Spec. Pap. Palaeontol.* **86**, 17–29 (2011).
10. Niedzwiedzki, G., Szrek, P., Narkiewicz, K., Narkiewicz, M. & Ahlberg, P. E. Tetrapod trackways from the early Middle Devonian period of Poland. *Nature* **463**, 43–48 (2010).
11. Gregory, W. K. & Raven, H. C. Origin of paired fins and limbs. *Ann. NY Acad. Sci.* **42**, 273–360 (1941).
12. Jarvik, E. *Basic Structure and Evolution of Vertebrates* Vol. 1 (Academic, 1980).
13. Jarvik, E. The Devonian tetrapod *Ichthyostega*. *Fossils Strata* **40**, 1–206 (1996).
14. King, H. M., Shubin, N. H., Coates, M. I. & Hale, M. E. Behavioural evidence for the evolution of walking and bounding before terrestriality in sarcopterygian fishes. *Proc. Natl Acad. Sci. USA* **108**, 21146–21151 (2011).
15. Edwards, J. L. in *Major Patterns of Vertebrate Evolution* (eds Hecht, M. K., Goody, P. C. & Hecht, B. M.) 553–577 (Plenum, 1977).
16. Rewcastle, S. C. Stance and gait in tetrapods: an evolutionary scenario. *Symp. Zool. Soc. Lond.* **48**, 239–267 (1981).
17. O'Gorman, F. Observations on terrestrial locomotion in Antarctic seals. *Proc. Zool. Soc. Lond.* **141**, 837–850 (1962).
18. Ashley-Ross, M. A. Hindlimb kinematics during terrestrial locomotion in a salamander (*Dicamptodon tenebrosus*). *J. Exp. Biol.* **193**, 255–283 (1994).
19. Reilly, S. M. & Elias, J. A. Locomotion in *Alligator mississippiensis*: kinematic effects of speed and posture and their relevance to the sprawling-to-erect paradigm. *J. Exp. Biol.* **201**, 2559–2574 (1998).
20. Jayne, B. C. & Irschick, D. J. Effects of incline and speed on the three-dimensional hindlimb kinematics of a generalized iguanian lizard (*Dipsosaurus dorsalis*). *J. Exp. Biol.* **202**, 143–159 (1998).
21. Ashley-Ross, M. A., Lundin, R. & Johnson, K. L. Kinematics of level terrestrial and underwater walking in the California newt, *Taricha torosa*. *J. Exp. Zool.* **311A**, 240–257 (2009).
22. Jenkins, F. A. Jr & Goslow, G. E. Jr. The functional anatomy of the shoulder of the savannah monitor lizard (*Varanus exanthematicus*). *J. Morphol.* **175**, 195–216 (1983).
23. Pridmore, P. A. Submerged walking in the epaulette shark *Hemiscyllium ocellatum* (Hemischyllidae) and its implications for locomotion in rhipidistian fishes and early tetrapods. *Zoology* **98**, 278–297 (1994).
24. Pace, C. M. & Gibb, A. C. Mudskipper pectoral fin kinematics in aquatic and terrestrial environments. *J. Exp. Biol.* **212**, 2279–2286 (2009).
25. Markey, M. J. & Marshall, C. R. Terrestrial-style feeding in a very early aquatic tetrapod is supported by evidence from experimental analysis of suture morphology. *Proc. Natl Acad. Sci. USA* **104**, 7134–7138 (2007).
26. Daeschler, E. B., Shubin, N. H., Thomson, K. S. & Amaral, W. W. A Devonian tetrapod from North America. *Science* **265**, 639–642 (1994).
27. Neyt, C. *et al.* Evolutionary origins of the vertebrate appendicular muscle. *Nature* **408**, 82–88 (2000).
28. Cole, N. J. *et al.* Development and evolution of the muscles of the pelvic fin. *PLoS Biol.* **9**, e1001168 (2011).

Supplementary Information is linked to the online version of the paper at www.nature.com/nature.

Acknowledgements We thank J. Molnar for assistance with segmentation, model construction, and movie generation; L. Witmer for access to platypus scan data; Digimorph for access to salamander scan data (National Science Foundation grant IIS-9874781 and IIS-0208675 to T. Rowe); M. Lowe for collections support at the University Museum of Zoology, Cambridge; G. Cuny for access to collections housed in the Geological Museum at the University of Copenhagen; J. Rankin for musculoskeletal modelling support; and P. Ahlberg for commenting on an earlier draft of this manuscript. For access to μCT scanning equipment in their care, we also acknowledge R. Abel, C. Martin and A. Heaver. This research was supported by Natural Environment Research Council grants NE/G005877/1 and NE/G00711X/1.

Author Contributions All authors contributed to project concept and design. S.E.P. collected and analysed the data and wrote the manuscript, including main text, figures and Supplementary Information. J.A.C. and J.R.H. provided a critical review of all aspects of manuscript development. All authors approved the final draft.

Author Information Reprints and permissions information is available at www.nature.com/reprints. The authors declare no competing financial interests. Readers are welcome to comment on the online version of this article at www.nature.com/nature. Correspondence and requests for materials should be addressed to S.E.P. (spierce@rvc.ac.uk).

LETTER

doi:10.1038/nature11128

The bonobo genome compared with the chimpanzee and human genomes

Kay Prüfer[1], Kasper Munch[2], Ines Hellmann[3], Keiko Akagi[4], Jason R. Miller[5], Brian Walenz[5], Sergey Koren[6], Granger Sutton[5], Chinnappa Kodira[7], Roger Winer[7], James R. Knight[7], James C. Mullikin[8], Stephen J. Meader[9], Chris P. Ponting[9], Gerton Lunter[10], Saneyuki Higashino[11], Asger Hobolth[2], Julien Dutheil[2], Emre Karakoç[12], Can Alkan[12]†, Saba Sajjadian[12], Claudia Rita Catacchio[13], Mario Ventura[12,13], Tomas Marques-Bonet[12,14], Evan E. Eichler[12], Claudine André[15], Rebeca Atencia[16], Lawrence Mugisha[17], Jörg Junhold[18], Nick Patterson[19], Michael Siebauer[1], Jeffrey M. Good[1,20], Anne Fischer[1,21], Susan E. Ptak[1], Michael Lachmann[1], David E. Symer[4], Thomas Mailund[2], Mikkel H. Schierup[2,22], Aida M. Andrés[1], Janet Kelso[1] & Svante Pääbo[1]

Two African apes are the closest living relatives of humans: the chimpanzee (*Pan troglodytes*) and the bonobo (*Pan paniscus*). Although they are similar in many respects, bonobos and chimpanzees differ strikingly in key social and sexual behaviours[1–4], and for some of these traits they show more similarity with humans than with each other. Here we report the sequencing and assembly of the bonobo genome to study its evolutionary relationship with the chimpanzee and human genomes. We find that more than three per cent of the human genome is more closely related to either the bonobo or the chimpanzee genome than these are to each other. These regions allow various aspects of the ancestry of the two ape species to be reconstructed. In addition, many of the regions that overlap genes may eventually help us understand the genetic basis of phenotypes that humans share with one of the two apes to the exclusion of the other.

Whereas chimpanzees are widespread across equatorial Africa, bonobos live only south of the Congo River in the Democratic Republic of Congo (Fig. 1a). As a result of their relatively small and remote habitat, bonobos were the last ape species to be described[2] and are the rarest of all apes in captivity. As a consequence, they have, until recently, been little studied[2]. It is known that whereas DNA sequences in humans diverged from those in bonobos and chimpanzees five to seven million years ago, DNA sequences in bonobos diverged from those in chimpanzees around two million years ago. Bonobos are thus closely related to chimpanzees. Moreover, comparison of a small number of autosomal DNA sequences has shown that bonobo DNA sequences often fall within the variation of chimpanzees[3].

Bonobos and chimpanzees are highly similar to each other in many respects. However, the behaviour of the two species differs in important ways[1]. For example, male chimpanzees use aggression to compete for dominance rank and obtain sex, and they cooperate to defend their home range and attack other groups[3]. By contrast, bonobo males are commonly subordinate to females and do not compete intensely for dominance rank[1]. They do not form alliances with one another and there is no evidence of lethal aggression between groups[3]. Compared with chimpanzees, bonobos are playful throughout their lives and show intense sexual behaviour[3] that serves non-conceptive functions and often involves same-sex partners[4]. Thus, chimpanzees and bonobos each possess certain characteristics that are more similar to human traits than they are to one another's. No parsimonious reconstruction of the social structure and behavioural patterns of the common ancestor of humans, chimpanzees and bonobos is therefore possible. That ancestor may in fact have possessed a mosaic of features, including those now seen in bonobo, chimpanzee and human.

To understand the evolutionary relationships of bonobos, chimpanzees and humans better, we sequenced and assembled the genome of a female bonobo individual (Ulindi) and compared it to those of chimpanzees and humans. Compared with the 6× Sanger-sequenced chimpanzee genome[6] (panTro2), the bonobo genome assembly has a similar number of bases in alignment with the human genome, a similar number of lineage-specific substitutions and similar indel error rates (Table 1 and Supplementary Information, sections 2 and 3), suggesting that the two ape genomes are of similar quality. Segmental duplications affect at least 80 Mb of the bonobo genome, according to excess sequence read-depth predictions. Owing to over-collapsing of duplications, only 14.6 Mb are present in the final assembly (Supplementary Information, section 4), a common error seen in assemblies from shorter-read technologies[7]. We used the finished chimpanzee sequence of chromosome 21 together with the human genome sequence to estimate an error rate of approximately two errors per 10 kb in the bonobo genome, with comparable qualities for the X chromosome and autosomes. The bonobo genome can therefore serve as a high-quality sequence for comparative genome analyses.

On average, the two alleles in single-copy, autosomal regions in the Ulindi genome are approximately 99.9% identical to each other, 99.6% identical to corresponding sequences in the chimpanzee genome and 98.7% identical to corresponding sequences in the human genome. A comprehensive analysis of the bonobo genome is presented in Supplementary Information. Here we summarize the most interesting results.

We identified and validated experimentally a total of 704 kb of DNA sequences that occur in bonobo-specific segmental duplications. They contain three partially duplicated genes (*CFHR2*, *DUS2L* and *CACNA1B*) and two completely duplicated genes (*CFHR4* and

[1]Max Planck Institute for Evolutionary Anthropology, D-04103 Leipzig, Germany. [2]Bioinformatics Research Centre, Aarhus University, DK-8000 Aarhus C, Denmark. [3]Max F. Perutz Laboratories, University Vienna, A-1030 Vienna, Austria. [4]Human Cancer Genetics Program and Department of Molecular Virology, Immunology and Medical Genetics, The Ohio State University Comprehensive Cancer Center, Columbus, Ohio 43210, USA. [5]J. Craig Venter Institute, Rockville, Maryland 20850, USA. [6]University of Maryland, College Park, Maryland 20742, USA. [7]454 Life Sciences, Branford, Connecticut 06405, USA. [8]Genome Technology Branch, National Human Genome Research Institute, National Institutes of Health, Bethesda, Maryland 20892, USA. [9]MRC Functional Genomics Unit, Department of Physiology, Anatomy and Genetics, University of Oxford, South Parks Road, Oxford OX1 3QX, UK. [10]The Wellcome Trust Centre for Human Genetics, Roosevelt Drive, Oxford OX3 7BN, UK. [11]Graduate School of Bioscience and Biotechnology, Tokyo Institute of Technology, Kanagawa 226-8503, Japan. [12]Department of Genome Sciences, University of Washington and the Howard Hughes Medical Institute, Seattle, Washington 98195, USA. [13]Sezione di Genetica-Dipartimento di Anatomia Patologica e Genetica, University of Bari, I-70125 Bari, Italy. [14]ICREA, Institut de Biologia Evolutiva (UPF-CSIC), 08003 Barcelona, Catalonia, Spain. [15]Lola Ya Bonobo Bonobo Sanctuary, "Petites Chutes de la Lukaya", Kinshasa, Democratic Republic of Congo. [16]Réserve Naturelle Sanctuaire à Chimpanzés de Tchimpounga, Jane Goodall Institute, Pointe-Noire, Republic of Congo. [17]Chimpanzee Sanctuary and Wildlife Conservation Trust (CSWCT), Entebbe, Uganda. [18]Zoo Leipzig, D-04105 Leipzig, Germany. [19]Department of Genetics, Harvard Medical School, Boston, Massachusetts 02115, USA. [20]Division of Biological Sciences, University of Montana, Missoula, Montana 59812, USA. [21]International Center for Insect Physiology and Ecology, 00100 Nairobi, Kenya. [22]Department of Bioscience, Aarhus University, DK-8000 Aarhus C, Denmark. †Present address: Department of Computer Engineering, Bilkent University, Ankara 06800, Turkey.

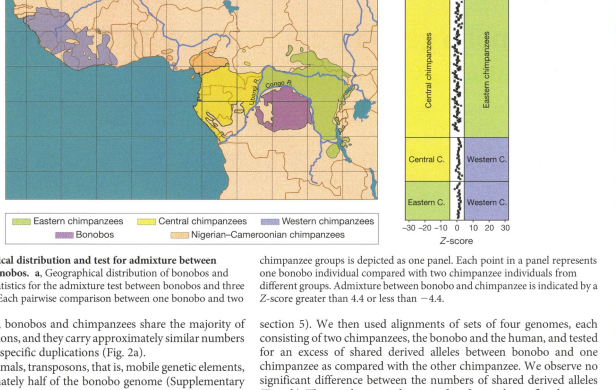

Figure 1 | Geographical distribution and test for admixture between chimpanzees and bonobos. a, Geographical distribution of bonobos and chimpanzees. **b**, *D* statistics for the admixture test between bonobos and three chimpanzee groups. Each pairwise comparison between one bonobo and two chimpanzee groups is depicted as one panel. Each point in a panel represents one bonobo individual compared with two chimpanzee individuals from different groups. Admixture between bonobo and chimpanzee is indicated by a *Z*-score greater than 4.4 or less than −4.4.

DDX28). However, bonobos and chimpanzees share the majority of segmental duplications, and they carry approximately similar numbers of bases in lineage-specific duplications (Fig. 2a).

As in other mammals, transposons, that is, mobile genetic elements, make up approximately half of the bonobo genome (Supplementary Information, section 6). In agreement with previous results[6], we find that *Alu* insertions accumulated about twice as fast on the human lineage as on the bonobo and chimpanzee lineages (Fig. 2b). We identified two previously unreported *Alu* subfamilies in bonobos and chimpanzees, designated *Alu*Yp1, which is present in 5 copies in the human genome and in 54 and 114 copies in the bonobo and chimpanzee genomes, respectively, and *Alu*Yp2, which is absent from humans and present in 24 and 37 copies, respectively, in the two apes. We found that, as in mice[8], African-ape-specific L1 insertions are enriched near genes involved in neuronal activities or cell adhesion and are depleted near genes encoding transcription factors or involved in nucleic-acid metabolism (Supplementary Information, section 6). In humans, L1 retrotransposition has been shown to occur preferentially in neuronal precursor cells and has been speculated to contribute to functional diversity in the brain[9]. The tendency of new L1 integrants to accumulate near neuronal genes on evolutionary timescales may mimic the somatic variation found in the brain.

To investigate whether bonobos and chimpanzees exchanged genes subsequent to their separation, we used a test (the *D* statistic[10]) to investigate the extent to which the bonobo genomes might be closer to some chimpanzees than to others (Supplementary Information, section 10). To this end, we generated Illumina shotgun sequences from two western, seven eastern, and seven central chimpanzees (Fig. 1a) and from three bonobos (Supplementary Information, section 5). We then used alignments of sets of four genomes, each consisting of two chimpanzees, the bonobo and the human, and tested for an excess of shared derived alleles between bonobo and one chimpanzee as compared with the other chimpanzee. We observe no significant difference between the numbers of shared derived alleles (Fig. 1b). There is thus no indication of preferential gene flow between bonobos and any of the chimpanzee groups tested. Such a complete separation contrasts with reports of hybridization between many other primates[11]. It is, however, consistent with the suggestion that the formation of the Congo River 1.5–2.5 million years ago created a barrier to gene flow that allowed bonobos and chimpanzees to evolve different phenotypes over a relatively short time.

Because the population split between bonobo and chimpanzee occurred relatively close in time to the split between the bonobo–chimpanzee ancestor (*Pan* ancestor) and humans, not all genomic regions are expected to show the pattern in which DNA sequences from bonobos and chimpanzees are more closely related to each other than to humans. Previous work using very low-coverage sequencing of ape genomes has suggested that less than 1% of the human genome may be more closely related to one of the two apes than the ape genomes are to one another[12]. To investigate the extent to which such so-called incomplete lineage sorting (ILS) exists between the three species, we used the bonobo genome and a coalescent hidden Markov model (HMM) approach[13] to analyse non-repetitive parts of the bonobo, chimpanzee[6], human[14] and orang-utan[15] genomes. This showed that 1.6% of the human genome is more closely related to the

Table 1 | Bonobo genome assembly characteristics and genomic features compared with the chimpanzee genome (panTro2)

	Bonobo	Chimpanzee
Bases in contigs	2.7 Gb	3.0 Gb
N50 contigs	67 kb	29 kb
N50 scaffolds	9.6 Mb	9.7 Mb
Human bases covered by alignments	2.74 Gb	2.72 Gb
Lineage-specific substitutions	5.71 million	5.67 million
Indel error rate	0.14 errors kb^{-1}	0.13 errors kb^{-1}
Segmental duplication content (>20 kb)	77.2 Mb	76.5 Mb
Lineage-specific retrotransposon integrants	1,445	1,039

See also Supplementary Information, sections 2–4 and 6. kb, kilobase; Mb, megabase; Gb, gigabase.

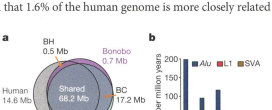

Figure 2 | Segmental duplications and transposon accumulation. a, Venn diagram showing segmental duplications in the human (H), chimpanzee (C) and bonobo (B) genomes. Each number of megabases refers to the total amount of sequence that occurs in segmental duplications (Supplementary Information, section 4). **b**, Accumulation of different retrotransposon classes on each lineage.

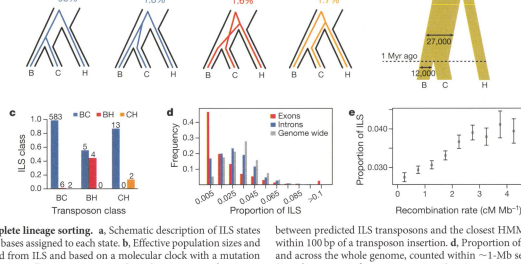

Figure 3 | Incomplete lineage sorting. **a**, Schematic description of ILS states and percentage of bases assigned to each state. **b**, Effective population sizes and split times inferred from ILS and based on a molecular clock with a mutation rate of 10^{-9} yr^{-1}. Myr, million years. We note that other estimates of mutation rates will correspondingly affect the estimates of the split times. **c**, Overlap between predicted ILS transposons and the closest HMM ILS assignments within 100 bp of a transposon insertion. **d**, Proportion of ILS in exons, introns and across the whole genome, counted within ~1-Mb segments of alignment (Supplementary Information, section 8). **e**, Proportion of ILS dependent on recombination rates. Errors, 95% confidence interval.

bonobo genome than to the chimpanzee genome, and that 1.7% of the human genome is more closely related to the chimpanzee than to the bonobo genome (Fig. 3a).

To test this result independently, we analysed transposon integrations, which occur so rarely in ape and human genomes that the chance of two independent insertions of the same type of transposon at the same position and in the same orientation in different species is exceedingly low. We identified 991 integrations of transposons absent from the orang-utan genome but present in two of the three species bonobo, chimpanzee and human. Of these, 27 are shared between the bonobo and human genomes but are absent from the chimpanzee genome, and 30 are shared between the chimpanzee and human genomes but are absent from the bonobo genome, suggesting that approximately 6% (95% confidence interval, 4.1–7.0%) of the genome is affected by ILS among the three species. The HMM estimation of ILS is further supported by the fact that the HMM tree topology assignments tend to match the ILS status of the neighbouring transposons ($P = 7.2 \times 10^{-6}$ and 0.025 for bonobo–human and chimpanzee–human ILS, respectively; Fig. 3c and Supplementary Information, section 6). We conclude that more than 3% of the human genome is more closely related to either bonobos or chimpanzees than these are to each other.

Such regions of ILS may influence phenotypic similarities that humans share with one of the apes but not the other. In fact, about 25% of all genes contain regions of ILS (Supplementary Information, section 8), and genes encoding membrane proteins and proteins involved in cell adhesion have a higher fraction of bases assigned to ILS than do other genes. Amino-acid substitutions that are fixed in the apes and show ILS may be particularly informative about phenotypic differences. We identified 18 such amino-acid substitutions shared between humans and bonobos and 18 shared between chimpanzees and humans (Supplementary Information, section 12). These are candidates for further study. An interesting example is the gene encoding the trace amine associated receptor 8 (TAAR8), a member of a family of G-coupled protein receptors that in the mouse detect volatile amines in urine that may provide social cues[16]. Although this gene seems to be pseudogenized independently on multiple ape lineages, humans and bonobos share a single amino-acid change in the first extracellular domain and carry the longest open reading frames (of 342 and 256 amino acids, respectively; open reading frames in all other apes, <180 amino acids) (SI 12). Further work is needed to clarify if TAAR8 is functional in humans and apes.

The ILS among bonobos, chimpanzees and humans opens the possibility of gauging the genetic diversity and, hence, the population history of the *Pan* ancestor. We used the HMM to estimate the effective population size of the *Pan* ancestor to 27,000 individuals (Fig. 3b), which is almost three times larger than that of present-day bonobos (Supplementary Information, section 9) and humans[17] but is similar to that of central chimpanzees[5,18,19]. We also estimated a population split time between bonobos and chimpanzees of one million years, which is in agreement with most previous estimates[18,19].

Differences in female and male population history, for example, with respect to reproductive success and migration rates, are of special interest in understanding the evolution of social structure. To approach this question in the *Pan* ancestor, we compared the inferred ancestral population sizes of the X chromosome and the autosomes. Because two-thirds of X chromosomes are found in females whereas autosomes are split equally between the two sexes, a ratio between their effective population sizes (X/A ratio) of 0.75 is expected under random mating. The X/A ratio in the *Pan* ancestor, corrected for the higher mutation rate in males, is 0.83 (0.75–0.91) (Fig. 4 and Supplementary Information, section 8). Similarly, we estimated an X/A ratio of 0.85 (0.79–0.93) for present-day bonobos using Ulindi single nucleotide polymorphisms in 200-kb windows (Supplementary Information, section 9). Under the assumption of random mating, this would mean that on average two females reproduce for each reproducing male. The

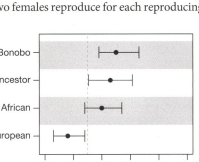

Figure 4 | X/A ratios. The X/A ratios for Ulindi (bonobo), an African human and a European human were inferred from heterozygosity, and that for the *Pan* ancestor was inferred from ILS. The low X/A ratio for the European has been suggested to be due to demographic effects connected to migrating out of Africa[20]. Errors, 95% confidence interval (Supplementary Information, sections 8 and 9).

difference in the variance of reproductive success between the sexes certainly contributes to this observation, as does the fact that whereas bonobo females often move to new groups upon maturation, males tend to stay within their natal group[20]. Because both current and ancestral X/A ratios are similar to each other and also to some human groups (Fig. 4), this suggests that they may also have been typical for the ancestor shared with humans.

Because factors that reduce the effective population size, in particular positive and negative selection, will decrease the extent of ILS, the distribution of ILS across the genome allows regions affected by selection in the *Pan* ancestor to be identified. In agreement with this, we find that exons show less ILS than introns (Fig. 3d and Supplementary Information, section 8). We also find that recombination rates are positively correlated with ILS (Fig. 3e), probably because recombination uncouples regions from neighbouring selective events. Unlike positive and negative selection, balancing selection is expected to increase ILS. In agreement with this, we find that ILS is most frequent in the major histocompatibility complex (MHC), which encodes cell-surface proteins that present antigens to immune cells (Supplementary Information, section 10) and is known to contain genes that evolve under balancing selection[21].

To identify regions affected by selective sweeps in the *Pan* ancestor, we isolated long genomic regions devoid of ILS. The largest such region is 6.1 Mb long and is located on human chromosome 3. This region contains a cluster of tumour suppressor genes[22], has an estimated recombination rate of 10% of the human genome average[23] and has been found to evolve under strong purifying selection in humans[24]. The diversity in the region, corrected for mutation rate, is lower than in neighbouring regions in chimpanzee but not in bonobos (Fig. 5a), and parts of the region show signatures of positive selection in humans[10,25,26]. Apparently this region evolves in unique ways that may involve both strong background selection and several independent events of positive selection among apes and humans.

The fact that the chimpanzee diversity encompasses bonobos for most regions of the genome can be exploited to identify regions that have been positively selected in chimpanzees after their separation from bonobos, because in such regions bonobos will fall outside the chimpanzee variation. We implemented a search for such regions, which is similar to a test previously applied to humans to detect selective sweeps since their split from Neanderthals[10] (*Homo neanderthalensis*), in an HMM that uses coalescent simulations for parameter training, the chimpanzee resequencing data and the megabase-wide average of the human recombination rates (Supplementary Information, section 7). Because the size of a region affected by a selective sweep will be larger the faster fixation was reached, the intensity of selection will correlate positively with genetic length. We therefore ranked the regions according to genetic length and further corrected for the effect of background selection[24]. The highest-ranking region contains an miRNA, miR-4465, that has not yet been functionally characterized. Four of the ten highest-ranking regions contain no protein- or RNA-coding genes, and may thus contain structural or regulatory features that have been subject to selection. Notably, four of these ten regions are on chromosome 6, and two of these four are within 2 Mb of the MHC (Fig. 5b). This suggests that the MHC and surrounding genomic regions have been a major target of positive selection in chimpanzees, presumably as a result of infectious diseases. Indeed, chimpanzees have experienced a selective sweep that targeted MHC class-I genes and reduced allelic diversity across a wide region surrounding the MHC[27], perhaps caused by the HIV-1/SIV$_{CPZ}$ retrovirus[27,28].

The bonobo genome shows that more than 3% of the human genome is more closely related to either bonobos or chimpanzees than these are to each other. This can be used to illuminate the population history and selective events that affected the ancestor of bonobos and chimpanzees. In addition, about 25% of human genes contain parts that are more closely related to one of the two apes than the other. Such regions can now be identified and will hopefully contribute to the unravelling of the genetic background of phenotypic similarities among humans, bonobos and chimpanzees.

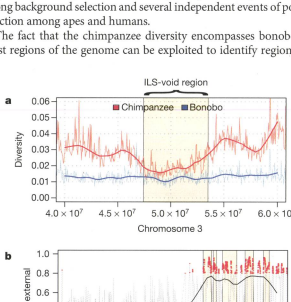

Figure 5 | Selection in the bonobo–chimpanzee common ancestor and chimpanzees. a, Diversity in chimpanzee and bonobo around the region on chromosome 3 devoid of ILS. **b**, Regions where bonobos fall outside the variation of chimpanzee upstream of the MHC. The MHC region is not plotted because the SNP density is sparse there as a result of duplications. Five regions among the 50 longest regions are shown in yellow. Red points show posterior probabilities >0.8.

METHODS SUMMARY

We generated a total of 86 Gb of DNA sequence from Ulindi, a female bonobo who lives in Leipzig Zoo (Supplementary Information, section 1). All sequencing was done on the 454 sequencing platform and included 10 Gb of paired-end reads from clones of insert sizes of 3, 9 and 20 kb. The genome was assembled using the open-source Celera Assembler software[29] (Supplementary Information, section 2). In addition, we sequenced 19 bonobo and chimpanzee individuals on the Illumina GAIIx platform to about one-fold genomic coverage per individual (Supplementary Information, section 5). Supplementary Information provides a full description of our methods.

Received 8 December 2011; accepted 5 April 2012.
Published online 13 June 2012.

1. Boesch, C., Hohmann, G. & Marchant, L. *Behavioural Diversity in Chimpanzees and Bonobos* (Cambridge Univ. Press, 2002).
2. de Waal, F. & Lanting, F. *Bonobo: the Forgotten Ape* (Univ. California Press, 1997).
3. Hare, B., Wobber, V. & Wrangham, R. The self-domestication hypothesis: evolution of bonobo psychology is due to selection against aggression. *Anim. Behav.* **83,** 573–585 (2012).
4. Kano, T. *The Last Ape: Pygmy Chimpanzee Behavior and Ecology* (Stanford Univ. Press, 1992).
5. Fischer, A. *et al.* Bonobos fall within the genomic variation of chimpanzees. *PLoS ONE* **6,** e21605 (2011).
6. The. Chimpanzee Sequencing and Analysis Consortium. Initial sequence of the chimpanzee genome and comparison with the human genome. *Nature* **437,** 69–87 (2005).
7. Alkan, C., Sajjadian, S. & Eichler, E. E. Limitations of next-generation genome sequence assembly. *Nature Methods* **8,** 61–65 (2011).
8. Akagi, K., Li, J., Stephens, R. M., Volfovsky, N. & Symer, D. E. Extensive variation between inbred mouse strains due to endogenous L1 retrotransposition. *Genome Res.* **18,** 869–880 (2008).
9. Baillie, J. K. *et al.* Somatic retrotransposition alters the genetic landscape of the human brain. *Nature* **479,** 534–537 (2011).
10. Green, R. E. *et al.* A draft sequence of the Neandertal genome. *Science* **328,** 710–722 (2010).
11. Arnold, M. L. & Meyer, A. Natural hybridization in primates: one evolutionary mechanism. *Zoology* **109,** 261–276 (2006).

12. Caswell, J. L. *et al.* Analysis of chimpanzee history based on genome sequence alignments. *PLoS Genet.* **4,** e1000057 (2008).
13. Hobolth, A., Christensen, O. F., Mailund, T. & Schierup, M. H. Genomic relationships and speciation times of human, chimpanzee, and gorilla inferred from a coalescent hidden Markov model. *PLoS Genet.* **3,** e7 (2007).
14. Lander, E. S. *et al.* Initial sequencing and analysis of the human genome. *Nature* **409,** 860–921 (2001).
15. Locke, D. P. *et al.* Comparative and demographic analysis of orang-utan genomes. *Nature* **469,** 529–533 (2011).
16. Liberles, S. D. & Buck, L. B. A second class of chemosensory receptors in the olfactory epithelium. *Nature* **442,** 645–650 (2006).
17. Takahata, N. Allelic genealogy and human evolution. *Mol. Biol. Evol.* **10,** 2–22 (1993).
18. Hey, J. The divergence of chimpanzee species and subspecies as revealed in multipopulation isolation-with-migration analyses. *Mol. Biol. Evol.* **27,** 921–933 (2010).
19. Wegmann, D. & Excoffier, L. Bayesian inference of the demographic history of chimpanzees. *Mol. Biol. Evol.* **27,** 1425–1435 (2010).
20. Eriksson, J. *et al.* Y-chromosome analysis confirms highly sex-biased dispersal and suggests a low male effective population size in bonobos (Pan paniscus). *Mol. Ecol.* **15,** 939–949 (2006).
21. Gyllensten, U. B. & Erlich, H. A. Ancient roots for polymorphism at the HLA-DQ alpha locus in primates. *Proc. Natl Acad. Sci. USA* **86,** 9986–9990 (1989).
22. Hesson, L. B., Cooper, W. N. & Latif, F. Evaluation of the 3p21.3 tumour-suppressor gene cluster. *Oncogene* **26,** 7283–7301 (2007).
23. Kong, A. *et al.* Fine-scale recombination rate differences between sexes, populations and individuals. *Nature* **467,** 1099–1103 (2010).
24. McVicker, G., Gordon, D., Davis, C. & Green, P. Widespread genomic signatures of natural selection in hominid evolution. *PLoS Genet.* **5,** e1000471 (2009).
25. Voight, B. F., Kudaravalli, S., Wen, X. & Pritchard, J. K. A map of recent positive selection in the human genome. *PLoS Biol.* **4,** e72 (2006).
26. Wang, E. T., Kodama, G., Baldi, P. & Moyzis, R. K. Global landscape of recent inferred Darwinian selection for Homo sapiens. *Proc. Natl Acad. Sci. USA* **103,** 135–140 (2006).
27. de Groot, N. G. *et al.* AIDS-protective HLA-B*27/B*57 and chimpanzee MHC class I molecules target analogous conserved areas of HIV-1/SIVcpz. *Proc. Natl Acad. Sci. USA* **107,** 15175–15180 (2010).
28. Yohn, C. T. *et al.* Lineage-specific expansions of retroviral insertions within the genomes of African great apes but not humans and orangutans. *PLoS Biol.* **3,** e110 (2005).
29. Miller, J. R. *et al.* Aggressive assembly of pyrosequencing reads with mates. *Bioinformatics* **24,** 2818–2824 (2008).
30. Gottipati, S., Arbiza, L., Siepel, A., Clark, A. G. & Keinan, A. Analyses of X-linked and autosomal genetic variation in population-scale whole genome sequencing. *Nature Genet.* **43,** 741–743 (2011).

Supplementary Information is linked to the online version of the paper at www.nature.com/nature.

Acknowledgements The sequencing effort was made possible by the ERC (grant 233297, TWOPAN) and the Max Planck Society. We thank D. Reich and L. Vigilant for comments; the 454 Sequencing Center, the MPI-EVA sequencing group, M. Kircher, M. Rampp and M. Halbwax for technical support; the staff of Zoo Leipzig (Germany), the Ngamba Island Chimpanzee Sanctuary (Entebbe, Uganda), the Tchimpounga Chimpanzee Rehabilitation Center (Pointe-Noire, Republic of Congo) and the Lola ya Bonobo bonobo sanctuary (Kinshasa, Democratic Republic of Congo) for providing samples; and A. Navarro, E. Gazave and C. Baker for performing the ArrayCGH hybridizations. The ape distribution layers for Fig. 1a were provided by UNEP-WCMC and IUCN 2008 (IUCN Red List of Threatened Species, Version 2011.2, http://www.iucnredlist.org). The National Institutes of Health provided funding for J.R.M., B.W., S.K., G.S. (2R01GM077117-04A1), J.C.M. (Intramural Research Program of the National Human Genome Research Institute) and E.E.E. (HG002385). E.E.E is an Investigator of the Howard Hughes Medical Institute. T.M.-B. was supported by a Ramón y Cajal grant (MICINN-RYC 2010) and an ERC Starting Grant (SIG_20091118); D.E.S., K.A. and S.H. were supported by the Ohio State University Comprehensive Cancer Center, the Ohio Supercomputer Center (#PAS0425) and the Ohio Cancer Research Associates (GRT00024299); and G.L. was supported by a Wellcome Trust grant (090532/Z/09/Z). The US National Science Foundation provided an International Postdoctoral Fellowship (OISE-0754461) to J.M.G. The Danish Council for Independent Research | Natural Sciences (grant no. 09-062535) provided funding for K.M. and M.H.S.

Author Contributions K.P., K.M., I.H., K.A., J.R.M., B.W., S.K., G.S., C.K., R.W., J.R.K., J.C.M., S.J.M., C.P.P., G.L., S.H., A.H., J.D., E.K., C. Alkan, S.S., C.R.C., M.V., T.M.-B., E.E.E., N.P., M.S., J.M.G., A.F., S.E.P., M.L., D.E.S., T.M., M.H.S., A.M.A., J.K. and S.P. analysed genetic data. C. André, R.A., L.M. and J.J. provided samples. K.P., J.K. and S.P. wrote the manuscript.

Author Information The bonobo genome assembly has been deposited with the International Nucleotide Sequence Database Collaboration (DDBJ/EMBL/GenBank) under the EMBL accession number AJFE01000000. 454 shotgun data of Ulindi have been made available through the NCBI Sequence Read Archive under study ID ERP000601; Illumina sequences of 19 chimpanzee and bonobo individuals are available under study ID ERP000602. Reprints and permissions information is available at www.nature.com/reprints. This paper is distributed under the terms of the Creative Commons Attribution-Non-Commercial-Share Alike licence, and is freely available to all readers at www.nature.com/nature. The authors declare competing financial interests: details accompany the full-text HTML version of the paper at www.nature.com/nature. Readers are welcome to comment on the online version of this article at www.nature.com/nature. Correspondence and requests for materials should be addressed to K.P. (pruefer@eva.mpg.de) or S.P. (paabo@eva.mpg.de).

LETTER

doi:10.1038/nature11156

Emergence of *KRAS* mutations and acquired resistance to anti-EGFR therapy in colorectal cancer

Sandra Misale[1,2]*, Rona Yaeger[3]*, Sebastijan Hobor[1]*, Elisa Scala[1,2]*, Manickam Janakiraman[4]*, David Liska[5], Emanuele Valtorta[6], Roberta Schiavo[7], Michela Buscarino[1,2], Giulia Siravegna[1], Katia Bencardino[7], Andrea Cercek[3], Chin-Tung Chen[5], Silvio Veronese[6], Carlo Zanon[1], Andrea Sartore-Bianchi[7], Marcello Gambacorta[6], Margherita Gallicchio[8], Efsevia Vakiani[9], Valentina Boscaro[8], Enzo Medico[2,10], Martin Weiser[5], Salvatore Siena[7], Federica Di Nicolantonio[1,11], David Solit[3,4] & Alberto Bardelli[1,2,11]

A main limitation of therapies that selectively target kinase signalling pathways is the emergence of secondary drug resistance. Cetuximab, a monoclonal antibody that binds the extracellular domain of epidermal growth factor receptor (EGFR), is effective in a subset of *KRAS* wild-type metastatic colorectal cancers[1]. After an initial response, secondary resistance invariably ensues, thereby limiting the clinical benefit of this drug[2]. The molecular bases of secondary resistance to cetuximab in colorectal cancer are poorly understood[3–8]. Here we show that molecular alterations (in most instances point mutations) of *KRAS* are causally associated with the onset of acquired resistance to anti-EGFR treatment in colorectal cancers. Expression of mutant *KRAS* under the control of its endogenous gene promoter was sufficient to confer cetuximab resistance, but resistant cells remained sensitive to combinatorial inhibition of EGFR and mitogen-activated protein-kinase kinase (MEK). Analysis of metastases from patients who developed resistance to cetuximab or panitumumab showed the emergence of *KRAS* amplification in one sample and acquisition of secondary *KRAS* mutations in 60% (6 out of 10) of the cases. *KRAS* mutant alleles were detectable in the blood of cetuximab-treated patients as early as 10 months before radiographic documentation of disease progression. In summary, the results identify *KRAS* mutations as frequent drivers of acquired resistance to cetuximab in colorectal cancers, indicate that the emergence of *KRAS* mutant clones can be detected non-invasively months before radiographic progression and suggest early initiation of a MEK inhibitor as a rational strategy for delaying or reversing drug resistance.

Defining the molecular bases of secondary resistance to anti-EGFR therapies is crucial to monitor, prevent and/or overcome drug refractoriness. To identify potential mechanisms of cetuximab resistance, we generated cetuximab-resistant variants of two colorectal cancer (CRC) cellular models (DiFi and Lim1215 cells) that are highly sensitive to EGFR inhibition (Supplementary Fig. 1a). DiFi cells overexpress EGFR as a result of high level amplification of the *EGFR* gene locus[9]. By contrast, Lim1215 cells express 'normal' EGFR levels but are similarly sensitive to cetuximab (Supplementary Fig. 1b, c). Both cell lines are wild type for *KRAS*, *BRAF* and *PIK3CA*, paralleling the molecular features of the patients with CRC who are most likely to respond to cetuximab[10].

Continuous drug treatment using two different protocols (see Methods and Supplementary Fig. 2) led to the emergence of cetuximab-resistant variants (termed DiFi-R and Lim1215-R; Figs 1a and 2a). To identify the molecular basis of cetuximab resistance in these cells, we performed gene copy number analysis and mutational profiling of the resistant and parental lines. Cetuximab-resistant DiFi-R cells differed from their sensitive parental counterpart by two focal molecular alterations: the *EGFR* gene copy number was reduced, whereas the *KRAS* gene was amplified (Fig. 1b, c and Supplementary Fig. 3). These genomic changes were accompanied by reduced EGFR and increased KRAS protein expression in the cetuximab-resistant cells (Fig. 1d). Sequence analysis confirmed that the *EGFR*, *KRAS*, *NRAS*, *HRAS*, *BRAF* and *PIK3CA* genes were all wild type in the cetuximab-resistant clones.

Sequence analysis of the Lim1215 cetuximab-resistant variants identified acquisition of either KRAS(G13D) or KRAS(G12R) mutations (Fig. 2b). In both DiFi-R and Lim1215-R cells, *KRAS* amplification and mutations, respectively, were accompanied by increased KRAS activation relative to their parental counterparts. In the presence of *KRAS* amplification, cetuximab could partially abrogate phosphorylation of MEK and extracellular signal-regulated kinase (ERK) but, as in *KRAS* mutant cells, was unable to induce growth arrest (Figs 1a, d and 2a, c).

To determine whether resistance was due to selection of pre-existing drug-resistant cells, we analysed the parental cell lines in depth for the presence of a minority population of *KRAS* amplified or mutant cells. In the parental DiFi cells, we identified a sub-population with high level *KRAS* amplification at a prevalence of approximately 1:40,000 (Supplementary Fig. 4). Similarly, deep sequencing and BEAMing (bead, emulsion, amplification and magnetics)[11] indicated that approximately 0.2% of the parental Lim1215 cells contained the KRAS(G13D) mutation (Supplementary Table 1). Notably, the G12R mutation was not detectable in the earliest available passage of parental cells, even when the analysis was performed at high coverage (>50,000-fold). These results suggest that the emergence of a cetuximab-resistant population could derive from selection of a pre-existing *KRAS* amplified or mutant clone or as the result of '*de novo*' acquisition of a *KRAS* mutation under the pressure of cetuximab treatment. To assess this latter possibility formally, we performed dilution cloning of the earliest available passage of Lim1215 cells to generate a homogenous, *KRAS* wild-type Lim1215 sub-line. As schematized in Supplementary Fig. 5, two successive dilution cloning experiments were performed and the derivative cells (hereafter referred to as E4.1) were confirmed as *KRAS* wild-type by both mass spectrometry (MS)-based genotyping and 454 pyrosequencing analysis. We then cultured the E4.1 cells in increasing concentrations of cetuximab, analogous to the experiment performed with the original Lim1215 parental line. Cells were collected during intermediate passages and subjected to MS-based genotyping and/or 454 sequencing analysis (Supplementary Fig. 5a).

[1]Laboratory of Molecular Genetics, Institute for Cancer Research and Treatment (IRCC), 10060 Candiolo (Torino), Italy. [2]Department of Oncological Sciences, University of Torino Medical School, 10060 Candiolo (Torino), Italy. [3]Department of Medicine, Memorial Sloan-Kettering Cancer Center, New York, New York 10065, USA. [4]Human Oncology and Pathogenesis Program, Memorial Sloan-Kettering Cancer Center, New York, New York 10065, USA. [5]Department of Surgery, Memorial Sloan-Kettering Cancer Center, New York, New York 10065, USA. [6]Division of Pathology, Ospedale Niguarda Ca' Granda, 20162 Milano, Italy. [7]Falck Division of Medical Oncology, Ospedale Niguarda Ca' Granda, 20162 Milano, Italy. [8]Dipartimento di Scienza e Tecnologia del Farmaco, University of Torino, 10125 Torino, Italy. [9]Department of Pathology, Memorial Sloan-Kettering Cancer Center, New York, New York 10065, USA. [10]Laboratory of Functional Genomics, Institute for Cancer Research and Treatment (IRCC), 10060 Candiolo (Torino), Italy. [11]FIRC Institute of Molecular Oncology (IFOM), 20139 Milano, Italy.
*These authors contributed equally to this work.

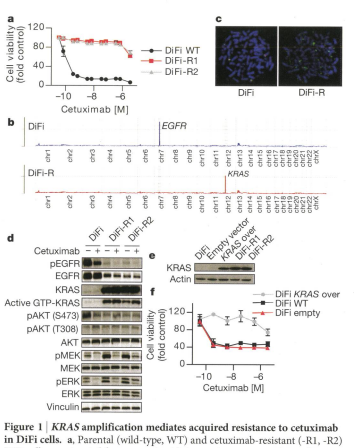

Figure 1 | *KRAS* amplification mediates acquired resistance to cetuximab in DiFi cells. **a**, Parental (wild-type, WT) and cetuximab-resistant (-R1, -R2) DiFi cells were treated for one week with increasing concentrations of cetuximab. Cell viability was assayed by the ATP assay. Data points represent the mean ± s.d. of three independent experiments. **b**, Whole exome gene copy number analysis of parental and cetuximab-resistant DiFi cells. Individual chromosomes are indicated on the *x*-axis. The lines indicate the sequencing depth (*y*-axis) over exome windows of 100,000 base pairs. **c**, Fluorescent *in situ* hybridization (FISH) analysis confirming *KRAS* amplification in resistant (DiFi-R) but not parental DiFi cells. *KRAS* locus bacterial artificial chromosome (BAC) DNA (probe RP11-707G18; green) and chromosome 12 paint (red) were hybridized to the metaphase spreads of DiFi cells. Original magnification, ×100. **d**, DiFi cells were treated with 35 nM cetuximab for 24 h, and whole-cell extracts were then subjected to western blot analysis and compared with untreated cells. DiFi-R1 and -R2 cells were plated in the absence of cetuximab for 7 days or maintained in their normal growth medium (with 35 nM cetuximab) before protein analysis. Active KRAS (GTP-KRAS) was assessed by glutathione *S*-transferase (GST)–RAF1 pull-down. Whole-cell extracts were blotted with phosphorylated EGFR (pEGFR; Tyr 1068), total EGFR, total KRAS, phosphorylated AKT (Thr 308), phosphorylated AKT (Ser 473), total AKT, total MEK1/2 and phosphorylated MEK1/2, total ERK1/2 and phosphorylated ERK1/2 antibodies. Vinculin was included as a loading control. **e**, Western blot analysis of KRAS protein in DiFi cells infected with a *KRAS* lentivirus. Actin is shown as a loading control. **f**, Ectopic expression of wild-type *KRAS* in parental DiFi cells confers resistance to cetuximab. Data points represent the mean ± s.d. of three independent experiments.

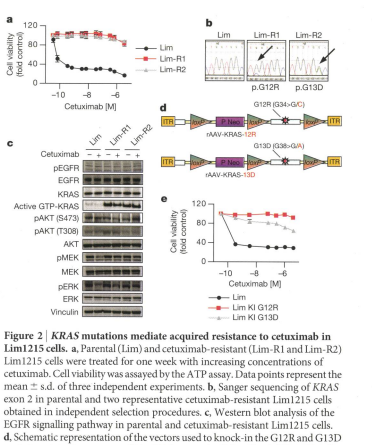

Figure 2 | *KRAS* mutations mediate acquired resistance to cetuximab in Lim1215 cells. **a**, Parental (Lim) and cetuximab-resistant (Lim-R1 and Lim-R2) Lim1215 cells were treated for one week with increasing concentrations of cetuximab. Cell viability was assayed by the ATP assay. Data points represent the mean ± s.d. of three independent experiments. **b**, Sanger sequencing of *KRAS* exon 2 in parental and two representative cetuximab-resistant Lim1215 cells obtained in independent selection procedures. **c**, Western blot analysis of the EGFR signalling pathway in parental and cetuximab-resistant Lim1215 cells. **d**, Schematic representation of the vectors used to knock-in the G12R and G13D mutations into the genome of Lim1215 parental cell lines by AAV-mediated homologous recombination. Targeting was assessed by Sanger sequencing. ITR, inverted terminal repeat; P Neo, neomycin-resistance plasmid. **e**, Parental and isogenic Lim1215 cells carrying the indicated mutations were treated for one week with increasing doses of cetuximab. KI, knock-in. Data points represent the mean ± s.d. of three independent experiments.

MS genotyping identified a KRAS(A146T) mutation after four passages in increasing concentrations of cetuximab (20 nM and higher; Supplementary Fig. 5b). These cells were indeed resistant to the drug (Supplementary Fig. 5c, d), and showed biochemical activation of KRAS (Supplementary Fig. 5e). In parallel, genetic analysis of the E4.1 cells grown in medium without cetuximab found them to be *KRAS* wild type. In summary, these data suggest that resistance to cetuximab in Lim1215 cells may emerge not only from the selection of pre-existing *KRAS* mutant clones but also as a result of continuing mutagenesis.

To prove that amplification or mutations of *KRAS* were causally responsible for cetuximab resistance in our *in vitro* models, we performed two sets of forward genetic experiments. First, ectopic overexpression of wild-type *KRAS* in DiFi conferred resistance to cetuximab (Fig. 1e, f). Second, adeno-associated virus (AAV)-mediated targeted homologous recombination was used to introduce (knock-in) the G13D and G12R alleles into the endogenous *KRAS* locus of Lim1215 cells[12]. Knock-in of the G13D or G12R mutant alleles rendered Lim1215 cells resistant to cetuximab (Fig. 2d, e).

Patients with chemotherapy-refractory CRC, who initially respond and then become resistant to cetuximab, have no further therapeutic options. We reasoned that cetuximab resistance resulting from constitutive KRAS activation could be prevented or reversed by pharmacological inhibition of KRAS signalling. We thus co-treated the resistant clones with cetuximab and selective inhibitors of MEK kinase and phosphatidylinositol-3-OH kinase (PI(3)K)—two key downstream effectors of oncogenic KRAS. Although PI(3)K inhibitors were ineffective in the cetuximab-resistant cells, both the Lim1215-R and DiFi-R cells were sensitive to combinatorial targeting of MEK and EGFR (Supplementary Fig. 6).

To determine whether *KRAS* mutation and/or amplification are clinically relevant mechanisms of acquired cetuximab resistance, we examined tumour biopsies from ten patients with CRC who had become refractory to either cetuximab or the anti-EGFR antibody panitumumab (Supplementary Table 2). We identified one individual (patient 11, Supplementary Table 3a) whose tumour at progression displayed *KRAS* amplification that was not present in a matched pre-cetuximab biopsy (Supplementary Fig. 7). In a different patient (patient 8, Supplementary Table 3a) Sanger sequencing identified a KRAS(Q61H) mutation in a biopsy obtained after disease progression on cetuximab treatment; the remaining eight tumour samples

obtained in patients with acquired resistance to anti-EGFR therapy were wild-type *KRAS* by this technique (Supplementary Table 3a). To determine whether the Sanger technology may have been underpowered to detect *KRAS* mutations in the biopsies obtained after cetuximab or panitumumab progression, these remaining cases were analysed using either 454 deep sequencing or BEAMing. These techniques identified the KRAS(G13D) mutation in four samples, and the simultaneous presence of G12D and G13D mutations in one case (Fig. 3b). In the six patients for whom sufficient pre-treatment tumour samples were available for high coverage 454 sequence analysis or BEAMing, *KRAS* mutations were absent pre-treatment (Supplementary Table 3b). Tumours from a further eight patients treated with cytotoxic chemotherapy but not previously exposed to anti-EGFR therapies were also analysed by 454 deep sequencing. In all eight cases (patients 13–21), 454 sequence analyses identified no evidence of *KRAS* mutation (Fig. 3a). These results indicate that treatment with anti-EGFR antibodies but not cytotoxic chemotherapy is associated with the acquisition of *KRAS* mutations ($P = 0.0193$) (Fig. 3c). Our data support the initiation of clinical trials to define the prevalence of *KRAS* alterations as a mechanism of acquired resistance to anti-EGFR therapies through systematic collection of biopsies.

Emergence of secondary resistance to cetuximab (disease progression) is presently established by radiological evaluation, and typically occurs within 9 to 18 months. We reasoned that the detection of *KRAS* mutant alleles in the plasma of patients treated with cetuximab or panitumumab may allow the early identification of individuals at risk for this mechanism of drug resistance before radiographic documentation of disease progression. We thus performed BEAMing analysis of serial plasma samples from patients treated with cetuximab (Supplementary Table 4a, b). This analysis confirmed that the same *KRAS* variants that were ultimately identified in the post-treatment (disease progression) biopsies were detectable in plasma as early as 10 months before the documentation of disease progression by radiological assessment (Fig. 4).

Drugs that target activated kinase pathways have profound but often temporary anti-tumour effects in subsets of patients with advanced solid tumours. In patients with advanced CRC, antibodies that bind to the extracellular domain of EGFR induce tumour regressions in 10–15% of patients when used alone, and enhance the effects of cytotoxic chemotherapies when used in combination[13,14]. Although several previous studies have identified somatic mutations in the *KRAS* gene as a biomarker of intrinsic resistance to EGFR-targeted agents in patients with CRC[2,15], the molecular basis for acquired resistance has remained obscure. We now report, for the first time, that a substantial fraction of CRC patients who exhibit an initial response to anti-EGFR therapies have, at the time of disease progression, tumours with focal amplification or somatic mutations in *KRAS* that were not detectable before the initiation of therapy. Our data indicate that drug resistance resulting from alterations in *KRAS* can be attributed not only to the selection of pre-existent *KRAS* mutant and amplified clones, but also to new mutations that arise as the result of continuing mutagenesis. The percentage of *KRAS* mutant alleles detected in the resistant tumours ranged from 0.4 to 17% (Fig. 3). At least three (not mutually exclusive) possibilities could account for this low allele frequency. First, despite our efforts to maximize tumour content by macrodissecting each sample, the individual tumour biopsies consisted of variable proportions of tumour and intermixed wild-type *KRAS* stromal cells. Second, only a fraction of the tumour cells in the disease progression samples may have contained the 'resistance' mutation. The latter model has been observed in patients with lung cancer with secondary resistance to the EGFR inhibitor erlotinib, in which only a fraction of the tumour cells collected at the time of radiographic disease progression contain

a

	Chemotherapy-resistant tumours *KRAS* mutational status		
Patient ID	Mutation	Percentage	Reads*/events†
2	WT*	0%	0/30,000
7	WT*	0%	0/11,262
8	WT†	0.01%	5/76,200
9	WT†	0%	0/89,760
10	WT†	0%	0/34,500
11	WT†	0%	0/190,600
13	WT*	0%	0/18,277
14	WT*	0%	0/27,942
15	WT*	0%	0/43,279
16	WT*	0%	0/41,693
17	WT*	0%	0/30,174
18	WT*	0%	0/16,400
19	WT*	0%	0/29,578
21	WT*	0%	0/18,277

b

	Anti-EGFR-resistant tumours *KRAS* mutational status		
Patient ID	Mutation	Percentage	Reads*/events†
1	WT*	0%	0/12,123
2	G13D*	10%	859/8,556
4	G13D*	5.9%	461/7,764
5	G13D*	14.3%	1,037/7,247
6	G13D*	8.6%	651/7,577
7	WT*	0%	0/17,142
8	Q61H†	17.3%	5,960/190,200
9	G12D†	0.04%	17/40,200
	G13D†	0.44%	117/26,400
10	WT†	0%	0/50,300
11	WT† (KRAS amplified)	0%	0/30,400

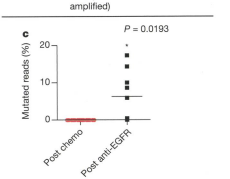

Figure 3 | Mutational analysis of the *KRAS* gene in patients. a, Mutational analysis of *KRAS* in patients with chemotherapy-refractory CRC. **b**, Mutational analysis of the *KRAS* gene in patients who progressed on anti-EGFR antibodies. The results in **a** and **b** are based on assays performed by deep sequencing technologies, either 454 pyrosequencing (*) or BEAMing (†). **c**, Dot plot of the percentage of mutated *KRAS* alleles in patients with chemotherapy-refractory and anti-EGFR-resistant CRC. *P* value was calculated using a two-tailed unpaired Mann–Whitney test.

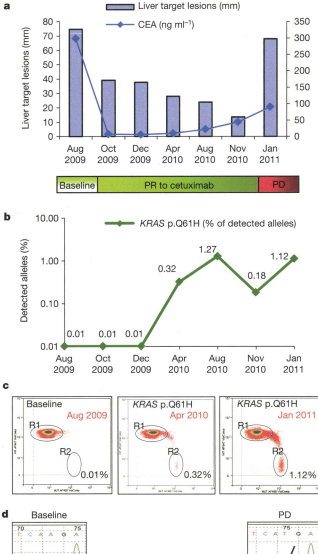

Figure 4 | Detection of circulating *KRAS* mutant DNA in a patient with acquired resistance to cetuximab therapy. a, Size of liver metastasis (blue bars) and carcinoembryonic antigen (CEA) levels in blood (blue line) at the indicated time points, showing an initial response to cetuximab followed by progression (patient 8). PR, partial response; PD, progressive disease. **b**, Quantitative analysis of KRAS(Q61H) mutant DNA in plasma, as assessed by BEAMing. **c**, Two-dimensional dot plot showing quantitative analysis of the KRAS(Q61H) mutation in plasma using BEAMing at individual time points. **d**, Mutational analysis of *KRAS* on tumour samples collected before cetuximab treatment and at the time of disease progression.

the EGFR(T790M) 'resistant' allele[16–18]. Analogously, a recent study indicates that a subset of colorectal cancers found to be wild-type *KRAS* by conventional Sanger sequencing, but *KRAS* mutant by more sensitive techniques, do not respond to anti-EGFR treatment[19]. These data suggest that clinical drug resistance may result from the acquisition of a drug-resistant allele in a sub-population of tumour cells. Finally, it is plausible that independent cell populations containing different resistance mechanisms evolve in parallel within the same metastatic lesion. Nevertheless, our functional analyses in cell models show that *KRAS* mutations are causally responsible for acquired resistance to cetuximab.

Furthermore, we find that the *KRAS* mutant alleles found in the tumours of patients collected after radiographic disease progression can be detected in plasma using highly sensitive DNA analysis methods. As such tumours may be sensitive to combined treatment with a MEK inhibitor, our results suggest that blood-based non-invasive monitoring of patients undergoing treatment with anti-EGFR therapies for the emergence of *KRAS* mutant clones could allow for the early initiation of combination therapies that may delay or prevent disease progression.

METHODS SUMMARY

DiFi and Lim1215 cells were exposed to different doses of cetuximab as described in Supplementary Fig. 2 to obtain the resistant variants. Cell viability was assessed by ATP content. Cells were seeded in 100 µl medium in 96-well plastic culture plates. The experimental procedures for knock-in of cancer mutations, the vectors, AAV production, cell infection and screening for recombinants have been described elsewhere[12]. Tumour specimens were obtained through protocols approved by the Institutional Review Board of Memorial Sloan-Kettering Cancer Center (protocol 10-029) and Ospedale Niguarda Ca' Granda (protocols 1014/09 and 194/2010). Details about the clinical characteristics of patients are provided in Supplementary Table 2. Identification of cancer mutations in the *KRAS*, *HRAS*, *NRAS*, *BRAF*, *PIK3CA* and *EGFR* genes was performed with different sequencing platforms (Sanger, 454 pyrosequencing and mass spectrometry), as described in detail in the Methods. For immunoblot analysis, total cellular proteins were extracted by solubilizing the cells in boiling SDS buffer. Western blot detection was done by enhanced chemiluminescence. The analysis of KRAS activation was performed by immunoprecipitation assay with a glutathione *S*-transferase (GST) fusion protein containing the Ras-binding domain (RBD) of RAF1 (GST–RAF1-RBD). Real-time PCR was performed using an ABI PRISM 7900HT apparatus (Applied Biosytems). KRAS protein expression was evaluated by immunohistochemistry performed on 3-µm-thick tissue sections using a specific KRAS (F234) antibody (SC-30, mouse monoclonal IgG_{2a} Santa Cruz Biotechnology). BEAMing was performed essentially as described previously[10], with deviations from the original protocol outlined in Methods. FISH experiments were conducted with the histology FISH accessory kit (Dako). Data are presented as mean ± s.d. and $n = 3$. Statistical significance was determined by a paired Student's *t*-test or unpaired Mann–Whitney test. $P < 0.05$ was considered statistically significant.

Full Methods and any associated references are available in the online version of the paper at www.nature.com/nature.

Received 8 December 2011; accepted 23 April 2012.
Published online 13 June 2012.

1. Ciardiello, F. & Tortora, G. EGFR antagonists in cancer treatment. *N. Engl. J. Med.* **358,** 1160–1174 (2008).
2. Karapetis, C. S. *et al. K-ras* mutations and benefit from cetuximab in advanced colorectal cancer. *N. Engl. J. Med.* **359,** 1757–1765 (2008).
3. Wheeler, D. L. *et al.* Mechanisms of acquired resistance to cetuximab: role of HER (ErbB) family members. *Oncogene* **27,** 3944–3956 (2008).
4. Benavente, S. *et al.* Establishment and characterization of a model of acquired resistance to epidermal growth factor receptor targeting agents in human cancer cells. *Clin. Cancer Res.* **15,** 1585–1592 (2009).
5. Li, C., Iida, M., Dunn, E. F., Ghia, A. J. & Wheeler, D. L. Nuclear EGFR contributes to acquired resistance to cetuximab. *Oncogene* **28,** 3801–3813 (2009).
6. Hatakeyama, H. *et al.* Regulation of heparin-binding EGF-like growth factor by miR-212 and acquired cetuximab-resistance in head and neck squamous cell carcinoma. *PLoS ONE* **5,** e12702 (2010).
7. Yonesaka, K. *et al.* Activation of ERBB2 signaling causes resistance to the EGFR-directed therapeutic antibody cetuximab. *Sci. Transl. Med.* **3,** 99ra86 (2011).
8. Montagut, C. *et al.* Identification of a mutation in the extracellular domain of the Epidermal Growth Factor Receptor conferring cetuximab resistance in colorectal cancer. *Nature Med.* **18,** 221–223 (2012).
9. Moroni, M. *et al.* Gene copy number for epidermal growth factor receptor (EGFR) and clinical response to antiEGFR treatment in colorectal cancer: a cohort study. *Lancet Oncol.* **6,** 279–286 (2005).
10. De Roock, W. *et al.* Effects of *KRAS*, *BRAF*, *NRAS*, and *PIK3CA* mutations on the efficacy of cetuximab plus chemotherapy in chemotherapy-refractory metastatic colorectal cancer: a retrospective consortium analysis. *Lancet Oncol.* **11,** 753–762 (2010).
11. Diehl, F. *et al.* Circulating mutant DNA to assess tumor dynamics. *Nature Med.* **14,** 985–990 (2008).
12. Di Nicolantonio, F. *et al.* Replacement of normal with mutant alleles in the genome of normal human cells unveils mutation-specific drug responses. *Proc. Natl Acad. Sci. USA* **105,** 20864–20869 (2008).
13. Bardelli, A. & Siena, S. Molecular mechanisms of resistance to cetuximab and panitumumab in colorectal cancer. *J. Clin. Oncol.* **28,** 1254–1261 (2010).
14. Van Cutsem, E. *et al.* Cetuximab and chemotherapy as initial treatment for metastatic colorectal cancer. *N. Engl. J. Med.* **360,** 1408–1417 (2009).

15. Amado, R. G. *et al.* Wild-type KRAS is required for panitumumab efficacy in patients with metastatic colorectal cancer. *J. Clin. Oncol.* **26,** 1626–1634 (2008).
16. Janne, P. A. Challenges of detecting EGFR T790M in gefitinib/erlotinib-resistant tumours. *Lung Cancer* **60** (suppl. 2), S3–S9 (2008).
17. Engelman, J. A. *et al.* Allelic dilution obscures detection of a biologically significant resistance mutation in EGFR-amplified lung cancer. *J. Clin. Invest.* **116,** 2695–2706 (2006).
18. Arcila, M. E. *et al.* Rebiopsy of lung cancer patients with acquired resistance to EGFR inhibitors and enhanced detection of the T790M mutation using a locked nucleic acid-based assay. *Clin. Cancer Res.* **17,** 1169–1180 (2011).
19. Molinari, F. *et al.* Increased detection sensitivity for *KRAS* mutations enhances the prediction of anti-EGFR monoclonal antibody resistance in metastatic colorectal cancer. *Clin. Cancer Res.* **17,** 4901–4914 (2011).

Supplementary Information is linked to the online version of the paper at www.nature.com/nature.

Acknowledgements We are particularly indebted to S. Lamba for generating the KRAS(G12R) knock-in in Lim1215 cells. We thank C. Cancelliere and S. Destefanis for technical assistance. We thank S. Arena, M. Russo and D. Zecchin for critically reading the manuscript. We also thank A. Heguy, A. Viale, N. Socci and M. Pirun for assistance with analysis of next generation sequencing data. This work was supported by European Union Seventh Framework Programme, grant 259015 COLTHERES (A.B. and S.S.); Associazione Italiana per la Ricerca sul Cancro (AIRC) 2010 Special Program Molecular Clinical Oncology 5 × 1000, project 9970 (A.B. and S.S.); Regione Piemonte (A.B. and F.D.N.); Fondazione Piemontese per la Ricerca sul Cancro (FPRC) Intramural Grant, 5xmille 2008, ONLUS (A.B. and F.D.N.); AIRC MFAG 11349 (F.D.N.); Oncologia Ca' Granda ONLUS (OCGO) (S.S.); Mr William H. Goodwin and Mrs Alice Goodwin and the Commonwealth Foundation for Cancer Research; the Experimental Therapeutics Center of Memorial Sloan-Kettering Cancer Center (D.S.); the Society of MSKCC (M.W.); the National Institutes of Health (D.S.); the Beene Foundation (D.S.) and Regione Lombardia and Ministerio Salute grant 'Gene Mutation Monitoring in mCRC' (S.S.).

Author Contributions A.B., D.S., S.S. and F.D.N. planned the project and supervised all research. A.B., D.S. and F.D.N. wrote the manuscript. S.M., R.Y., S.H., E.S., M.W. and F.D.N. designed the experiments. A.B. conceived the molecular analysis of plasma samples. S.M., R.Y., S.H., E.S., M.J., D.L., E.V., R.S., M.B., G.S., C.-T.C., S.V., M.G. and V.B. performed the experiments. C.Z., A.S.-B., M.G. and E.M. analysed data. K.B., A.C. and E.V. provided samples for analysis. S.S., D.S. and A.B. devised dual biopsy clinical protocols for EGFR mAb resistant mCRC.

Author Information Reprints and permissions information is available at www.nature.com/reprints. The authors declare no competing financial interests. Readers are welcome to comment on the online version of this article at www.nature.com/nature. Correspondence and requests for materials should be addressed to D.S. (solitd@mskcc.org) or A.B. (alberto.bardelli@ircc.it).

LETTER

doi:10.1038/nature11219

The molecular evolution of acquired resistance to targeted EGFR blockade in colorectal cancers

Luis A. Diaz Jr[1,2], Richard T. Williams[3], Jian Wu[1,4], Isaac Kinde[1], J. Randolph Hecht[5], Jordan Berlin[6], Benjamin Allen[7], Ivana Bozic[7], Johannes G. Reiter[7,8], Martin A. Nowak[7], Kenneth W. Kinzler[1], Kelly S. Oliner[3] & Bert Vogelstein[1]

Colorectal tumours that are wild type for *KRAS* are often sensitive to EGFR blockade, but almost always develop resistance within several months of initiating therapy[1,2]. The mechanisms underlying this acquired resistance to anti-EGFR antibodies are largely unknown. This situation is in marked contrast to that of small-molecule targeted agents, such as inhibitors of ABL, EGFR, BRAF and MEK, in which mutations in the genes encoding the protein targets render the tumours resistant to the effects of the drugs[3–6]. The simplest hypothesis to account for the development of resistance to EGFR blockade is that rare cells with *KRAS* mutations pre-exist at low levels in tumours with ostensibly wild-type *KRAS* genes. Although this hypothesis would seem readily testable, there is no evidence in pre-clinical models to support it, nor is there data from patients. To test this hypothesis, we determined whether mutant *KRAS* DNA could be detected in the circulation of 28 patients receiving monotherapy with panitumumab, a therapeutic anti-EGFR antibody. We found that 9 out of 24 (38%) patients whose tumours were initially *KRAS* wild type developed detectable mutations in *KRAS* in their sera, three of which developed multiple different *KRAS* mutations. The appearance of these mutations was very consistent, generally occurring between 5 and 6 months following treatment. Mathematical modelling indicated that the mutations were present in expanded subclones before the initiation of panitumumab treatment. These results suggest that the emergence of *KRAS* mutations is a mediator of acquired resistance to EGFR blockade and that these mutations can be detected in a non-invasive manner. They explain why solid tumours develop resistance to targeted therapies in a highly reproducible fashion.

One major barrier to testing any hypothesis about the nature of acquired resistance to anti-EGFR antibodies is limited access to post-treatment tumour tissue. Even when post-treatment tumour tissue is available, sampling bias confounds interpretation because only a small portion of one tumour is usually biopsied, precluding assessment of genetic heterogeneity within or among lesions. To circumvent the tissue access problem, we have examined circulating, cell-free DNA—a form of 'liquid biopsy'. It has been previously shown that circulating tumour DNA (ctDNA) can be found in the majority of patients with metastatic colorectal cancers[7–9]. Analysis of ctDNA is informative because not only it can identify a specific mutant genotype, but it can also provide a measurement of the total tumour burden[7]. If tumours became resistant to anti-EGFR antibodies as a result of the emergence of *KRAS* mutations in their tumours, we expected that mutant *KRAS* genes would be released into the circulation in a time frame consistent with the emergence of resistance.

We retrospectively analysed longitudinal serum samples from 28 patients with chemorefractory metastatic colorectal cancer (CRC) receiving single-agent therapy with panitumumab[10]. Four patients with *KRAS* mutant tumours, who never achieved disease control, were selected as controls. As expected, these four patients were found to have progressive disease at the time of first tumour assessment, 7 ± 2 weeks (mean $\pm$ 1 standard deviation) after initiating treatment with panitumumab (Supplementary Table 1)[1,2]. The other 24 patients with wild-type *KRAS* tumours achieved a partial response ($n = 8$), had prolonged stable disease ($n = 14$), or had retrospectively-determined progressive disease but remained on study for an extended period ($n = 2$). These 24 patients developed clinically evident progressive disease 25 ± 10 weeks (mean $\pm$ 1 standard deviation) following initiation of treatment (Supplementary Table 1) as determined by radiographic imaging.

Serum samples obtained from patients before the initiation of therapy were evaluated for all common mutations at codons 12 and 13 of *KRAS* using a digital ligation assay with a detection limit of one mutant molecule per ml of serum (examples in Supplementary Fig. 1)[11]. Mutations were independently confirmed in a second aliquot of the same serum and the results quantified via a PCR assay that can digitally enumerate the fraction of rare variants in a complex mixture of DNA template molecules (examples in Supplementary Fig. 1 and Supplementary Table 2)[12].

Of the four cases whose archival tumours harboured *KRAS* mutations, three had detectable levels of mutant *KRAS* in the serum before treatment with panitumumab (Supplementary Table 2). In these three patients, the *KRAS* mutations found in the circulation were identical to those found in the patients' tumour tissues even though the time of serum assessment was, on average, 88 weeks after the diagnosis of metastatic disease and even longer after the initial tumour excision (Supplementary Tables 1 and 2). No mutations in *KRAS* were detected in the pre-treatment serum DNA from patients whose archival tumour tissue was wild type for *KRAS* (Supplementary Table 2).

Next, we examined 169 serially acquired serum samples from the 28 patients for the presence of mutant *KRAS* fragments (Supplementary Fig. 2). These samples were collected at approximately 4-week intervals until disease progression (Supplementary Table 2). Serum was assessed for mutations at *KRAS* codons 12 and 13 as described above. When sufficient serum was available (23 of 28 patients), it was assessed for *BRAF* mutations at codons 600 and 601 using the identical assay. Of the 24 patients who did not have *KRAS* mutations at baseline, nine (38%) were found to develop *KRAS* mutations during the course of therapy (Supplementary Table 2), whereas none developed *BRAF* mutations. In three cases (patients no. 1, 12 and 22), several *KRAS* mutations appeared in the circulation—two different mutants in one case and four different mutants in the two other cases (examples in Fig. 1). In each of these cases, the time to appearance of all mutations in the circulation was very similar (Fig. 2). Circulating mutant *KRAS* templates were identified before radiographic evidence of disease progression in three of the nine cases (patients no. 1, 10 and 24). The lead time (that is, the interval between detectable ctDNA and radiographic

[1]Ludwig Center for Cancer Genetics and Therapeutics and Howard Hughes Medical Institute at Johns Hopkins Kimmel Cancer Center, Baltimore, Maryland 21287, USA. [2]Swim Across America Laboratory at Johns Hopkins, Baltimore, Maryland 21287, USA. [3]Amgen Inc., Thousand Oaks, California 91320, USA. [4]State Key Laboratory of Cancer Biology, Cell Engineering Research Center & Department of Cell Biology, The Fourth Military Medical University, Xi'an 710032, China. [5]Division of Hematology/Oncology, David Geffen School of Medicine, University of California, Los Angeles, California 90095, USA. [6]Vanderbilt University Medical Center, Nashville, Tennessee 37232, USA. [7]Program for Evolutionary Dynamics, Harvard University, Cambridge, Massachusetts 02138, USA. [8]IST Austria (Institute of Science and Technology Austria), Klosterneuburg 3400, Austria.

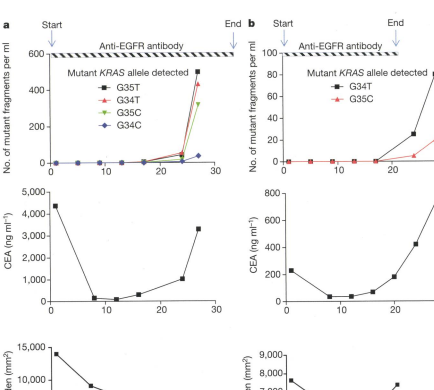

Figure 1 | Emergence of circulating mutant *KRAS*. **a**, **b**, The time course of circulating mutant *KRAS* alleles, CEA and tumour burden are depicted in two patients where fragments of circulating DNA containing mutant *KRAS* were detected. The emergence of four different mutant *KRAS* alleles in codon 12 (cDNA nucleotides 35T, 34T, 35C and 34C) in the serum of patient 1 is shown in **a**, and the emergence of two different mutant *KRAS* alleles in codon 12 (cDNA nucleotides 34T and 35C) in the serum of patient 12 is shown in **b**. Tumour burden refers to the aggregate cross-sectional diameter of the index lesions.

evidence of disease progression) averaged 21 weeks (Supplementary Table 2). The level of ctDNA generally paralleled that of CEA (carcinoembryonic antigen), the standard biomarker used for following disease progression in metastatic CRC (Supplementary Table 3 and Supplementary Fig. 2).

In the three patients (patients no. 8, 20 and 28) with detectable mutant *KRAS* in their tumours as well as in their circulation, no new mutations in *KRAS* emerged (Supplementary Table 2).

The progression-free survival (hazard ratio 0.9; 95% confidence interval 0.3366 to 2.453; $P = 0.85$; log-rank test) and overall survival (hazard ratio 0.42; 95% confidence interval 0.1599 to 1.144; $P = 0.09$; log-rank test) of patients was not significantly different whether they developed secondary *KRAS* mutations or not (Supplementary Fig. 3)

The availability of serially collected serum samples provided a unique opportunity to model the tumour evolutionary process in those patients that responded to panitumumab. The first question we addressed was whether *KRAS* mutations were likely to be present before the initiation of therapy with panitumumab. To estimate the average tumour growth rate, we used the ctDNA data (Supplementary Table 2) from the nine patients that developed *KRAS* mutations during therapy. The average tumour growth rate was found to be 0.069—that is, the number of tumour cells resistant to panitumumab doubled approximately every ten days (doubling time = ln2/0.069 days; see Supplementary Appendix). The growth rate represents the difference between the cell birth rate b and the cell death rate d, that is, $b - d$. Previous studies[13] have shown that $b \approx 0.25$ for colorectal cancer cells, corresponding to one cell division every 4 days, yielding a value of 0.18 ($= 0.25 - 0.069$) for d.

Using these data-derived estimates of b and d, a branching process model was used to test the null hypothesis that there were no cells with *KRAS* mutations in the tumours before the initiation of therapy. We calculated the probability that the number of mutant *KRAS* cells could have grown to at least the observed levels at the times they were measured, assuming this null hypothesis (see Supplementary Appendix). Using the known tumour burdens and pre-treatment ctDNA levels measured in patients 8 and 20 who harboured *KRAS* mutations in their tumours before therapy, as well as data obtained on previously studied patients with metastatic disease[2], we calculated that one mutant *KRAS* template per ml of serum corresponds to a tumour containing 44 million *KRAS*-mutant cells. We performed the statistical valuation separately for each patient. In the three patients that developed more than one circulating *KRAS* mutation, we assumed that each of the detected *KRAS* mutations originated from a different lesion (see below). Thus a total of 16 lesions from nine patients were analysed. For each lesion, the possibility that the observed mutations were absent at the start of treatment could be rejected (thus confirming the presence of pre-existing *KRAS* mutations) with >95% confidence (in most cases, >99.9% confidence; Supplementary Table 4)[14,15]. Furthermore, we varied the birth rate b around the previously calculated value of 0.25, allowing it to be as small as 0.15 or as large as 0.35, and found that this did not affect our conclusion that the mutations were present before therapy, although for one lesion the confidence fell below 95% as the birth rate was increased (Supplementary Table 4).

Next, we estimated how many mutations gave rise to resistance to panitumumab in patients *in vivo*. The total number of lesions large enough to detect by imaging averaged 7.0 lesions per patient in the 24

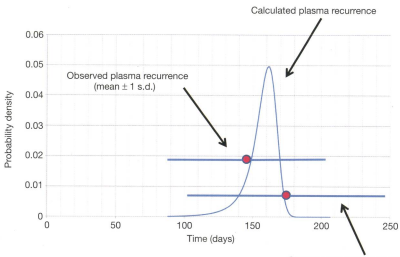

Figure 2 | Predicted probability distribution of times from when treatment starts until resistance mutations become observable in circulating DNA. The observed time to detection of mutant *KRAS* fragments (21 ± 8.5 weeks, mean ± 1 standard deviation) is overlaid with time to clinical progression (25 ± 10 weeks, mean ± 1 standard deviation) in the patients studied. Predictions were based on the Luria–Delbrück model with death, as introduced in ref. 14, or equivalently, the branching process model from ref. 16.

patients studied with wild-type *KRAS* tumours (Supplementary Table 1). Assuming that each individual *KRAS* mutation detected in the serum emanated from a single metastatic lesion, the 16 lesions responsible for contributing ctDNA (Supplementary Table 2) accounted for 9.6% of the total 167 lesions. The other 90% of lesions presumably had developed genetic alterations that were not assessed in our study. As we assessed four different mutated nucleotides of *KRAS* (at codons 12 and 13, Supplementary Table 5), this analysis suggests that a total of approximately 42 ($=4\times167/16$) nucleotides gave rise to resistance in our 24 patients. These remaining 38 nucleotides (42 minus 4) would represent a maximum of 38 genes (one potential mutant nucleotide per gene), or approximately 10 genes if, like *KRAS*, there was an average of four nucleotides per gene that could give rise to resistance when mutated.

Would at least one of these 42 mutant nucleotides be expected to be present in a metastatic lesion initiated by a single cell that was wild type at all 42 nucleotides? We analysed this question using a Luria–Delbrück model generalized to incorporate cell death[14–16]. If we conservatively assume that cancer cells have the same mutation rate as normal cells and the same birth rate described above (0.25)[15,17], then a tumour detectable by computed tomography scanning (one billion cells) is almost certain (probability $>1-10^{-52}$) to contain at least one cell with a mutation at one of these 42 nucleotides. The expected number of such cells is about 3,200 (Supplementary Appendix)[16,17]. These 3,200 cells are distributed among various clones that arose during the growth of the metastatic lesion before therapy with panitumumab. The largest clonal subpopulation is in most cases the progeny of the subpopulation containing the first resistance mutation to arise and survive stochastic drift. Using the equations described in the Supplementary Appendix, we calculated the expected size of this clonal subpopulation as 2,200 cells; thus, 69% (2,200/3,200) of the resistant cells should be derived from a single clone. As described in the Supplementary Appendix, varying the number of possible mutations conferring resistance from 4 to 100 did not change this expectation: there are hundreds to thousands of cells with resistance mutations in each metastasis before the initiation of panitumumab therapy and more than half of these resistant cells are expected to be derived from a single clone.

Our mathematical model also accounts for the very similar times at which circulating *KRAS* fragments were observed across patients and lesions. We calculated the probability distribution for the times at which circulating *KRAS* fragments should become detectable (Supplementary Appendix). As shown in Fig. 2, the mean of this distribution was 22 weeks with a 95% confidence interval ranging from 18 to 25 weeks. These predicted times are strikingly similar to those actually observed in the patients analysed in this study (21 ± 8.5 weeks, mean ± 1 standard deviation) and just slightly sooner than when clinical progression was observed (25 ± 10 weeks, mean ± 1 standard deviation). Finally, we performed simulations to further validate these analytical findings. The results were similar: mutant *KRAS* fragments were predicted to become evident at 22 ± 1.5 weeks (mean ± 1 standard deviation) following treatment (Supplementary Appendix).

Our study indicates that the resistance mutations in *KRAS* and other genes were highly likely to be present in a clonal subpopulation within the tumours *prior* to the initiation of panitumumab therapy. Although we base this conclusion on new data and mathematical analyses, it is consistent with earlier experimental data on other targeted agents[18–21] as well as theoretical predictions[22–24]. As noted in several previous studies of targeted therapeutic agents[18–21], most lesions recur at approximately the same time following therapy. This was also true in our selected group of patients, in which disease progression occurred at the same time in patients who did or did not develop circulating *KRAS* mutations (Supplementary Fig. 3).

Our study suggests that only a limited number of nucleotide mutations and genes are likely to be able to exert a resistance phenotype. If there were many more genes with this capacity, then it would be unlikely that such a high fraction of patients (38%) and lesions (9.6%) would develop mutations in a single gene (*KRAS*). This finding is consistent with earlier studies in that only a small number of genes has been found to be expressed differentially in resistant tumours and an even smaller number to be mutated—none as frequently as *KRAS*[18,25,26]. That only a small number of genes can confer resistance is encouraging; if there were a very large number of genes (and nucleotides) that had the capacity to produce resistance to panitumumab, there would be little hope of combining this drug with others to circumvent resistance.

In sum, our results suggest the following scenario for the development of resistance to panitumumab. Each relatively large metastatic lesion is expected to contain a subclone containing hundreds or thousands of cells with one of about 42 mutations conferring resistance to the antibody. Resistance is therefore a fait accompli—the time to recurrence is simply the interval required for the subclone to repopulate the lesion. This generally takes 5 to 6 months (Fig. 2) and is due to

the rapid expansion of the resistant subclone immediately following treatment initiation. To make these remissions last longer than 5 to 6 months, combination therapies targeting at least two different pathways will be required.

METHODS SUMMARY

Patients and specimens. Patients with chemorefractory metastatic colorectal carcinoma were enrolled into one of two panitumumab monotherapy studies (NCT00083616)[19]. The study protocols were approved by the institutional review boards and all patients signed a written consent form. A subset of patients was selected for this analysis from a total of 388 patients. Patients received panitumumab 6 mg kg^{-1} every two weeks until disease progression. Tumour scans were read centrally by a panel of at least two blinded independent radiologists using a modification of the WHO criteria. Assessments were performed at 4-week intervals through week 28 and every 3 months thereafter until progression of disease. Responses were confirmed at least 4 weeks after response criteria were first met. *KRAS* mutational status in the tissue was predetermined using the DxS assay (Qiagen).

DNA purification. DNA was purified from of 0.2–1 ml of banked serum using the QIAamp circulating nucleic acid kit (Qiagen, catalogue no. 55114) following the manufacturer's recommendations. Amplifiable DNA was quantified with quantitative PCR, using primers and conditions as previously described[27].

Assessments of circulating mutant *KRAS* DNA. The ligation assays were performed as previously described[11] using the primers and probes indicated in Supplementary Table 5. In brief, *KRAS* fragments containing codons 12 and 13 were amplified with primers designed to yield a small PCR product (106 base pairs) to accommodate the degraded DNA found in serum[28]. Note that some of the probes contained locked nucleic acid (LNA) linkages (Exiqon). To confirm and further quantify samples containing *KRAS* mutations, BEAMing assays were used[17] with the primers and probes listed in Supplementary Table 5. The number of mutant fragments per ml of serum was determined from the fraction of alleles containing the mutant allele (determined by BEAMing[17]) and the number of alleles assessed per ml of plasma (determined by qPCR[27] and reported in Supplementary Table 6).

Received 10 December 2011; accepted 8 May 2012.
Published online 13 June 2012.

1. Amado, R. G. *et al.* Wild-type *KRAS* is required for panitumumab efficacy in patients with metastatic colorectal cancer. *J. Clin. Oncol.* **26,** 1626–1634 (2008).
2. Karapetis, C. S. *et al. K-ras* mutations and benefit from cetuximab in advanced colorectal cancer. *N. Engl. J. Med.* **359,** 1757–1765 (2008).
3. Pao, W. *et al. KRAS* mutations and primary resistance of lung adenocarcinomas to gefitinib or erlotinib. *PLoS Med.* **2,** e17 (2005).
4. Engelman, J. A. *et al. MET* amplification leads to gefitinib resistance in lung cancer by activating ERBB3 signaling. *Science* **316,** 1039–1043 (2007).
5. Corcoran, R. B. *et al. BRAF* gene amplification can promote acquired resistance to MEK inhibitors in cancer cells harboring the BRAF V600E mutation. *Sci. Signal.* **3,** ra84 (2010).
6. Johannessen, C. M. *et al.* COT drives resistance to RAF inhibition through MAP kinase pathway reactivation. *Nature* **468,** 968–972 (2010).
7. Diehl, F. *et al.* Circulating mutant DNA to assess tumor dynamics. *Nature Med.* **14,** 985–990 (2008).
8. Diehl, F. *et al.* Detection and quantification of mutations in the plasma of patients with colorectal tumors. *Proc. Natl Acad. Sci. USA* **102,** 16368–16373 (2005).
9. Holdhoff, M., Schmidt, K., Donehower, R. & Diaz, L. A. Jr. Analysis of circulating tumor DNA to confirm somatic *KRAS* mutations. *J. Natl. Cancer Inst.* **101,** 1284–1285 (2009).
10. Hecht, J. R. *et al.* Lack of correlation between epidermal growth factor receptor status and response to panitumumab monotherapy in metastatic colorectal cancer. *Clin. Cancer Res.* **16,** 2205–2213 (2010).
11. Wu, J. *et al.* Recurrent *GNAS* mutations define an unexpected pathway for pancreatic cyst development. *Sci. Transl. Med.* **3,** 92ra66 (2011).
12. Diehl, F. *et al.* BEAMing: single-molecule PCR on microparticles in water-in-oil emulsions. *Nature Methods* **3,** 551–559 (2006).
13. Jones, S. *et al.* Comparative lesion sequencing provides insights into tumor evolution. *Proc. Natl Acad. Sci. USA* **105,** 4283–4288 (2008).
14. Dewanji, A., Luebeck, E. G. & Moolgavkar, S. H. A generalized Luria–Delbrück model. *Math. Biosci.* **197,** 140–152 (2005).
15. Luria, S. E. & Delbrück, M. Mutations of bacteria from virus sensitivity to virus resistance. *Genetics* **28,** 491–511 (1943).
16. Iwasa, Y., Nowak, M. A. & Michor, F. Evolution of resistance during clonal expansion. *Genetics* **172,** 2557–2566 (2006).
17. Tomasetti, C. & Levy, D. Role of symmetric and asymmetric division of stem cells in developing drug resistance. *Proc. Natl Acad. Sci. USA* **107,** 16766–16771 (2010).
18. Montagut, C. *et al.* Identification of a mutation in the extracellular domain of the epidermal growth factor receptor conferring cetuximab resistance in colorectal cancer. *Nature Med.* **18,** 221–223 (2012).
19. Maheswaran, S. *et al.* Detection of mutations in *EGFR* in circulating lung-cancer cells. *N. Engl. J. Med.* **359,** 366–377 (2008).
20. Turke, A. B. *et al.* Preexistence and clonal selection of *MET* amplification in *EGFR* mutant NSCLC. *Cancer Cell* **17,** 77–88 (2010).
21. Leder, K. *et al.* Fitness conferred by BCR-ABL kinase domain mutations determines the risk of pre-existing resistance in chronic myeloid leukemia. *PLoS ONE* **6,** e27682 (2011).
22. Durrett, R. & Moseley, S. Evolution of resistance and progression to disease during clonal expansion of cancer. *Theor. Popul. Biol.* **77,** 42–48 (2010).
23. Lenaerts, T., Pacheco, J. M., Traulsen, A. & Dingli, D. Tyrosine kinase inhibitor therapy can cure chronic myeloid leukemia without hitting leukemic stem cells. *Haematologica* **95,** 900–907 (2010).
24. Komarova, N. L. & Wodarz, D. Drug resistance in cancer: principles of emergence and prevention. *Proc. Natl Acad. Sci. USA* **102,** 9714–9719 (2005).
25. Lu, Y. *et al.* Epidermal growth factor receptor (EGFR) ubiquitination as a mechanism of acquired resistance escaping treatment by the anti-EGFR monoclonal antibody cetuximab. *Cancer Res.* **67,** 8240–8247 (2007).
26. Yonesaka, K. *et al.* Activation of ERBB2 signaling causes resistance to the EGFR-directed therapeutic antibody cetuximab. *Sci. Transl. Med.* **3,** 99ra86 (2011).
27. Rago, C. *et al.* Serial assessment of human tumor burdens in mice by the analysis of circulating DNA. *Cancer Res.* **67,** 9364–9370 (2007).
28. Fan, H. C., Blumenfeld, Y. J., Chitkara, U., Hudgins, L. & Quake, S. R. Noninvasive diagnosis of fetal aneuploidy by shotgun sequencing DNA from maternal blood. *Proc. Natl Acad. Sci. USA* **105,** 16266–16271 (2008).

Supplementary Information is linked to the online version of the paper at www.nature.com/nature.

Acknowledgements The authors thank J. Schaeffer, J. Ptak, N. Silliman and L. Dobbyn for technical assistance and M. Ekdahl for operational assistance. This work was supported by The Virginia and D. K. Ludwig Fund for Cancer Research, the National Colorectal Cancer Research Alliance, NIH grants CA129825, CA43460, CA57345, CA62924, CA095103, and R01GM078986, NCI contract N01-CN-43309, ERC Start grant (279307: Graph Games), FWF NFN Grant No S11407-N23 (Rise), and the John Templeton Foundation. Simulations were performed on the Orchestra cluster supported by the Harvard Medical School Research Information Technology Group.

Author Contributions L.A.D., K.S.O. and B.V. designed experiments, analysed data and wrote the paper. B.V., I.K. and J.W. performed experiments, analysed data and provided input to the manuscript. R.T.W., J.B. and J.R.H. provided critical materials, reagents, analysed data and provided input to the manuscript. B.A., I.B., J.G.R. and M.A.N. analysed data, performed the mathematical modelling and provided input to the manuscript.

Author Information Reprints and permissions information is available at www.nature.com/reprints. The authors declare competing financial interests: details accompany the full-text HTML version of the paper at www.nature.com/nature. Readers are welcome to comment on the online version of this article at www.nature.com/nature. Correspondence and requests for materials should be addressed to L.A.D. (ldiaz1@jhmi.edu) and K.S.O. (koliner@amgen.com).

LETTER

doi:10.1038/nature11134

Autoregulation of microRNA biogenesis by *let-7* and Argonaute

Dimitrios G. Zisoulis[1]*, Zoya S. Kai[1]*, Roger K. Chang[1,2] & Amy E. Pasquinelli[1]

MicroRNAs (miRNAs) comprise a large family of small RNA molecules that post-transcriptionally regulate gene expression in many biological pathways[1]. Most miRNAs are derived from long primary transcripts that undergo processing by Drosha to produce ~65-nucleotide precursors that are then cleaved by Dicer, resulting in the mature 22-nucleotide forms[2,3]. Serving as guides in Argonaute protein complexes, mature miRNAs use imperfect base pairing to recognize sequences in messenger RNA transcripts, leading to translational repression and destabilization of the target messenger RNAs[4,5]. Here we show that the miRNA complex also targets and regulates non-coding RNAs that serve as substrates for the miRNA-processing pathway. We found that the Argonaute protein in *Caenorhabditis elegans*, ALG-1, binds to a specific site at the 3′ end of let-7 miRNA primary transcripts and promotes downstream processing events. This interaction is mediated by mature let-7 miRNA through a conserved complementary site in its own primary transcript, thus creating a positive-feedback loop. We further show that ALG-1 associates with let-7 primary transcripts in nuclear fractions. Argonaute also binds let-7 primary transcripts in human cells, demonstrating that the miRNA pathway targets non-coding RNAs in addition to protein-coding messenger RNAs across species. Moreover, our studies in *C. elegans* reveal a novel role for Argonaute in promoting biogenesis of a targeted transcript, expanding the functions of the miRNA pathway in gene regulation. This discovery of autoregulation of let-7 biogenesis establishes a new mechanism for controlling miRNA expression.

Recent studies from our laboratory provided a global map of interactions between Argonaute and endogenous messenger RNAs (mRNAs) in *C. elegans* at the fourth larval (L4) stage of development[6]. Using cross-linking immunopurification with high-throughput sequencing (CLIP-seq), we found that more than 3,000 mRNA transcripts have sequences bound by *C. elegans* ALG-1 (Argonaute Like Gene 1). Unexpectedly, the non-coding let-7 primary transcripts (pri-let-7), which are processed into the mature let-7 miRNA, were among the RNAs targeted by Argonaute, as indicated by the presence of an ALG-1-binding site towards the 3′ ends of the transcripts (Fig. 1a and Supplementary Fig. 1). To verify that Argonaute associates with pri-let-7, we performed RNA immunopurification (RIP) assays, using an anti-ALG-1 antibody, in L4-stage lysates from wild-type worms and *alg-1(gk214)* mutants, which lack the anti-ALG-1 epitope and show slightly delayed development (Supplementary Fig. 2). A robust signal for pri-let-7 sequences was observed in wild-type but not *alg-1(gk214)*

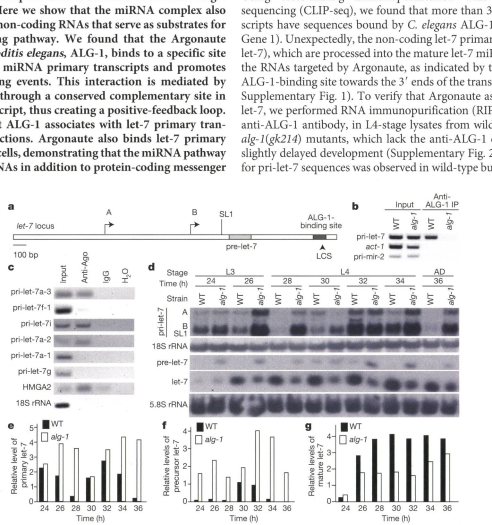

Figure 1 | Argonaute binds and regulates pri-let-7. a, The *let-7* gene: precursor sequence; two transcriptional start sites (A and B); splice site for SL1 trans-splicing; and the ALG-1-binding site, which includes a let-7 complementary site (LCS), are indicated. **b**, **c**, Detection of the indicated transcripts by RIP of wild type and *alg-1(gk214)* or HeLa cell extracts. IP, immunopurification. **d**, Northern blot analysis of RNA from wild type (WT) and *alg-1(gk214)*. **e**–**g**, Levels of pri-let-7 (**e**) relative to 18S ribosomal RNA (rRNA) and precursor (**f**) and mature (**g**) let-7 relative to 5.8S rRNA in wild type or *alg-1(gk214)* quantified from **d**.

[1]Division of Biology, University of California, San Diego, La Jolla, California 92093-0349, USA. [2]Department of Biology Education, Stockholm University, 106 91 Stockholm, Sweden.
*These authors contributed equally to this work.

extracts (Fig. 1b and Supplementary Fig. 3a). Two unspliced (A and B) and one SL1 trans-spliced primary let-7 isoforms are produced by the *let-7* gene in *C. elegans*[7], and they all seem to associate with Argonaute (Supplementary Fig. 3a). Control *actin* mRNA or pri-mir-2 transcripts were not detected in ALG-1 immunopurifications, demonstrating the specificity of Argonaute association with primary let-7 transcripts (Fig. 1b and Supplementary Fig. 3a). Human Argonaute (AGO) proteins also associate with a subset of let-7 primary transcripts, suggesting that this interaction is conserved in more complex organisms (Fig. 1c and Supplementary Fig. 3b).

Argonaute-mediated post-transcriptional regulation can result in mRNA degradation[4,5], and many established miRNA targets in *C. elegans* are upregulated in *alg-1*(*gk214*) mutant worms[6]. To test whether *alg-1* also regulates the levels of primary let-7 transcripts, we performed northern blotting on RNA extracted from wild-type and *alg-1*(*gk214*) worms after every 2 h of development from mid L3, when mature let-7 starts to accumulate, until early adulthood. The three primary let-7 transcripts were detected at similar levels in wild-type and *alg-1*(*gk214*) worms after 24 h of development (Fig. 1d). However, 4 h later the total let-7 primary transcript levels in wild type had decreased to almost undetectable levels, whereas the levels in *alg-1*(*gk214*) remained high (Fig. 1d, e). Although the expression of let-7 primary transcripts in both strains still followed the previously described oscillation behaviour[8], the cycling was muted in the *alg-1*(*gk214*) worms. Overall the pattern is consistent in independent biological replicates, although the rapid cycling of let-7 can shift the expression peaks of individual time courses (Supplementary Fig. 3d, e). By contrast with let-7, the levels of other primary miRNA transcripts showed modest, if any, changes in *alg-1*(*gk214*) compared with wild type at the L4 stage, and none of these primary miRNAs were detected in ALG-1 RIP assays (Supplementary Fig. 3c and data not shown). At all time points, precursor let-7 (pre-let-7) accumulated to higher levels in *alg-1*(*gk214*) compared with wild type, whereas mature let-7 was more abundant in wild type (Fig. 1d, f, g and Supplementary Fig. 3d, f, g). An accumulation of the precursor form and a diminished level of the mature form was observed in *alg-1*(*gk241*) compared with wild-type worms for all miRNAs tested (mir-58, mir-90 and lin-4), regardless of changes in primary transcript levels (Supplementary Fig. 3d and data not shown). These observations are consistent with previous reports of a general role for Argonaute in precursor processing and stabilization of mature miRNA[9–12].

The Argonaute-bound region in let-7 primary transcripts is about 500 nucleotides downstream of the mature let-7 sequence and covers about 100 nucleotides, as mapped by ALG-1 CLIP-seq[6] (Fig. 1a). To test whether this site is required for interaction of ALG-1 with let-7 primary transcripts, we created transgenic strains with a single copy insertion of the *let-7* locus lacking the ALG-1-binding site. These animals express the endogenous primary let-7 transcripts from the X chromosome (wild-type pri-let-7) and primary let-7 transcripts with the ALG-1-binding site deleted (Δalg-1 pri-let-7) from chromosome II. Both the wild-type and the Δalg-1 pri-let-7 transcripts were expressed in the transgenic animals, but only the wild-type pri-let-7 transcript with the ALG-1-binding site intact immunopurified with Argonaute (Fig. 2a and Supplementary Fig. 4a).

Compared with the control strain, worms harbouring the Δalg-1 pri-let-7 transgene expressed levels of primary let-7 that were higher overall (Fig. 2b and Supplementary Fig. 4b). In these assays, primary transcripts expressed from the endogenous let-7 locus are detected in addition to those of transgenic origin. To specifically analyse transgenic *let-7* expression, we crossed the transgenic strains into the *let-7*(*mn112*) background. The *let-7*(*mn112*) mutation removes 190 base pairs just upstream and including the first nucleotide of the let-7 precursor, resulting in undetectable production of precursor or mature miRNA[13]. Northern blotting showed higher levels of primary let-7 transcripts lacking the ALG-1-binding site than of wild type for most time points in the *let-7*(*mn112*) background (Fig. 2c and

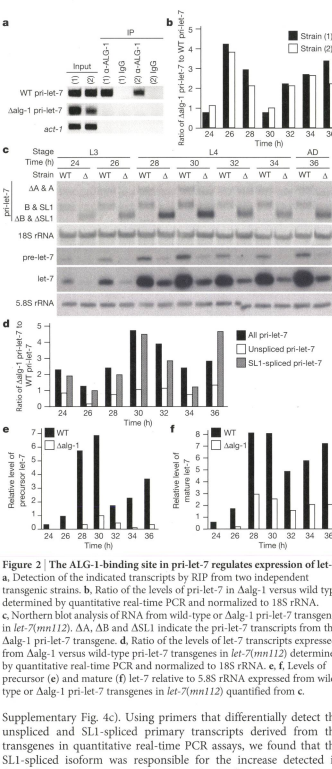

Figure 2 | The ALG-1-binding site in pri-let-7 regulates expression of let-7. **a**, Detection of the indicated transcripts by RIP from two independent transgenic strains. **b**, Ratio of the levels of pri-let-7 in Δalg-1 versus wild type determined by quantitative real-time PCR and normalized to 18S rRNA. **c**, Northern blot analysis of RNA from wild-type or Δalg-1 pri-let-7 transgenes in *let-7*(*mn112*). ΔA, ΔB and ΔSL1 indicate the pri-let-7 transcripts from the Δalg-1 pri-let-7 transgene. **d**, Ratio of the levels of let-7 transcripts expressed from Δalg-1 versus wild-type pri-let-7 transgenes in *let-7*(*mn112*) determined by quantitative real-time PCR and normalized to 18S rRNA. **e**, **f**, Levels of precursor (**e**) and mature (**f**) let-7 relative to 5.8S rRNA expressed from wild-type or Δalg-1 pri-let-7 transgenes in *let-7*(*mn112*) quantified from **c**.

Supplementary Fig. 4c). Using primers that differentially detect the unspliced and SL1-spliced primary transcripts derived from the transgenes in quantitative real-time PCR assays, we found that the SL1-spliced isoform was responsible for the increase detected in the Δalg-1 pri-let-7 transgenic worms (Fig. 2d and Supplementary Fig. 4d). Unexpectedly, although the Δalg-1 pri-let-7 levels were higher, the levels of precursor and mature let-7 in those animals were 2–5-fold lower than the levels in their wild-type counterparts (Fig. 2c, e, f and Supplementary Fig. 4c, e, f). This deficiency reduced the rescue activity of the Δalg-1 pri-let-7 transgene in the *let-7*(*mn112*) background (Supplementary Fig. 4g).

We found a potential let-7 complementary site within the ALG-1-binding region of pri-let-7 that is conserved in other *Caenorhabditis* species (Fig. 3a and Supplementary Fig. 5a,b). To test whether let-7 miRNA mediates association of ALG-1 with primary let-7 transcripts, we performed RIP assays, using L4-stage wild-type and *let-7*(*n2853*)

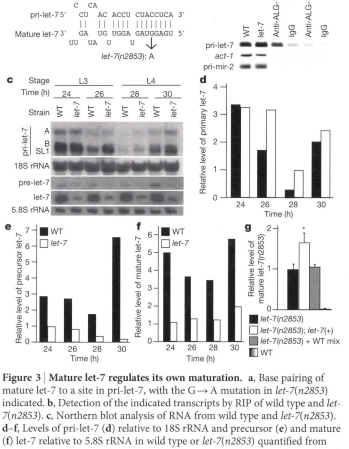

Figure 3 | Mature let-7 regulates its own maturation. **a**, Base pairing of mature let-7 to a site in pri-let-7, with the G→A mutation in *let-7(n2853)* indicated. **b**, Detection of the indicated transcripts by RIP of wild type and *let-7(n2853)*. **c**, Northern blot analysis of RNA from wild type and *let-7(n2853)*. **d**–**f**, Levels of pri-let-7 (**d**) relative to 18S rRNA and precursor (**e**) and mature (**f**) let-7 relative to 5.8S rRNA in wild type or *let-7(n2853)* quantified from **c**. **g**, Analysis of mature let-7(n2853) relative to 18S rRNA from the indicated strains or a 1:1 mix of RNA from *let-7(n2853)* and wild type (mean ± s.e.m., $n = 3$, $^*P < 0.05$).

mutant animals. The *let-7(n2853)* mutant animals harbour a point mutation (G→A) at the fifth nucleotide of the mature miRNA (Fig. 3a), which disrupts base pairing to target mRNAs[13–17]. Primary let-7 immunopurified with ALG-1 in wild-type but not *let-7(n2853)* extracts (Fig. 3b and Supplementary Fig. 6a), indicating that the association of Argonaute with primary let-7 transcripts requires the mature let-7 miRNA.

Northern blot analysis of primary let-7 in staged *let-7(n2853)* and wild-type animals during development from the mid L3 stage until the mid L4 stage showed similar or higher levels in *let-7(n2853)* than in wild-type animals (Fig. 3c, d and Supplementary Fig. 6b–d). Despite the generally higher levels of primary let-7, precursor and mature let-7 were substantially reduced in *let-7(n2853)* compared with wild-type worms (Fig. 3c–f and Supplementary Fig. 6b–f).

Our cumulative data indicate that binding of ALG-1 through mature let-7 miRNA to pri-let-7 results in reduced transcript levels and increased mature levels, consistent with a role for ALG-1 in promoting the processing of primary let-7 transcripts. To test this idea further, we investigated whether introduction of wild-type *let-7* would boost the levels of mature let-7(n2853). Because the let-7(n2853) primary transcript has an intact let-7 complementary site, the presence of wild-type mature let-7 miRNA is predicted to recruit ALG-1 to the transcript to promote processing and increase levels of mature let-7(n2853). Strains containing the wild-type *let-7* gene integrated on chromosome II and the *let-7(n2853)* allele on the X chromosome (denoted *let-7(n2853)*;*let-7*(+)) were tested for effects on the levels of mature let-7(n2853) RNAs. Compared with the *let-7(n2853)* strain, the levels of mature let-7(n2853) were increased in the *let-7(n2853)*; *let-7*(+) strain (Fig. 3g). This upregulation is probably muted by destabilization of the mature miRNA attributed to the n2853 mutation, which impairs the target-mediated protection conferred on mature miRNAs by their target mRNAs[15].

Because processing of miRNA primary transcripts typically occurs in the nucleus, we investigated the association of ALG-1 with pri-let-7 in this compartment. About 20% of ALG-1 protein localized to the nuclear fraction (Fig. 4a). Notably, almost half of the mature let-7 miRNA—double the amount of three other tested miRNAs (Fig. 4a)—was associated with the nuclear fraction. Using ALG-1 RIP assays of whole-cell and nuclear fractions from wild-type animals, we observed strong and specific association of pri-let-7 with ALG-1 in both extracts (Fig. 4b).

Recently, the nuclear transport receptor exportin-1 (XPO-1) was implicated in regulating primary miRNA processing through an unknown mechanism[18]. As previously reported, depletion of *xpo-1* by RNA interference (RNAi) resulted in a twofold decrease in mature let-7 levels[18] (Fig. 4c). Moreover, *xpo-1* depletion reduced the nuclear localization of ALG-1 by a factor of 3.5 ± 0.1 (mean ± s.e.m., $n = 5$, $P < 0.001$), but did not affect total ALG-1 levels, compared with wild-type controls (Fig. 4d). Additionally, RIP assays revealed reduced association of ALG-1 with pri-let-7 in *xpo-1*-depleted animals (Fig. 4e). Although exportin-1 is best characterized as a nuclear export factor, it has been shown to interact with Argonaute proteins in mammalian cells[19], and it thus remains to be determined how direct a role XPO-1 has in mediating nuclear interactions between ALG-1 and pri-let-7.

Our studies reveal a novel picture of non-coding RNAs as targets of miRNA-induced silencing complexes. We find that Argonaute associates with let-7 miRNA primary transcripts in *C. elegans* and with a

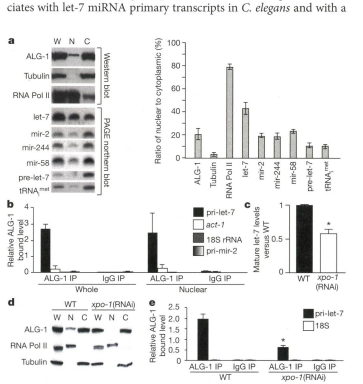

Figure 4 | Association of ALG-1 with pri-let-7 in nuclear fractions. **a**, Detection in whole cell (W), nuclear (N) or cytoplasmic (C) fractions of the indicated proteins or RNAs (mean ± s.e.m., $n = 3$). PAGE, polyacrylamide gel electrophoresis; tRNA$_i^{met}$, initiator methionine transfer RNA. **b**, Levels of the indicated transcripts relative to their respective inputs analysed by RIP and detected by quantitative real-time PCR (mean ± s.e.m., $n = 2$). **c**, Ratio of mature let-7 from *xpo-1* relative to control RNAi after normalization to 18S rRNA (mean ± s.e.m., $n = 7$, $^*P < 0.001$). **d**, Detection of the ALG-1 protein in fractions from wild-type and *xpo-1*-depleted animals. **e**, Analysis of pri-let-7 or 18S rRNA relative to their respective inputs by RIP and quantitative real-time PCR of control (wild type) or *xpo-1* RNAi (mean ± s.e.m., $n = 4$, $^*P < 0.001$).

subset of pri-let-7 RNAs in human cells, indicating that transcripts other than miRNAs can also be miRNA targets and should be considered in target prediction endeavours. Argonaute is best understood in its role in directing deadenylation and translational repression of bound mRNAs through incompletely resolved mechanisms[4,5]. Although the mechanism by which ALG-1 regulates let-7 primary transcripts is yet to be fully elucidated, it seems to depend on the subcellular localization of Argonaute, as regulated by XPO-1, and to be independent of LIN-28 (Supplementary Fig. 7). Recently miR-709 was reported to inhibit the processing of pri-miR-15a/16-1 in mouse cells[20]. The discovery that the miRNA complex can regulate the processing of primary transcripts reveals a new role for Argonaute in the miRNA pathway. Moreover, this is the first example of a direct miRNA autoregulatory loop, whereby mature let-7 binds and promotes processing of its own primary transcript. This amplification mechanism may be important for efficient production of mature let-7 from the oscillating levels of primary transcript substrates during development of *C. elegans*. Our demonstration of direct miRNA regulation of let-7 biogenesis adds to the growing list of factors that impose post-transcriptional control on production of this important miRNA[8,21–27]. Because misregulation of let-7 leads to disease[28], the let-7 positive-feedback loop presents a new target for therapeutic interventions designed to restore appropriate miRNA levels.

METHODS SUMMARY

Caenorhabditis elegans were grown and synchronized by standard methods at 25 °C. Polyacrylamide gel electrophoresis and agarose northern blotting methods were used to detect smaller and larger RNA species, respectively[7]. For PCR assays with reverse transcription, RNA was extracted and complementary DNA was synthesized using random hexamers[8]. For quantification of mature let-7 miRNA from the *let-7(n2853)* strain, we used Taqman Small RNA Assays with a custom-made reverse-transcription primer specific to the mutant sequence (Applied Biosystems). RIP assays in *C. elegans* were performed with anti-ALG-1 antibodies (Thermo Fisher Scientific) and in HeLa cells with antibodies (4F9, sc-53521, Santa Cruz; 2e12/1c9, Sigma) that recognize AGO1 to AGO4 (refs 8, 29).

Full Methods and any associated references are available in the online version of the paper at www.nature.com/nature.

Received 19 April 2011; accepted 2 April 2012.
Published online 3 June 2012.

1. Suh, N. & Blelloch, R. Small RNAs in early mammalian development: from gametes to gastrulation. *Development* **138,** 1653–1661 (2011).
2. Kim, V. N., Han, J. & Siomi, M. C. Biogenesis of small RNAs in animals. *Nature Rev. Mol. Cell Biol.* **10,** 126–139 (2009).
3. Krol, J., Loedige, I. & Filipowicz, W. The widespread regulation of microRNA biogenesis, function and decay. *Nature Rev. Genet.* **11,** 597–610 (2010).
4. Huntzinger, E. & Izaurralde, E. Gene silencing by microRNAs: contributions of translational repression and mRNA decay. *Nature Rev. Genet.* **12,** 99–110 (2011).
5. Fabian, M. R., Sonenberg, N. & Filipowicz, W. Regulation of mRNA translation and stability by microRNAs. *Annu. Rev. Biochem.* **79,** 351–379 (2010).
6. Zisoulis, D. G. *et al.* Comprehensive discovery of endogenous Argonaute binding sites in *Caenorhabditis elegans*. *Nature Struct. Mol. Biol.* **17,** 173–179 (2010).
7. Bracht, J., Hunter, S., Eachus, R., Weeks, P. & Pasquinelli, A. E. Trans-splicing and polyadenylation of let-7 microRNA primary transcripts. *RNA* **10,** 1586–1594 (2004).
8. Van Wynsberghe, P. M. *et al.* LIN-28 co-transcriptionally binds primary let-7 to regulate miRNA maturation in *Caenorhabditis elegans*. *Nature Struct. Mol. Biol.* **18,** 302–308 (2011).
9. Grishok, A. *et al.* Genes and mechanisms related to RNA interference regulate expression of the small temporal RNAs that control *C. elegans* developmental timing. *Cell* **106,** 23–34 (2001).
10. Duchaine, T. F. *et al.* Functional proteomics reveals the biochemical niche of *C. elegans* DCR-1 in multiple small-RNA-mediated pathways. *Cell* **124,** 343–354 (2006).
11. Diederichs, S. & Haber, D. A. Dual role for argonautes in microRNA processing and posttranscriptional regulation of microRNA expression. *Cell* **131,** 1097–1108 (2007).
12. Tan, G. S. *et al.* Expanded RNA-binding activities of mammalian Argonaute 2. *Nucleic Acids Res.* **37,** 7533–7545 (2009).
13. Reinhart, B. J. *et al.* The 21-nucleotide let-7 RNA regulates developmental timing in *Caenorhabditis elegans*. *Nature* **403,** 901–906 (2000).
14. Bagga, S. *et al.* Regulation by let-7 and lin-4 miRNAs results in target mRNA degradation. *Cell* **122,** 553–563 (2005).
15. Chatterjee, S., Fasler, M., Bussing, I. & Grosshans, H. Target-mediated protection of endogenous microRNAs in *C. elegans*. *Dev. Cell* **20,** 388–396 (2011).
16. Chatterjee, S. & Grosshans, H. Active turnover modulates mature microRNA activity in *Caenorhabditis elegans*. *Nature* **461,** 546–549 (2009).
17. Vella, M. C., Choi, E. Y., Lin, S. Y., Reinert, K. & Slack, F. J. The *C. elegans* microRNA let-7 binds to imperfect let-7 complementary sites from the lin-41 3′ UTR. *Genes Dev.* **18,** 132–137 (2004).
18. Büssing, I., Yang, J. S., Lai, E. C. & Grosshans, H. The nuclear export receptor XPO-1 supports primary miRNA processing in *C. elegans* and *Drosophila*. *EMBO J.* **29,** 1830–1839 (2010).
19. Castanotto, D., Lingeman, R., Riggs, A. D. & Rossi, J. J. CRM1 mediates nuclear-cytoplasmic shuttling of mature microRNAs. *Proc. Natl Acad. Sci. USA* **106,** 21655–21659 (2009).
20. Tang, R. *et al.* Mouse miRNA-709 directly regulates miRNA-15a/16–1 biogenesis at the posttranscriptional level in the nucleus: evidence for a microRNA hierarchy system. *Cell Res* **22,** 504–515 (2012).
21. Heo, I. *et al.* Lin28 mediates the terminal uridylation of let-7 precursor microRNA. *Mol. Cell* **32,** 276–284 (2008).
22. Lehrbach, N. J. *et al.* LIN-28 and the poly(U) polymerase PUP-2 regulate let-7 microRNA processing in *Caenorhabditis elegans*. *Nature Struct. Mol. Biol.* **16,** 1016–1020 (2009).
23. Michlewski, G. & Caceres, J. F. Antagonistic role of hnRNP A1 and KSRP in the regulation of let-7a biogenesis. *Nature Struct. Mol. Biol.* **17,** 1011–1018 (2010).
24. Newman, M. A., Thomson, J. M. & Hammond, S. M. Lin-28 interaction with the Let-7 precursor loop mediates regulated microRNA processing. *RNA* **14,** 1539–1549 (2008).
25. Rybak, A. *et al.* A feedback loop comprising lin-28 and let-7 controls pre-let-7 maturation during neural stem-cell commitment. *Nature Cell Biol.* **10,** 987–993 (2008).
26. Trabucchi, M. *et al.* The RNA-binding protein KSRP promotes the biogenesis of a subset of microRNAs. *Nature* **459,** 1010–1014 (2009).
27. Viswanathan, S. R., Daley, G. Q. & Gregory, R. I. Selective blockade of microRNA processing by Lin28. *Science* **320,** 97–100 (2008).
28. Büssing, I., Slack, F. J. & Grosshans, H. let-7 microRNAs in development, stem cells and cancer. *Trends Mol. Med.* **14,** 400–409 (2008).
29. Hendrickson, D. G., Hogan, D. J., Herschlag, D., Ferrell, J. E. & Brown, P. O. Systematic identification of mRNAs recruited to argonaute 2 by specific microRNAs and corresponding changes in transcript abundance. *PLoS ONE* **3,** e2126 (2008).

Supplementary Information is linked to the online version of the paper at www.nature.com/nature.

Acknowledgements We thank J. Lykke-Andersen and members of the Pasquinelli lab for reading the manuscript, and we thank D. Hogan for discussions. We thank F. Slack for originally pointing out the let-7 complementary site in pri-let-7; the M. David lab for sharing their real-time PCR machine; P. Van Wynsberghe for the Δalg-1 primary let-7 plasmid; C. Mello for the worm fractionation protocol; E. Moss for LIN-28 antibodies; and A. Gorin, H. Jeng and S. Verma for technical assistance. Funding was provided by a Leukemia & Lymphoma Society Special Fellow Award 3611-11 (D.G.Z.); US National Institutes of Health (NIH) CMG and NIH/NCI T32 CA009523 Training Grants (Z.S.K.); the Swedish Board of Study Support (R.K.C.); and NIH grant GM071654, the Keck Foundation and the Peter Gruber Foundation (A.E.P.).

Author Contributions A.E.P., D.G.Z. and Z.S.K. designed the project and wrote the paper. D.G.Z. (Figs 1b, c, 2a, 3b, g and 4b–e and Supplementary Figs 2, 3a–c, 4a and 6a), Z.S.K. (Figs 1d, 2c, d and 3c and Supplementary Figs 3d, 4c, d, g and 6b), R.K.C. (Figs 2b, 3g and 4a and Supplementary Fig. 4b) and A.E.P. (Fig. 4a and Supplementary Fig. 7) performed the experiments and analysed the data. A.E.P. supervised the studies.

Author Information Reprints and permissions information is available at www.nature.com/reprints. The authors declare no competing financial interests. Readers are welcome to comment on the online version of this article at www.nature.com/nature. Correspondence and requests for materials should be addressed to A.E.P. (apasquinelli@ucsd.edu).

LETTER

doi:10.1038/nature11098

Generalized Lévy walks and the role of chemokines in migration of effector CD8$^+$ T cells

Tajie H. Harris[1], Edward J. Banigan[2], David A. Christian[1], Christoph Konradt[1], Elia D. Tait Wojno[1], Kazumi Norose[3], Emma H. Wilson[4], Beena John[1], Wolfgang Weninger[5,6], Andrew D. Luster[7], Andrea J. Liu[2] & Christopher A. Hunter[1]

Chemokines have a central role in regulating processes essential to the immune function of T cells[1–3], such as their migration within lymphoid tissues and targeting of pathogens in sites of inflammation. Here we track T cells using multi-photon microscopy to demonstrate that the chemokine CXCL10 enhances the ability of CD8$^+$ T cells to control the pathogen *Toxoplasma gondii* in the brains of chronically infected mice. This chemokine boosts T-cell function in two different ways: it maintains the effector T-cell population in the brain and speeds up the average migration speed without changing the nature of the walk statistics. Notably, these statistics are not Brownian; rather, CD8$^+$ T-cell motility in the brain is well described by a generalized Lévy walk. According to our model, this unexpected feature enables T cells to find rare targets with more than an order of magnitude more efficiency than Brownian random walkers. Thus, CD8$^+$ T-cell behaviour is similar to Lévy strategies reported in organisms ranging from mussels to marine predators and monkeys[4–10], and CXCL10 aids T cells in shortening the average time taken to find rare targets.

T. gondii is an opportunistic pathogen that causes encephalitis in patients with acquired defects in T-cell function[11]. Several studies have established that resistance to this parasite in the central nervous system (CNS) relies on T-cell production of interferon (IFN)-γ and cytotoxic T cells, but little is known about the factors that regulate the behaviour of effector T cells at this site[12–14]. To understand the role of chemokines in directing T cells to regions of infection during toxoplasmic encephalitis, real-time PCR (rtPCR) was performed to assess changes in chemokine-receptor expression in the brains of infected mice (Supplementary Fig. 1a). Notably, messenger RNA transcripts for CXCR3, a receptor expressed by activated and memory T cells and associated with T-helper 1 (T_H1)-type responses[15,16] and its ligands, CXCL9 and CXCL10, were highly expressed during toxoplasmic encephalitis (Fig. 1a). Previous studies have demonstrated extensive production of *Cxcl10* mRNA by activated astrocytes during toxoplasmic encephalitis[17]. Analysis of lymphocytes isolated from the brains of mice infected with ovalbumin (OVA)-expressing Prugniaud-strain (Pru^{OVA}) tachyzoites showed that CD8$^+$ T cells, including those specific for ovalbumin, express CXCR3 (Fig. 1b) and migrate towards CXCL10 *ex vivo* (Fig. 1c). Thus, parasite-specific CD8$^+$ T cells present in the CNS during toxoplasmic encephalitis are responsive to CXCR3 ligands.

Although CXCL10 is required for resistance to acute *T. gondii* infection[18], little is known about how this molecule affects T-cell responses during chronic toxoplasmic encephalitis. Therefore, we treated chronically infected mice with anti-CXCL10 antibodies. One week later, mononuclear cells from the brain were isolated, and T cells were quantified by flow cytometry. Anti-CXCL10 treatment led to a 40% decrease in the number of CD8$^+$ T cells (Fig. 2a, $P = 0.04$) and an increase in parasite burden (Fig. 2b, $P = 0.04$). Immunohistochemical staining for *T. gondii* showed latent cyst forms in control mice (Fig. 2c), whereas regions of active parasite replication were observed in the brains of anti-CXCL10-treated mice (Fig. 2d). To address the role of CXCL10 in the recruitment and maintenance of antigen-specific T cells in the CNS, we used an adoptive-transfer system. *In vitro*-activated OVA-specific OT-I cells were transferred to mice chronically infected with Pru^{OVA}, resulting in the migration and accumulation of these cells within the CNS[19]. When OT-I T cells were transferred to chronically infected wild-type C57BL/6 or *Cxcl10*-deficient mice, knockout mice had 60% fewer transferred cells in the brain in comparison to wild-type mice, whereas equivalent numbers were recovered from the spleen and lymph node in both groups (Supplementary Fig. 1b, c). Similar results were obtained when *Cxcr3*$^{-/-}$ and wild-type OT-I cells were transferred to wild-type mice chronically infected with Pru^{OVA} (Supplementary Fig. 1d, e).

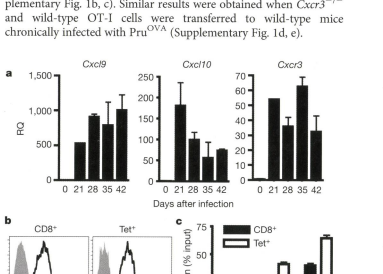

Figure 1 | Chemokine and chemokine receptor expression in the brain during chronic toxoplasmosis. C57BL/6 mice were infected with Pru^{OVA} and RNA was isolated from whole brain tissue. **a**, rtPCR specific for *Cxcl9*, *Cxcl10* and *Cxcr3* was performed and normalized to *Hprt* mRNA. Results are depicted as mean and s.e.m. of fold increase over uninfected brain. Data are representative of two independent experiments with three mice per group. RQ, relative quantity. **b**, Brain mononuclear cells were purified on day 35 after infection. CXCR3 expression (solid line) by CD8$^+$ and K^b-SIINFEKL$^+$ (tet$^+$) cells was measured by flow cytometry. The grey histogram represents the fluorescence minus one control. Data are representative of three independent experiments. **c**, Purified brain mononuclear cells were used in *ex vivo* chemotaxis assays. The mean and s.e.m. percentage of cells that migrated towards CXCL10 are depicted. Results are representative of three independent experiments.

[1]Department of Pathobiology, School of Veterinary Medicine, University of Pennsylvania, 380 South University Avenue, Philadelphia, Pennsylvania 19104, USA. [2]Department of Physics and Astronomy, School of Arts and Sciences, University of Pennsylvania, 209 South 33rd Street, Philadelphia, Pennsylvania 19104, USA. [3]Department of Infection and Host Defense, Graduate School of Medicine, Chiba University 1-8-1, Inohana, Chuo-ku, Chiba 260-8670, Japan. [4]Division of Biomedical Sciences, University of California-Riverside, Riverside, California 92521, USA. [5]The Centenary Institute, Newtown, New South Wales 2042, Australia. [6]Discipline of Dermatology, Sydney Medical School, Sydney, New South Wales 2006, Australia. [7]Center for Immunology and Inflammatory Diseases, Division of Rheumatology, Allergy and Immunology, Massachusetts General Hospital, Building 149, 13th Street, Room 8301, Charlestown, Massachusetts 02129, USA.

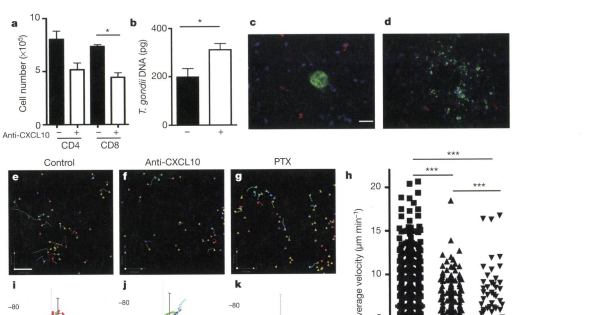

Figure 2 | CXCL10 affects the CD8$^+$ T-cell population and the control of parasite replication. a, **b**, Mice chronically infected with Pru^{OVA} were treated with anti-CXCL10 (+) antibody or control antibody (−). T cells isolated from the brain were identified by flow cytometry (**a**) and parasite burden was measured in the brain using rtPCR (**b**). Results are depicted as mean and s.e.m. of three independent experiments, with 3–4 mice per group. *$P \leq 0.05$, paired Student's *t*-test. **c**, **d**, Immunohistochemical staining of brain sections for *T. gondii* (green), CD8 (red) and 4′,6-diamidino-2-phenylindole (DAPI; blue) in anti-CXCL10-treated mice (**c**) and control animals (**d**). Scale bar, 20 μm. OT-I^{GFP} cells were expanded *in vitro* and transferred to mice chronically infected with Pru^{OVA} parasites. On day 7 after transfer, brains from mice that received PBS (control), 300 μg anti-CXCL10, or 8 μg PTX intraperitoneally (i.p.) were imaged in three dimensions over 10 min. **e**–**g**, Representative cells tracks from control (**e**), anti-CXCL10-treated (**f**), and PTX-treated (**g**) mice are shown. Scale bar, 100 μm. **h**, Volocity software was used to calculate the average track velocity (the average over all cells of the total displacement divided by the total observation time). Ctrl, control. **i**–**k**, Cell motility was visualized by plotting individual cell tracks from the origin from control (**i**), anti-CXCL10-treated (**j**) and PTX-treated (**k**) mice. ***$P < 0.001$ by one-way analysis of variance. Cell track data were obtained from three independent experiments with two mice per group. Control, 12 movies, $n = 507$ cells; anti-CXCL10, 10 movies, $n = 280$ cells; and PTX, 7 movies, $n = 192$ cells.

These studies show that CXCL10 and CXCR3 are required for optimal recruitment and/or retention of antigen-specific CD8$^+$ T cells in the CNS during toxoplasmic encephalitis. To determine whether CXCL10 and chemokine signals also affect the migration of CD8$^+$ T cells once they enter the CNS, we used multi-photon imaging to track green fluorescent protein (GFP)-expressing OT-I T cells (OT-I^{GFP}) in explant brain after short-term anti-CXCL10 treatment (Supplementary Movies 1 and 2). In addition, chemokine signals were inhibited using pertussis toxin (PTX), an inhibitor of $G\alpha_i$ signalling[2] (Supplementary Movie 3). We imaged cells for 10–30 min because cells migrate out of the field of view during longer imaging periods, biasing our sample towards cells that are less motile. Analysis of the cell tracks (Fig. 2e–g) showed that anti-CXCL10 treatment reduced the average cell velocity by 23%, from 6.35 μm min^{-1} in control-treated mice to 4.88 μm min^{-1} (Fig. 2h), whereas PTX reduced the track velocity by 46% to 3.45 μm min^{-1}. Plots of individual cell tracks demonstrate that cells cover less area over a 10-minute time span in the absence of CXCL10 or when treated with PTX (Fig. 2i–k).

We performed a standard analysis to determine quantitatively how chemokines affect the migratory behaviour of CD8$^+$ T cells by extracting the motility coefficient (Supplementary Fig. 2). This analysis implicitly assumes a Brownian walk, as the motility coefficient is extracted from the slope of the best linear fit to the mean-squared displacement (m.s.d.), $\langle r^2(t)\rangle$, as a function of time, *t* (ref. 20). However, when we plot the m.s.d. on a log–log plot, it grows with time approximately as t^{α}, with $\alpha \approx 1.4$ (Fig. 3a). This finding suggests that the T-cell tracks are not Brownian walks.

To determine the type of random walk that best describes the migration data, we focused not only on the behaviour of the m.s.d., but also on the shape of the tracks; the probability distribution $P(\mathbf{r}(t))$ of cell displacements, $\mathbf{r}(t)$, as a function of the time interval, *t*; and the decay of normalized displacement correlations, $\langle \hat{X}(\tau,t)\rangle = \langle \mathbf{r}(0,t)\cdot\mathbf{r}(\tau,\tau+t)\rangle / \langle r^2(0,0)\rangle$, as a function of τ, where $\mathbf{r}(\tau,\tau+t)$ is the displacement between times τ and $\tau + t$. Together, these properties provide a more complete description of the walk statistics than the m.s.d. alone, and therefore provide far more constraints that must be satisfied by a candidate random-walk model. First, by analysing statistics of the cell-trajectory shapes, we established that CD8$^+$ T cells do not exhibit directional migration on the time and length scales relevant to this experiment (see Supplementary Fig. 3 and Supplementary Discussion). To analyse the displacement distribution, we introduced a time-dependent variable, $\zeta(t)$, to scale the cell displacements. For Brownian walks, the distribution, $\hat{P}(\rho)$, of scaled displacements, $\rho(t) \equiv r(t)/\zeta(t)$, should be Gaussian, $\hat{P}(\rho) = \frac{1}{\sqrt{2\pi}} e^{-\rho^2/2}$, and the scale factor, $\zeta(t)$, should be the root m.s.d. (r.m.s.d.). However, for the migrating CD8$^+$ T cells, the distribution $\hat{P}(\rho)$ is not Gaussian (Fig. 3b, inset); the probability of large displacements is much larger than expected at all times studied. Notably, $\hat{P}(\rho)$ has the same shape at all times, indicating that the tracks are also not well described by persistent random walks. Moreover, the scale factor obeys $\zeta(t) \sim t^{\gamma}$, with $\gamma = 0.63$, and not $\gamma = 1/2$, as expected for Brownian walks (Fig. 3c), and clearly differs from the r.m.s.d. (Supplementary Fig. 4) at all times studied. Finally, the displacement correlations do not decay exponentially in time, as for Brownian walks (Fig. 3c, inset). Thus,

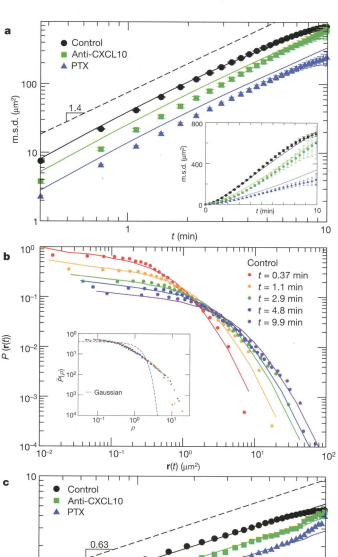

Figure 3 | CD8$^+$ T-cell migration tracks are consistent with generalized Lévy walks. **a**, We compare experimental data for cells in control (black circles), anti-CXCL10-treated (green squares), and PTX-treated (blue triangles) mice with results for the generalized Lévy walk model (solid lines). The m.s.d. grows nonlinearly in time, scaling approximately as t^{α}, where $\alpha \approx 1.4$ (dashed line). Inset shows linear plot of the m.s.d. Error bars denote s.e.m. **b**, The probability distributions, $P(\mathbf{r}(t))$, of T-cell displacements at several different times, t, for cells from control mice only. To avoid artefacts[30], histograms were constructed by placing 2,500, 2,000, 1,500, 1,300 or 600 displacements in each bin for $t = 0.37$ min, 1.1 min, 2.9 min, 4.8 min or 9.9 min, respectively. Inset shows that displacement probability distributions at different times collapse onto a single curve when the displacement is scaled by $\zeta(t)$. For comparison, a scaled Gaussian distribution is shown (dashed line). **c**, $\zeta(t)$, used to rescale displacements in **b** increases approximately as a power law, t^{γ}, where $\gamma \approx 0.63$. Inset shows that normalized displacement correlations, $\langle K(\tau,t)\rangle = \langle \mathbf{r}(0,t)\cdot\mathbf{r}(\tau,\tau+t)\rangle / \langle r^2(0,0)\rangle$, for control cells decay more slowly than exponentially (dashed line) with time τ.

Brownian walks do not describe effector T-cell migration during toxoplasmic encephalitis.

On the basis of these walk statistics, we considered several variations of Lévy walks (see Supplementary Table 1, Supplementary Fig. 5 and Supplementary Discussion). We find that, consistent with early observations of runs and pauses in lymphocytes[21], T-cell migration is well described by the following model of a generalized Lévy walk[22]. Walkers make straight runs at fixed velocity in random directions over distances chosen randomly from a Lévy distribution, $L_{\mu}(\ell) \sim \ell^{-\mu}$, with $\mu_{\mathrm{run}} = 2.15$. After each run, a walker pauses for a duration of time that is drawn from a Lévy distribution with $\mu_{\mathrm{pause}} = 1.7$. The values of the exponents μ_{run} and μ_{pause} were determined from a maximum-likelihood analysis[23] (see Supplementary Discussion). The model captures quantitatively the observed displacement distributions at different times (Fig. 3b), the time evolution of the m.s.d. and scale factor (Fig. 3a and c, respectively), the decay of displacement correlations (Fig. 3c, inset), and qualitative features of cell tracks (Supplementary Fig. 6). An Akaike weight analysis[24] indicates that the generalized Lévy walk model does a better job of fitting the displacement distributions than any of the other models we have considered, including, for example, bimodal correlated random walks[25] (see Supplementary Table 1, Supplementary Fig. 5 and Supplementary Discussion). The generalized Lévy walk model is consistent with our data over 30 min (Supplementary Fig. 7), and also describes the behaviour of polyclonal CD8$^+$ T cells, transgenic lymphocytic choriomeningitis virus-specific CD8$^+$ T cells migrating in the absence of cognate antigen, and CD8$^+$ T cells migrating in the brains of live animals (Supplementary Fig. 8).

In the absence of CXCL10 or signals through $G\alpha_i$-coupled receptors, the migration statistics for CD8$^+$ T cells are well described by the same generalized Lévy walk model, characterized by $\mu_{\mathrm{run}} = 2.15$ and $\mu_{\mathrm{pause}} = 1.7$ (Supplementary Figs 6 and 8), as for control cells, but with either a reduced instantaneous speed during runs or longer pauses. Therefore, the chemokine CXCL10 and signals through $G\alpha_i$-coupled receptors speed up migration without otherwise changing the walk statistics. This result, together with the fact that we find no evidence of directed migration over the timescales investigated (see Supplementary Discussion), suggests a chemokinetic role for CXCL10 during toxoplasmic encephalitis.

Previous studies have demonstrated that neutrophil or CD8$^+$ T-cell control of bacteria or tumour cells, respectively, can be understood by a rate equation in which the killing of targets is modelled as a collision-based process[26,27]. We incorporated the generalized Lévy walk statistics into a similar model to predict the time required to find rare target cells. In our model, we placed N generalized Lévy walkers randomly in a sphere of volume V with a target of radius a at the origin (Supplementary Fig. 9a). We find that cells migrating by generalized Lévy walks are considerably more efficient in finding target cells than those performing Brownian walks (Fig. 4 and Supplementary Fig. 9b, c). Here, the efficiency is the inverse of the sum of the displacements of all the walkers at the instant when the first walker reaches the target[28]. In the absence of CXCL10 or signals through $G\alpha_i$-coupled receptors, our model predicts that for estimated values of a, V and N, the capture time for a CD8$^+$ T cell to reach the target is increased by factors of 1.9 or 3.0, respectively, in comparison to the control setting (see Supplementary Fig. 9d–f and Supplementary Discussion). These results suggest that the ability of CD8$^+$ T cells to find and control *T. gondii*-infected targets in the CNS is aided by a generalized Lévy walk search strategy, and the capture time is shortened by CXCL10, and probably by other chemokines as well. We emphasize that the generalized Lévy walk is not necessarily an optimal search strategy, and a model with $\mu_{\mathrm{run}} = 2.0$ would be more efficient according to this definition[28]. Moreover, the efficiency is highly dependent on details of the environment and search/capture process[29] that are not presently known, so determination of the optimal search strategy remains an open question.

Lévy search strategies may be used by diverse species, including microzooplankton, fruitflies, honeybees, mussels, predatory fish, sea turtles, penguins and spider monkeys[4–10]. Our results show that a

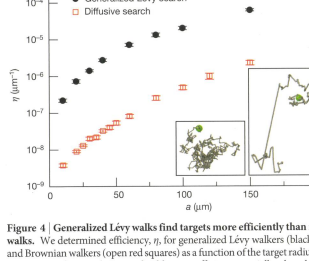

Figure 4 | Generalized Lévy walks find targets more efficiently than random walks. We determined efficiency, η, for generalized Lévy walkers (black circles) and Brownian walkers (open red squares) as a function of the target radius, a. The generalized Lévy search is considerably more efficient, especially when the targets are small. Error bars denote s.e.m. Small inset shows an example trajectory for Brownian walks and the large inset shows the generalized Lévy walk model.

generalization of this search strategy seems to be relevant, at the single-cell level, to the ability of effector cells to find rare targets. In addition, our findings provide a new insight into the role of CXCL10 as a chemokine that specifically influences the capture time for $CD8^+$ T cells to find infected targets during toxoplasmic encephalitis. Altogether, our findings raise several fundamental questions as to whether lymphocytes execute generalized Lévy walks in other environments, how activation status affects walk statistics, and whether the pauses suggested by our model arise from factors internal to the cell or from interactions of the cells with their external environment.

METHODS SUMMARY

T. gondii infection was established by intraperitoneal injection of Pru^{OVA}. rtPCR was performed for chemokine receptor expression and *T. gondii* DNA quantification. Brain mononuclear cells were stained with fluorescently conjugated antibodies for flow-cytometric analysis. OT-I cells were activated *in vitro* and transferred to recipient mice. Mice were treated with four doses of 100 μg anti-CXCL10 for week-long depletion studies or 300 μg 18 h before imaging studies. PTX was administered at 400 μg kg^{-1} 6 h before imaging. For multi-photon microscopy, explant brain was imaged using a Leica SP5 2-photon microscopy system. Cell tracking was performed using Volocity software. To create displacement histograms without binning artefacts[30] (Supplementary Tables 2 and 3), a constant number of displacements were placed in each bin. Various statistical methods were applied to test the validity of the generalized Lévy walk model (see Fig. 3, Supplementary Figs 3, 5, 7, 8, 10, Supplementary Table 1 and Supplementary Discussion). Brownian dynamics-like simulations were performed to simulate the general behaviour and searching capability of Gaussian ('random') and Lévy walkers (see Supplementary Discussion). N searchers were placed in a spherical volume of radius b, and they moved stochastically until finding the target of radius a, which was stationary at the centre of the sphere. During random walks, searchers moved $6D\Delta t = 0.1$ μm in the x-, y-, or z-direction each time step; here D is the motility coefficient and Δt is the time step. In Lévy walk simulations, a direction for a run was chosen at random, and run lengths were drawn from a Lévy distribution with exponent $\mu_{\text{sim}} = 2.15$. Searchers moved a distance $v\Delta t$ each time step until the run was completed. After each run, the walker paused for a time drawn from Lévy distribution with $\mu_{\text{pause}} = 1.7$.

Full Methods and any associated references are available in the online version of the paper at www.nature.com/nature.

Received 26 July 2011; accepted 30 March 2012.
Published online 27 May 2012.

1. Bromley, S. K., Mempel, T. R. & Luster, A. D. Orchestrating the orchestrators: chemokines in control of T cell traffic. *Nature Immunol.* **9,** 970–980 (2008).
2. Cyster, J. G. Chemokines, sphingosine-1-phosphate, and cell migration in secondary lymphoid organs. *Annu. Rev. Immunol.* **23,** 127–159 (2005).
3. Ebert, L. M., Schaerli, P. & Moser, B. Chemokine-mediated control of T cell traffic in lymphoid and peripheral tissues. *Mol. Immunol.* **42,** 799–809 (2005).
4. Bartumeus, F., Peters, F., Pueyo, S., Marrase, C. & Catalan, J. Helical Lévy walks: adjusting searching statistics to resource availability in microzooplankton. *Proc. Natl Acad. Sci. USA* **100,** 12771–12775 (2003).
5. Reynolds, A. M. & Frye, M. A. Free-flight odor tracking in *Drosophila* is consistent with an optimal intermittent scale-free search. *PLoS ONE* **2,** e354 (2007).
6. Humphries, N. E. *et al.* Environmental context explains Lévy and Brownian movement patterns of marine predators. *Nature* **465,** 1066–1069 (2010).
7. de Jager, M., Weissing, F. J., Herman, P. M. J., Nolet, B. A. & van de Koppel, J. Lévy walks evolve through interaction between movement and environmental complexity. *Science* **332,** 1551–1553 (2011).
8. Boyer, D. *et al.* Scale-free foraging by primates emerges from their interaction with a complex environment. *Proc. R. Soc. Lond. B* **273,** 1743–1750 (2006).
9. Reynolds, A. M. *et al.* Displaced honey bees perform optimal scale-free search flights. *Ecology* **88,** 1955–1961 (2007).
10. Sims, D. W. *et al.* Scaling laws of marine predator search behaviour. *Nature* **451,** 1098–1102 (2008).
11. Montoya, J. G. & Liesenfeld, O. Toxoplasmosis. *Lancet* **363,** 1965–1976 (2004).
12. Denkers, E. Y. *et al.* Perforin-mediated cytolysis plays a limited role in host resistance to *Toxoplasma gondii*. *J. Immunol.* **159,** 1903–1908 (1997).
13. Gazzinelli, R., Xu, Y., Hieny, S., Cheever, A. & Sher, A. Simultaneous depletion of $CD4^+$ and $CD8^+$ T lymphocytes is required to reactivate chronic infection with *Toxoplasma gondii*. *J. Immunol.* **149,** 175–180 (1992).
14. Suzuki, Y., Orellana, M. A., Schreiber, R. D. & Remington, J. S. Interferon-γ: the major mediator of resistance against *Toxoplasma gondii*. *Science* **240,** 516–518 (1988).
15. Sallusto, F., Geginat, J. & Lanzavecchia, A. Central memory and effector memory T cell subsets: function, generation, and maintenance. *Annu. Rev. Immunol.* **22,** 745–763 (2004).
16. Sallusto, F., Lanzavecchia, A. & Mackay, C. R. Chemokines and chemokine receptors in T-cell priming and Th1/Th2-mediated responses. *Immunol. Today* **19,** 568–574 (1998).
17. Strack, A., Schluter, D., Asensio, V. C., Campbell, I. L. & Deckert, M. Regulation of the kinetics of intracerebral chemokine gene expression in murine Toxoplasma encephalitis: impact of host genetic factors. *Glia* **40,** 372–377 (2002).
18. Khan, I. A. *et al.* IP-10 is critical for effector T cell trafficking and host survival in *Toxoplasma gondii* infection. *Immunity* **12,** 483–494 (2000).
19. Wilson, E. H. *et al.* Behavior of parasite-specific effector $CD8^+$ T cells in the brain and visualization of a kinesis-associated system of reticular fibers. *Immunity* **30,** 300–311 (2009).
20. Cahalan, M. D. & Parker, I. Choreography of cell motility and interaction dynamics imaged by two-photon microscopy in lymphoid organs. *Annu. Rev. Immunol.* **26,** 585–626 (2008).
21. Miller, M. J., Wei, S. H., Parker, I. & Cahalan, M. D. Two-photon imaging of lymphocyte motility and antigen response in intact lymph node. *Science* **296,** 1869–1873 (2002).
22. Zumofen, G. & Klafter, J. Laminar–localized-phase coexistence in dynamical systems. *Phys. Rev. E* **51,** 1818–1821 (1995).
23. Newman, M. E. J. Power laws, Pareto distributions and Zipf's law. *Contemp. Phys.* **46,** 323–351 (2005).
24. Johnson, J. B. & Omland, K. S. Model selection in ecology and evolution. *Trends Ecol. Evol.* **19,** 101–108 (2004).
25. Potdar, A. A., Lu, J., Jeon, J., Weaver, A. M. & Cummings, P. T. Bimodal analysis of mammary epithelial cell migration in two dimensions. *Ann. Biomed. Eng.* **37,** 230–245 (2009).
26. Budhu, S. *et al.* $CD8^+$ T cell concentration determines their efficiency in killing cognate antigen-expressing syngeneic mammalian cells *in vitro* and in mouse tissues. *J. Exp. Med.* **207,** 223–235 (2010).
27. Li, Y., Karlin, A., Loike, J. D. & Silverstein, S. C. Determination of the critical concentration of neutrophils required to block bacterial growth in tissues. *J. Exp. Med.* **200,** 613–622 (2004).
28. Viswanathan, G. M. *et al.* Optimizing the success of random searches. *Nature* **401,** 911–914 (1999).
29. Reynolds, A. M. & Bartumeus, F. Optimising the success of random destructive searches: Lévy walks can outperform ballistic motions. *J. Theor. Biol.* **260,** 98–103 (2009).
30. Sims, D. W., Righton, D. & Pitchford, J. W. Minimizing errors in identifying Lévy flight behaviour of organisms. *J. Anim. Ecol.* **76,** 222–229 (2007).

Supplementary Information is linked to the online version of the paper at www.nature.com/nature.

Acknowledgements This work was supported by grants from the National Institutes of Health AI-41158 (C.A.H.), AI-42334 (C.A.H.), EY-021314 (C.A.H.), T32-AI-055400 (T.H.H.), AI-081478 (T.H.H.), CA-069212 (A.D.L.), RNS-072298 (E.H.W.) and AI-090234 (B.J.); the National Science Foundation DMR-0520020 (E.J.B.) and DMR-1104637 (E.J.B. and A.J.L.); the state of Pennsylvania; Japan Society for the Promotion of Science Grant-in-Aid for Scientific Research Grant 20592071 (K.N.); and the Ministry of Education, Culture, Sports, Science and Technology of Japan (K.N.). We acknowledge L. Zhang and the Penn Vet Imaging Facility for technical assistance.

Author Contributions T.H.H. and E.J.B. contributed equally to this work. T.H.H. performed the immunological *in vivo* and imaging studies and wrote the paper. E.J.B. performed analysis of T-cell migration and designed the mathematical model. K.N. and E.D.T.W. collected data. A.J.L. and C.A.H. were involved in study design and contributed equally. All authors discussed the results and commented on the manuscript.

Author Information Reprints and permissions information is available at www.nature.com/reprints. The authors declare no competing financial interests. Readers are welcome to comment on the online version of this article at www.nature.com/nature. Correspondence and requests for materials should be addressed to A.J.L. (ajliu@physics.upenn.edu) or C.A.H. (chunter@vet.upenn.edu).

LETTER

doi:10.1038/nature11132

PPAR-γ is a major driver of the accumulation and phenotype of adipose tissue T_{reg} cells

Daniela Cipolletta[1], Markus Feuerer[3]†, Amy Li[1], Nozomu Kamei[2]†, Jongsoon Lee[2], Steven E. Shoelson[2], Christophe Benoist[1] & Diane Mathis[1]

Obesity and type-2 diabetes have increased markedly over the past few decades, in parallel. One of the major links between these two disorders is chronic, low-grade inflammation[1]. Prolonged nutrient excess promotes the accumulation and activation of leukocytes in visceral adipose tissue (VAT) and ultimately other tissues, leading to metabolic abnormalities such as insulin resistance, type-2 diabetes and fatty-liver disease. Although invasion of VAT by pro-inflammatory macrophages is considered to be a key event driving adipose-tissue inflammation and insulin resistance, little is known about the roles of other immune system cell types in these processes. A unique population of VAT-resident regulatory T (T_{reg}) cells was recently implicated in control of the inflammatory state of adipose tissue and, thereby, insulin sensitivity[2]. Here we identify peroxisome proliferator-activated receptor (PPAR)-γ, the 'master regulator' of adipocyte differentiation, as a crucial molecular orchestrator of VAT T_{reg} cell accumulation, phenotype and function. Unexpectedly, PPAR-γ expression by VAT T_{reg} cells was necessary for complete restoration of insulin sensitivity in obese mice by the thiazolidinedione drug pioglitazone. These findings suggest a previously unknown cellular mechanism for this important class of thiazolidinedione drugs, and provide proof-of-principle that discrete populations of T_{reg} cells with unique functions can be precisely targeted to therapeutic ends.

A unique population of $Foxp3^+$ $CD4^+$ T_{reg} cells was recently found in the VAT of normal individuals[2], at a much higher fraction of the $CD4^+$ T-cell compartment than that usually observed in lymphoid or other non-lymphoid tissues. VAT T_{reg} cells had a readily distinguishable phenotype from that of their counterparts in the spleen and lymph nodes, including a distinct gene expression profile, T-cell receptor repertoire, and pattern of chemokine and chemokine receptor expression. Adipose tissue inflammation and both local and systemic metabolic indices were improved or worsened by global enrichment or impoverishment, respectively, of T_{reg} cells[2–4]. However, a lack of appropriate reagents has so far precluded an assessment of the precise role of fat-resident T_{reg} cells.

The molecules that orchestrate the distinctive properties of VAT T_{reg} cells are unknown. Comparing the gene expression profiles of mouse visceral fat and lymphoid organ T_{reg} cells, we were struck by the increased level of transcripts encoding the nuclear receptor PPAR-γ in the former (Fig. 1a and Supplementary Fig. 1a). The specificity of this increase was highlighted by a comparison of *Pparg* transcript levels across a large library of microarray data sets (more than 350) encompassing T cells of diverse subsets, activation statuses and localizations (Fig. 1b). Because of the crucial role of PPAR-γ in adipocyte differentiation, as well as its anti-inflammatory activities[5], we speculated that its expression in VAT T_{reg} cells might be responsible for at least some of their unique features.

To identify genes that were positively or negatively correlated with *Pparg* expression, we performed a clustering analysis across transcript profiles obtained from VAT and lymph node T_{reg} cells of mice differing in their metabolic state: either lean (C57Bl/6 (B6) animals of various ages kept on normal chow) or obese ($B6.Lep^{ob/ob}$ (ob/ob) animals of varying age on normal chow or B6 animals on a high-fat diet (HFD)) (Supplementary Fig. 1b, c). The set of loci whose expression was co- or anti-correlated with *Pparg* transcript levels encompassed the majority of those most strongly up- (red) or down- (blue) regulated, respectively, in visceral fat versus lymphoid tissue T_{reg} cells[2] (Fig. 1c). The co-clustered transcripts included many that encode chemokines or chemokine receptors involved in leukocyte migration and extravasation (for example, *Ccr1*, *Ccr3*, *Cxcr6*, *Cxcl2* and *Cxcl3*), several encoding molecules involved in lipid metabolism (*Pcyt1a* and *Dgat1*), and *Il10* transcripts.

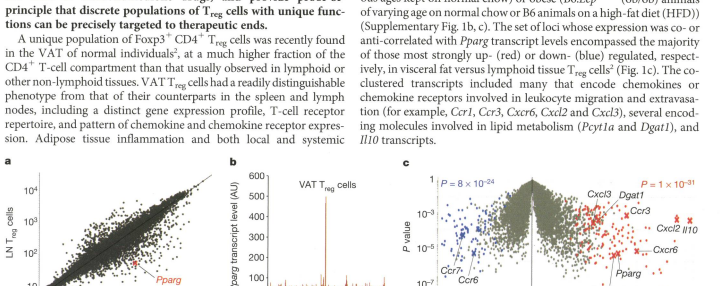

Figure 1 | Transcripts directly or inversely correlated with *Pparg* expression in VAT T_{reg} cells. a, Microarray analysis. Normalized expression values for transcripts isolated from T_{reg} cells from epididymal fat versus lymph node (LN) of 30-week-old retired-breeder B6 males (in triplicate). **b**, Expression of *Pparg* in a library of microarray data sets from diverse T-cell populations: different subsets, activation statuses or locations. AU, arbitrary units. **c**, A volcano plot comparing gene expression in VAT and lymph node T_{reg} cells of normal-chow-fed B6 mice. The *Pparg* co- and anti-cluster transcripts defined in Supplementary Fig. 1b are superimposed in red and blue, respectively. Some of the characteristic VAT T_{reg} genes are indicated. *P* values are from a chi-squared test.

[1]Division of Immunology, Department of Microbiology and Immunobiology, Harvard Medical School, Boston, Massachusetts 02115, USA. [2]Joslin Diabetes Center and Department of Medicine, Harvard Medical School, Boston, Massachusetts 02215, USA. †Present addresses: German Cancer Research Center (DKFZ), 69120 Heidelberg, Germany (M.F.); The University of Tokyo, Tokyo 113-8655, Japan (N.K.).

We directly evaluated the role of PPAR-γ in specifying the VAT T_{reg} cell phenotype by retrovirally transducing *Foxp3* alone or together with *Pparg* into naive $CD4^+$ T cells activated *in vitro* with anti-CD3/CD28-coated beads (neither transcription factor being expressed at detectable levels in the host $CD4^+$ T cells). Two isoforms of PPAR-γ have been described, referred to as PPAR-γ1 and PPAR-γ2 (ref. 5); although adipocytes are known to express both of them, the isoform(s) made by T lymphocytes is not well characterized. Feature-level analysis of *Pparg* transcripts, exploiting our existing Affymetrix ST 1.0 microarray data, showed that messenger RNAs corresponding to both PPAR-γ1 and PPAR-γ2 were expressed by VAT T_{reg} cells, with predominance of the former (Supplementary Fig. 2a), whereas the low-level transcripts made by the other T-cell populations primarily encoded PPAR-γ2 (not shown). Therefore, we evaluated the ability of each isoform to cooperate with Foxp3 to promote the VAT T_{reg} cell gene expression signature. Most transcripts are distributed in a grey cloud along the diagonal in the fold-change/fold-change (FC/FC) plot of Fig. 2a, showing that *Pparg1* and *Pparg2* induced the expression of a similar set of genes when co-transduced with *Foxp3*; the slight tilt towards the *x*-axis indicates that *Pparg1* transduction was slightly more potent. Each isoform promoted expression of the above-discussed *Pparg* co-cluster (red cloud along the diagonal), although only *Pparg1* repressed expression of the bulk of the *Pparg* anti-cluster (blue cloud along the *x*-axis). Similarly, as illustrated most clearly by the *Pparg* plus *Foxp3* versus *Foxp3* alone 'volcano plots' (Fig. 2b, c), each PPAR-γ isoform could collaborate with Foxp3 to upregulate a substantial fraction of the genes characteristic of the VAT T_{reg} cell up-signature (pink, skewed to the right in Fig. 2b, c). However, the corresponding down-signature was partially recapitulated only after *Pparg1* plus *Foxp3* transduction (green, skewed to the left in Fig. 2c but not in Fig. 2d).

Because adequate PPAR-γ ligand might not be available in this *in vitro* context, we explored the effect of adding a synthetic agonist, the thiazolidinedione (TZD) drug pioglitazone (Pio). Twenty-four hours after retroviral infection, double (*Pparg1* plus *Foxp3*, or *Pparg2* plus *Foxp3*) or single (*Foxp3* alone) transductants were treated with Pio for 48 h. The most notable effect of this agonist, whether in the context of *Pparg1* or *Pparg2*, was the augmentation of a set of 'lipid metabolism' genes, some of which were reported to be differentially expressed in VAT versus lymph node T_{reg} cells in a previous *ex vivo* microarray analysis[2]. This influence was most obvious on FC/FC plots (Fig. 2d, e), which isolate the effect of Pio in the context of each isoform (as aligned towards the *x*-axis). Upregulated genes involved in lipid metabolism included those coding for fatty-acid transporters (*Cd36* and *Slc27a2*), enzymes involved in fatty-acid synthesis (*Lipe* and *Scd1*), an enzyme essential for fatty-acid oxidation (*Cpt1a*), an enzyme responsible for the synthesis of triglycerides (*Dgat1*), and a lipid-droplet-associated protein (*Plin2*). Similar results were obtained with rosiglitazone, another TZD drug, or with GW1929, a potent non-TZD PPAR-γ agonist (Supplementary Fig. 2b, c; note change in axis labels compared with Fig. 2d, e). The fact that PPAR-γ could cooperate with Foxp3 to impose a VAT T_{reg} cell phenotype on naive $CD4^+$ T cells raised the question of whether the two transcription factors interact in some way. Indeed, both PPAR-γ isoforms were co-immunoprecipitated with Foxp3 in transduced HEK293 cells, arguing that they have the potential to interact, either directly or within a shared complex (Fig. 2f). (Unfortunately, we could not obtain adequate material from *ex vivo* T cells to perform an analogous experiment.)

To assess the importance of PPAR-γ for the VAT T_{reg} phenotype *in vivo*, we abrogated its expression specifically in T_{reg} cells by crossing a mouse line carrying 'floxed' *Pparg* with a line expressing the Cre recombinase under the dictates of *Foxp3* promoter/enhancer elements. The T_{reg} cell specificity of Cre expression in such mice has been validated in several contexts. At 25 weeks, the resulting mutants had lower fractions and numbers of VAT T_{reg} cells than their *Pparg* wild-type littermates (carrying the *Foxp3-Cre* transgene); by contrast, the

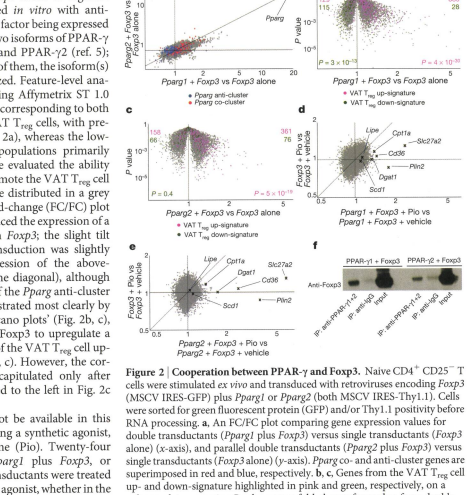

Figure 2 | Cooperation between PPAR-γ and Foxp3. Naive $CD4^+$ $CD25^-$ T cells were stimulated *ex vivo* and transduced with retroviruses encoding *Foxp3* (MSCV IRES-GFP) plus *Pparg1* or *Pparg2* (both MSCV IRES-Thy1.1). Cells were sorted for green fluorescent protein (GFP) and/or Thy1.1 positivity before RNA processing. **a**, An FC/FC plot comparing gene expression values for double transductants (*Pparg1* plus *Foxp3*) versus single transductants (*Foxp3* alone) (*x*-axis), and parallel double transductants (*Pparg2* plus *Foxp3*) versus single transductants (*Foxp3* alone) (*y*-axis). *Pparg* co- and anti-cluster genes are superimposed in red and blue, respectively. **b**, **c**, Genes from the VAT T_{reg} cell up- and down-signature highlighted in pink and green, respectively, on a volcano plot comparing *P* value versus fold-change for probes from double transductants (*Foxp3* and *Pparg1*, **c**; *Foxp3* and *Pparg2*, **d**) versus single transductants (*Foxp3* alone). The VAT T_{reg} cell up- and down-signatures were defined in Methods. *P* values from a chi-squared test. **d**, **e**, Twenty-four hours after transduction of naive $CD4^+$ T cells, cultures were treated with Pio (1 μM) for 48 h. FC/FC plots comparing gene expression values of Pio-treated versus vehicle-treated double transductants (*Pparg1* plus *Foxp3*, **d**; *Pparg2* plus *Foxp3*, **e**) (*x*-axis), and equivalent Pio-treated versus vehicle-treated single transductants (*Foxp3* alone) (*y*-axis). Some genes involved in lipid metabolism are indicated. Mean expression values calculated from three independent experiments. **f**, The association of Foxp3 with PPAR-γ was determined by co-immunoprecipitation. An anti-PPAR-γ1 + 2 antibody was used to immunoprecipitate (IP) PPAR-γ1 and PPAR-γ2 from nuclear lysates of HEK293 cells co-transduced with *Foxp3* and *Pparg1* or *Pparg2*. Immunoblots were probed with anti-Foxp3.

representation of T_{reg} cells in the lymphoid organs of mutants was normal (Fig. 3a). Although VAT T_{reg} cells in wild-type mice increased >2.5-fold between 15 and 25 weeks to eventually constitute more than 40% of the $CD4^+$ T cell compartment, this subset remained below ~10% in the mutant mice (Supplementary Fig. 3a). The T_{reg} cells remaining in the VAT (but not those in the spleen) of mutants had a lower mean fluorescence intensity (MFI) of Foxp3 expression than that of their wild-type counterparts (Supplementary Fig. 3b). A volcano plot comparing gene expression in VAT T_{reg} cells from *Pparg* wild-type and mutant mice showed the VAT T_{reg} cell up-signature (pink, skewed to the right) to be underrepresented in mutant T cells, whereas, conversely, the down-signature (green, skewed to the left) was over-represented (Fig. 3b). VAT and lymphoid organ T_{reg} cells were much more similar in the *Pparg* mutant than in the wild-type mice (Supplementary Fig. 3c); this difference reflected alterations at the level

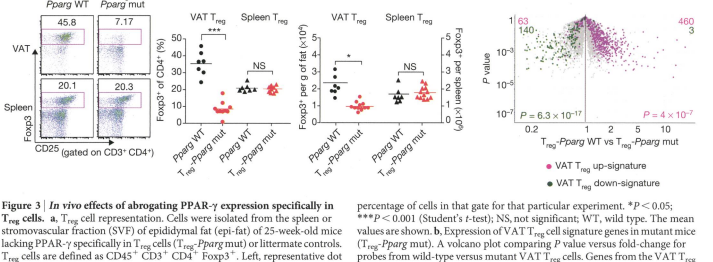

Figure 3 | *In vivo* effects of abrogating PPAR-γ expression specifically in T_{reg} cells. **a**, T_{reg} cell representation. Cells were isolated from the spleen or stromovascular fraction (SVF) of epididymal fat (epi-fat) of 25-week-old mice lacking PPAR-γ specifically in T_{reg} cells (T_{reg}-*Pparg* mut) or littermate controls. T_{reg} cells are defined as $CD45^+$ $CD3^+$ $CD4^+$ $Foxp3^+$. Left, representative dot plots (of at least three experiments); centre, summary data (for fraction of $CD4^+$ cells); right, cell numbers per g of tissue. Dot plot numbers indicate the percentage of cells in that gate for that particular experiment. $^*P < 0.05$; $^{***}P < 0.001$ (Student's *t*-test); NS, not significant; WT, wild type. The mean values are shown. **b**, Expression of VAT T_{reg} cell signature genes in mutant mice (T_{reg}-*Pparg* mut). A volcano plot comparing *P* value versus fold-change for probes from wild-type versus mutant VAT T_{reg} cells. Genes from the VAT T_{reg} up- and down-signature are highlighted in pink and green, respectively. *P* values from a chi-squared test.

of VAT T_{reg} cells, as the absence of PPAR-γ expression in lymph node T_{reg} cells had little impact (Supplementary Fig. 3d). This observation was confirmed at the protein level (Supplementary Fig. 4): downregulation of CCR2, GATA3, KLRG1 and CD69 in mutant versus wild-type VAT T_{reg} cells to resemble the lower levels in lymphoid tissue T_{reg} cells; upregulation of CD103 and CD86 in mutant VAT T_{reg} cells to approach the higher levels in lymphoid T_{reg} cells. Thus, PPAR-γ is an important factor controlling the accumulation and phenotype of T_{reg} cells residing in adipose tissue.

How the loss of PPAR-γ influences the turnover of T_{reg} cells residing in VAT is unclear. Addressing this issue was more complex than simply comparing the half-life of VAT T_{reg} cells in wild-type and mutant mice because the residual T_{reg} cells in the latter animals are likely to be atypical 'survivors' and/or recruits from the lymphoid T_{reg} cell pool exploiting a niche empty of the usual competitors. So we performed an acute assay, monitoring T_{reg} cell populations in wild-type mice over a few days of treatment with the irreversible PPAR-γ inhibitor GW9662 (Supplementary Fig. 5a). There were no significant differences in the VAT or spleen T_{reg} cell fraction or numbers in the drug- versus vehicle-treated animals (Supplementary Fig. 5b, c). However, there was a progressive decline in the fraction of $GATA3^+$ T_{reg} cells in VAT (but not in spleen), and a parallel decrease in the GATA3 MFI (Supplementary Fig. 5d, e). The GATA3 transcription factor is highly overrepresented in VAT versus lymphoid tissue T_{reg} cells, and is downregulated in the absence of PPAR-γ (Supplementary Fig. 4). Altogether, our data indicate that PPAR-γ may control both the establishment and the maintenance of the VAT T_{reg} cell phenotype.

Secondarily, the mutant mice had fractional and numerical increases in some, but not all, adipose tissue monocyte/macrophage subsets: pro-inflammatory $CD11b^+$ $CD11c^+$ $F4/80^+$ macrophages (Supplementary Fig. 6a, c) and pro-inflammatory $CD11b^+$ $Ly6c^{hi}$ monocytes (left panels in Supplementary Fig. 6b, d), but not $CD11b^+$ $Ly6c^{low}$ monocytes (right panels in Supplementary Fig. 6b, d), considered to be anti-inflammatory. There were no changes in the fractions or numbers of $CD8^+$ T or B cells in VAT of mutant mice (Supplementary Fig. 6e–h).

Pio is a well-known insulin-sensitizing agent that improves metabolic indices in obese mice and humans. Given its ability to enhance the unique fat T_{reg} cell signature in cultured cells (Fig. 2d, e), we wondered how this drug might affect VAT T_{reg} cells in obese (HFD-fed) mice. There was an impressive enrichment of the fraction and number of T_{reg} cells in epididymal adipose tissue of animals treated with Pio (Fig. 4a and Supplementary Fig. 7a); this effect was specific, and not seen in the spleen, subcutaneous fat, perirenal fat or liver (Fig. 4a and Supplementary Fig. 7b). There were also marked phenotypic changes in the epididymal fat T_{reg} cell population of Pio-treated and equivalent untreated obese mice: an overall shift of the gene expression profile towards that typical of VAT T_{reg} cells (Fig. 4b); an increase in the Foxp3 MFI (Supplementary Fig. 7c); a PPAR-γ-dependent enrichment of cells expressing GATA3 (Supplementary Fig. 7d); and enhanced cell-surface display of the lipid scavenger CD36 (Fig. 4c). As PPAR-γ ligands are known to stimulate oxidized low-density lipoprotein uptake by augmenting levels of CD36 on the surface of macrophages[6], we stained T_{reg} cells with Nile red, a dye that selectively binds to intracellular lipid droplets. VAT, but not spleen, T_{reg} cells readily took up lipids, especially in response to Pio (Fig. 4d). This process was PPAR-γ-dependent as the Pio-induced increase in CD36 expression and Nile red staining were both greatly dampened in *Pparg* mutant mice (Supplementary Fig. 7e, f). Thus, Pio accentuates the accumulation and phenotype of fat T_{reg} cells in epididymal fat depots of obese mice.

The marked increase in the representation of and alterations in the phenotype of VAT T_{reg} cells provoked by Pio treatment of obese mice raised the question of whether this population contributes to the insulin-sensitizing effect of Pio. In analogy to the human context, we compared immunological and metabolic parameters in obese (HFD-fed) *Pparg* wild-type and mutant mice as a function of Pio co-treatment. As anticipated, the VAT T_{reg} cell population of wild-type animals fed a HFD was quite low, and it increased substantially when Pio was included in the diet (Fig. 4e). Also as expected, the representation of VAT T_{reg} cells in mutant animals on a HFD was similar to that of their wild-type counterparts: a HFD in and of itself results in death and/or evacuation of typical VAT T_{reg} cells, so abrogation of PPAR-γ expression in this context has no further effect. Pio could not expand VAT T_{reg} cells in the mutant (Fig. 4e). Pio had differential effects on conventional adipose tissue monocyte/macrophage populations in HFD-fed mutant mice: pro-inflammatory macrophages ($CD11b^+$ $CD11c^+$ $F4/80^+$) were diminished, although not to the degree seen in wild-type littermates (Supplementary Fig. 8a); by contrast, pro-inflammatory monocytes ($CD11b^+$ $Ly6c^{hi}$) did not undergo their usual reduction (Supplementary Fig. 8b, left); whereas anti-inflammatory monocytes ($CD11b^+$ $Ly6c^{low}$) uncharacteristically declined (Supplementary Fig. 8b, right). Pio treatment of obese mutant mice was less effective than the treatment of their wild-type counterparts at normalizing systemic metabolic parameters: homeostatic model assessment of insulin resistance (Fig. 4f), glucose and insulin tolerance

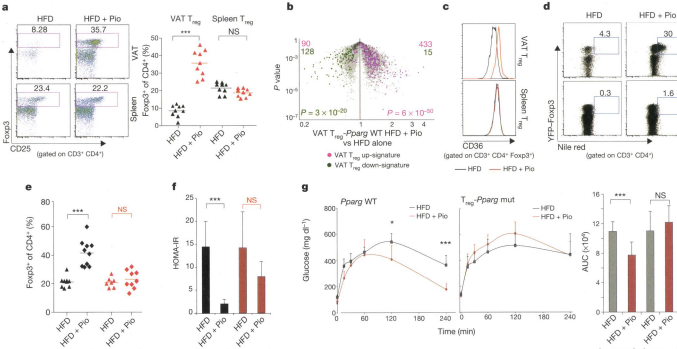

Figure 4 | Pio promotion of epididymal fat T_{reg} cell numbers and phenotype. At 9 weeks of age, wild-type and mutant *Pparg* mice (T_{reg}-*Pparg* mut) were fed a HFD with or without Pio for 13 weeks. Cells from the spleen and epididymal fat SVF were stained and analysed by flow cytometry. Numbers on dot plots indicate the percentage of cells in that gate for that particular experiment (representative of at least three experiments). **a**, T_{reg} cells from *Pparg* wild-type mice on a HFD with or without Pio. Left, representative dot plots; right, summary data. **b**, Expression of VAT T_{reg} cell signature genes in *Pparg* wild-type mice on a HFD with or without Pio. Volcano plot compares *P* value versus fold-change for probes from VAT T_{reg} cells isolated from *Pparg* wild-type mice on a HFD plus Pio versus a HFD alone. Genes from the VAT T_{reg} up- and down-signature are highlighted in pink and green, respectively. *P* values from a chi-squared test. **c**, MFI of CD36 expression by T_{reg} cells. ΔMFI indicates, for gated $CD3^+$ $CD4^+$ $Foxp3^+$ cells, the difference in CD36 expression for HFD-fed mice with or without Pio treatment. Epi-fat ΔMFI = 3,828 ± 1,362 (*$P = 0.039$); spleen ΔMFI = −182 ± 597 (NS). **d**, Cells were isolated from the spleen or epi-fat SVF of B6. *Foxp3-(YFP-)Cre* mice kept on a HFD with or without Pio for 13 weeks, and stained for CD3, CD4 and Nile red. YFP, yellow fluorescent protein. *$P = 0.01$. **e**, T_{reg} cell fraction. Cells from spleen or epi-fat SVF were stained and analysed by flow cytometry. **f**, Insulin sensitivity. Mice were assessed for blood fasting-glucose and fasting-insulin levels. These values were used to calculate the homeostatic model assessment of insulin resistance (HOMA-IR). **g**, Glucose tolerance. Left, intraperitoneal glucose tolerance test (GTT) on wild-type mice. Centre, GTT on mutant mice. Right, area under the curve (AUC) calculations. $n = 13$–14 mice per group. *$P < 0.05$, ***$P < 0.001$ (Student's *t*-test). Error bars denote mean ± s.d. for immunological parameters, mean ± s.e.m. for metabolic parameters, as is standard practice in the respective fields.

(Fig. 4g and Supplementary Fig. 8c), and phosphorylated (p)AKT levels in multiple organs (Supplementary Fig. 8d). At least some of the muted metabolic response to Pio reflected events in VAT, evidenced by the lack of normalization of pAKT values at that site. The Pio treatment clearly worked, however, as we observed in both wild-type and mutant drug-treated HFD-fed mice the expected increase in epididymal fat-pad weight (Supplementary Fig. 9a), although not in total body weight (not shown); a coupled decrease in adipocyte numbers and an increase in adipocyte size (Supplementary Fig. 9b, c); and increased levels of serum adiponectin and *Adipoq* transcripts (Supplementary Fig. 9d). Leptin (*Lep*) transcript levels were unchanged in both wild-type and HFD-fed individuals (Supplementary Fig. 9e), as anticipated[7].

The main conclusion from our results is that PPAR-γ is a major orchestrator of the unique properties of VAT T_{reg} cells. This nuclear receptor collaborates with Foxp3 to impose on naive $CD4^+$ T cells the transcriptional profile characteristic of VAT T_{reg} cells. Interestingly, both PPAR-γ isoforms can promote the fat T_{reg} up-signature in conjunction with Foxp3, but only isoform 1 drives the down-signature. This constitutes a rare dysjunction in the activities of the two PPAR-γ isoforms, which differ by only an extra 30 amino acids at the amino terminus of PPAR-γ2. Experimental manipulation of PPAR-γ specifically in $Foxp3^+$ cells had a clear and precise impact on the accumulation and phenotype of T_{reg} cells in epididymal fat depots. A newly discovered property was that VAT, but not lymphoid tissue, T_{reg} cells can take up lipids, an intriguing adaptation to the tissular environment, not shared by conventional T cells residing at the same site. It remains to be determined whether this feature promotes T_{reg} cell survival or effector functions, or whether it is an epiphenomenon.

Our data also indicate that PPAR-γ expressed by T_{reg} cells contributes substantially to the insulin-sensitizing activity of Pio. It was initially assumed, given the role of this transcription factor in fat-cell differentiation, that TZD drugs improve metabolic parameters in obese individuals by activating PPAR-γ in adipocytes. Although this notion has received experimental support[8], other studies have argued for the importance of PPAR-γ expression in macrophages[9,10], muscle[11] and the central nervous system[12,13]. On first consideration, it seems difficult to explain the need for PPAR-γ across such a broad range of cell types, but several points should be kept in mind. First, TZD drugs may affect several processes upstream of insulin resistance, for example, ingestive behaviour, adipocity and inflammation; PPAR-γ-driven programs in different cell types may influence these processes differentially. Second, abrogating PPAR-γ expression in different cell types seems to have organ-specific effects on insulin resistance[11–13]. And third, there is increasing appreciation that the gene promoters used to generate transgenic mouse lines with cell-type-specific ablation of PPAR-γ can be 'leaky'. Delineating the cell type(s) crucial for the protective effect of Pio on metabolic disorders is imperative given current concerns over the side effects of the TZD class of compounds and the resultant search for alternative drugs[14].

Lastly, our results provide proof-of-principle that it is possible to target a designated population of T_{reg} cells for a particular therapeutic goal. The emerging notion that the Foxp3$^+$ CD4$^+$ T_{reg} cell compartment includes several subtypes with distinct phenotypes, localizations and effector functions[15] has evoked the exciting possibility of developing strategies to expand or contract disease-relevant T_{reg} cells, leaving the bulk of the compartment intact to maintain immune homeostasis.

METHODS SUMMARY

Source and maintenance of mice are described in Methods. Experimentals and controls were always littermate-matched males (for example, *Pparg*$^{fl/fl}$-*Foxp3*$^{YFP\text{-}Cre}$ and *Pparg*^{wt}-*Foxp3*$^{YFP\text{-}Cre}$). HFD and normal-chow animals were fed a diet containing 60 kcal% and 10 kcal% fat, respectively. Mice on a HFD plus Pio were fed Pio at 100 mg per kg of food. Metabolic studies were performed on mice fed a HFD with or without Pio for 12 weeks. For GTTs, glucose (2.0 g per kg body weight) was administered by intraperitoneal (i.p.) injection after an overnight fast. For insulin tolerance tests, insulin (0.75 U) was administered by i.p. injection after 4 h of fasting.

CD4$^+$ CD25$^-$ T cells were activated for 48 h with anti-CD3/CD28 antibody-coated beads plus recombinant human IL-2 before retroviral transduction and cultured for 72 h after transduction. In selected experiments, 24 h after infection, transduced cells were treated with 1 μM Pio, rosiglitazone or GW1929, or with vehicle (dimethylsulphoxide) for 48 h before sorting. For T-cell analysis, cells were stained with anti-CD45, -CD3, -CD4, -CD8, -CD25 and sometimes anti-CD36, fixed, permeabilized and intracellularly stained for Foxp3 and GATA3. For intracellular lipids, cells were stained with anti-CD3, anti-CD4 and Nile red (1 μg ml^{-1}). RNA from double-sorted cells was prepared for microarray analysis[2], and hybridized to GeneChip Mouse Genome M1.0 ST arrays (Affymetrix).

Full Methods and any associated references are available in the online version of the paper at www.nature.com/nature.

Received 21 June 2011; accepted 3 April 2012.
Published online 16 May 2012.

1. Osborn, O. & Olefsky, J. M. The cellular and signaling networks linking the immune system and metabolism in disease. *Nature Med.* **18,** 363–374 (2012).
2. Feuerer, M. *et al.* Lean, but not obese, fat is enriched for a unique population of regulatory T cells that affect metabolic parameters. *Nature Med.* **15,** 930–939 (2009).
3. Winer, S. *et al.* Normalization of obesity-associated insulin resistance through immunotherapy. *Nature Med.* **15,** 921–929 (2009).
4. Ilan, Y. *et al.* Induction of regulatory T cells decreases adipose inflammation and alleviates insulin resistance in ob/ob mice. *Proc. Natl Acad. Sci. USA* **107,** 9765–9770 (2010).
5. Tontonoz, P. & Spiegelman, B. M. Fat and beyond: the diverse biology of PPARgamma. *Annu. Rev. Biochem.* **77,** 289–312 (2008).
6. Tontonoz, P. *et al.* PPARγ promotes monocyte/macrophage differentiation and uptake of oxidized LDL. *Cell* **93,** 241–252 (1998).
7. Miyazaki, Y. *et al.* Effect of pioglitazone on circulating adipocytokine levels and insulin sensitivity in type 2 diabetic patients. *J. Clin. Endocrinol. Metab.* **89,** 4312–4319 (2004).
8. Sugii, S. *et al.* PPARγ activation in adipocytes is sufficient for systemic insulin sensitization. *Proc. Natl Acad. Sci. USA* **106,** 22504–22509 (2009).
9. Hevener, A. L. *et al.* Macrophage PPARγ is required for normal skeletal muscle and hepatic insulin sensitivity and full antidiabetic effects of thiazolidinediones. *J. Clin. Invest.* **117,** 1658–1669 (2007).
10. Odegaard, J. I. *et al.* Macrophage-specific PPARγ controls alternative activation and improves insulin resistance. *Nature* **447,** 1116–1120 (2007).
11. Hevener, A. L. *et al.* Muscle-specific *Pparg* deletion causes insulin resistance. *Nature Med.* **9,** 1491–1497 (2003).
12. Ryan, K. K. *et al.* A role for central nervous system PPAR-γ in the regulation of energy balance. *Nature Med.* **17,** 623–626 (2011).
13. Lu, M. *et al.* Brain PPAR-γ promotes obesity and is required for the insulin-sensitizing effect of thiazolidinediones. *Nature Med.* **17,** 618–622 (2011).
14. Olefsky, J. M., Lazar, M. A. & Scherer, P. E. Antidiabetes wars: a new hope. *Nature Med.* **16,** 972–973 (2010).
15. Josefowicz, S. Z., Lu, L. F. & Rudensky, A. Y. Regulatory T cells: mechanisms of differentiation and function. *Annu. Rev. Immunol.* **30,** 531–563 (2012).

Supplementary Information is linked to the online version of the paper at www.nature.com/nature.

Acknowledgements We thank A. Rudensky, F. Gonzalez, R. Kahn, B. Spiegelman and D. Vignali for providing materials; K. Hattori, M. Davenport, J. LaVecchio, G. Buruzala, J. Ericson, K. Leatherbee and S. Davis for technical assistance; A. Ergun, A. Morton and J. Shu for experimental help; and M. Wilson and J. Hill for discussions. Supported by grants from the National Institutes of Health (NIH; DK092541) and Ellison Foundation (Boston) to D.M. and C.B., Dana Foundation to D.M. and S.E.S.; the American Diabetes Association (RA 110BS97) to J.L., and the NIH (DK51729) to S.E.S.; as well as by core facilities of the Joslin Diabetes Center (P30DK36836). M.F. received a postdoctoral fellowship from the King Trust.

Author Contributions All authors designed research; D.C. and A.L. performed research; D.C., S.E.S., C.B. and D.M. analysed data; D.C., C.B. and D.M. wrote the paper.

Author Information Microarray data have been deposited in the Gene Expression Omnibus under accession codes GSE37532, GSE37533, GSE37534 and GSE37535. Reprints and permissions information is available at www.nature.com/reprints. The authors declare competing financial interests: details accompany the full-text HTML version of the paper at www.nature.com/nature. Readers are welcome to comment on the online version of this article at www.nature.com/nature. Correspondence and requests for materials should be addressed to D.M. (cbdm@hms.harvard.edu).

LETTER

doi:10.1038/nature11147

Immune self-reactivity triggered by drug-modified HLA-peptide repertoire

Patricia T. Illing[1,2], Julian P. Vivian[3], Nadine L. Dudek[2], Lyudmila Kostenko[1], Zhenjun Chen[1], Mandvi Bharadwaj[1], John J. Miles[4,5], Lars Kjer-Nielsen[1], Stephanie Gras[3], Nicholas A. Williamson[2], Scott R. Burrows[4], Anthony W. Purcell[2]*, Jamie Rossjohn[3,5]* & James McCluskey[1,6]*

Human leukocyte antigens (HLAs) are highly polymorphic proteins that initiate immunity by presenting pathogen-derived peptides to T cells[1]. HLA polymorphisms mostly map to the antigen-binding cleft, thereby diversifying the repertoire of self-derived and pathogen-derived peptide antigens selected by different HLA allotypes[2]. A growing number of immunologically based drug reactions, including abacavir hypersensitivity syndrome (AHS) and carbamazepine-induced Stevens–Johnson syndrome (SJS), are associated with specific HLA alleles[3–7]. However, little is known about the underlying mechanisms of these associations, including AHS, a prototypical HLA-associated drug reaction occurring exclusively in individuals with the common histocompatibility allele *HLA-B*57:01*, and with a relative risk of more than 1,000 (refs 6, 7). We show that unmodified abacavir binds non-covalently to HLA-B*57:01, lying across the bottom of the antigen-binding cleft and reaching into the F-pocket, where a carboxy-terminal tryptophan typically anchors peptides bound to HLA-B*57:01. Abacavir binds with exquisite specificity to HLA-B*57:01, changing the shape and chemistry of the antigen-binding cleft, thereby altering the repertoire of endogenous peptides that can bind HLA-B*57:01. In this way, abacavir guides the selection of new endogenous peptides, inducing a marked alteration in 'immunological self'. The resultant peptide-centric 'altered self' activates abacavir-specific T-cells, thereby driving polyclonal CD8 T-cell activation and a systemic reaction manifesting as AHS. We also show that carbamazepine, a widely used anti-epileptic drug associated with hypersensitivity reactions in *HLA-B*15:02* individuals, binds to this allotype, producing alterations in the repertoire of presented self peptides. Our findings simultaneously highlight the importance of HLA polymorphism in the evolution of pharmacogenomics and provide a general mechanism for some of the growing number of *HLA*-linked hypersensitivities that involve small-molecule drugs.

Abacavir (Supplementary Fig. 1) is a guanosine-related pro-drug that causes reverse transcriptase chain termination in HIV-1 infection[8]. T cells carrying the CD8 antigen ($CD8^+$ T cells) from patients with resolved AHS, and from abacavir-naive, *HLA-B*57:01*$^+$ healthy donors, proliferate and acquire effector functions in response to abacavir *in vitro*[8]. Moreover, abacavir-specific T cells are not activated by antigen-presenting cells expressing the closely related natural allotypes HLA-B*57:03 (Asp114Asn; Ser116Tyr), HLA-B*57:02 (Asp114Asn; Ser116Tyr; Leu156Arg) and HLA-B*58:01 (Met45Thr; Ala46Glu; Val97Arg; Val103Leu)[8], suggesting that abacavir-HLA-B*57:01 specificity is particularly sensitive to the F-pocket architecture, namely residue 116. We examined the functional capacity of the natural allotype HLA-B*57:11, which differs from HLA-B*57:01 in the C/E pocket and environs (Ile94Thr; Ile95Leu; Val97Trp) to stimulate abacavir-specific T cells. Like HLA-B*57:03, HLA-B*57:02 and HLA-B*58:01 (ref. 8), HLA-B*57:11 was not functional in activating abacavir-specific T cells from HLA-B*57:01 donors (Fig. 1a), indicating that abacavir-HLA-B*57:01 specificity maps to the C-terminal end of the antigen-binding cleft (C, D, E and F pockets).

We speculated that abacavir, or a metabolite thereof, might either covalently modify a cellular protein or peptide to generate a novel immunogenic ligand or alter the peptide repertoire in some other way. Two of the most functionally important positions (114 and 116) controlling abacavir reactivity distinguish HLA-B*57:01 from HLA-B*57:03 (ref. 8), allowing us to probe how these positions alter the specificity of bound peptides and the impact of abacavir on the peptide repertoire. We therefore characterized the peptides bound to affinity-purified HLA-B*57:01 and HLA-B*57:03 molecules from untreated and abacavir-treated cell lines by mass spectrometry[9]. In abacavir-treated cells, reverse-phase high-performance liquid chromatography fractions from purified HLA-B*57:01, but not HLA-B*57:03, contained unmodified abacavir (Fig. 1b). Abacavir is a pro-drug, but none of its metabolites were detected by liquid chromatography–tandem mass spectrometry (LC–MS/MS) analysis of the eluted material. These findings indicated that abacavir itself interacted non-covalently and specifically with HLA-B*57:01.

The repertoire of self peptides presented by HLA-B*57:01, HLA-B*57:03 and HLA-B*58:01 in the presence and absence of abacavir was examined further (Fig. 2 and Supplementary Table 1). The sequence motif characteristic of peptides that bind HLA-B*57:01 (ref. 10) was verified to contain a Ser/Thr→Ala/Val at peptide position 2 (P2) and a Trp→Phe at the C terminus of the peptide (PΩ) (Supplementary Table 1). HLA-B*57:03 had the same P2 preference as HLA-B*57:01, but the PΩ preference was reversed with Phe→Trp (Supplementary Table 1). After treatment of antigen-presenting cells with abacavir we observed a change in the nature of the peptides bound to HLA-B*57:01, but not for peptides bound to HLA-B*57:03 or HLA-B*58:01 (Fig. 2a and Supplementary Table 1). This was characterized by an increase in the number of HLA-B*57:01 ligands with non-canonical Ile or Leu at PΩ (Fig. 2a and Supplementary Table 1). In contrast, no change was detected in the preferred P2 residues selected by HLA-B*57:01 (Fig. 2a and Supplementary Table 1) or the length of peptides recovered (Fig. 2b–d). These novel peptides represented about 20–25% of the recoverable peptide repertoire, indicating a massive shift in self-antigen presentation (Fig. 2a, e), which was consistent with the 33% estimated occupancy of HLA-B*57:01 complexed with abacavir (Supplementary Table 2a). The impact of F-pocket polymorphism on abacavir recognition by T cells (Fig. 1a), the co-purification of abacavir with HLA-B*57:01-peptide complexes (Fig. 1b) and the impact of abacavir on selection of PΩ residues

[1]Department of Microbiology & Immunology, University of Melbourne, Parkville, Victoria 3010, Australia. [2]Department of Biochemistry and Molecular Biology and Bio21 Molecular Science and Biotechnology Institute, University of Melbourne, Parkville, Victoria 3010, Australia. [3]Department of Biochemistry and Molecular Biology, School of Biomedical Sciences, Monash University, Clayton, Victoria 3800, Australia. [4]Queensland Institute of Medical Research and Australian Centre for Vaccine Development, Brisbane, Queensland 4029, Australia. [5]Institute of Infection and Immunity, Cardiff University School of Medicine, Heath Park, Cardiff CF14 4XN, UK. [6]Victorian Transplantation and Immunogenetics Service, Australian Red Cross Blood Service, 100–154 Batman Street, West Melbourne, Victoria 3003, Australia.
*These authors contributed equally to this work.

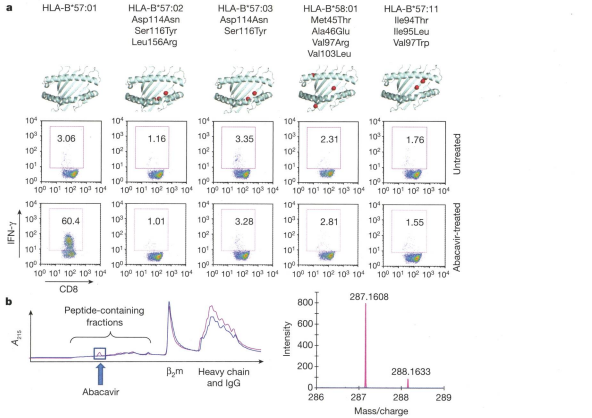

Figure 1 | Specificity of abacavir T-cell responses and binding to HLA-B*57:01. a, An abacavir-responsive T-cell line raised *in vitro* from an *HLA-B*57:01*$^+$ donor was re-stimulated with C1R or B-LCL antigen-presenting cells expressing the indicated HLA allotypes, in the presence or absence of abacavir[22]. Flow plots are shown of responding T cells gated for CD3 and co-stained for CD8 and IFN-γ. Boxed areas indicate the percentage of responding T cells. Schematics show the location of HLA polymorphisms. **b,** Separation of peptides from HLA-B*57:01 (magenta) and HLA-B*57:03 (blue) by reverse-phase high-performance liquid chromatography after treatment of cells with abacavir. Arrow indicates the standard retention time for abacavir. β_2m, β_2-microglobulin. Fractions were analysed by LC–MS/MS (right). Abacavir was detected in HLA-B*57:01 preparations (mass spectra: predicted $MH^+ = 287.1615$, Dmass (the mass difference between observed and theoretical) = 0.0007 a.m.u., 2 p.p.m. mass accuracy).

(Fig. 2a) led us to propose that abacavir bound specifically to the antigen-binding cleft of HLA-B*57:01. This is consistent with the dependence of abacavir presentation on TAP (transporter associated with antigen processing) and tapasin, implying a normal pathway of peptide loading[8]. This would result in a large proportion of the normal repertoire of peptides being sterically hindered from binding to and stabilizing HLA-B*57:01. The altered stereochemistry of the antigen-binding cleft facilitates the binding of a new repertoire of peptides containing immunogenic neo-epitopes. Consistent with this view, HLA-B*57:01 bound to peptides (Supplementary Table 2b) containing a PΩ-Trp did not further stabilize recombinant HLA-B*57:01 in the presence of abacavir. In contrast, for five of the neo-self peptides eluted specifically in the presence of abacavir, the corresponding refolded HLA-B*57:01–neo-self-peptide–abacavir complexes were approximately 5–10 °C more thermostable than the corresponding HLA-B*57:01–neo-self-peptide complexes (Supplementary Table 2b).

To test whether abacavir-specific T-cell reactivity was dependent on simultaneous presentation of abacavir and novel self peptides, we first established that T-cell-receptor (TCR) genes from a single abacavir-specific T-cell clone, transfected into Jurkat cells, specifically conferred reactivity to C1R-B*57:01 cells in the presence of abacavir (Supplementary Fig. 2a). Second, we examined the abacavir-specific T-cell response towards five neo-self peptides exclusively identified from HLA-B*57:01 complexes isolated from abacavir-treated cells. T-cell lines were raised from two different healthy *HLA-B*57:01*$^+$ donors and interferon-γ (IFN-γ) enzyme-linked immunosorbent spot (ELISPOT) assays were conducted using C1R-B*57:01 and T2-B*57:01 target cells with or without pretreatment with abacavir (Supplementary Fig. 2b). The addition of abacavir to T2-B*57:01 cells without the exogenous peptides did not activate T-cell clones. In contrast, the five pooled abacavir-dependent peptides added exogenously to the T2-B*57:01 cells in the presence of abacavir activated many T-cell clones (spot-forming units) in each of the two T-cell lines (Supplementary Fig. 2b). This data shows that self peptides bound to HLA-B*57:01 in the presence of abacavir specifically stimulate abacavir-responsive T cells. Thus, the selection of a novel HLA-B*57:01-peptide repertoire by abacavir exposes the normally self-tolerant T-cell compartment to previously unseen neo-self peptides resembling antigen presentation by allogeneic HLA molecules to T cells, as occurs in graft rejection[11] and graft-versus-host disease[12]. In these circumstances a diverse repertoire of αβ TCRs may be selected by responding T cells, reflecting reactivity towards the diverse array of novel self peptides bound to HLA-B*57:01. To test this hypothesis we examined the Vβ repertoire of the TCRs selected by abacavir-specific T cells in seven unrelated *HLA-B*57:01*$^+$ donors. Broadly polyclonal TCR usage (in which different T cell clones undergo expansion in response to abacavir) was observed in all donors (Fig. 3). In addition, for donors 6 and 7 the T-cell repertoire was assessed before and after stimulation with abacavir, revealing modest 'private' biases in immune repertoire that differed between these donors (Fig. 3; compare Vβ2 with Vβ8 in these donors before and after stimulation). Moreover, analysis of the antigen-binding complementarity-determining region 3 sequences in abacavir-specific TCRs did not reveal biased patterns (Supplementary Table 3). TCR selection was therefore consistent with the diverse array of stimulating ligands in abacavir-treated cells, with no evidence of TCR bias as frequently observed in T-cell responses to single, novel ligands[13]. This observation is distinct from the reported sharing of a narrow repertoire of drug-specific T cells reactive in *HLA-B*15:02*$^+$

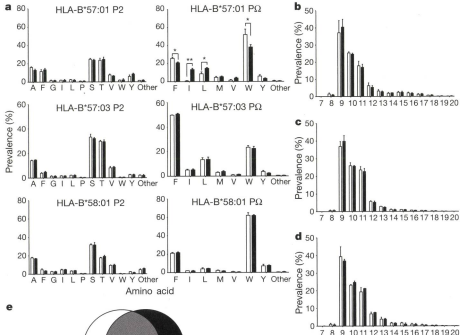

Figure 2 | Abacavir modifies the PΩ F-pocket anchor residue preference of HLA-B*57:01 but not that of HLA-B*57:03. a, Frequency of amino acids occurring at P2 and PΩ in nine-residue peptides eluted from HLA-B*57:01, HLA-B*57:03 and HLA-B*58:01. Asterisk, $P < 0.05$; two asterisks, $P < 0.001$ (unpaired Student's *t*-test). **b**–**d**, The distribution of peptide lengths from the data sets HLA-B*57:01 (**b**) HLA-B*57:03 (c) and HLA-B*58:01 (**d**). Filled and clear bars represent values from abacavir-treated and untreated cells, respectively. Values are derived from averaging prevalence across three replicate data sets of up to 3,000 distinct peptide sequences per condition. Error bars indicate s.d. across these data sets. **e**, The distribution of all peptides eluted from HLA-B*57:01 highlighting shared and unique peptides sequenced from untreated and abacavir-treated cells.

patients with carbamazepine-induced SJS or toxic epidermal necrolysis (TEN)[14]. The abacavir-specific, polyclonal TCR usage is consistent with the presentation of diverse neo-self peptides as a result of drug-induced 'altered self'.

Next we individually expressed and refolded HLA-B*57:01 in complex with two self peptides (LTTKLTNTNI, 'LTTK', cytochrome *c* oxidase subunit 2; RVAQLEQVYI, 'RVAQ', small nuclear ribonucleoprotein Sm D3) that had been exclusively isolated from HLA-B*57:01 in the presence of abacavir and both of which possessed the preferred PΩ residue, Ile, common in neo-peptides eluted in the presence of abacavir. Indeed, HLA-B*57:01 refolded extremely poorly with these self peptides in the absence of abacavir, which is consistent with the altered binding motif revealed by the peptide elution data. We crystallized the HLA-B*57:01–LTTK–abacavir and HLA-B*57:01–RVAQ–abacavir complexes and determined their structures to 1.9 Å and 1.6 Å resolution, respectively (Supplementary Table 4). The structure of the HLA-B*57:01–LTTK–abacavir complex was very similar to that of the HLA-B*57:01–RVAQ–abacavir complex (Supplementary Fig. 3a), revealing that the mode of abacavir binding is conserved when disparate abacavir-specific self peptides are presented by HLA-B*57:01. The HLA-B*57:01–LTTK–abacavir complex closely resembled the structure of the previously reported complex of HLA-B*57:01 with the self peptide LSSPVTKSF (ref. 8). Thus, the presence of abacavir, which was unambiguously observed to be non-covalently bound within the antigen-binding cleft (Fig. 4a, b), did not markedly alter the conformation of the antigen-binding cleft itself. Moreover, the conformation of the bound peptide, although not sitting as deep within the antigen-binding cleft as the LTTK self peptide, nevertheless adopted a slightly bulged conformation that was reminiscent of how longer major histocompatibility complex (MHC) class I peptides (more than 10 residues long)[15] can bind within the antigen-binding cleft (Fig. 4b).

Within the HLA-B*57:01–LTTK–abacavir and HLA-B*57:01–RVAQ–abacavir complexes, abacavir was bound in an extended manner, at the base of the antigen-binding cleft, in which the plane of the aromatic rings were positioned approximately diagonally across the cleft's β-sheet, with the cyclopentyl and purinyl moieties located in the D and E pockets, respectively, while the cyclopropyl moiety extended towards, and protruded into, the F pocket (Fig. 4c–e). The binding of abacavir did not impinge on the B pocket, which is consistent with the unchanged anchor preference at this site in abacavir-treated cells (Fig. 2a). However, the conformation of abacavir within the cleft provided a basis for understanding the global peptide repertoire shift induced by the drug, in that abacavir resided within several HLA-B*57:01 binding pockets (C, D, E and F), thereby affecting the nature of the peptides bound. For example, P7-Lys of the conventional LSSPVTKSF self peptide bound in the absence of abacavir would clash with the cyclopentyl and purinyl moieties of abacavir (Fig. 4f).

Abacavir made extensive contacts with the HLA molecule (buried surface area 450 $Å^2$), forming numerous van der Waals contacts, five hydrogen bonds and three water-mediated hydrogen bonds, yet made few contacts with the self peptides bound within the cleft, with direct abacavir–peptide contacts being limited to P3-Thr, P5-Leu and P10-Ile for the LTTK complex and to the P10-Ile in the RVAQ complex (Fig. 4c, e). Abacavir was completely buried within the antigen-binding cleft of HLA-B*57:01–LTTK, with the peptide accounting for only 24% of the buried surface area; the HLA-B*57:01 contributed to burying the remaining 76% of abacavir's surface area. The extensive contacts made by HLA-B*57:01 and the three moieties of abacavir (Fig. 4c–e and Supplementary Fig. 1) provided a basis for understanding why only abacavir, and not its closely related metabolites (such as carbovir), was specifically bound within the antigen-binding cleft: the abacavir metabolites are likely to have a much reduced affinity for HLA-B*57:01. Specifically, the cyclopentyl moiety of abacavir nestled against Tyr 99 (Fig. 4c), in which the O^{η} moiety hydrogen-bonded to Tyr 74-OH (Fig. 4d), whereas the purinyl moiety of abacavir was flanked by aromatic residues Tyr 74 and Trp 147, as well as forming van der Waals contacts with Val 97, Ser 116 and Ile 124 (Fig. 4d).

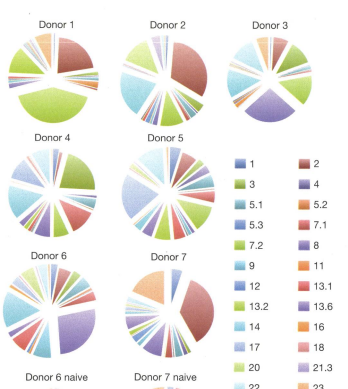

Figure 3 | Vβ usage of abacavir-reactive CD8 T cells from HLA-B*57:01 positive healthy blood donors. T-cell receptor Vβ usage of abacavir-reactive T cells determined by flow cytometry of *in vitro* activated T cells from the blood of seven *HLA-B*57:01*$^{+}$ healthy donors. Abacavir-reactive cells were identified on the basis of IFN-γ production in response to abacavir-loaded C1R-B*57:01 and their Vβ usage is shown. The Vβ repertoire of the total CD8 T-cell population before stimulation with abacavir (naive) is shown for donors 6 and 7 for comparison.

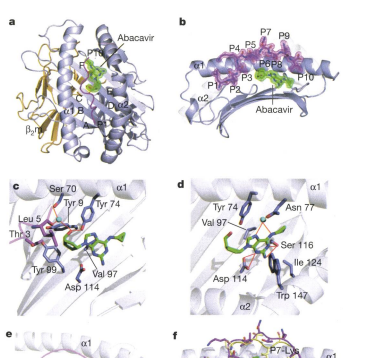

Figure 4 | Structure of HLA-B*57:01–abacavir–peptide complex. **a**, Abacavir within the peptide-binding groove, with the HLA pockets labelled A–F. β_2m, β_2-microglobulin. **b**, Orientation of abacavir orthogonal to **a**. **c**–**e**, HLA-B*57:01–LTTK–abacavir contacts cyclopentyl group (**c**), purine group (**d**) and cyclopropyl group (**e**). **f**, Superposition of the LSSPVTKSF peptide[9] (yellow) on LTTK peptide (magenta) with abacavir bound to HLA-B*57:01; P7-Lys is labelled. Polymorphic differences between HLA-B*57:01, HLA-B*57:03 and HLA-B*58:01 are shown as transparent cyan sticks. Key for all panels: blue, HLA-B*57:01; orange, β_2-microglobulin; magenta, peptide; green, abacavir; cyan spheres, water; red lines, hydrogen bonds; mesh, $2F_o$–F_c electron density contoured at 1σ.

Moreover, the N^4 group of the purinyl moiety hydrogen-bonded to Asp 114, and the N^1 and N^2 groups hydrogen-bonded to Ser 116 (Fig. 4d). The cyclopropyl moiety, which resided within the F pocket, packed against Ser 116 and Tyr 123 and additionally formed van der Waals contacts with Ile 95. The presence of the cyclopropyl group within the F pocket would disfavour the presence of larger amino-acid side chains at the PΩ position (Fig. 4e), thereby providing a basis for understanding why the presence of abacavir induces a preference for smaller residues at PΩ (Fig. 4f).

The structure of the HLA-B*57:01–LTTK–abacavir complex also provided a basis for understanding the impact of HLA micropolymorphism on abacavir specificity (Fig. 4f) and our observation of abacavir co-purification only with HLA-B*57:01 (Fig. 1b). For example, abacavir cannot bind HLA-B*58:01, because the polymorphic position 97 (HLA-B*57:01 Val97Arg HLA-B*58:01) sat directly beneath, and contacted abacavir such that the presence of the long charged side chain of Arg 97 in HLA-B*58:01 would disfavour abacavir binding (Fig. 4f). Moreover, in HLA-B*57:02 and HLA-B*57:03, the replacement of Ser 116 at the base of the F pocket with the more bulky Tyr 116 residue would prevent abacavir from binding these allotypes, because the central purine group would not be accommodated (Fig. 4f). Indeed, when the HLA-B*57:01–abacavir contact sites are mapped against the HLA sequence database (http://www.ebi.ac.uk/imgt/hla/), it is evident that the constellation of contact residues is unique to HLA-B*57:01, thereby providing a basis for the exquisite specificity of abacavir towards this HLA allomorph. These findings help explain the low prevalence of AHS in African Americans who have relatively high frequencies of *HLA-B*58:01*, *HLA-B*57:02* and *HLA-B*57:03*, and in whom the frequency of *HLA-B*57:01* is lower than in Europe[16]. The penetrance of AHS in *HLA-B*57:01*$^{+}$ individuals is about 50%, indicating that additional factors determine whether abacavir treatment induces AHS[17]. It is unclear whether these cofactors are genetic[18] or are related to environmental factors such as drug dose. Either way, the basic mechanism involves specific co-occupancy of the HLA-B*57:01 antigen-binding cleft by abacavir and novel self peptides presenting a new 'immunological self' to host T cells.

Next we sought to establish the likely generality of our HLA–abacavir-associated observations, and focused on carbamazepine (CBZ) (Supplementary Fig. 4a–e). A strong HLA association is well established between *HLA-B*15:02* and CBZ-induced SJS/TEN in Asian populations with odds ratios of more than 1,000 (refs 3, 4, 14). We first established that a non-covalent association existed between CBZ and HLA-B*15:02 by purifying HLA-B*15:02 peptide complexes from CBZ-treated cells (Supplementary Fig. 4). Second, sequencing of peptides bound to HLA-B*15:02 in the presence of CBZ revealed a

shift in the preferred amino-acid side-chain selection with an increase in the hydrophobicity at several positions and a preference for smaller residues at the P4 and P6 positions, but no shift in anchor residue preference (P2 and PΩ) (Supplementary Fig. 4 and Supplementary Table 5a, b). The magnitude of the CBZ-induced repertoire shift, about 15%, was smaller than that observed for abacavir. This was predicted, because CBZ is likely to bind at secondary anchor sites in HLA-B*15:02, adjacent to position 156. This is based on the observation that the closely related allele, *HLA-B*15:01*, is not associated with CBZ-induced SJS, and a notable non-conservative difference between these two allomorphs is at position 156 (Leu, HLA-B*15:02; Trp HLA-B*15:01). The small shift in peptide repertoire might explain the restricted TCR usage against drug-specific T cells reactive in *HLA-B*15:02*$^{+}$ patients with CBZ-induced SJS. Furthermore, automated *in silico* docking of CBZ into the cleft of HLA-B*15:02 predicted that CBZ binds underneath the P4/P6 residues of the peptide, adjacent to position 156 in HLA-B*15:02 (Supplementary Fig. 4c–e). Taken together, these observations for CBZ-HLA-B*15:02 peptide complexes resonated with those for abacavir–HLA-B*57:01, suggesting a general mechanism for hypersensitivity reactions towards at least two commonly used drugs with known HLA associations.

It is well established that HLA molecules can bind peptide ligands; our findings show that small-molecule drugs can specifically and non-covalently interact with defined HLA class I molecules, and subsequently alter peptide repertoire in a clinical context (Supplementary Fig. 5). These findings suggest that HLA molecules, and most probably other antigen-presenting molecules, may be surprisingly susceptible to drug modulation of antigen selection that in turn induces altered T-cell immunity. Although the observed mechanism is unlikely to account for all HLA-associated drug associations, our observations provide a potential basis for illuminating other HLA-linked drug hypersensitivities such as the very strong link between *HLA-B*58:01* and allopurinol hypersensitivity syndrome[19]. Indeed, the extensive polymorphism of HLA molecules, the similarity of small-molecule drugs possessing ring structures (Supplementary Fig. 1) and the plethora of different drug hypersensitivities make it likely that this is a general mechanism. In this regard, the capacity of small molecular moieties to modulate immunological self could have implications for understanding the origins of autoimmunity.

METHODS SUMMARY

T-cell assays. Peripheral blood mononuclear cell samples from healthy blood donors were from the Australian Bone Marrow Donor Registry and Australian Red Cross Blood Bank. Stimulation with abacavir and cytokine assays have been described previously[4].

Peptide repertoire analyses. HLA–peptide complexes were immunoaffinity purified using solid-phase-bound W6/32 monoclonal antibody[20] and analysed essentially as described[9].

Jurkat-transfection and activation assay. An abacavir-responsive T-cell clone (ABC12.20) was cloned into a retroviral vector (pMIG) and transduced into the Jurkat cell line. Activation was measured as the mean fluorescence intensity of staining for the early activation marker CD69.

ELISPOT assays. IFN-γ ELISPOT assays were performed using cytokine capture and detection reagents in accordance with the instructions of the manufacturer (Mabtech).

HLA-B*57:01 expression, refolding and purification. The peptides LTTKLTNTNI (cytochrome *c* oxidase subunit 2) and RVAQLEQVYI (small nuclear ribonucleoprotein Sm D3) were refolded with HLA-B*57:01 and abacavir and purified as described previously[21].

Thermal stability assays. These were conducted on pHLA-B*57:01 samples (±abacavir) with the fluorescent dye Sypro orange in the Real Time Detection system (Corbett RotorGene 3000), to monitor protein unfolding.

***In silico* docking.** Computational docking was performed to probe the binding of carbamazepine into HLA-B*15:02.

Crystallization and data collection. The HLA-B*57:01–LTTK–abacavir and HLA-B*57:01–RVAQ–abacavir complexes were crystallized and their structures were determined.

Full Methods and any associated references are available in the online version of the paper at www.nature.com/nature.

Received 6 January; accepted 16 April 2012.
Published online 23 May 2012.

1. McCluskey, J. & Peh, C. A. The human leucocyte antigens and clinical medicine: an overview. *Rev. Immunogenet.* **1,** 3–20 (1999).
2. Parham, P. & Ohta, T. Population biology of antigen presentation by MHC class I molecules. *Science* **272,** 67–74 (1996).
3. Bharadwaj, M. *et al.* Drug hypersensitivity and human leukocyte antigens of the major histocompatibility complex. *Annu. Rev. Pharmacol. Toxicol.* **52,** 401–431 (2012).
4. Chung, W. H. *et al.* Medical genetics: a marker for Stevens–Johnson syndrome. *Nature* **428,** 486 (2004).
5. Daly, A. K. *et al.* HLA-B*5701 genotype is a major determinant of drug-induced liver injury due to flucloxacillin. *Nature Genet.* **41,** 816–819 (2009).
6. Mallal, S. *et al.* Association between presence of HLA-B*5701, HLA-DR7, and HLA-DQ3 and hypersensitivity to HIV-1 reverse-transcriptase inhibitor abacavir. *Lancet* **359,** 727–732 (2002).
7. Hetherington, S. *et al.* Genetic variations in HLA-B region and hypersensitivity reactions to abacavir. *Lancet* **359,** 1121–1122 (2002).
8. Chessman, D. *et al.* Human leukocyte antigen class I-restricted activation of CD8^{+} T cells provides the immunogenetic basis of a systemic drug hypersensitivity. *Immunity* **28,** 822–832 (2008).
9. Purcell, A. W. *et al.* Quantitative and qualitative influences of tapasin on the class I peptide repertoire. *J. Immunol.* **166,** 1016–1027 (2001).
10. Barber, L. D. *et al.* Polymorphism in the α1 helix of the HLA-B heavy chain can have an overriding influence on peptide-binding specificity. *J. Immunol.* **158,** 1660–1669 (1997).
11. Macdonald, W. A. *et al.* T cell allorecognition via molecular mimicry. *Immunity* **31,** 897–908 (2009).
12. Archbold, J. K., Macdonald, W. A., Burrows, S. R., Rossjohn, J. & McCluskey, J. T-cell allorecognition: a case of mistaken identity or déjà vu? *Trends Immunol.* **29,** 220–226 (2008).
13. Turner, S. J., Doherty, P. C., McCluskey, J. & Rossjohn, J. Structural determinants of T-cell receptor bias in immunity. *Nature Rev. Immunol.* **6,** 883–894 (2006).
14. Ko, T. M. *et al.* Shared and restricted T-cell receptor use is crucial for carbamazepine-induced Stevens–Johnson syndrome. *J. Allergy Clin. Immunol.* **128,** 1266–1276 (2011).
15. Burrows, S. R., Rossjohn, J. & McCluskey, J. Have we cut ourselves too short in mapping CTL epitopes? *Trends Immunol.* **27,** 11–16 (2006).
16. Hughes, A. R. *et al.* Association of genetic variations in HLA-B region with hypersensitivity to abacavir in some, but not all, populations. *Pharmacogenomics* **5,** 203–211 (2004).
17. Mallal, S. *et al.* HLA-B*5701 screening for hypersensitivity to abacavir. *N. Engl. J. Med.* **358,** 568–579 (2008).
18. Martin, A. M. *et al.* Predisposition to abacavir hypersensitivity conferred by HLA-B*5701 and a haplotypic Hsp70-Hom variant. *Proc. Natl Acad. Sci. USA* **101,** 4180–4185 (2004).
19. Hung, S. I. *et al.* HLA-B*5801 allele as a genetic marker for severe cutaneous adverse reactions caused by allopurinol. *Proc. Natl Acad. Sci. USA* **102,** 4134–4139 (2005).
20. Brodsky, F. M., Bodmer, W. F. & Parham, P. Characterization of a monoclonal anti-β2-microglobulin antibody and its use in the genetic and biochemical analysis of major histocompatibility antigens. *Eur. J. Immunol.* **9,** 536–545 (1979).
21. Macdonald, W. *et al.* Identification of a dominant self-ligand bound to three HLA B44 alleles and the preliminary crystallographic analysis of recombinant forms of each complex. *FEBS Lett.* **527,** 27–32 (2002).
22. Zemmour, J., Little, A. M., Schendel, D. J. & Parham, P. The HLA-A,B 'negative' mutant cell line C1R expresses a novel HLA-B35 allele, which also has a point mutation in the translation initiation codon. *J. Immunol.* **148,** 1941–1948 (1992).

Supplementary Information is linked to the online version of the paper at www.nature.com/nature.

Acknowledgements We thank R. Holdsworth and M. Diviney for support; N. Croft for discussions, and the staff at the MX2 beamline of the Australian synchrotron for assistance with data collection. This research was supported by a Program Grant from the National Health and Medical Research Council of Australia (NHMRC) and the Australian Research Council (ARC). S.G. is supported by a Senior Fellowship from Monash University. A.W.P. is supported by an NHMRC Senior Research Fellowship; J.R. is supported by an NHMRC Australia Fellowship.

Author Contributions P.J. undertook functional analyses, data generation and writing of the manuscript. J.V. solved the structure and undertook structural analysis. N.D., Z.C., M.B., N.A.W., L.K., J.J.M., S.R.B., S.G. and L.K.N. contributed to data collection, experimentation and/or the provision of technical and scientific advice. A.W.P., J.McC. and J.R. are joint senior and corresponding authors—together they led the investigation, devised the project, analysed the data and wrote the manuscript.

Author Information The atomic coordinates and structure factors for the pHLA-B*57:01–abacavir complexes are deposited in the Protein Data Bank under accession numbers 3VRJ and 3VRI. Reprints and permissions information is available at www.nature.com/reprints. The authors declare no competing financial interests. Readers are welcome to comment on the online version of this article at www.nature.com/nature. Correspondence and requests for materials should be addressed to J.McC. (jamesm1@unimelb.edu.au), A.W.P. (apurcell@unimelb.edu.au) or J.R. (jamie.rossjohn@monash.edu).

Product Focus: Microarrays

Microarray Momentum

Technological strides in microarrays enhance traditional research techniques

ITSI-Biosciences is utilizing iTRAQ (5-plex assay) to simultaneously detect and quantify selenium responsive proteins in human plasma samples collected at five different time points (0 months, 3 months, 6 months, 9 months and 12 months) by investigators from Pennsylvania State University Cancer Center. The typical turnaround time is 2 weeks for most experiments. As little as 5 µg to 100 µg of protein can be analyzed. The deliverable includes raw and analyzed data, fold-difference of proteins that show difference in expression between the test and reference samples and gene ontology classification of the identified proteins.

Fluidigm has announced the availability of the **Access Array™ Barcode Library** for the Ion Torrent Personal Genome Machine (PGM) sequencer. This barcode library allows multiplexing of up to 96 different samples in a single sequencing run. "The Access Array Barcode Library for the Ion Torrent PGM enables the growing base of Ion Torrent users to dramatically improve their sample preparation for amplicon sequencing. The library uses a bidirectional amplicon tagging approach to allow reads to be obtained from both ends and across the full length of the amplicon with single-read sequencing. This eliminates the need for paired-end read sequencing," said Gajus Worthington, Fluidigm President and CEO. **The Fluidigm Access Array System** prepares amplicons for resequencing without the need for any additional library preparation and can operate with any next-generation sequencer (NGS) on the market. It prepares these amplicons in just hours, instead of days, and performs the sample preparation for less than $10 per sample. In addition, using the Access Array Barcode Libraries developed for the Illumina, Roche, and Ion Torrent sequencing platforms, researchers can test the same amplicon pools to cross-validate sequencing results across different NGS platforms.

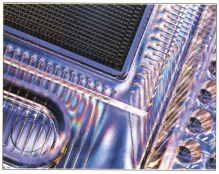

Fluidigm Microfluidic system chip

Oxford Gene Technology (OGT), provider of innovative clinical genetics and diagnostic solutions to advance molecular medicine, has released the first in a number of new microarrays for use in cancer research. The new **CytoSure™ Haematological Cancer +SNP array** is optimized for the study of the hematological malignancies Chronic Lymphocytic Leukemia (CLL) and Multiple Myeloma (MM), as well as Myeloproliferative Neoplasms (MPN) and Myelodysplastic Syndromes (MDS). The new array offers confident detection of both copy number variation (CNV) and loss of heterozygosity (LOH) on a single chip for these diseases. This is achieved by utilizing OGT's novel array design, which combines long oligo array comparative genomic hybridization (aCGH) probes for CNV detection with fully validated single nucleotide polymorphism (SNP) content for identifying LOH. The probes on the new array have been optimized to target regions known to be important predictors of disease progression and patient prognosis in hematological cancers, while providing good backbone coverage. These features facilitate the rapid, reliable identification of key genomic aberrations, while the complimentary, industry-leading CytoSure Interpret Software allows intuitive, single-click data analysis. Using the new array, researchers can move quickly and assuredly from processing their samples to generating relevant biological insight. James Clough, Vice President OGT Clinical & Genomic Solutions, commented: "OGT has worked in collaboration with leading researchers to develop the CytoSure Haematological Cancer +SNP array. The new array is the first member of a rapidly expanding portfolio we are developing for the genetic analysis of cancerous lesions, with several other additions set to be released in the near future." The new CytoSure™ Haematological Cancer +SNP array offers reliable and accurate aCGH and LOH detection on a single array by utilizing a unique SNP probe design. Analysis is carried out using an intensity-based comparison between the two SNP alleles, meaning that no changes to the standard aCGH protocol are required and any reference sample can be used. This allows the two tests to operate effectively on the same array. In addition, CytoSure arrays utilize 60-mer oligonucleotide probes, which have been shown to offer higher signal-to-noise ratios and increased specificity and sensitivity, providing the highest data quality possible. For optimum performance, the array can be combined with the CytoSure Genomic DNA Labelling Kit, which offers high signal intensities enabling easier allele discrimination.

Porvair has launched a microsite dedicated to providing detailed information on its solid state **Chromatin Immunoprecipitation**

Material compiled by Kenyon Hoag Life Science

KENYONHOAG

Product Focus: Microarrays

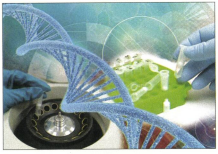

Porvair launched a microsite dedicated to its Chromatin Immunoprecipitation (ChIP) technology

(ChIP) technology. The microsite provides an informative background on ChIP technology and introduces the solid state approach pioneered by Porvair. A collaborative case study on the site compares the Chromatrap protocol with results from using a Protein G Magnetic Beads technique. Under optimal conditions, the Chromatrap protocol resulted in a 25.5 fold increase in the percentage DNA pull-down using the exact same sample of MCF7 breast cancer cells, targeting the RNA polymerase II protein bound to the GAPDH target gene. A further independent case study compares Porvair Chromatrap technology with alternative traditional ChIP methods (Sepharose and Dynabeads). In this study Chromatrap columns were shown to provide a greater level of enrichment of the DNA of interest due to low levels of background binding compared to specific antibody binding. Also, the DNA pull down (percentage input) was significantly higher for the Chromatrap columns than for the other matrices in these assays.

Thermo Fisher Scientific, the world leader in serving science, announced that it will exclusively distribute the **Bellbrook Labs iuvo™ Microconduit Array** products, including the **iuvo™ Microchannel 5250** and the **iuvo™ Chemotaxis Assay plates**. These products, coupled with Thermo Scientific high-content cellular analysis tools, enable scientists to build advanced cell models and conduct functional assays in a miniaturized, high-throughput format. Such assays offer more relevant models of living systems for drug discovery and basic cell research, without sacrificing productivity. When compared with traditional manual methods, the combination of these tools offers clear advantages such as automation, standardization, quantification and cost savings. The plates may be used for studying a wide variety of cell functions of interest to cancer, inflammation and immunology researchers, including chemotaxis, cell invasion, cell migration and angiogenesis. In addition, these assay plates enable researchers to reproduce complex microenvironments in vitro and study their role in cell function in order to improve the search for new drugs. The iuvo Microconduit plates are fully compatible with the **Thermo Scientific ArrayScan VTI HCS Reader** and **Thermo Scientific CellInsight Image Cytometer** as well as automated microscopes and plate readers. All Thermo Scientific high-content platforms have been optimized for use with the iuvo Microconduit Array plates, providing a simple workflow with sophisticated image analysis to deliver multi-parameter data on cell function.

QIAGEN recently launched the PyroMark CpG Assays, consisting of PCR and **sequencing primers for analyzing the methylation status** of specific targets across the human and mouse genomes by Pyrosequencing. Over 60,000 pre-designed assays are available, based on carefully tailored algorithms to generate the optimal assay design. Researchers can thereby minimize the time spent on assay optimization. Combined with other dedicated products of the PyroMark line, including PCR and sequencing reagents specially optimized for Pyrosequencing, the PyroMark CpG Assays enable methylation analysis of virtually any CpG island, with a simple and streamlined workflow. Also new from QIAGEN are the EpiTect Plus Bisulfite Kits, which provide a fast and streamlined procedure for complete DNA bisulfite conversion and cleanup from various starting materials, including FFPE tissue. The integrated sample lysis and bisulfite conversion saves time, and the reliable DNA Protect Technology minimizes DNA degradation from the harsh reaction conditions. The result is highly concentrated high-quality bisulfite-converted DNA and an increased sensitivity in downstream assays of up to 200-fold.

Companies mentioned in this Product Focus

ITSI	www.itsibio.com
Oxford Gene Technology	www.ogt.co.uk
Fluidigm	www.fluidigm.com
Porvair Filtration Group	www.porvairfiltration.com
Thermo Fisher Scientific	www.thermoscientific.com
QIAGEN	www.qiagen.com

"This article was compiled by Kenyon Hoag Life Science and submitted to Nature. It has not been written by or reviewed by the Nature editorial team and Nature takes no responsibility for the accuracy or otherwise of the information provided. Submit press releases for consideration to productfocus@nature.com with the topic in the subject line."

A key thread in your scientific career

Since 1869 we've made it our mission to share the greatest developments in science and advance the discussion among the global scientific community. Whether in print, online or mobile, *Nature* is always at the forefront of science and is your forum to read, watch, listen and engage with key research, news and opinion.

How will you access the next landmark discovery?

➲ NATURE.COM/NATURE

nature publishing group npg

WATCH THIS AD COME TO LIFE IN YOUR HANDS

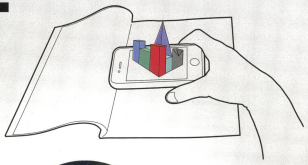

Download the Kaust AR App and experience this interactive ad in 3D!

What you will discover:

The King Abdullah University of Science and Technology (KAUST) is an international, graduate level, Research University located on the Red Sea. We have used augmented reality technology to create a 3D interactive experience of the KAUST campus (newly opened in September 2009). Come and discover the research departments at KAUST and our current job vacancies available through **naturejobs.com**.

How to interact with this ad:

Download your '**Kaust AR App**' from your App Store, Google Play or visit **bit.ly/kaust-app**. After launching the application, simply point your camera at this ad (hold your camera 12-24 inches away from this page) and the globe will spin to life, opening up to reveal the KAUST campus. The KAUST Augmented Reality Application was developed in association with *Naturejobs* and Inition.

naturejobs.com

جامعة الملك عبد الله للعلوم والتقنية
King Abdullah University of Science and Technology

INITION
Everything in 3D

nature publishing group npg

Download the Kaust AR App from bit.ly/kaust-app

Available on the App Store

ANDROID APP ON Google play

Android is a trademark of Google Inc.

RW225621

POSTDOCS NIH committee calls for workforce reforms **p.561**

PROFESSIONAL DEGREES Most graduates from new programmes head to industry **p.561**

NATUREJOBS For the latest career listings and advice **www.naturejobs.com**

GRANT APPLICATIONS

Find me the money

Some consultants offer to help researchers to find and secure grants. But scientists should carefully consider whether and how a consultant is worth the time and expense.

BY LUCAS LAURSEN

The e-mails were arriving in Pete Kissinger's inbox almost every day: "TODAY ONLY: Extra 25% Off… Craft your R01 Grants Management… Only 1 Day Left." They were from consultants trying to charge him to do something that scientists have long done for themselves: search for research-grant opportunities, write proposals and, in some cases, manage the grant once it has been won. Eventually, Kissinger's curiosity got the better of him.

Having founded his first company in the 1970s, Kissinger, an entrepreneur and bioanalytical chemist who works part-time at Purdue University in West Lafayette, Indiana, is no stranger to the challenges of raising start-up capital and research money. But he says that it is harder to get funding now than when he began. For one thing, the paperwork is more onerous. "And that's not really the thing most of us in science enjoy doing," he says. So about 18 months ago, when he needed money to develop a device for sampling blood to speed up clinical diagnoses, Kissinger hired FreeMind, a funding consultancy with offices ▶

nature MIDDLE EAST
Emerging science in the Arab world

twitter facebook google+

RESEARCH
NEWS JOBS
BLOGS EVENTS

Ensure you're part of the scientific and medical community gaining access to **the latest research in the region**.

Nature Middle East is your free comprehensive portal keeping you at the centre of science in the Arabic speaking Middle East.

nature.com/nmiddleeast

Download the free app for your phone at http://gettag.mobi

Sponsored by

nature publishing group npg

in Boston, Massachusetts, and in Jerusalem. He is waiting for decisions on two applications that he made last year with their help, and on another that was put together in March.

Types of funding finder range from services offering online information packs that cost a few hundred dollars to consulting firms such as FreeMind, which can charge up to 10% of the grant total. In return, they offer familiarity with the applications process and established relationships with the programme officers and businesses that are offering the funds. Nothing stops a scientist from going directly to the US National Science Foundation for funding information, notes Ram May-Ron, vice-president of FreeMind. "We don't claim to have any special powers, but we have lots of experience."

Consultants say that they can help to highlight and emphasize the aspects of a proposal that increase the chances of funding. "It's not just about how you raise money, it's about how to direct what you're doing in a fashion that will extract the social, medical and financial value of it," says Mark Goldstein, chief scientific officer of MammaCare, a medical-device firm based in Gainesville, Florida. Goldstein has worked with Kirk Macolini, a funding finder at Centurion Technologies in Ithaca, New York, for more than 10 years.

Making the most of that help means knowing when to seek assistance, whom to ask for it and how to work well with a consultant.

REACHING OUT

The emergence of funding finders reflects the growing specialization and competition in science. Just as postdocs and technicians handle the nitty-gritty of experiments so that principal investigators can concentrate on guiding their laboratory's research, some lab leaders are also seeking help with finding, winning and maintaining funding. "The nice thing is he does it all, from soup to nuts. It's free and clear of my office," says Ajit Varki, a glycobiologist at the University of California, San Diego, who hired Macolini to help him to get funding for a pharmaceutical start-up now called Sialix, based in Vista, California.

But hiring a funding finder itself requires careful planning. Researchers must consider how they will work with the consultant and other project collaborators to make the most of the time invested in the grant application. It helps to understand that funding finders cannot do all the work themselves. "If somebody drops an idea in our lap and says, 'Write a proposal', it would be quite difficult," says Ian Eden, a senior consultant at Arttic in Derby, UK. "We work with them, not on our own." Researchers need to set aside time to discuss their goals, answer technical questions about their research, evaluate suggestions from the consultant and produce and execute a strategy based on those discussions.

However, young researchers should begin by seeking funding advice from their home

Ram May-Ron's consultancy shows researchers how to maximize their chances of winning a grant.

institutions, says Alan Rebar, executive director of Discovery Park, a research-coordination centre at Purdue that organizes networking events with other grant seekers. Universities often skim off a percentage of their researchers' grants for overhead costs and devote administrative resources to helping scientists seek funding, so they usually prefer researchers to seek help internally, and may even prohibit them from using university funds to pay outsiders. The situation can become complicated, however, when researchers want to transfer their research from the academic to the commercial sector. "I can't use university resources to do an outside business application," says Kissinger.

Funding finders all say that their clients have higher success rates on average than scientists acting alone, although such claims are impossible to verify. The US National Institutes of Health reports that 11% of applications to the first round of its Small Business Innovation Research grants, which aim to help small businesses to commercialize research results, are successful. May-Ron says that 30–40% of his clients' applications for those grants are successful.

In addition to proposal-writing help, some firms offer networking tips and strategic guidance. Gonzalo de Silva, a consultant at the Euro-Funding Advisory Group in Madrid, notes that to be eligible for many European grants, research teams must include scientists in different countries as well as an industry partner; funding finders can help to make connections between potential collaborators. "That's where we add the most value, because we have a lot of contacts with businesses and experience," says de Silva.

Funding consultants tend to deal repeatedly with the same contacts in business and

at funding bodies, so they can build up an understanding of what such people are looking for. "If you have absolutely no clue as to what the interest of the programme officers is, then you really have no chance," says May-Ron. "We try to close this gap through conversations with programme officers and researchers." By talking to programme officers about a project idea before submitting the proposal, he explains, a consultant might learn that the funder puts increased value on certain components of the application. "So we tell the scientist to focus on those," says May-Ron.

In other cases, programme officers might mention that they are about to open a call for proposals, giving the consultant time to alert a client. The applicant could get such information for free by contacting a programme officer directly, but making dozens of requests to keep on top of all opportunities would be very time-consuming. And consultants can get to know a programme officer's preferences and interests. May-Ron recalls a case where one programme officer encouraged one of his clients, an influenza researcher, to submit a proposal in response to a call with guidelines that did not actually specify influenza research as a candidate area. The researcher won the award.

THE RIGHT CHOICE

Once scientists are convinced that they or their projects would benefit from external consultancy, they have to choose a firm. Universities sometimes contact grant consultants to supplement their in-house staff, notes Rebar, so researchers might be able to get a list of contacts. Or they could do some digging for themselves: Goldstein found Macolini through an Internet search.

PURDUE UNIVERSITY

"It's really easy to submit a long proposal. It's much harder to write a short one."
Pete Kissinger

The size of a potential project will make a difference to the type of consultancy the researcher should approach. Arttic, like many large firms, won't work on grants smaller than about €10 million (US$13 million), says Eden, and its fee is 5–7% of the grant money.

Macolini's fees include an upfront project charge and a percentage-based success fee, with the proportions varying from project to project. This creates a higher initial cost for the researcher than does a contingency fee alone, but consultants argue that it helps to prevent researchers sending them half-baked ideas just because they have nothing to lose when the grants don't materialize.

Researchers can ask for references from consultants' previous clients, but should treat them with caution. "The scientist has to evaluate the record of the consultants," says de Silva. There are no obvious ways of comparing one company's claimed success rate with another's, because they have no reporting requirements and different scientific disciplines have different funding constraints, which could affect success. However, it is possible to compare companies' years of experience and the number of grants they have facilitated, as well as the types of grants and collaborations.

Goldstein says he chose Macolini because he had a history of helping "really bright" research teams, an apparently sincere interest in the project and a willingness to offer criticism. It is particularly important to make sure that the scientist's and the consultant's aims are compatible, because one project may lead to another. "You need someone to tell you when you're barking up the wrong tree," says Goldstein.

MAKING THE MOST OF IT

The more information researchers share, the more likely the consultants are to be able to find funding for the project — or improve the odds of winning a grant. "We try to fully understand their project and regroup and rearrange them to reflect what funding sources would expect to see," says May-Ron. That could mean recommending that a researcher restrict an application to one avenue of research and hold off on another. Or it could mean bringing in components from other disciplines to strengthen a proposal.

The consultant runs through multiple drafts and revisions of the proposal in cooperation with the investigator, boiling down the content until it is simple, succinct and a good match for the ideas of the programme officers. "It's really easy to submit a long proposal. It's much harder to write a short one," says Kissinger. External reminders make it easier to hit goals, he adds: "They help find opportunities, keep you on track with the format and make you remember deadlines." In addition to the technical help, says Goldstein, good funding finders offer strategic advice. During brainstorming sessions, Macolini asks business-type questions such as how long it will take to explore an idea and what the client will do next with it. The ability to do that comes from "having a leg in each field", says Goldstein.

It is still too early for Kissinger to know whether his funding-finding gamble will pay off. But at least his inbox is now overflowing not with marketing *e*-mails, but with tailored messages from his own consultant. ■

Lucas Laursen *is a freelance journalist based in Madrid, Spain.*

POSTDOCS

Pay rise recommended

Biomedical postdoctoral researchers supported by US National Institutes of Health (NIH) fellowships should earn US$42,000 in their first year, with 4–6% increases in each of years two to seven, says an NIH committee report. Released on 14 June and commissioned by NIH director Francis Collins, the report offers recommendations to ease long training periods and overproduction of PhDs. It advises that NIH-supported postdocs receive the same benefits as employed colleagues, including health insurance, retirement plans and paid time off; calls to double the number of Early Independence awards, which speed postgraduates into careers and skip excessive postdoctoral training; and recommends training grants to prepare graduate students for varied career paths.

PROFESSIONAL DEGREES

Career paths mixed

Most graduates of professional science master's (PSM) degree programmes in the United States go on to work in industry, according to an independent analysis that used social media to track employment outcomes. Of more than 1,800 graduates tracked, some two-thirds now have industry positions. About one-quarter of the graduates are pursuing a university position or another degree, and fewer than 8% are working at non-profit organizations or in government. PSM degrees were initially designed to meet industry needs, although many programmes are now expanding, says Michael Teitelbaum, senior adviser to the Alfred P. Sloan Foundation in New York, which supported development of the PSM and funded the analysis. "These are very encouraging data," he says.

PHD PROGRAMMES

Universities must evolve

PhD students at US universities need better preparation for careers outside academia, says a report released on 14 June by the US National Academies in Washington DC in response to a congressional directive. *Research Universities and the Future of America* makes ten recommendations, including a call to use research collaborations to align graduate programmes more closely with business. It also recommends that the US government attract and retain talent by streamlining immigration processes.

European Head Office, London naturejobs@nature.com
The Macmillan Building, 4 Crinan Street, London N1 9XW, UK
Tel: +44 (0) 20 7843 4961 Fax: +44 (0) 20 7843 4996

European Manager:
Nils Moeller,+44 (0) 20 7843 4953 n.moeller@nature.com
Southwest UK/RoW:
Emma Hare, +44 (0) 20 7843 4944 e.hare@nature.com
Northeast UK/Ireland:
Matthew Ward, +44 (0) 20 7014 4059 m.ward@nature.com
France/Switzerland/Belgium:
Julie Aramburu, +44 (0) 20 7843 4994 j.aramburu@nature.com
Scandinavia/Spain/Portugal/Italy:
Megan Ball, +44 (0) 20 7843 4973 m.ball@nature.com
North Germany/The Netherlands/Eastern Europe:
Kristin Doelling, +44 (0) 20 7843 4970 k.doelling@nature.com
South Germany/Austria:
Maria Kubalova, +44 (0) 20 7014 4084 m.kubalova@nature.com
Natureevents:
Matthew Clare, +44 (0) 20 7014 4015 m.clare@nature.com
Business Development Manager, Middle East:
Jon Giuliani, +44 (0) 20 7843 4922 j.giuliani@nature.com

USA Head Office, New York naturejobs@us.nature.com
75 Varick Street, 9th Floor, New York, NY 10013-1917
Tel: +1 800 989 7718 Fax: +1 800 989 7103

US Sales Manager:
Ken Finnegan, +1 212 726 9248 k.finnegan@us.nature.com

Japan Head Office, Tokyo
Chiyoda Building, 2–37 Ichigayatamachi, Shinjuku-ku, Tokyo 162-0843
Tel: +81 3 3267 8751, Fax: +81 3 3267 8746

Asia-Pacific Sales & Business Development Manager:
Yuki Fujiwara, +81-3-3267-8765 y.fujiwara@natureasia.com
Business Development Manager, Greater China/Singapore:
Gloria To, +852 2811 7191 g.to@natureasia.com

India
3a, 4th Floor, DLF Corporate Park, Gurgaon, 122 002, India

Advertisement Sales:
Vikas Chawla, +91 1242881057 v.chawla@nature.com

Translational Health Science and Technology Institute

PRINCIPAL INVESTIGATORS HIV-1 Vaccine Design Program

THSTI an autonomous institute set up by Government of India conduct multidisciplinary research to help translate scientific ar technological advancements into innovative affordab technologies and health solutions and IAVI a global, not-for-prof public-private partnership organization working to speed the searc for a vaccine to prevent HIV infection are seeking Principa Investigators for their joint collaborative *HIV Vaccine Desig Program located in National* Capital Region of Delhi, India.

This innovative discovery research initiative for discovering an advancing novel new generation HIV vaccine candidates directed at HIV-1 envelope-based immunogen screening selection and prioritization using unique industrial-type high throughput strategies. It shall expand the number of vaccin candidates for testing and enhance the speed with which the can be assayed. It shall be an integral part of the THSTI cluster c research centers and linked to IAVI's Neutralizing Antibod Consortium & IAVI's Design and Development lab in Brooklyn, New York. Interdisciplinary interaction, international collaboration, high quality science and vaccine-oriented applied research shall be c key to program success.

The Principal Investigator will formulate, lead, and guide all scientific aspects of the Program related to his/her area of research unde the broad direction of the Program Director.

For further details on this and other positions please visit the website: http://www.thsti.res.in

RW226004

nature

Ecology and Evolution Editor

Nature the international weekly journal of science, seeks to appoint a Locum Ecology and Evolution Editor to join a team dedicated to publishing the world's best original research in the biological sciences.

This position is a locum position covering a Paternity leave for a 6-7 month period starting in December 2012.

The successful candidate will play a key role in determining how biological sciences are represented - through the selection and preparation of manuscripts for publication and by acting as *Nature*'s interface with the relevant research communities. These are demanding and intellectually stimulating positions, and call for a keen interest in the practice and communication of science.

The ideal candidate will have a strong track record of research in ecology and evolution and ideally theoretical biology, but highly qualified candidates from other areas of the biological sciences are also encouraged to apply. Applicants should hold or expect shortly to receive a PhD or equivalent degree.

This position is preferably based in *Nature*'s London office but positions in US offices may also be considered.

Please apply by sending your CV, covering letter (including your class of degree, a brief account of your research and other relevant experience, and details of your current salary) and a concise discussion of recent scientific developments which you have found particularly exciting (stating why).

Please upload your application to job http://jobs.macmillan.com/ - ref. **NPG/062/12**.

nature publishing group npg

IN225428R

SINGAPORE CLINICAL RESEARCH INSTITUTE

SINGAPORE CLINICAL RESEARCH INSTITUTE

The Singapore Clinical Research Institute (SCRI), an Academic Research Organization tasked with enhancing and developing core infrastructure, as well as providing scientific leadership for the conduct of both investigator-initiated and industry-sponsored clinical research. We are currently seeking:

CHIEF EXECUTIVE OFFICER

The CEO is responsible for the following:

- Provide strategic leadership and direction to SCRI
- Support collaborative research funded by private commercial and government
- Develop scientific excellence, infrastructure and professional staff to conduct clinical research
- Manage resources and oversee performance of the organization

Requirements:

- Minimum a Medical Degree with specialization
- Extensive experience in managing clinical research entities
- Experience in proposing and conducting investigator-initiated and industry- sponsored clinical research in academic medical centers

If you meet our requirements, we would like to hear from you. Please send your detailed resume, indicating your current and expected salaries to:

Chairman, Search Committee
SINGAPORE CLINICAL RESEARCH INSTITUTE
31, Biopolis Way,
#02-01, Nanos
Singapore 138669
Email address: recruit@scri.edu.sg

(Only shortlisted candidates will be contacted)

JP225698

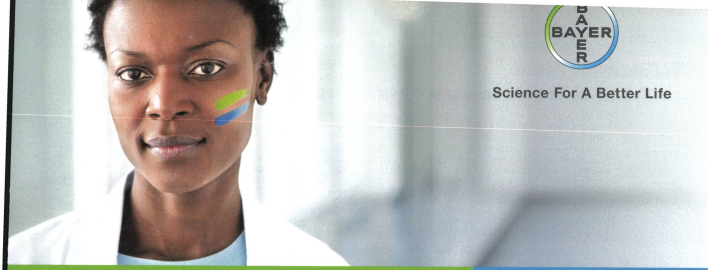

Dr. Esther Johnson wants to make the world a better place - for everyone. As a lab head at Bayer, Esther knows she is doing just that. Searching for solutions and never giving up. That is the passion that unites all of us at Bayer. We call it the Bayer Spirit. If you feel it, too, then it is high time we had a chance to talk about a career at Bayer.

Lab Head Inflammation

Bayer Pharma AG, Berlin, Germany

Job description As part of Global Drug Discovery at Bayer, the department Common Mechanism Research – Inflammation has the goal of discovering new treatment options for patients with severe inflammatory and autoimmune diseases, with a current focus on inflammatory bowel disease and systemic lupus erythematosus. As a Laboratory head in the department, you will be responsible for the direction and management of laboratory technicians and for establishing and implementing state of the art disease models and assays systems. A major aspect of your work will be to generate new projects in our indication areas and to lead interdisciplinary projects (both early and advanced projects), interacting with colleagues from different R&D functions and across different research sites. You will develop an external network of academic and CRO partners to support your projects and the work of the department. You will also participate actively in the interdisciplinary Early Research Group "Inflammation" and will contribute to the department strategy.

Your qualifications You have a degree in medicine, veterinary medicine, pharmacology or a related discipline, with postgraduate qualification to Ph.D. or M.D. / Ph.D. level. You already have extensive post-doctoral experience in a relevant field, preferably in an international setting, and you have broad expertise in immunology and pharmacology, with focus on autoimmune and chronic inflammatory diseases. You have extensive experience with in vitro assays and in vivo models relevant to the department's indication areas (in both assay/model development and validation, and efficient day-to-day running). Furthermore, you are experienced in initiating, leading and managing complex interdisciplinary projects, and have the ability to represent your projects at all levels within the company. You possess excellent interpersonal and communication skills, together with good problem-solving skills and the ability to think outside the box. You also have experience in managing laboratory staff and efficient deployment of resources. Due to our international working environment a fluent command of written and spoken English is essential.

Your application We offer a competitive salary in an international environment as well as excellent opportunities for professional and personal development. If your background and personal experience fits this profile, please send us your complete application at www.myBayerjob.de (Reference Code 0000038092), submitting a cover letter, your CV and references.

www.myBayerjob.de

Fon +49 214 30 9 97 79

W225991R

London

Centre for Infection Prevention and Management
Department of Medicine

CIPM Research Posts:

Research Assistant, Research Associates, Research Fellow

The National Centre for Infection Prevention and Management (CIPM), Imperial College London is expanding, with new posts for PhDs and Masters level researchers. Applications are invited to the CIPM for one postdoctoral scientist (Research Associate or Research Fellow grade) in Health Informatics, another (Research Associate or Research Fellow grade) in Epidemiology and one Researcher (Research Assistant or Research Associate grade) in Health Management and Innovation Adoption. These are unusual and exciting opportunities for three different motivated research scientists to build their careers in Infectious Diseases within the dynamic environment of the CIPM (www.imperial.ac.uk/cipm) and in the NHS.

The CIPM focuses on infection prevention policy, improving the quality of antimicrobial prescribing, and access to safe and effective healthcare in different settings. Our multidisciplinary teams work in collaboration with one another and the posts advertised will continue to expand this collaborative work.

The CIPM is currently looking for two postdoctoral scientists with a focus in infectious diseases.

1. **Research Associate or Fellow in Epidemiology:** You should have a background in classical epidemiology (e.g. study design, direct observational data collection, etc) and applied statistics.

2. **Research Associate or Fellow in Health Informatics:** You should have experience in health informatics and computational statistics.

The ideal candidates will have PhDs in the field of infectious diseases epidemiology, health informatics or a related field and can be at either the junior or senior level. They will have a record of high-quality publications in peer-reviewed journals and a successful track record in research. Enthusiasm and motivation in innovative research are also essential.

3. **Research Assistant or Associate Health Management Research:** The third CIPM post is for a Research Assistant/Associate in Health Management Research and in particular Innovation Adoption. The post will require the holder to use institutional and innovation diffusion theories to examine and model factors which influence the adoption of new technologies or changes in the NHS. The ideal candidate must have a PhD or be working towards a qualification in Health Management or a closely related discipline and have knowledge and experience of health services research and health services research programmes.

All three CIPM post holders will have a particular remit to develop applied research that can have an impact on public health policy, antimicrobial prescribing, patient care, or access to healthcare. This is a unique opportunity for three different individuals to build their careers in translational infectious diseases research in a new and expanding Centre. Support for continuation of these research posts and career advancement is highly promoted within the Centre through fellowships and collaborative research funding.

For more information about the Centre please visit www.imperial.ac.uk/cipm

For specific information relating to the CIPM Epidemiology or Health Informatics posts please contact Professor Alison Holmes at email: alison.holmes@imperial.ac.uk

For specific information relating to the CIPM Health Management Research Innovation Adoption post please contact Professor Rifat Atun at email: r.atun@imperial.ac.uk

Our preferred method of application is online via our website at http://www3.imperial.ac.uk/employment (please select "Job Search" then enter the job title or vacancy reference number into "Keywords"). Please complete and upload an application form as directed **quoting the relevant reference number**. Please make sure you upload your CV along with your application for consideration.

Reference numbers:

- **HM2012093 - Research Associate or Fellow (Epidemiology)**
- **HM2012096 - Research Associate or Fellow (Health Informatics)**
- **HM2012095 - Research Assistant or Associate (Health Management)**

Alternatively, if you are unable to apply online, please email hmrecr@imperial.ac.uk to request an application form.

Closing Date: 17 July 2012 (Midnight BST).

Stonewall DIVERSITY CHAMPION

Committed to equality and valuing diversity. We are also an Athena Bronze SWAN Award winner, a Stonewall Diversity Champion and a Two Ticks Employer.

U226016R

www.naturejobs.com

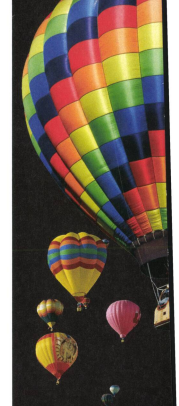

HIGHER & HIRE!

Post all your vacancies for FREE on the largest dedicated job board for the scientific community:

naturejobs.com

nature publishing group npg

Queen Mary
University of London

Investing in Scientific Excellence

Queen Mary, University of London (QMUL), is one of the UK's most successful higher education institutions with a reputation for excellent and innovative research that has a positive impact across the globe. In the last RAE exercise we were ranked 11th overall in the UK[1] and from August 2012 we will be a member of the Russell Group of leading UK research intensive universities.

We recognise that excellent research is dependent on outstanding researchers and are making an exciting and significant investment in the development of future excellence with the establishment of a number of new Early Career Fellowships in our Faculties of Science and Engineering and Medicine and Dentistry.

If you are an Early Career Researcher with ambitious plans to develop significant, independent programmes of research we'd like to hear from you. Appointments will be to three-year fellowships leading to permanent posts within the Faculties.

For more information and to apply please visit:
www.hr.qmul.ac.uk/jobs/earlycareersfellowships

[1] Guardian RAE 2008 League Tables

www.qmul.ac.uk

U2260009R

The **Helmholtz Centre for Infection Research** (*HZI*), a member of the Helmholtz Association of German Research Centres, invites applications in a joint appointment with **Hannover Medical School (*MHH*)** for a

Professorship in Virology (Professorial Grade W3)

starting at the earliest opportunity.

The successful applicant will have demonstrated expertise in virology at both research and teaching levels. In particular, applicants should have acquired an international research reputation pertaining to specific, clinically relevant, human pathogenic virus. Active involvement in raising external grant support and engagement with local research networks (graduate colleges, consortium grants (e.g. SFBs), German Centre for Infection Research) as well as experience in leading a research group is expected. The appointee should significantly strengthen the Cell and Molecular Biology expertise and Virology networking within the Braunschweig/Hanover region.

The holder of the position will be concurrently appointed as head of department at HZI and as a professor of virology at Hannover Medical School.

The successful applicant will be expected to have an excellent track record of publications and in winning competitive research grants and should have shown commitment towards undergraduate education and postgraduate teaching. We invite applications from both science and medical graduates.

A central focus of this position is the translation of research findings to the clinic.

Disabled candidates with equivalent qualifications will receive preferential consideration.

The Helmholtz Centre for Infection Research and Hannover Medical School are seeking to increase the proportion of female scientific personnel and thus especially welcome applications from women.

Applicants must fulfil the employment requirements of the Higher Education Act of Lower Saxony (§ 25). These include "Habilitation" or equivalent postgraduate research experience. Further information can be obtained on request.

Applications including personal data sheet, scientific and clinical career history, full documentation on teaching experience, a teaching concept, a complete and categorised list of publications, and a selection of reprints of five major publications, should be submitted by 27 July 2012 to:

President of the Hannover Medical School, Carl-Neuberg-Str. 1, D-30625 Hannover, Germany

W226019R

School of Sport, Exercise and Health Sciences

Loughborough University

Bioinformatician **Fixed-term for 48 months**

£27,578 to £35,939 per annum

Do you wish to contribute to some of Europe's most innovative translational medicine projects with access to unrivalled novel human genomics bio-bank data? We are seeking talented informatics researchers or biologists with a strong mathematical background to implement informatics and molecular classification strategies to yield novel and clinically relevant diagnostics for ageing and diabetes.

Ideally you will have a strong interest in translational medicine and be comfortable working with an international team of researchers applying Systems Biology approaches to human ageing, cardiovascular and metabolic disease. Our projects are funded by the, BBSRC, MRC and EU PF7 and the successful applicant will be afforded excellent collaboration and training opportunities. You may have an MSc in bioinformatics or programming and ideally a PhD in a relevant discipline.

The ideal applicant will have track-record in informatics, statistics or programming with a proven record of publication. Alternatively you will have a strong record in biological sciences, be highly numerate and have a strong commitment to obtaining informatics skills. It would be desirable if you have experience in a biological sciences at some stage of your training or specific knowledge of gene-chip informatics and molecular classification techniques.

You will work as part of a multi-disciplinary team and must therefore have excellent communication skills and a real desire to work in a team environment where projects are shared. The candidate will benefit from being part of an international team working across the EU, USA and Canada and thus gain experience managing and contributing to international collaborations and meetings.

This post is offered on a 4-year fixed-term contract, subject to satisfactory completion of a 12-month probation period.

School details can be found at www.lboro.ac.uk/departments/ssehs.

Curriculum Vitae will only be accepted if accompanied by a fully completed University application form. Closing date: 20 July 2012. Please quote reference **REQ1214537/6208.**

U029011R

www.lboro.ac.uk/jobs

Department of Biology, Chemistry and Pharmacy - Institute of Chemistry and Biochemistry
invites applications for a tenured

Professorship in Inorganic Chemistry (W 3)

The successful applicant will be required to cover the area named above in teaching and research.
Appointment requirements are governed by article 100 of the Berlin Higher Education Act (Berliner Hochschulgesetz).
The appointee will have an outstanding track record of university teaching and research in a contemporary field of inorganic chemistry, such as main group chemistry, with a strong international component. She or he should have experience teaching courses independently as well as acquiring funding for, and carrying out, sponsored research.
The successful candidate will cover the area of inorganic chemistry in its entirety within the degree programs offered at the Institute - in particular for students enrolled in bachelor's and bilingual master's programs in chemistry. She or he is expected to cooperate with colleagues working in other specialized research areas and complement their efforts effectively. The professor should participate in the graduate school Fluorine as a Key Element (1582), the collaborative research center Multivalency as Chemical Organization and Action Principle (SFB 765) or other research associations established in Berlin, as well as help create new research initiatives within the natural sciences at Freie Universität Berlin.
Applications quoting the **reference code W3-Anorg**, should include a CV, copies of all certificates of academic qualification, a list of publications, evidence of educational competence (such as courses previously taught) as well as involvement in ongoing and future research endeavors, joint research projects and externally funded projects (specifying the amount of funding). Furthermore, applicants are asked to submit an overview (not exceeding two pages in length) of their envisioned focal areas - along with potential partners for cooperation - in the region as well as a detailed list (with brief explanations) of required space, personnel and financial resources. All materials must be received, electronically and in hard copy, no later than **July 30th, 2012** at Freie Universität Berlin, Fachbereich Biologie, Chemie, Pharmazie, Dekan Herrn Prof. Dr. Hans-Ulrich Reißig, Takustr. 3, 14195 Berlin, Germany.
For additional details, please visit www.fu-berlin.de, www.bcp.fu-berlin.de, www.bcp.fu-berlin.de/chemie/gkf/uor and www.sfb765.de.

Department of Biology, Chemistry and Pharmacy - Institute of Chemistry and Biochemistry
invites applications for a tenured

Professorship in Biochemistry with a Focus on Membrane Biochemistry (W 3)

The successful applicant will be required to teach courses in biochemistry and focus on membrane biochemistry in her or his research.
Appointment requirements are governed by article 100 of the Berlin Higher Education Act (Berliner Hochschulgesetz).
The appointee will have an outstanding track record of university teaching and research with a strong international component. She or he will be an aspiring scientist with an international reputation and a research interest in contemporary issues of biological membranes applying biochemical and biophysical processes. The range of methods to be employed should complement the expertise at the Institute and be compatible with other research groups at the Department. Candidates should have experience acquiring funding for, and carrying out, sponsored research as well as designing and implementing curricula in biochemistry.
The newly appointed professor will be active in the development of the Department's strategy to implement new biomolecular and biomedical research initiatives. Active participation in local research networks such as the Collaborative Research Center Scaffolding of Membranes - Molecular Mechanisms and Cellular Functions (SFB 958) and graduate schools is desirable.
Applications quoting the **reference code W3-Membranbioche**, and including, apart from standard documents (CV, publications, diplomas and certificates), a list of previously acquired third-party funds (including the amounts raised) and previous courses taught; a description of planned future research and potential partners in Berlin (2 pages max.) as well as a brief overview and justification of rooms, equipment and personnel needed must be received in hard copy and on a CD-ROM no later than **July 30th, 2012** at Freie Universität Berlin, Fachbereich Biologie, Chemie, Pharmazie, Dekan Herrn Prof. Dr. Hans-Ulrich Reißig, Takustr. 3, 14195 Berlin, Germany.
For additional details, please visit www.fu-berlin.de, www.bcp.fu-berlin.de and www.sfb958.de.

Application guidelines and general information on the appointment procedure as well as requirements for professorships at Freie Universität Berlin can be found at www.fu-berlin.de/praesidialamt.

W226006R

"When trying to recruit good scientists for such a remote institutions like ours, in the Canary Is., the high visibility and wide-range exposure that Naturejobs provides has been crucial. I'm very happy to have international candidates who applied to our position from places ranging between St. Petersburg and Cincinnati. Thanks a lot!"

Eduardo Salido, MD, PhD,
Hospital Universitario de Canarias

naturejobs

Aalto University
School of Electrical
Engineering

Smart power. Novel networks.

Aalto University School of Electrical Engineering transforms scientific and technological research results to advanced solutions and applications ranging from nanotechnology to space robotics.

SEVEN Tenure Track or Tenured PROFESSOR Positions

Aalto University School of Electrical Engineering seeks experts especially in the following fields:

- Electrical Engineering (power and energy), Automatic Control, Embedded Systems, Smart Living Environment;
- Radio Science and Engineering, Radio Astronomy, Space Science and Engineering, Optoelectronics;
- Communications Engineering and Networking Technology.

The positions are open at all levels from assistant professor to full tenured professor.

Applicants must have a doctoral degree in a relevant field. For assistant and associate professor levels evaluation focuses on merits and potential for excellence, for full professors we look for demonstrated excellence in research and teaching. Relevant industrial experience is appreciated.

Application deadline is September 30, 2012. For further information and application details, please visit at:
www.elec.aalto.fi/tenuretrack

Aalto University is a new university with over a century of experience. Created from a high-profile merger between three leading universities in Finland – the Helsinki School of Economics, the Helsinki University of Technology and the University of Art and Design Helsinki – Aalto University opens up new possibilities for strong multi-disciplinary education and research. The university's ambitious goal is to rank among the top universities in the world in its areas of specialization. At Aalto University, there are 20 000 students and a staff of 5 000, of which 350 are professors.

aalto.fi

W225854R

ETH

Eidgenössische Technische Hochschule Zürich
Swiss Federal Institute of Technology Zurich

Schweizerischer Erdbebendienst
Swiss Seismological Service

Professor of Seismology and Director of the Swiss Seismological Service (SED)

The Department of Earth Sciences (www.erdw.ethz.ch) and the Swiss Seismological Service (www.seismo.ethz.ch) at ETH Zurich invite applications for the above-mentioned position.

The successful candidate will lead a diverse team of currently 80 scientists, staff members, and students. The SED is a national service and competence centre for earthquake related risk analysis and research, service, and education. It operates the national seismic network, consisting of more than 120 real-time stations, a 24/7 alert service, is responsible for seismic hazard assessment at a national scale and acts as the Swiss National Data Centre for the CTBT. Presently, the SED conducts research and development covering a wide range of topics, including seismic hazard assessment, engineering seismology, induced seismicity, computational and statistical seismology, real-time seismology and seismotectonics.

The new Professor and Director should have expertise in any domain of seismology and will direct the national seismological service and shape the research activities at the SED responding to the increasingly cross-disciplinary challenges of the future. He or she has an outstanding research record, proven ability to raise competitive funding and demonstrated managerial as well as communication skills. A contribution to teaching within the Department of Earth Sciences at both undergraduate level (German or English) and graduate level courses (English) is expected. Furthermore, a willingness to learn German is required.

Your application should include your curriculum vitae, publication list, statement of research interests, and the names of three potential referees. The letter of application should be addressed **to the President of ETH Zurich, Prof. Dr. Ralph Eichler. The closing date for applications is 16 September 2012.** ETH Zurich is an equal opportunity and affirmative action employer. In order to increase the number of women in leading academic positions, we specifically encourage women to apply. ETH Zurich is further responsive to the needs of dual career couples and qualifies as a family friendly employer. **Please apply online at www.facultyaffairs.ethz.ch.**

W225943R

UNIVERSITY of OULU
OULUN YLIOPISTO

TENURE TRACK POSITIONS AT THE UNIVERSITY OF OULU, FINLAND

The University of Oulu in Northern Finland is an international, multidisciplinary research university with a rich pool of creative and intellectual talent. It is one of the largest universities in Finland with an exceptionally wide academic base and ranked among the top 301–400 universities in the world on the ARWU list (The Academic Ranking of World Universities, conducted by researchers at the Center for World-Class Universities of Shanghai Jiao Tong University CWCU).

The strengths of the University of Oulu are its broad academic base, top-level research in its chosen focus areas, and quality education. The University promotes advanced research, education and culture, and strengthens the knowledge and skills base leading to enhanced wellbeing. Its activities ensure the availability of a highly-trained specialist workforce and research capacity.

The University of Oulu **seeks candidates for tenure track positions** to begin in 2013 in the following topics:

Biosciences and Health

Information Technology

Cultural Identity and Interaction

Environment, Natural Resources and Materials

Business Studies and Economics

Research-Based Teacher Education

More information on the positions and how to apply at **www.oulu.fi/english/jobs** and from Director Sinikka Eskelinen, e-mail sinikka.eskelinen@oulu. Application deadline is **October 1, 2012 before 3:00 p.m. local time.**

www.oulu.fi/english/jobs

W226061R

Program Officer

GLOBAL HEALTH ADVANCED PROFESSIONALS PROGRAM

The Bill & Melinda Gates Foundation is hiring advanced degreed professionals for a two-year introduction to the fields of Global Development and Global Health. In this two-year role, you will:

- Work on a range of challenging issues, such as polio eradication and global hunger.
- Serve with some of the world's most renowned experts in the field.
- Leverage your expertise to contribute to programmatic strategy.
- Gain in-depth knowledge of the key drivers of philanthropy.
- Establish a strong networking relationship with the Bill & Melinda Gates Foundation.

We're seeking exceptional individuals with any of the following backgrounds:

- Advanced scientific degrees.
- MD, PhD, PharmD plus 1-3 years of post doc experience.
- MBA plus 1-3 years experience in management consulting, investments/private equity.

These are full-time salaried positions located at our headquarters in Seattle, Washington. In this beautiful and vibrant setting, you'll enjoy a lifestyle that is as richly rewarding as the work you will contribute to. Apply at: **www.gatesfoundation.org/jobs**. Resumes must be submitted by **July 13, 2012.**

BILL & MELINDA GATES *foundation*

EOE

NW225985

Philipps Universität Marburg

The Medical Faculty of the Philipps-Universität Marburg and the University Hospital Gießen and Marburg GmbH, Department of Internal Medicine, Division of Hematology, Oncology and Immunology in Marburg offer the following position

Full Professorship (W3) for Molecular and Tumor Immunology

Research activities at the Medical Faculty of the Philipps-Universität Marburg are focused on tumor biology and immunology. To link and expand these research topics, a full professorship for Molecular and Tumor Immunology is established which is affiliated to the Clinical Department of Hematology, Oncology and Hematology (Director: Prof. Dr. Andreas Neubauer). The position is provided with ample lab space located in our new research building for tumor biology and immunology.

Candidates are expected to hold a M.D. and/or PhD. degree and to be qualified through excellent scientific research experience and activities in at least one of the research fields mentioned. Clinical work is possible within the limits of a secondary employment. Experience in the acquisition of third party funding is required. Successful candidates are expected to have contributed significantly in the fields of "Ras signaling in human cancer" (Collaborative Research Centre Transregio 17), "Genetics of drug resistance in cancer" (Clinical Research Group KFO210), "Allogeneic stem cell transplantation" and/or "Immunology of graft-versus-host disease".

Conditions of employment based on § 61 and § 62 Hessisches Hochschulgesetz (HHG) are valid. Philipps-Universität Marburg places great importance on the intensive mentoring of students and doctoral candidates; therefore, the regular presence of the teaching staff is required.

We are supporting females and therefore particularly encourage female candidates to apply. Applicants with children are welcome. The Philipps-Universität Marburg aims to position itself as a family-friendly university. In case of equal qualifications, preference will be given to people with disabilities in the context of the valid regulations.

Candidates are requested to fill out the form for applicants listed under (http://www.uni-marburg.de/fb20/formulare) with the office and home address. Applications should be received by July 27, 2012 by the President of the Philipps-Universität Marburg, 35032 Marburg, Germany.

W225956R

Wellcome Trust Sanger Institute

The Wellcome Trust Sanger Institute, based south of Cambridge, is one of the world's leading genomic research centres funded primarily by the Wellcome Trust. Our mission is to use genome sequences to advance understanding of the biology of humans and pathogens in order to improve human health.

The Institute conducts research in four thematic areas – human genetics, pathogen genetics, model organism genetics and informatics. Building on its expertise in the genetic manipulation of ES cells and the production of iPS cells, we are developing plans for a new scientific programme in Stem Cells and Cellular Phenotyping [SCCP]. The programme will have two major components – a resource of stem cells/iPS cells and a high-throughput cellular phenotyping platform.

We are currently drawing together the scientific leadership and technical expertise to develop and shape the resources and the platform. The significant infrastructure requirements are being progressed in parallel and include major laboratory refurbishment, equipment specification and purchase, defining resource needs and recruitment and training of technical groups. The new platform will sit alongside our established large scale experimental pipelines as part of an extensive scientific infrastructure including sequencing, genotyping, sample management, large scale PCR and others which support and drive numerous projects both internally and externally.

We are now looking to recruit a number of roles for the Stem Cell Pipeline in the facility. This pipeline will be responsible for generating, maintaining and genetically manipulating large numbers of high quality stem cells and differentiated cell lines. These cell lines will be generated from human and model organism tissues before being passed to other teams for phenotyping at the genetic and cellular level. Once implemented this fully operational pipeline will support new lines of scientific enquiry by allowing us to assess the impact of genetic variation at a cellular level across all areas of interest. This is a fantastic opportunity to deliver stem cell services at the forefront of science and technology with the potential for significant scientific advances and health impacts.

Senior Scientific Manager – Cell Culture Team: Ref: 81217
Senior Scientific Manager – Cellular Phenotyping Team: Ref: 81232
Salary range: £37,140 - £52,511 pa plus excellent benefits
Scientific Pipeline Managers with a strong track record of operational scientific, project & people management, you will work with the Senior Management Team to set up and ultimately run the high throughput cell culture and cellular phenotyping aspect of our stem cell facility. Reporting to the Head of Operations, you will be accountable for the operational delivery of the services provided by your teams in the stem cell pipeline, ensuring these meet customer requirements, motivating and managing the performance of your team. You will also be involved in identifying and implementing developments to ensure the pipeline remains at the cutting edge of stem cell technology.

Research Assistants – Cell Culture and Cellular Phenotyping Teams: Ref: 81207 and 81227
Salary range: £17,188 - £23,692 pa plus excellent benefits
We are seeking self-motivated and enthusiastic individuals with an undergraduate degree in a biological science and cell culture expertise to support the programme. Post-holders will be involved in deriving and maintaining iPS & ES cell cultures from primary cell tissues and consequently quality controlling them using a diversity of assays.

Technical Assistant – Tissue Culture: Ref: 81208
Salary range: £13,965 - £18,953 pa plus excellent benefits
This key role will ensure that on-going supplies of tissue culture, media and consumables are available for the smooth running of the project. The post holder's main responsibility will be to ensure that the necessary culture media and feeder plates are generated for growing hIPCSC lines.

Other information
Informal enquiries may be made to James Ellis, SCCP Programme Manager - email: je5@sanger.ac.uk tel: 01223 494763

Please apply via our vacancy web pages
https://jobs.sanger.ac.uk

Please refer to our website for details on closing dates

www.sanger.ac.uk
Working towards diversity through equality

wellcome trust sanger institute

Genome Research Limited is a Registered Charity No.1021457

U226031R

BROWN

Environmental Remote Sensing:
The Environmental Change Initiative (ECI) (http://www.eci.brown.edu/), Brown University, invites applications for a Brown University tenure-track faculty position in Environmental Remote Sensing. We seek a scholar who uses remotely sensed data to analyze the multiscalar and complex relationships between human societies and the natural environment. Requirements include a Ph.D. in an environmentally-relevant social or natural science, a record of achievement in the use of remotely sensed data in environmental science-focused research demonstrated by peer reviewed publications and/or externally funded research, and a commitment to excellence in graduate and undergraduate teaching. We seek candidates whose research interests and expertise complement and strengthen existing ECI research foci in land change science, biogeochemical processes, and conservation science. The successful candidate should integrate research efforts with environmentally relevant natural and social sciences spanning sociology, ecology, evolutionary biology and geological and climate science and have experience working in an interdisciplinary team. In addition to remotely sensed data, we are interested in candidates who broadly incorporate geospatial technologies in their research. S/he will maintain an active, externally-funded research program and be involved in teaching at both undergraduate and graduate levels. ECI fosters interdisciplinary research and education in the environmental sciences at Brown. The University is making investments in the ECI including new resources for interdisciplinary research, post-doctoral research appointments, graduate education and a cooperative graduate program with the Marine Biological Laboratory (MBL) at Woods Hole. The candidate will be a core faculty member of the ECI with an appointment in a tenure-granting department such as Sociology, Geological Sciences, or Ecology and Evolutionary Biology. Appointment is expected at the Assistant Professor level, although exceptional circumstances would warrant appointment at a higher level. The department appointment will require that the candidate's qualifications are commensurate with the tenuring department's standards for a tenured or tenure-track appointment.

Requirements include a Ph.D. in an environmentally-related discipline, a record of achievement in the use of remotely sensed data in environmental science-focused research, and a commitment to graduate and undergraduate teaching.

To apply, please submit a letter of interest addressed to Jack Mustard, Search Committee Chair, Environmental Change Initiative, along with a current CV, teaching and research statements, and 3 letters of reference for the Assistant Professor position. Applications should be submitted through Interfolio at http://www.interfolio.com/apply/12528 and must be received by September 6, 2012 in order to receive full consideration.

For administrative questions regarding this position please contact Bonnie Horta at Bernadette_Horta@brown.edu or (401) 863-3032.

Brown University is an EEO/AA employer. Minorities and women are encouraged to apply.

NW225789R

SAHA INSTITUTE OF NUCLEAR PHYSICS
KOLKATA, INDIA
www.saha.ac.in

Faculty Positions

SINP invites applications for faculty positions at different levels from scientists having outstanding academic records and research achievements. At present, major research activities of the Institute are in the following broad areas: Atomic, Nuclear and Plasma Physics, Condensed Matter & Surface Physics, High Energy Physics, Theoretical & Mathematical Physics and Biophysical Sciences. SINP is an autonomous organization funded by the Department of Atomic Energy of Government of India to carry out basic research in the above broad areas. SINP has excellent state-of-the-art in-house facilities and also has collaborative access to various high-energy accelerators and synchrotron facilities across the world. We seek applicants, who will complement and extend our current research activities. Prospective applicants should also have interest in graduate teaching. This is a rolling advertisement (refer **http://www.saha.ac.in/cs/www/position/Selection_Procedure.pdf)** and applications may be submitted anytime of the year in plain papers/e-mails with details like cover letter, resume giving entire list of publications, a statement of research plan and contact details of 5 referees. Salary and rank will be commensurate with qualifications and research experience - minimum of two years of postdoctoral experience is required.

Director, Saha Institute of Nuclear Physics, 1/AF, Bidhannagar, Kolkata 700064, INDIA; director.sinp@saha.ac.in

RW226005R

The University of Manchester

Faculty of Medical and Human Sciences
School of Biomedicine

Research Associate

£29,249 - £33,884 p.a. **Ref: M&HS/0125**

The University of Manchester invites applications from candidates with a proven track research record in the area of cell, developmental or stem cell biology for the position of Postdoctoral Research Associate.

You will join the School of Biomedicine, performing most of the work in the laboratory of A V Hill Building in Dr Tao Wang's research group and in the North West Embryonic Stem Cell Centre based in the Core Technology Facility led by Professor Sue Kimber. Some experimental work will also be conducted in King's College London in collaboration with Professor Qingbo Xu.

You will focus on the development of induced pluripotent stem cells (iPSCs) by reprogramming skin fibroblasts from CADASIL patients and differentiating the iPSCs into smooth muscle cells. The aim is to establish a cell model for CADASIL disease for the purpose of elucidating the molecular mechanisms of this condition and identify therapeutic options.

You should have a PhD degree or equivalent in the area of biology or biomedicine and have a demonstrated research experience in cell biology and molecular biology. Experience in stem cells or molecular biology is desirable.

Informal enquiries can be made to Dr Tao Wang at tao.wang@manchester.ac.uk or telephone 0161 275 1508.

Application forms and further particulars are available from our website www.manchester.ac.uk/jobs If you are unable to go online you can request a hard copy of the details from the Faculty HR Office, telephone 0161 275 8835 or e-mail mhs-hr@manchester.ac.uk

Closing date: 26 July 2012.

The University of Manchester values a diverse workforce and welcomes applications from all sections of the community.

www.manchester.ac.uk/jobs

U226010R

The Laboratory of Photonics and Interfaces (LPI) of the EPFL, SWITZERLAND, has openings for postdoctoral positions in the group of Prof. Michael Graetzel/ Dr. Md. K. Nazeeruddin.

ÉCOLE POLYTECHNIQUE FÉDÉRALE DE LAUSANNE

The positions involve synthesis, characterization of quantum dots and their application in solar energy conversion into electricity. The candidates are expected to be independent, highly ambitious, career oriented, and hard working with an excellent track record in preparation of QD's, cell fabrication and measurements.

One exclusive position is for somebody who is familiar with DSSC fabrication and testing. She/He should concentrate on making high efficiency cells and test all the dyes that are synthesized at LPI.

We offer excellent working conditions, an environment strongly conducive to academic research and/or industrial carrier. The EPFL offers a full benefits package, and the salary commensurate with skills and experience, starting from US$85,000.

michael.graetzel@epfl.ch mdkhaja.nazeeruddin@epfl.ch
Tel.: +41 21 693 31 12 ; +41 21 693 61 24.

Review of applications will continue until October 2012 or until the positions are filled.

W226007R

"Thank you for assisting in advertising the 6x 'Research Associate' positions on the Naturejobs website. I was advised thoroughly on the inventory that would be the best for our organisation and the web inventory worked. We received a huge response and will contact you for future advertisements."

Nanda Rahman,
Bio Nano Consulting, UK

nature jobs

ADVANCING PROTEIN CRYSTALLIZATION USING MICROGRAVITY

Issue Date:
June 26, 2012

Letters of Intent Due:
July 31, 2012

Proposals Due:
August 15th, 2012

Full Details of this CASIS RFP available at:
www.iss-casis.org/solicitations

CASIS
CENTER FOR THE ADVANCEMENT OF SCIENCE IN SPACE

The Center for the Advancement of Science in Space (CASIS) is an IRC Section 501(c) (3) entity responsible for management of the International Space Station U.S. National Laboratory under a Cooperative Agreement with NASA. Per Section 504 of the NASA Authorization Act of 2010, the purpose of CASIS is to maximize the value of investment the U.S. government made in the station's National Lab and demonstrate the scientific and technological productivity of the National Lab over the next decade. CASIS seeks to advance scientific research and education in conjunction with the space station, managing a diverse research and education portfolio across a broad range of scientific fields.

This request for proposals (RFP) seeks to identify protein crystallography projects, which CASIS will support through grant funding, facilitation of service-provider interactions, and flight coordination to and from the space station.

The purpose of this RFP is to award research grants that will support space station use by commercial and academic investigators to advance understanding of protein crystallization in space, toward (1) improving yield and resolution in crystallographic studies and (2) developing new crystallization approaches that have commercial or scientific applications.

NW225737A

Bringing jobseekers and recruiters together.

Academic • Industry • Government

Search now at **naturejobs.com**

naturejobs
making science work

EMBO

Winner of the
EMBO Gold Medal 2012

Jiří Friml

Department of Plant Systems Biology, VIB and Ghent University, Flanders, Belgium

in recognition of his pioneering work on auxin transport and gradient formation in plants.

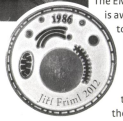

The EMBO Gold Medal is awarded annually to a young European researcher for outstanding contributions to research in the life sciences.

Further details:
www.embo.org
/aboutembo/embo-gold-medal.html

W225875A

REPROGRAPHICS: CTT, London E17 6BU UK and **The Charlesworth Group,** Wakefield, UK.
PRINTED BY: William Gibbons & Sons Ltd, UK; **Publishers Press,** Lebanon Junction, Ky, USA and **Obun Printing Co. Inc,** Tokyo, Japan

Nature and VIB present:

Frontiers in plant biology: From discovery to applications

Recent years have seen an explosion of new high throughput technologies which in turn have enabled ground-breaking discoveries in plant sciences. Next generation sequencing and advances in genome assembly and analysis are helping to crack the code of even the most complex genomes. Transcriptomics, proteomics and metabolomics are leading the way in providing new insights into the inner workings of plant cells and plant cell-cell communications. Equally importantly, the cell biology toolbox – previously mainly restricted to animal and yeast cells – has finally been built up in plants allowing researchers to explore the fundamental questions in plant cell biology and compare plant solutions with those of other organisms. Importantly, the 'omics' and cell biology tools also shed light on plant-environment interactions, including responses to abiotic signals and plant-pathogen interactions.

October 3-5, 2012
Aula Ghent University, Ghent, Belgium

SPEAKERS

Julia Bailey-Serres
Dominique Bergmann
Ralf Bock
Joanna Chory
José Dinneney
Caroline Dean
Xinnian Dong
Jiří Friml
Maria Harrison
David Jackson
Liwen Jiang
Sophien Kamoun
Salome Prat
Pamela Ronald
Kazuki Saito
Teva Vernoux
Olivier Voinnet
Philip Wigge
Zhenbiao Yang
Qifa Zhang

ORGANIZERS:

Jo Bury (VIB, Belgium)
Jiří Friml (VIB / Ghent University, Belgium)
Dirk Inzé (VIB / Ghent University, Belgium)
Deepa Nath (*Nature*, UK)
Magdalena Skipper (*Nature*, UK)
Detlef Weigel (Max Plank Institute for Developmental Biology, Germany)

Abstract submission and early booking (reduced fee) deadline: July 25, 2012

For more information and to register visit:
www.nature.com/natureconferences/fpb2012

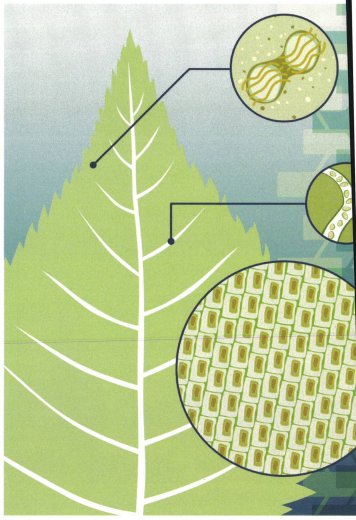

nature

VIB

IN224604E

nature jobs CAREER EXPO

Naturejobs Career Expos 2012
LONDON AND HEIDELBERG

Both events focus exclusively on the scientific world and offer a career fair and conference for those seeking opportunities and career guidance in the life sciences, physics, chemistry and medical sciences.

FREE Exhibition • Insightful Conference • Company Workshops

Naturejobs Career Expo

LONDON

20 SEPTEMBER 2012

Business Design Centre
London, United Kingdom

www.naturejobs.com/careerexpo

Organised by *Naturejobs*

Naturejobs Career Expo

HEIDELBERG

24 OCTOBER 2012

Print Media Academy
Heidelberg, Germany

www.spektrum.de/careerexpo

Organised by *Naturejobs* and *Spektrum der Wissenschaft*

nature publishing group npg

IN223178E

CELESTIAL BODIES

Love among the stars.

BY KEN LIU

So there I was, a new gas giant just waking up. The disk of nebular dust surrounded me like a fresh blanket of snow. Along with the rest of the planets, I marched around that dust cloud, absorbing everything I could, growing and loving every second.

Then I saw her.

A tiny, dainty thing. Rocky, hard, solid. Not at all like me, all swirls and ionized storms. She was closer to the sun, and she shone so brightly in that golden light, like a spinning jewel.

I was instantly smitten.

She was young, fiery and hot-tempered (and in truth, I suppose I was then, too). Volcanoes erupted constantly all over her surface, and she spun so fast. Gliding along in our separate orbits, we flirted, argued, got to know each other. For hundreds of millions of years, we danced our teasing dance: closer, farther apart, closer again.

I loved her for her fearless embrace of the Universe. Back then, the Oort cloud sent hailstorms of comets towards the heart of the solar system. She did not shrink from them, but laughed as the great balls of ice struck against her, singing all the while. She hummed as the ice melted, boiled against her skin, rained down and collected into rivers, lakes, seas.

Before I knew it, she had grown into a young planet of great beauty. Her blue oceans swelled and filled out gracefully, and the tan continents drifted over them like sunspots. She was still tempestuous and moody: lightning flashed in her atmosphere, studded by speeding cumulonimbus clouds. At her poles, shifting auroras lit up the darkness, dazzling even at my distance.

Finally, I worked up the courage to ask her to join me in my orbit. I even made a ring out of the prettiest bits of drifting dust. "We have been dancing long enough," I said. "Come, let us travel together, inseparable until the end of time."

She glowed, brightened, but then tilted her axis ever so slightly. "Look," she said, and opened her cloud-cover a sliver so that I could see.

Her oceans were teeming with tiny things, creatures that moved on their own. They dove and swam, chased each other and leapt out of the waves, as fleeting as flashing meteors.

"Some time ago, lightning struck the sea just so and formed a chain of complex organic molecules. At first, I didn't pay much attention to it, but it multiplied and grew. During the eon while you and I danced to the fixed measures of gravity, that simple beginning has evolved into these beautiful and wondrous forms."

"I don't understand," I said. "What do these … things have to do with us?"

"They're fragile," she said, her surface

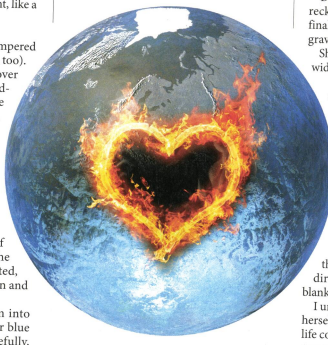

brightening again with that lovely, gentle glow. "I have to stay where I am so that they'll be warm and safe."

"Then I'll join you."

She wobbled in surprise. "No! Your radiation … I'm sorry, but we can't be together. I have responsibilities now."

I couldn't believe it. She was choosing a bunch of parasites over me.

I shouted and spun, and storms, each as big as she was, raged across my surface. But she just ignored me, and continued to tend to her babies, to life.

Something happened to me then. Maybe it was the pull of another star passing by, or a friendly gas giant that wandered closer to offer me comfort, but I shuddered and left my old path.

Now my travels were at an angle to the plane of the solar system. My orbit grew erratic, eccentric. I dove closer to the sun than even she did at perihelion, and flew as far away as the Oort cloud at aphelion. By turns I froze and burned. I approached her, imploring her to accept my devotion, and I ran from her, driven by despair.

I could see that my mass was affecting her, nudging her from her orbit.

"Stop," she pleaded. "Please. You're hurting the life dependent on me."

But I didn't stop, and I grew even more reckless. During one of my approaches, I finally moved too close, and she fell into my gravity well and was flung out of her orbit.

She drifted away from the sun on an ever-widening spiral.

As she passed me, she turned her face away. I could see a veil of ice forming over her once-clear blue oceans.

"I'm sorry!" I cried after her.

For a moment I saw her shudder, as her molten core grew hotter under the tidal forces of the sun's gravity and mine. "I have to save them," she murmured. "I have to save my babies."

The veil of ice soon covered all of her and grew thicker. And as she continued on her trajectory away from the sun, I could see her atmosphere turn directly into ice and fall onto her like a blanket of dry snow.

I understood. She was willing to entomb herself away from the Universe just so that life could continue to survive in her liquid oceans, heated by the fire of her core from below and protected from the void above by miles of ice.

"Goodbye," I said.

And I saw her ice shell crack just a bit, and a miles-long flow of magma oozed out, a blood red wound hissing against the ice.

"Goodbye," she said, already so far away.

In a moment the magma froze solid again and sealed the crack, like a scab. I'll never forget that sight. It was her heart, bleeding with pain and love.

I watched until she disappeared into the emptiness between the stars.

But I know she's still out there, dreaming under her ice shell, her heart ever fiery, giving life to a whole world. ■

Ken Liu *lives and writes in Massachusetts. For more, see http://kenliu.name/stories.*

This story is based on D. S. Abbott and E. R. Sitzer *Astrophys. J. Lett.* **735,** L27 (2011).

➲ NATURE.COM
Follow Futures on Facebook at:
go.nature.com/mfoodm

7,000 Recombinant Human Proteins

More Assays! Better Assays!

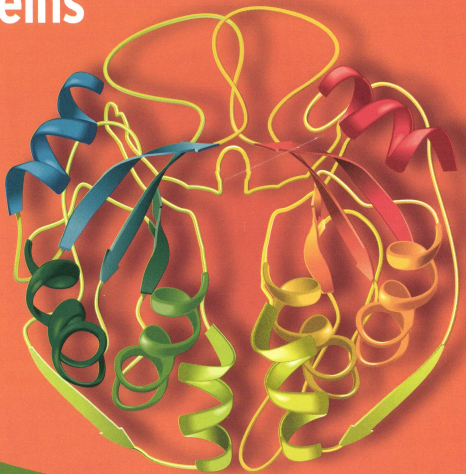

The Largest Collection of Mammalian Cell-Derived Proteins

Protein functional studies

Compound screening

Immunogens for antibody production

Assay standards: ELISA, Mass Spec, and more

Human MTOR protein activity verified in a kinase assay

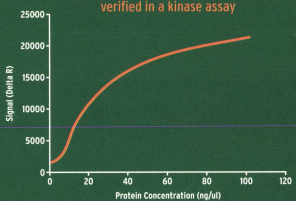

ORIGENE
Your Gene Company

origene.com/protein

More translational and predictive animal models.

Plot your pathway for breakthroughs in neuroscience with knockout rat models from SAGE® Labs.

Biosynaptic.

Advancements in neuroscience are yours to discover with targeted knockout rats from SAGE Labs. Our comprehensive suite of rat models can help move your neuroscience research forward. Map your next breakthrough with smarter rat models for studying neurodegenerative, mood, and affective disorders, including seven new models of autism.

SAGE® LABS
Sigma Advanced Genetic Engineering

Explore our collection of knockout rat models
sageresearchmodels.com

©2012 Sigma-Aldrich Co. LLC. All rights reserved. SIGMA and SIGMA-ALDRICH are trademarks of Sigma-Aldrich Co. LLC, registered in the US and other countries. SAGE is a registered trademark of Sigma-Aldrich Co. LLC. Where bio begins is a trademark of Sigma-Aldrich Co. LLC.